Biophysical investigations of hen lysozyme aggregation and its inhibition at alkaline pH

A Thesis Submitted in Partial Fulfillment of the Requirements for the Degree of

Doctor of Philosophy

By

Vijay Kumar Ravi

Department of Biotechnology
Indian Institute of Technology Guwahati
Assam, India.

August 2011

INDIAN INSTITUTE OF TECHNOLOGY GUWAHATI

Department of Biotechnology

STATEMENT

I do hereby declare that the matter embodied in this thesis is the result of investigations carried out by me in the Department of Biotechnology, Indian Institute of Technology Guwahati, India, under the guidance of Prof. Rajaram Swaminathan.

In keeping with the general practice of reporting scientific observations, due acknowledgements have been made wherever the work described is based on the findings of other investigators.

IIT Guwahati
August, 2011.

Vijay Kumar Ravi

INDIAN INSTITUTE OF TECHNOLOGY GUWAHATI

Department of Biotechnology

CERTIFICATE

It is certified that the work described in this thesis, entitled "*Biophysical investigations of hen lysozyme aggregation and its inhibition at alkaline pH"* done by Mr. Vijay Kumar Ravi for the award of degree of Doctor of Philosophy is an authentic record of the results obtained from the research work carried out under my supervision in the Department of Biotechnology, Indian Institute of Technology Guwahati, India, and this work has not been submitted elsewhere for a degree.

IIT Guwahati
August 2011.

Prof. Rajaram Swaminathan
Department of Biotechnology
IIT Guwahati

This thesis is dedicated to----------

My father- in- law, Late Shri Ramautar Mochi

&

My Bade Pitaji, Late Shri Ramsawrup Mochi

Acknowledgements

This my privileged to acknowledge my supervisor, Prof. R. Swaminathan for his excellent guidance, valuable suggestions for planning experiments, results discussion, data analysis and suggestions for my future plans.

I wish to thank all of my Doctoral committee members Dr. V. V. Dasu, Dr. Gopal Das, and Dr. A. Ramesh for their precious suggestions, comments and time to time evaluation of my Ph. D research work.

I am grateful to thanks to existing and as well as all former HOD for providing all state of art facility.

I would like to thank all the faculty members of my department.

I would like to thanks all present staffs and former staffs for their support.

I am thankful to CIF for providing fluorescence facility. I would like to thank Mr. Francis for his help during fluorescence measurements, and also to Dr. G. Krishnamoorthy and his group for providing experimental facility.

I am thankful to HOD department of Chemistry for allowing fluorescence measurements.

I would like to thanks Prof. G. Krishnamoorthy from Chemical Dynamics Lab, TIFR, Mumbai for organizing AFM training. I thanks to Mrs. Madhuri (Prof. G.K's lab) for giving AFM training.

I would like to acknowledge ministry of Social welfare and empowerment and UGC, New Delhi, Govt. of India, for giving financial support under RGNF scheme for the period of 2010-2011.

I am also thankful to IIT Guwahati for institute fellowship from Jan 2006-Jan2010.

I am thankful to DST, Govt. of India for giving financial support from Dec 2010 to 31st March 2011 for this work.

I wish to thank my all former lab members specially Dr. Satish Kumar for helping during my techniques learning period, Dr. M.V satish, Dr. Meher and Dr. L. Homchaudhuri. I am thankful to Mr. Nividh chandra for scientific and general discussion and also Mrs. Gunjan, Miss Tulsi and Miss Soumya.

I am thankful to Narendra, Aditya, Kapil, Mohit and Bhaskar.

I am thankful to Dr. Satish kumar for his help in DLS experiment.

I am thankful to Dr. Suresh and his lab members from IICB Kolkata for doing CD experiments.

I am very very thankful to all my friends who are always in my heart for moral support and help. I am also thankful to all my seniors (Dr. Mahanty, Dr. Sahu, Dr. Majumder, Dr. Gopi, Dr. Purama, Dr. Shiva, Dr. Atul, Dr. Ballav, Dr Sandeep, Dr. Dilip, and Dr. Ramakrishna), all my batch mates (Dr. Pallav, Dr. Sanjay, Dr. Achlesh, Dr. Shampa, Dr. Vigya) and all hostel friends (Narsihn, Gaurav, Kaushik, Beda, Sukhi, Shadab, Vijay Mishra, Himanshu jee, Arvind, Sandip, Zella, Rajendra, Yata, Asim, K. Hegdge, Sourabh, Ratual, Naresh,Kasturi, Rachna and Sachi) and all my M.Tech friends.

I am thankful to all my seniors and batch mates and juniors for his morals support.

Lastly…I sincerely thank to my blood relationship member my parents. They have always helped like anything and gave moral support and encouragement for making bright carrier. I wish to thanks my brothers, sisters, and all my family members for their moral support for Love & affection, encouragement. I wish to thanks my Chotte Dada ji and Dadi for their encouragement and moral support. I wish to thanks my mother- in- law, brothers and sisters-in- law for moral support in my Ph. D carrier. Finally, I express my heartiest and deepest thanks to my wife Suganti and cute son Vidyanshu. It is not enough for me to express their support during my Ph.D, especially in the last year of my research work.

I pray to God who always gives potency for struggling in adverse situation.

Abbreviations

:

HEWL	Hen egg white lysozyme
Dansyl	2-dimethyl aminonaphthalene 6-sulfonyl
Dabcyl	(4-((4-(dimethylamino) azo) benzoic acid
SDS	Sodium dodecyl sulphate
CTAB	Cetyltrimethylammonium bromide
DTT	Dithiothreitol
ThT	Thioflavin T
AFM	Atomic Force Microscopy
ANS	8-anilinonaphthalene-1-sulphonic acid
NAG	N-Acetyl-D-glucosamine
FRET	Fluorescence resonance energy transfer
Chitotriose	N,N′,N″-Triacetylchitotriose

ABSTRACT

Protein aggregation has been considered as undesired product, while incorrect folding of proteins. It is associated with the many of consequences like neurodegenerative diseases (e.g. Alzheimer's and Parkinson's) and non-neurodegenerative disease (e.g. Type II diabetes, systemic amylodosis), recovery of over expressed therapeutics proteins, and formulation for the protein drug. Protein aggregation occurs through different and complex pathway, forming intermediate products like oligomers. These oligomers further participate into amyloid fibril formation. Previously it has been considered that amyloid fibrils are responsible for amyloidogenic diseases. However recent finding indicates that oligomeric products are likely have a role in causing diseases like Alzheimer's, Parkinson's in late age. Apart from clinical significance of amyloid fibril, recent study impresses that amyloid fibers have a great potential to be used as biomaterials and nanodevices like nanovechicles, nano wire, nanopores and nanoscaffold. These intrinsic properties were developed because of its ordered cross β – sheet structure and self assembling property at a nanoscale. Hence, in this thesis some salient biophysical investigation was carried out on growth of hen lysozyme oligomers, amyloid fibers formation and its inhibition.

It has shown that hen lysozyme forms amorphous and ordered (fibrillar) aggregates in pH 12.2 at room temperature. These aggregates later stabilized through intermolecular disulfide bond formation among aggregates. Subsequently, it was also studied that how surfactants (SDS, CTAB) and DTT affects the aggregation of lysozyme. For this investigation, the lysozyme was incubated in pH 12.2 at room temperature and aggregation was monitored at different incubation period. Size heterogeneity and morphology of hen lysozyme aggregates was monitored employing gel filtration chromatography and atomic force microscopy techniques. The size heterogeneity was observed based on the spectral profile of gel filtration elution volume. Here, it was found that at early time lysozyme spontaneously forms mixture of aggregates containing more populated small aggregates in pH 12.2 at room temperature. However as time of incubation increases nearly 120 hours the big aggregates predominate. However in presence of SDS, HEWL forms large molecular mass or unusual shape. In presence of CTAB lysozyme aggregate was found relatively smaller and compact compare to SDS. Although in presence of DTT lysozyme conformation was remain compact and its size/shape was comparatively similar to monomer. Further,

morphology of aggregates, in absence and presence of surfactant (SDS, CTAB) and DTT was monitored employing atomic force microscopy. It was shown for the first time that HEWL forms both globular aggregates and fibrils in pH 12.2 at room temperature. We observed 120 μM HEWL grow with heterogeneous population of aggregates including fibril after 5 days incubation in pH 12.2 at room temperature. In presence of SDS, formation of HEWL-SDS complex was seen, in such manner like bound outer surface of micellar SDS around HEWL. This complex is making as a big molecular mass with adjoining small clusters situated nearby. In presence of CTAB, the aggregates were seen unbound to CTAB and single aggregates were comparatively smaller. Interestingly in presence of DTT, HEWL was observed like monomer morphology. The native protein was seen like monomer in pH 7.0. These aggregates feature was matching with gel –filtration elution profile in presence and absence of surfactants (SDS, CTAB) and DTT. From these finding it was quite evident that DTT has a strong influence in halting the progress of HEWL aggregation at alkaline pH 12.2 compare to surfactants.

After these studies, it was important to characterize the inhibition of hen lysozyme aggregation using small molecule. For this purpose HEWL was pre-incubated with its competitive inhibitor, chitotriose (or its smaller sugar derivatives) and NAG at neutral pH 7 was used to investigate any influence on its aggregation and fibrillogenesis in pH 12.2. Interestingly following features like size of aggregates change in helical content, reduction of free sulfhydryl and morphology was observed. Sizes of aggregates were characterized using gel filtration. Based on the elution profile, it was observed that overnight (12 hour) pre-incubation of HEWL with its competitive inhibitor, *N*,*N*′,*N*″-Triacetylchitotriose (chitotriose) at pH 12.2, significantly reduced presence of larger oligomers in comparison to samples containing absence of chitotriose. Subsequently in presence of NAG, at longer incubation times it was observed that mixture of large aggregates as well as moderately sized oligomers exist. This was similar to HEWL pH 12.2 aggregates feature. Using CD, helical structure of HEWL in presence of chitotriosoe was significantly retained whereas helical structures were reduced in presence of NAG and control HEWL pH 12.2 sample. Accessibility of sulfhydryl groups using DTNP assay was indicated that free –SH reduced significantly in presence of chitotriose and NAG compared to control where all free –SH were accessible to DTNP. It seems that these additives protect the disulfide bond from breakage at alkaline pH. Employing AFM, morphology of HEWL aggregates in presence and absence of chitotriose

and NAG were investigated. Results were shown that in presence of chitotriose, HEWL appears as small oligomers without forming amyloid fibrils. However in presence of NAG and control HEWL samples contains large globular aggregates and fibrillar aggregates after prolonged incubation in pH 12.2.

After showing feature of aggregates like size and morphlogy at fixed HEWL concentration in absence and presence of additives like surfactants, DTT, chitotriose, NAG. It was imperative to investigate the aggregates feature like oligomer and fibril at different concentration. As it has been discuss previously, oligomeric states are found to be toxic to neuronal cell and responsible for neuronal dysfunction diseases. Can be possible to isolate oligomer based on size and morphology with varying the concentration?. Due to this reason, concentration dependent size, structure and dynamics of oligomeric state was studied in this part of thesis. The growth dependent changes in structure and dynamics of lysozyme at pH 12.2 was screened from various HEWL concentration range 120 μM to 300 and 30 nM. For this investigation, various biophysical techniques such as fluorescence resonance energy transfer, ANS binding assay, Tryptophan quenching, steady state fluorescence anisotropy, fluorescence anisotropy decay kinetics and atomic force microscopy was employed. Based on these observations, different kinds of changes were found such that: (1) the reduction in size with decreasing the initial monomer concentration from 120-300 nM was observed from fluorescence resonance energy transfer, steady state and time resolved fluorescence anisotropy decay. (2) Exposure of deep hydrophobic interiors dependent on increasing initial monomer concentration range120 μM to 300 nM was found from emission maximum and blue shift of dansyl –HEWL conjugates spectra, ANS binding assay and tryptophan fluorescence quenching. (3) The growth of fibril was found at all concentration range 120 μM to 300 nM and 30 nM, which was not dependent on initial monomer concentration. At very low concentration like 300 nM fibril was seen originating from oligomers and rate of fibril growth is different and in very fascinating manner. (4) At higher monomer concentration like 120 μM tightly branched fibril was seen. (5) Here occurrence of fibril was observed at all possible detecting range concentrations which suggest that fibril is forming through isodesmic mechanism.

In last part of thesis, work was focused on suppression of HEWL aggregation using strategy like alkylation of free -SH group with iodoacetamide. For this purpose free -SH was methylated using iodoacetamide, which block formation of further intermolecular disulfide

bond (S-S) in pH 12.2. The role of intermolecular disulfide bond was seen in stable growth of aggregates. Subsequently aggregation process were investigated employing various techniques as follows Thioflavin –T, ANS assay, atomic force microscopy, steady state fluorescence anisotropy, and fluorescence anisotropy decay kinetics and fluorescence life time. Our Thioflavin –T and AFM data were shown that methylated free thiol HEWL in pH 12.2 unable to form a fibril, however moderate increase in Th-T intensity was found, possibly due to binding with intermediates like oligomers. With ANS data it was observed that methylated free –SH HEWL expose hydrophobic residues less compare to free –SH in aqueous environments. It was evident from increased fluorescence intensity and marginal red shift of spectra. We also observed low r_{ss} value of methylated free thiol HEWL- dansyl conjugates compare to control. The fluorescence anisotropy decay kinetics showed that methylated –SH HEWL-dansyl conjugates retains low longer rotational correlation time (ϕ_2) compare to control HEWL-dansyl conjugates after 30 hours of incubation in pH 12.2 at room temperature. Morpholgy of thiol blocked HEWL was shown, results indicates that oligomer does not participate in further fibril formation. All these investigations suggest that HEWL with blocked free- SH group forms only oligomers not fibril in pH 12.2 at room temperature.

Table of contents

1 Introduction

1.1 Protein aggregation

Proteins need correctly folded conformation for carrying out their specific biological functions (**Anfinsen et al., 1973**). However inside cells, the nature of protein synthesis, the high protein concentration, the action of molecular chaperones and proteases, the potential for post-translational modification, and the ‘‘molecular crowding effect’’ are all factors have a great potential to influence incorrect folding which leads to protein aggregation **(Minton et al., 2001).** Although out side cells, like *in vitro* condition, alterations of physicochemical parameters are responsible for incorrect folding which adopts non native conformation termed as misfolded and unfolded state. These non native states trigger the protein aggregation process. Protein aggregation process itself is a multi- complex phenomenon where different intermediates are formed. These intermediates are responsible for formation of soluble aggregates and insoluble aggregates. The insoluble aggregates characterized as well known ordered structure known as amyloid fibril. This amyloid accumulates as plaques extra cellularly in organs and intracellularly inside cells. These deposits induce cellular stress and affects immunity in neurodegenerative diseases, which cause neuronal dysfunction and loss. The accumulation of abnormal protein aggregates become toxic by disrupting intracellular transport, followed by protein degradation pathways, or disturbing vital cell functions. The current list of protein misfolding disorders includes, numerous neurodegenerative diseases such as Parkinson’s, Alzheimer’s and Huntington’s disease; Transmissible encephalopathies, Gerstmann Straussler Scheinker disease, fatal familial insomnia, multiple system atrophy, numerous synucleinopathies and taupathies, amyotrophic lateral sclerosis, and familial encephalopathy with neuroserpin inclusion bodies, as well as monoclonal protein systemic amyloidosis, reactive systemic amyloi-dosis, familial amyloidotic polyneuropathy, hereditary apoAI amyloidosis, hereditary lysozyme amyloidosis, senile systemic amyloidosis, isolated atrial amyloidosis, hereditary cerebral amyloid, Finnish hereditary amyloidosis, hereditary fibrinogen chain amyloidosis, insulin-related amyloid, cataracts, medullary carcinoma of the thyroid, late onset diabetes mellitus, symptomatic (haemodialysis related) β_2- microglobulin amyloidosis, arthritis, and many

other systemic, localized, and familial amyloidosis (**Dobson et al., 2004, Sunde et al., 1998, Uversky et al., 1999, Uversky et al., 2006**).

In addition, the formation of inclusion bodies is known to exhibit a major problem in the recombinant production of therapeutic proteins (**Fink et al., 1998**). Formulation of these therapeutic proteins into delivery systems and their in vivo delivery are often complicated because of protein association and protein aggregation problem **(Demidov et al., 2004)**. Thus, protein folding abnormalities and subsequent events underlie numerous difficulties with protein therapeutic applications. Current demographic trends indicate that need for age-related and other degenerative disorders and macromolecule therapeutics will be at the frontline of future medical developments.

1.1.1 History of amyloid deposits

The amyloid term was popular in 19th century due to its role in neurodegenerative diseases. Here it is very crucial to discuss in detail about history and feature of amyloid. The macroscopic abnormalities in liver (lardaceous and waxy liver) and spleen (spongy and "white stone" containing spleens) associated with proteinaceous misfoldings was perhaps reported first time in 1639 (reviewed by **Cohen et al., 1986).** From these concepts the history of amyloidosis was started from year 1854, when the German physician Rudolph Virchow introduced the term "amyloid" to examine a macroscopic tissue abnormality in cerebral corpora amylacea and the waxlike deposits in spleen, liver and kidney **(Virchow, 1854)**. Thereafter, Friedreich and Kekule extracted amyloid rich segments from the spleen of an amyloidosis patient. They employed chemical analyses of the extracted material and concluded that the main substance was proteinaeous in nature **(Friedreich et al., 1859)**. This was later confirmed by Hanssen, who showed that amyloids are digestable with pepsin **(Hanssen et al., 1908)**. The role of abnormal deposits in the progress of neurodegenerative disorders began with a report by Alois Alzheimer **(Alzheimer et al., 1907),** which was examined as senile plaques and neurofibrillary tangles in the brain of a middle aged woman. They were carrying memory deficits and a progressive loss of cognitive function. This was the first published evidence of Alzheimer's disease (AD) **(Forman et al., 2004)**. The neuropathological hallmarks of Parkinson's disease (PD), Lewy bodies (LBs), and Lewy

neuritis (LNs) were described briefly thereafter in 1912 by Friederich Lewy **(Lewy et al., 1912)**.

There are several proteins which bear no relation to protein deposition diseases even though they have been found to form amyloid like structure under *in vitro* condition, This finding indicates that formation of amyloid structure is an inherent or generic property of any polypeptide chain and this type of assembly has found in nature also **(Chiti et al., 2006)**. In support of the above statement, it has been discussed that functional amyloid like structure present in some organism which was evolved by self-assembly mechanism in nature. This is use for host defense for their survival. The well studied example of functional amyloid is formed from self assembly of protein curlin that is used by Escherichia coli to colonize inert surfaces and mediate binding to host proteins. This was consistent with the characteristics of other amyloid structures, 6–12 nm in diameter, containing extensive β-sheet structure. **(Chapman et al., 2002, Fowler et al., 2007).** Another example is filamentous bacterium *Streptomyces coelicolor* that produces aerial hyphae, which is a secreted protein called chaplins. This has been identified in the hyphae of this organism with the ability to form amyloid fibrils that act cooperatively to bring about aerial development **(Mankar et al., 2011)**.

1.1.2 The Structure of amyloid fibrils

The molecular structures of amyloid fibrils are interest of discussion, as atomic level structural information is crucial for an understanding of the interactions between the protein monomer that drive amyloid formation. These studies can facilitate understanding of fibrillization mechanisms and pathways, and for the design and development of fibrillization inhibitors. The low-resolution based methods were developed for the physical and structural characterization of amyloid fibrils, before development of high resolution techniques for atomic structure study of amyloid. The eminent biophysicist William Astbury proposed that every protein might have a fibrous state as well as a globular state (**Astbury et al., 1935)**. The amyloid fibril structured by secondary structure was first shown from tinctorial properties of amyloids in vivo, where Congo red exhibits yellow-green birefringence under cross-polarized light after binding with amyloid, indicating the presence of ordered structure in the amyloid aggregate (**Westermark et al., 1999**). Similarly, amyloid binding-induced

Thioflavin T fluorescence suggests the presence of ordered structure in the aggregates **(LeVine, H., 1999)**. William Astbury was first biophysicist who obtained cross-beta fibril diffraction pattern, that was accepted as the classical signature of the amyloid state of proteins. Subsequently repetitive nature of the cross- beta-sheet structure of amyloids was assayed by X-ray fiber diffraction **(Sunde et al., 1997)**. Other than X-ray fiber diffraction technique circular dichroism (CD) and fourier transform infrared spectroscopy (FTIR) are also used to measure the β-sheet content of amyloids **(Fradinger et al., 2005)**, whereas electron microcopy (EM) was used to observed the boundaries and shape of the amyloid fibrils to a resolution of approximately 10–25 Å **(Zhang et al., 2009)**. On the contrary electron paramagnetic resonance spectroscopy (EPR) **(Margittai et al., 2008)** and quenched hydrogen/ deuterium exchange coupled with mass spectrometry **(Kheterpal et al., 2006)** or two-dimensional nuclear magnetic resonance spectroscopy (NMR) was employed for providing significant details about the local structure of the amyloid fibrils **(Hoshino et al., 2002, Ritter et al., 2005, Toyama et al., 2007)**. These low resolution techniques were not relevant to study atomic resolution structures of amyloid. It was also stated that "amyloid fibrils cannot be characterized in detail at the molecular level because they are not crystalline yet. It is difficult to study by solution NMR spectroscopy due to its large mass. **(Chiti & Dobson 2006)**. As amyloid research became advance and progressive, the first solid state NMR studies of amyloid fibrils were performed by Spencer and coworkers Griffin (**Spencer et al., 1991)**. They proposed a structural model for Aβ (34-42) fibrils that contains anti parallel β-sheets with an alternating hydrogen bond arrangement **(Lansbury et al., 1995, Griffiths et al., 1995, Costa et al., 1997)**. Afterwards Tyco and other groups have studied a detail structure of the amyloid fibrils Aβ peptide (Aβ1−40) at pH 7.4 and 24^{o} C. Their structure shown using dipolar recoupling techniques, each Aβ1−40 molecule contributes a pair of β sheet approximately 12–24 residues and 30–40 on both sides of the core region of the fibrils (see Fig.1.1.2 a). These strands, connected by the loop 25–29, are not part of the same β-sheet, however, but participate in the formation of two distinct β-sheets within the same protofilament (Fig.1.1.2 a). The different Aβ molecules are stacked on to each other, in a parallel arrangement and in register, at least from residue 9 to 39 **(Antzutkin et al., 2000, Balbach et al., 2002, Tyco, 2006 and Ahmed et al, 2010)**.

1.1.3 Structural studies using high resolution techniques

With the help of high resolution techniques like X-ray crystallogarphy, illustrating three-dimensional and atomic structure of amyloid fibril is crucial for understanding the role of each and every amino acid in architecture of amyloid fibril. R. Nelsson and M.R Sawaya studied crystal structure of different amyloid protein (i.e. Sup35, insulin, Aβ, tau, and amylin) by X-ray crystallography **(Nelsson et al., 2005, Sawaya et al., 2007)**. In the case of the Sup35p fragment, the crystal consists of pairs of parallel β-sheets in which each individual peptide molecule contributes a single β-strand (Fig. 1.1.2 c). The stacked β-strands are arranged in parallel in both sheets. The two sheets interact with each other through the side chains of Asn2, Gln4, and Asn6 in such orientation that water is excluded from the region between them. The remaining side chains on the outer faces of the sheets are hydrated and more distant from the next pair of β-sheets, suggesting that this minimal interaction perhaps represent a crystal contact rather than a feature of the fibrillar state. The important aspect of these structures found similar which was proposed from cryo-electron microscopy (EM) analysis of the amyloid fibrils. Where fibril formed from an SH3 domain and from insulin, in which the electron density maps were interpreted as arising from pairs of relatively flat untwisted β- sheets **(Jimenez et al., 2002)**. Such similarities suggest that many amyloid fibrils could have core structures that have very similar features. The specific nature of the side-chain packing, including such characteristics as the alignment of adjacent strands and the separation of the sheets **(Fandrich et al, 2002)**, which provides an information for the occurrence of variation of the structures for specific types of fibrils in the details. Recently, the atomic structures presented small molecule binders complex inside fiber-forming segments of Aβ, determined by X-ray micro crystallography. This structure reveals that small molecules bind between pair of β-sheets nearly parallel to the fiber axis. The structures also indicate that apolar molecules float along the fiber, which is reliable with the observation of nonspecific binding from variety of amyloid proteins. In contrast, negatively charged orange-G binds specifically to lysine side chains of adjacent sheets (**Landau et al., 2011**). These structures would be beneficial molecular frameworks for the design of diagnostics and drugs for protein aggregation diseases. Recently Schneider and coworkers illustrated structure of ploy glutamine fibrils using solid state NMR spectroscopy. Using Solid-state 29 NMR dipolar correlation experiments, they have found mostly β-strand character and tight interdigitation of hydrogen-bonded glutamine side chains from different sheets (**Schneider et al., 2011**).

Apart from the structural studies of amyloid at atomic level, interestingly in very recent oligomers structural polymorphism of human islet amyloid polypeptide (hIAPP) was studied using solid-state NMR and mass-per-length (MPL), They model a series of hIAPP oligomers with different β-layers (one, two, and three layers), symmetries (symmetry and asymmetry), and associated interfaces using molecular dynamics simulations. Their report explains that different hIAPP oligomeric models contribute a general and intrinsic nature of amyloid polymorphism, and which is driven by different interfacial side-chain interactions. (**Zhao et al., 2011**).

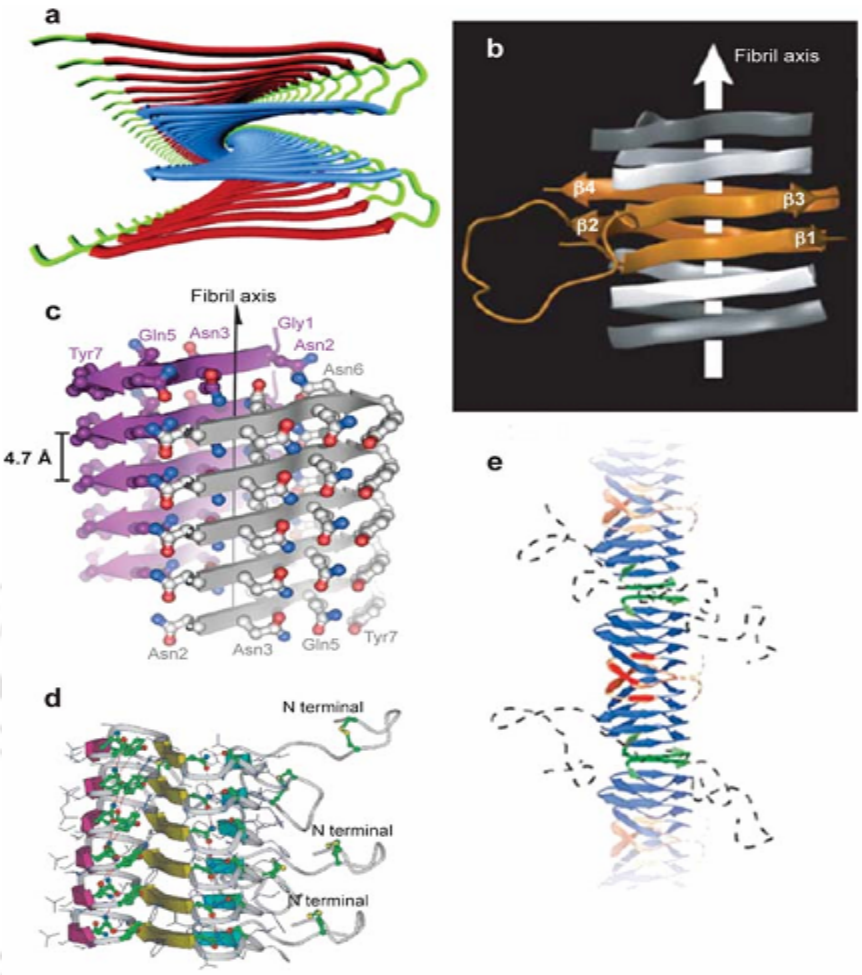

Figure 1.1.2: Three-dimensional structural models of fibrillar aggregates. (a) The protofilament of Aβ viewed down the long axis of the fibril. The segments 12–24 (red) and 30–40 (blue). (b) The fibril structure from the C-terminal domain 218–289 of the fungal prion protein HET-s. The ribbon diagram represents the four β-strands (orange) and the long loop between β_2 and β_3 from one molecule. Flanking molecules along the fibril axis (gray) (c) Atomic structure of the microcrystals assembled from the GNNQQNY peptide. (d) The protofilament shown from amylin peptide. Green, yellow, and pink β-strands indicate residues 12–17, 22–27, and 31–37, respectively. The unstructured N-terminal tail is shown on the right of the panel along with the disulfide Bridge between Cys2 and Cys7. (e) The fibril from the NM region of Sup35p. The colored ribbons indicate residues 25–38 (red), 39–90 (blue), and 91–106 (green). The unstructured regions 1–20 (red dashed lines) and 158–250 (black dashed lines) are shown. Adapted from (Chiti et al., 2006).

1.1.4 The polymorphism of amyloid fibrils

Before the study of molecular structure of amyloid fibrils, it was considered that morphological variation occurs between different fibrils formed from the similar peptide or protein **(Bauer et al., 1995).** Based on atomic level structural studies it was known that such morphological variations is associated with heterogeneity in molecular structure like change in the structural position of the polypeptide chains within the fibrils for example in peptide hormone glucagon, it was revealed that glucagon forms fibril at different temperature (25 ºC, 50 °C) which are morphologically distinct with difference in the secondary structure **(Pedersen et al., 2006).** The Aβ (1-40) forms polymorphic fibrils through variation of atomic structure of peptides **(Petkova et al., 2005).** It was also observed that yeast prion protein Ure2p formed polymorphic fibril because of conformational variation in atomic structure **(Baxa et al., 2005)**

1.1.5 Mechanism of protein aggregation

Mechanisms of protein aggregation are still elusive due to its complex process that dependent on several parameters. Basically protein aggregation process follows polymerization reaction pathways either kinetically or thermodynamically. Monomer which may temporarily assume an amyloidogenic conformation in solution, changes free energy crossing free energy barrier that is required to initiate the nucleation process. This step does not kinetically favor aggregation and this could be remain like dimer or pseudo dimer form. It is very difficult to characterize structurally due to its very dynamic multicomponent system and even low experimental resolution. However the distribution of nuclei concentration isolated recently using back-calculation. The *in vitro* concentration of nuclei for the model hormone, recombinant human insulin, is accounted in the picomolar range. This may rough estimate; reason is that the back-calculation method is likely to overestimate the nuclei concentration because it does not take into consideration of fibril fragmentation, which would lower the amount of nuclei (**Sorci et al., 2011**).

In the next steps these nuclei formed critical nucleus which prompt the fibril formation. The time taken for formation of critical nucleus from nuclei is considered as lag period which is slower process. This is known as the rate determining step (slow) that may be responsible for protecting normal individuals from amyloid formation. The time of the lag

phase is proportional to the steepness of the energy curve in the initial step (Fig. 1.1.5.1b), and protein concentration (**Kumar et al., 2010**). The dependence of the lag time on protein concentration is controlled by the rate of the association and dissociation of monomer as well as by the size of the nucleus (i.e. the number of monomers in the nucleus) (**Kodaka et al., 2004**)

This slow process can be avoided or make shorten by modifying the aggregation condition or adding the preformed fibril called seeding (see Fig. 1.2.5.2). Once a critical nucleus reaches, the conditions become favorable for aggregation with very fast kinetics and this is called elongation phase, from their any available monomers in the amyloidogenic conformation quickly participate in the fibril formation.

Nucleation dependent polymerization process starts only above the define concentration similarly for the fibril formation certain concentration are required. This characteristic monomer concentration is referred to as the critical concentration. The critical concentration for different protein is defined in different aggregation condition (**Mishra et al., 2007, Nag et al., 2011**). At equilibrium, a finite amount of the monomer would exist in equilibrium with the polymer (**Harper et al., 1997**). The critical concentration is usually determined from a plot of the rate of polymer formation (or amount of polymer) versus protein concentration (Fig. 1.1.5.1 d). It is interesting to know that micelle formation also requires a critical concentration, known as the critical micelle concentration (CMC). It has studied that amyloid fibril nucleation is much slower than micelle formation, probably due to attaining the greater entropic barrier which is involved in organizing a fibrillar structure (**Lansbury et al., 1995**).

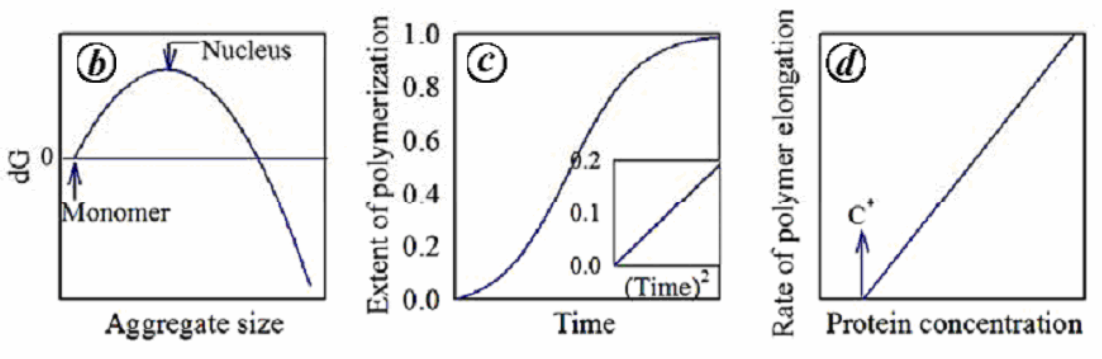

Figure 1.1.5.1: Indicates the kinetics of protein aggregation (b) Free energy barrier in an NDP reaction. (c) shows the characteristic kinetic features of an NDP reaction, namely, the presence of a lag phase (d) A critical concentration C*. Adopted from (Kumar et al., 2010).

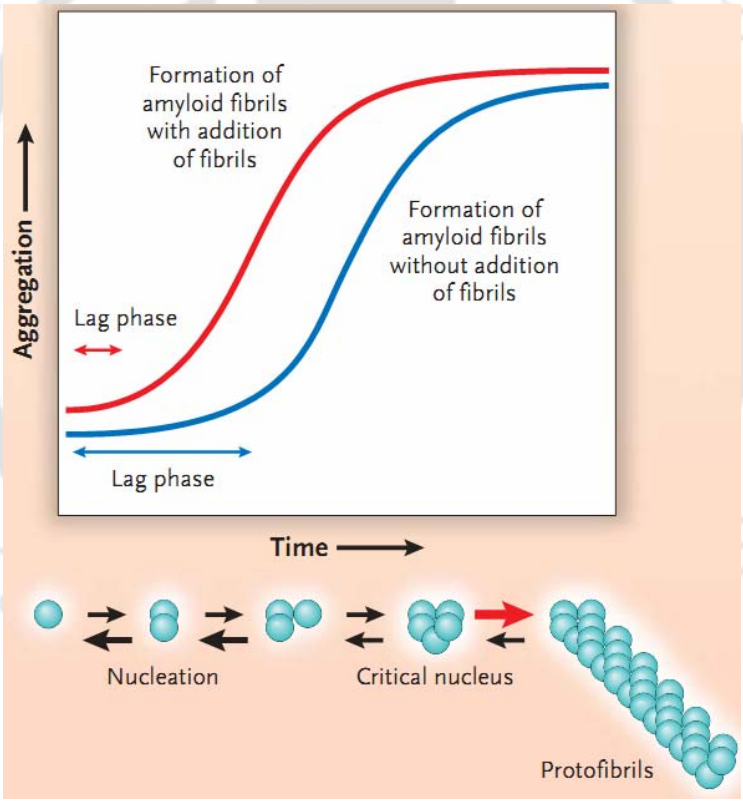

Figure 1.1.5.2: Kinetics of fibril formation is shown. The blue line indicates the formation of amyloid fibrils, beginning from a solution of monomer proteins. The red line represents a similar condition in which preformed fibrils are added, thus making the lag phase much shorter. Below the plot nucleus dependent scheme are shown.
Adopted from (Merlini et al., 2003).

1.1.5.1 Nucleated growth dependent amyloid formation

Nearly 50 years ago, in 1959 Oosawa first time proposed the nucleation based polymerization mechanism of G–F transformation of actin **(Oosawa et al., 1959)**. Further it has been discussed extensively that amyloid fibril formation occurs via nucleated growth mechanism. In This mechanism protein conformation changes into amyloid ordered structure via various intermediates such as template and nucleation, linear colloid-like assembly of spherical oligomers and domain-swapping **(Zerovinik et al., 2011, Ghosh et al., 2010**). Non-amyloidogenic protein cystatin (Cysteine protease inhibitor), temperature dependent and concentration dependent rate kinetics was pursue nucleus based aggregation growth. Based on thioflavin T assay, their finding suggests that faster rate of aggregation (fibrillation) was dependent on increasing temperature and lowering the cystatin concentration **(Skerget et al., 2009)**.

1.1.5.2 Structured Oligomers and protofibrils

Nowdays, substantially effort has been put for identifying, isolating and characterizing the oligomeric species. It has major role in mechanism of fibril formation, Moreover; oligomeric species are implicated as toxic for neuronal cells which may be responsible for the complications of neurodegenerative disease (**Winner et al., 2011, Kayed at al., 2003, Ahmed et al., 2010**). Different mixture of oligomers of β-Amyloid (1-40) as individual subunit like small oligomers, has been studied using single molecules fluorescence techniques by directly counting the photobleaching steps in the fluorescence. They found heterogeneity among β-Amyloid (1-40) oligomeric aggregates **(Ding et al., 2009).** The morphology of soluble oligomers was found as spherical and invariant in shape with 2.7 to 4.2 nm in diameter. The small oligomers can stabilize using low- temperature and low salt concentration. Ahmed and coworkers isolated the disc shaped oligomers (pentamers) using low –temperature and low salt concentration and it was found that these oligomers do not conatins β- sheets structure (**Ahmed et al., 2010**). Another form of aggregates exist like curvilinear with length of ~300 nm (**Shekher et al., 2011, Harper et al., 1997)** called protofibril which has characteristics feature like binding property to Thioflavin T dye, Congo red and it consist of β sheets confirmed by CD. One should not confuse with protofilament that is dissimilar to protofibril. The protofilament are constituents units of mature fibril. The

oligomers of all proteins like (α- synuclein, islet amyloid polypeptide, polyglutamine, lysozyme, human insulin and prion protein, tau protein) have common structural feature and follow common mechanism of toxocity which is confirmed by oligomer-specific antibody reaction (**Kayed et al., 2003**) and It is found different from fibril structure. It is obviously difficult to characterize the oligomers and for these purpose single molecules fluorescence techniques, monoclonal antibody –specific techniques have been used (**Orete et al., 2008**, **Patterson et al., 2011**). Patterson and his coworkers isolated dimeric species from tau oligomers. They found dimer forms higher oligomeric state by self associating mechanism and these dimer/oligomer presents as pathological inclusion in Alzheimer's diseases (**Patterson et al ., 2011**).

1.1.5.3 Unstructured oligomers and protofibrils

Some proteins form oligomers through covalent dimeriztion process like for example yeast prion Sup 35p. This dimer nucleates further to participate in formation of fibril. Basically covalent dimerization occurs if oligomer are maintained under oxidizing condition, where intermolecular disulfide bridges are created from cysteine residues **(Krishnan et al., 2005).**

In the case of Aβ 40, 42 soluble oligomers exist in rapid equilibrium between monomer and it was composed of 2-4 and 5-6 molecules, however these oligomers was disorganized and unstructured confirmed by CD measurements **(Bitan et al., 2003)**. Another example addressed about unstructured oligomers, which formed through rapid unfolding of the SH3 domain of bovine phosphatidylinositol 3' kinase at pH 3.6 and converted in thin and curly structured protofibril. It was concluded that structured protofibril species can form through reorganization or self assembly of small oligomers however disorganized oligomers that are formed quickly after the initiation of aggregation process **(Chiti & Dobson, 2006).**

1.1.5.4 Protein aggregation through isodesmic polymerization

Zhao and coworkers has discussed the isodesmic model in simplistic way and indicates that it is a simplest type of polymerization or aggregation process and which was considered as one dimensional polymer. This type of polymerization is assumed that any monomer can add to another monomer and fibril forms with identical free energy change, as a result while addition of monomer equilibrium constant for all steps are same (see Fig. 1.1.5.4 A). Hence in this system there is no energy difference between adding a monomer to a polymer or to

another monomer can be observed (see Fig. 1.1.5.4 B). It can considered that isodesmic model based protein aggregation occurs without nucleation formation process, however it has also assumed, if equilibrium constant is larger at the first step (i.e dimerization) than equilibrium constant of further monomer addition steps, the system considered to be as tight dimerzation which follow isodesmic elongation. Another important factor for isodesmic model is presence of no critical concentration barrier is needed (**Zhao et al., 2003**). There are very few example are available in support of isodesmic model protein aggregation mechanism (**Oosawa et al., 1962, Sekhar et al., 2011, Romberg et al., 2001, Frieden et al., 2007, Kumar et al., 2010**).

A

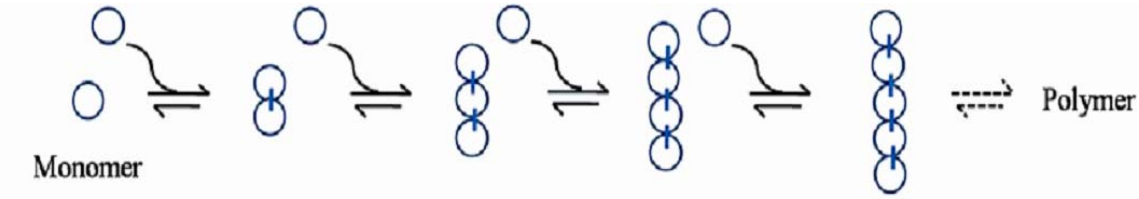

Figure 1.1.5.4 A: Schematic of isodesmic polymerization.

Polymerization of amyloidogenic yeast prion (Sup 35) has also suggested that prion (Sup 35) fiber grows by monomer addition and rapid polymerization occurs without intermediate formation. It was proposed that absence of oligomeric intermediates during fiber growth raises the possibility that agents designed to promote direct fiber formation and disfavoring oligomer formation, may help prevent the accumulation of potentially toxic oligomeric intermediates **(Collins et al., 2004)**.

B

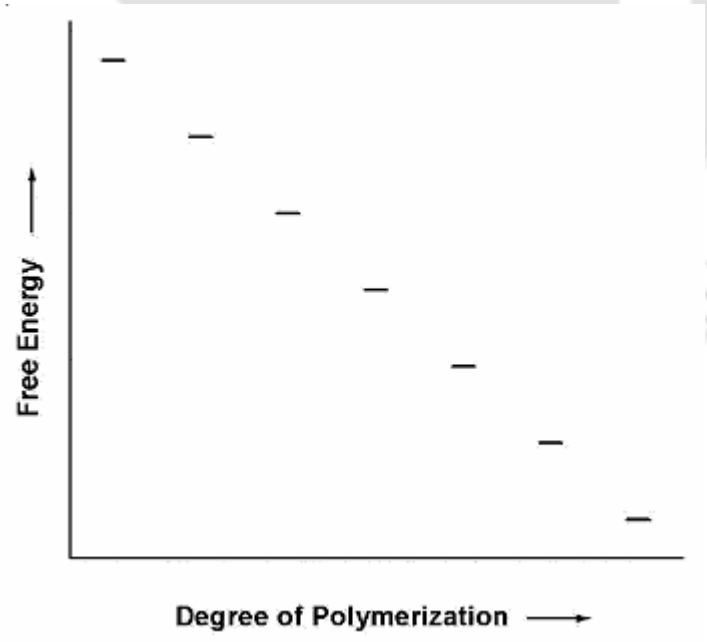

Figure 1.1.5.4 B: Qualitative plots of free energy as a function of degree of polymerization for isodesmic polymerization. Adapted from (Zhao et al., 2003).

1.1.6 Protein conformation versus protein aggregation

1.1.6.1 Globular protein aggregation from partial unfolding

In previous section system are found at structured and unstructured state prior to structured fibril formation. Here will be discussing some recent facts about globular protein aggregation. It was studied that globular proteins requires partially unfolding to form amyloid aggregates (**Kelly 1998, Dobson, 1999**). It was reported that globular protein have greater tendency to aggregate at such condition like high temperature, high pressure, low pH , high pH, and organic solvents in moderate condition where protein can partially unfold **(Gosal et al., 2005, Guijarro et al., 1998, Chiti et al., 2000, Villegas et al., 2000, Ferrao-Gonzales et al., 2000, Homchaudhuri et al., 2006).**

Based on the pathophysiological investigation, some famlial forms of diseases triggered through destabilization of the native structure. Destabilization native structure increases the population of non native state, through which natural mutations occurs and mediate the protein aggregation which responsible for the protein deposits disease (**Hammarstrom et al., 2002**). As an example aggregation human lysozyme and HypF-N can be started with less than 1% of partially folded population that remains in equilibrium with native conformation (**Canet et al., 2002, Marcon et al., 2005**)

1.1.6.2 Aggregation through native like oligomers

Recently some new study has strong evidence that globular proteins contains propensity to aggregates via small fluctuations in native structure (locally unfolded) like thermal fluctuations at physiological pH rather than destabilization of native structure. Interestingly, these oligomers containing native fluctuating conformations retain enzymatic activity and it has also native like topology (**Chiti & Dobson, 2009**). (see Fig. 1.1.6.2 a & b).

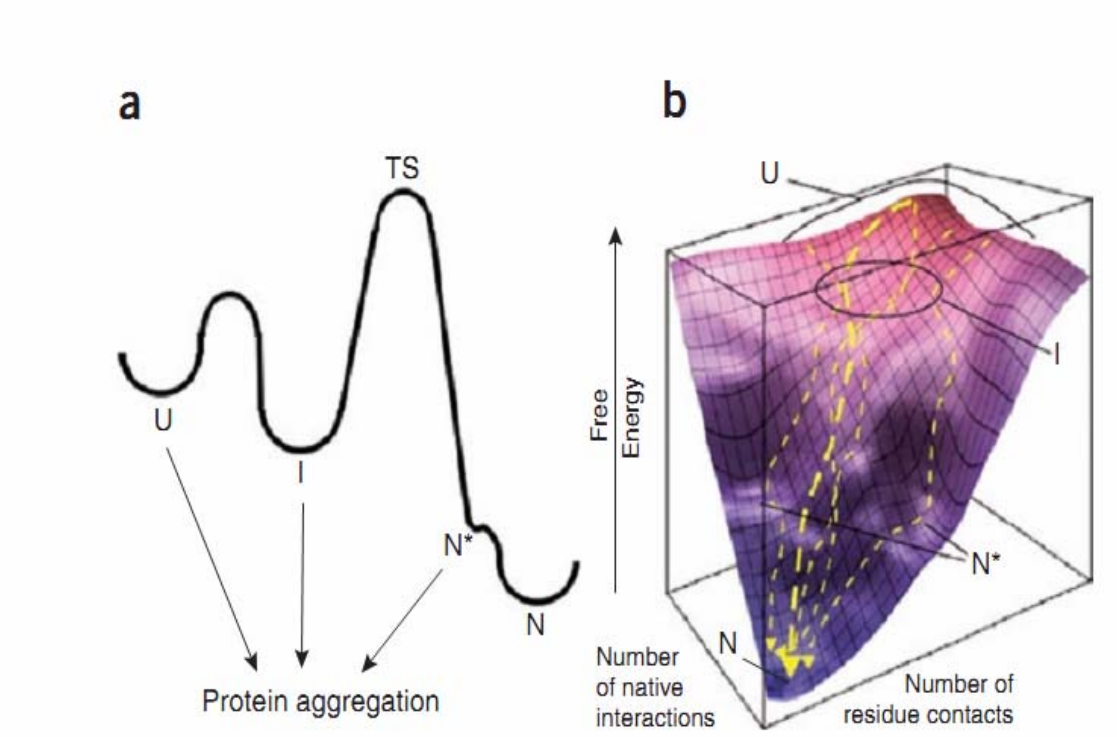

Figure 1.1.6.2: (a) Folding is shown according to classical thermodynamic and kinetic principles (b) a free energy landscape. Adopted from (Chiti et al., 2009).

From figure 1.1.6.2, it has shown that conformation changes essential for triggering the protein aggregation. The unfolded state (U), consisting of a large ensemble of unstructured conformations, can collapse to a partially folded state (I) and then fold across the major free energy barrier for folding to the native folded state (N). Both figures can be seen backward with N unfolding to form I through the major free energy barrier for unfolding. One or more locally unfolded states (N*) may attain from N due to thermal fluctuations. Such conformational changes indicate high energy states with respect to N under physiological conditions, but normally separated from N by a low energy barrier. Although it form temporarily and are rarely populated at equilibrium. Protein molecules adopting the U, I and N* states or conformations can all self-assemble and consequently trigger amyloid formation. However, under physiological conditions, N* is both thermodynamically and kinetically more readily changeable from N than are I and U. Therefore it may represent a key precursor to protein aggregation.

1.1.6.3 Changes in sequence influences amyloid formation

The polypeptide chains having different sequence can form amyloid at very different rates, either these processes occurs from fully or partially unfolded state (**Chiti et al., 2006**). The substitution in sequence affects the hydrophobicity of side chain, charge and secondary structure that influence the aggregation. It has been observed that change in sequence of amino acid affects the hydrophobicity, which may decrease or increase, playing a crucial role in aggregation (**Otzen et al., 2000, Chiti et al., 2002, Wurth et al., 2002, Campioni et al., 2010**).

Effect of charge is another key factor which influences the aggregation like higher net charge either globally or locally may hinder self association for example AcP aggregation triggered by single amino acid substitution (**Chiti et al., 2002**). The interaction of macromolecule which exhibits high compensatory charge can influence polypeptide chains aggregation (**Fernandez et al., 2004, Giasson et al., 2003**). Apart from charge and hydrophobicity, a low probability to attain α- helical structure and high probability to form β-sheet structure are also considered as important influential factor for protein aggregation (**Kollberg et al., 2001, William et al., 2004**).

1.2 Inhibition of protein aggregation

Alzheimer's disease is a distressing neurological disorder that affects more than 37 million people worldwide. The economic burden of Alzheimer's disease has been enormous; in the United States alone, the estimated direct and indirect annual cost for patient care is at least $100 billion. Current FDA approved drugs against Alzheimer's disease provide only modest symptomatic relief.

Therefore it is imperative and essential to discuss and address the different strategy which is implicated for suppression of the protein aggregation.

Ross and his coworkers worked out on some effective therapeutic strategies. Based on the scheme from figure 1.2, the therapeutic strategy against the inhibition of protein aggregation would be beneficial at early steps of aggregation, because it may suppress the formation of potentially toxic oligomers or other intermediates. However in such polymerization where linear addition occurs without formation of oligomeric intermediates would be itself considered as toxic.

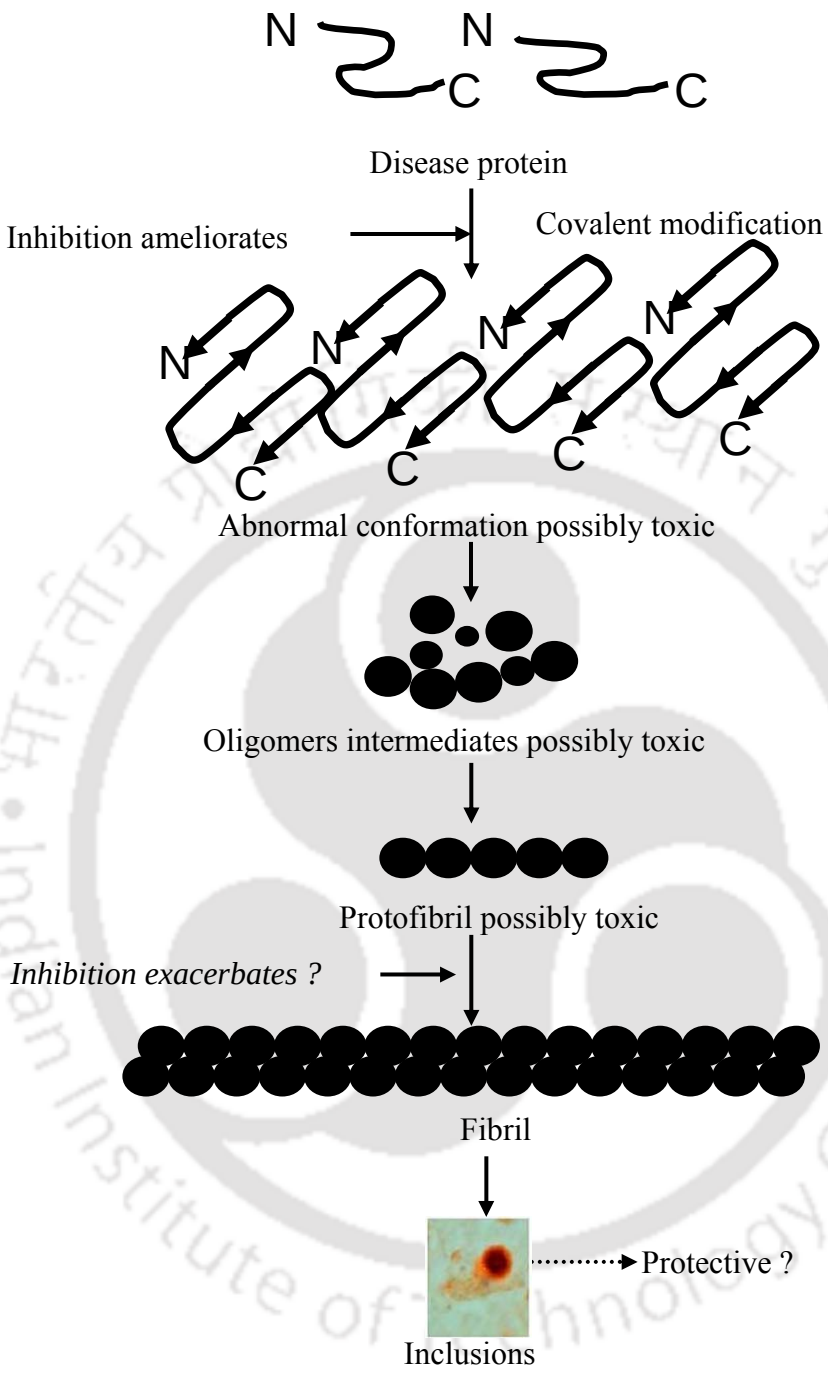

Figure 1.2: Scheme for therapeutic strategy (Ross et al., 2004).

In contrast inhibition at later stage could be disadvantageous for the reason that it may result in accumulation of toxic intermediates. Targeting intermediates steps for oligomeric inhibition can helpful for isolating the toxic species also and which would be helpful in development of better efficacy drugs molecules (**Ross et al., 2004**). Based on the schematic strategy represented by Ross and his coworkers, some small molecules characterized by Necula and group in 2006 has shown effect at step wise of aggregation process such as: a) Compounds that inhibit oligomerzation rather fibrillization for example azure C, basic blue, curcumin, Th T, indomethacin etc. b) Inhibitor for both oligomerization and fibrilization for example hemin, hematin, rhodmine B, phenol red, eosin Y etc. c) Molecules that inhibit fibrillization but not oligomerization for example apigenin, Chicagon sky blue, orange G etc (**Necula et al., 2007**). Another approach, chemical chaperones may be designed for blocking protein aggregation and including upregulation of molecular chaperones or aggregate clearance mechanisms (**Rochet, 2007; Herczenik and Gebbink, 2008**). The saccharide molecules like trehalose at very high concentration were used for suppression of polyglutamine diseases (**Tanaka et al., 2004**). Apart from this some small molecules have been developed to inhibit Aβ aggregation (**Bohrman et al., 2000, Wood et al., 1996, Reixach et al., 2000**), α-synuclein and prions (**Lee et al., 2004, May et al., 2003**). Further approach is proteolytic cleavage target like γ- secretase, β- secretase (**Citron et al., 2002, John et al., 2003**) for Aβ aggregation. Some of drug molecules are under clinical trial which targets the γ- secretase, β- secretase of Aβ. Immunotherapy, use of specific antibodies are promising strategy for inhibiting or reverse the in vitro and in vivo fibril formation by amyloidogenic proteins or peptides (**Schenk, 2002; White et al., 2003**). Recently new approach have implemented like toxicity can be substantially reduced if the hydrophobic residues are incorporated to a greater extent within the interior of the oligomeric assemblies, even in the absence of an effective change in morphology, because it was observed that solvent-exposed and structurally disorganized hydrophobic residues within small protein oligomers are associated to pathogenesis of protein misfolded human diseases and can act significantly as important molecular targets for therapeutic purpose (**Campioni et al., 2010**).

Furthermore, to reducing the toxicity of oligomers or converting into non-toxic conformers are of important approaches towards the therapeutic purpose. In this context few aromatic small molecules investigated which are applicable to remodel the aggregation steps of Aβ aggregates. These molecules categorized in three different classes such as Class I

molecules (e.g myricetin and NDGA) remodel soluble oligomers into large off pathway aggregates that are found to be non-toxic. The class II molecules converts soluble Aβ oligomers into fibrils but inactive against disintegration of fibrillar aggregates. Although Class III (e.g tannic acid, piceid molecule) disassemble soluble oligomers as well as fibril into low molecular mass species. Surprisingly these species found non toxic **(Ladiwala et al., 2011**).

Table 1.2: Selected Alzheimer's disease drug development programs, information was collected (**Rafii et al., 2009**)

Drugs	**Mecahanism of action**	**Stage of development**
Trampirosate	Direct Aβ binding to prevent Aβ aggregation	Completed phase III/ Discontinued
ACC-001	Active Aβ vaccine	Phase II (Safety, proof of concepts)
Bapineuzumab	Anti- Aβ monoclonal antibodies	Phase III (efficacy in AD)
Rember	Tau aggregation inhibitor	Entering phase III (efficacy in AD)
Tarenflurbil	γ- secretase modulator	Completed phase III/ discontinued
Semegacestat	γ- secretase inhibitor	Phase III (efficacy in AD)

1.3 Lysozyme aggregation

In 1922, Sir Alexander Fleming isolated a substance from nasal mucus of a patient suffering from common cold that could kill certain bacteria like *Micrococcus lysodeikticus* (**Fleming, 1922**). Later he coined the term of this substance 'lysozyme'. It was also found in other body fluids like tears, saliva and blood serum. Other than human tissues, egg white was identified as a rich source of lysozyme. The early work like antibacterial property of lysozyme has been

reviewed by Thompson (**Thompson, 1940**), while an account of the discovery of lysozyme is also available (**Maurois, 1963**). However after the initial euphoria in the investigation of antibacterial substances, it had evicted that lysozyme had little clinical value as an antibacterial, before discovery of penicillin. Lysozyme was used poorly, until hen egg white lysozyme was isolated, purified and crystallized succesfully. Later hen egg white lysozyme treated as model protein for studying biophysical property and folding process of proteins.

HEWL is a single polypeptide chain (14.3 kDa) of 129 amino acid residues with four intramolecular disulphide bridges **(Jolles, 1960; Jolles, 1964)** see figure 1.3 and an isoelectric point near ~11.3 (**Vasilescu et al., 1999**), having excellent solubility in aqueous medium **(Wetter and Deutsch, 1951)**. Based on enzyme properties, HEWL catalyses the hydrolysis of β (1→4) glycosidic bond between N-acetylmuramic acid and N-acetylglucosamine in peptidoglycan polysaccharide found in bacterial cell walls. The complete primary structure of HEWL was first elucidated in 1963 **(Jolles, 1963; Canfield, 1963)** and two year later in 1965, the three dimensional structure of HEWL was established, the first for an enzyme **(Blake et. al., 1965; Blake et. al., 1967; Johnson & Phillips, 1965; Phillips, 1966; Blake et. al., 1967; Phillips,1967).** The folding of this protein has been studied extensively **(Dobson et. al., 1994)**. Investigations on self-association or aggregation of HEWL became imperative when it was reported by Pepys and co-workers that point mutations in human lysozyme (with which HEWL shares 60% sequence identity,) associated with hereditary systemic amyloidosis (**Pepys et. al., 1993**). This disease was symptomatic with deposition of amyloid fibrils of human lysozyme (sometimes in kilogram quantities) in kidneys, gastrointestinal tract, lymph nodes, blood vessels, spleen and liver. Studies in vitro condition, focusing on the molecular mechanisms leading to aggregation of HEWL and human lysozyme have received a lot of attention giving rise to numerous conditions that yield amyloid fibrils by different pathways (**Trexler & Nilsson, 2007**).

A

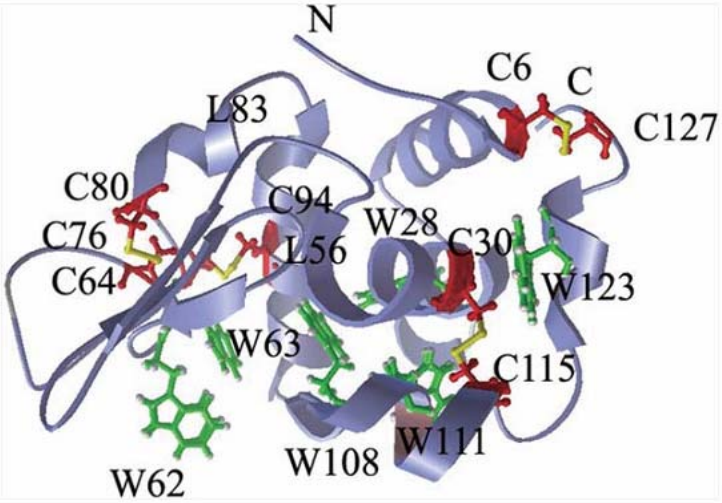

Figure 1.3: Structure of hen egg white lysozyme from PDB files 1HEW. It contains six tryptophan (Trp) residues marked with green color and eight cysteine (Cys) residues (red color) forming four native disulfide bonds (yellow color), that is, Cys6-Cys127, Cys30-Cys115, Cys64-Cys80, and Cys76-Cys94, respectively. There are six hydrophobic clusters with the maximal hydrophobicity around the residues cysteine 6, tryptophan 28, leucine 56, leucine 83, tryptophan 108, and tryptophan 123, respectively.

1.3.1 Aggregation of hen lysozyme in vitro

Tertiary structure, protein folding mechanism and functions of hen lysozyme are almost identical from human lysozyme. Due to inexpensively available, smaller size, excellent solubility in aqueous medium, stability and pI 11.35 (**Vasilescu et al., 1999**), HEWL can serve as a model protein to investigate protein aggregation in the context of developing a detailed understanding of lysozyme amyloidosis. Different conditions have been established

over the years where hen lysozyme likly to aggregates. Here some of conditions among these are discussed below:

1.3.1.1 Using alkaline pH

In 1961, Sophianopoulos and Van Holde were investigated first time of reversible association of hen egg white lysozyme (1 mM with 0.15 M KCl) in alkaline pH from equilibrium sedimentation data (**Sophianopoulos & Van Holde, 1961**). They observed monomer-dimer equilibrium between pH 5.4 and 10. The same group had earlier shown that the protein is monodisperse at pH 5.4 (**Van Holde & Baldwin, 1958**). More detailed investigations by these group showed that dimer population of lysozyme was quite prominent with increase in pH between 5 and 9 (see Fig. 1.3.1.1). They hypothesize that dimerization is favored when two monomers have each lost a proton from a group with a pKa of 6.2 (**Sophianopoulos & Van Holde, 1964**). This ionisable group was later identified as carboxylate from Glu 35 in the active site (**Sophianopoulos, 1969)**. Moreover, at above pH 10, a steep increase in molecular weight was noticeable indicating formation of higher order oligomers, However it was not investigated further by them. They mention that exposure of lysozyme above pH 11 likely to form amorphous precipitates (Sophianopoulos & Van Holde, 1964). However, it must be noted that the lysozyme concentrations were used by them near 1 mM. Obviously the formation of precipitates above pH 11 is not surprising because the isoelectric pH of HEWL was found 11.35 and protein concentration of 1 mM is higher, which could make easier to precipitates. Our group has initiated investigations of HEWL oligomerisation at pH 12.2, which is slightly above its isoelectric point (pI). Initial studies employing fluorescence anisotropy of covalently labelled dansyl probe showed that aggregation of HEWL at pH 12.2 proceeds spontaneously at room temperature (25 ^{o}C). The aggregation process follow by absence of a lag phase as concentration of the protein is varied between 4 and 200 μM. The dependence of the steady state anisotropy value on HEWL concentration reveals that probably size of aggregates formed are dependent on initial monomer concentration.

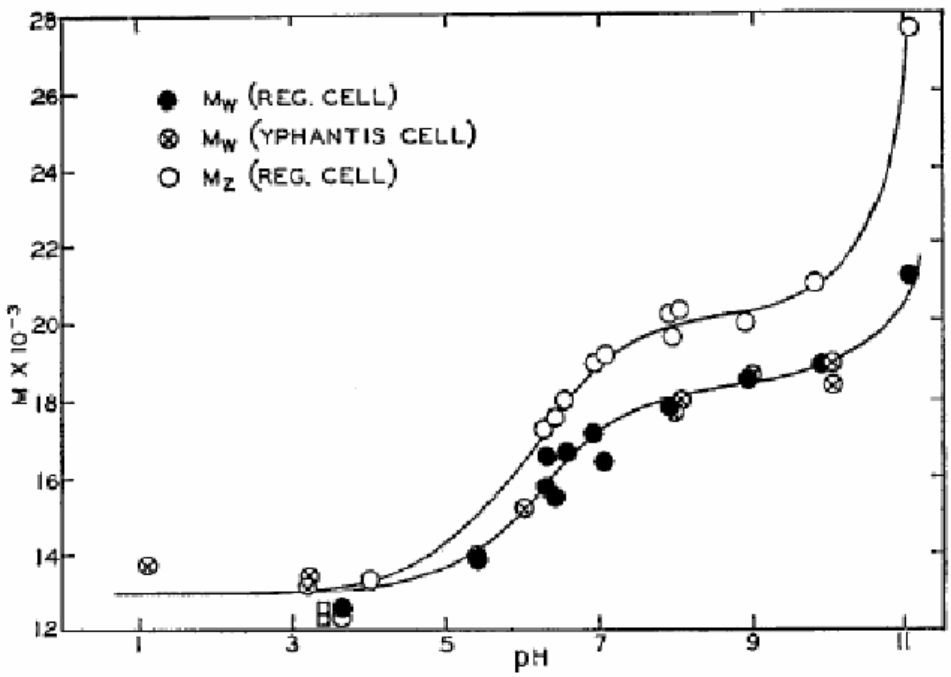

Figure 1.3.1.1: Change in apparent molecular weight against pH at 20°C. Protein concentration is 1.4 g per 100 ml, in 0.15 M KCl. M_W and M_Z denote the weight average and z-average molecular weights from sedimentation equilibrium experiment. Adapted from (Sophianopoulos & Van Holde, 1964).

Time-resolved fluorescence anisotropy decay analysis revealed a heterogeneous population of aggregates at 60 minutes after incubation in alkaline pH with a fast 1.4 ns rotational component suggesting significant freedom for local segmental motion of dansyl probe. With progress in time, this component rises to 5.3 ns at 100 minutes indicating loss of rotational freedom owing to dense molecular packing inside the aggregate, slowing segmental motion. After overnight incubation (~20 hours) in alkaline pH, this value settles down to 3.5 ns hinting at hindered rotational motion in the aggregate (**Homchaudhuri et. al, 2006**). Other than aggregation, Hameed and co-workers have found significant decrease in mean residue ellipticity, that confirms HEWL undergoes a structural transition like a molten globule between pH 11 and 13.5, having a midpoint near pH 12.8 (**Hameed et. al., 2007**). Some HEWL aggregation was reported at pH 9.2 in presence of SDS also (**Moosavi-Movahedi et. al., 2007; Jain et. al., 2011**). As previously has been already demonstrated that HEWL can dimerize at alkaline pH in absence of SDS (**Sophianopoulos & Van Holde, 1961**),

conversely anionic detergents like SDS are likely to bind to positively charged surfaces of HEWL and enhance amyloid formation by minimizing electrostatic repulsions (**Moosavi-Movahedi et. al., 2007**). Subsequently, HEWL in presence of 20% t-butanol at pH 12.75, an enormous increase in thioflavin T fluorescence intensity and large increase in hydrodynamic radius was observed in which suggests possibility of amyloid like fibrils (**Hameed et al., 2009**). Apart from the alkaline pH lysozyme has a propensity to aggregates at several conditions like acidic pH, higher temperature, different solvent, different additives, some physical treatment like UV etc. It is imperative and useful to acquire detail information in this regard (**Swaminathan et al., 2011**).

1.3.1.2 Using acidic pH

In 2000, Krebs and co-workers (**Krebs et. al., 2000**) reported formation of amyloid fibrils from full length HEWL, its peptide (49-64) from β-sheet region and a mutant peptide (I55T) of same region. They have performed experiment using several conditions like elevated temperatures (37 and 65 ^{o}C), rapid heating and cooling followed by incubation at 37 ^{o}C, incubation at low pH (2.0 and 4.0) and pH 7.4 subsequent to addition of trifluoroethanol. They found at all the above conditions are suitable for fibrils formation, however the fastest rate of formation was observed with pH 2.0 followed by incubation at 65^{o}C. Interestingly, the conditions required for forming fibrils from peptide above were relatively milder compared to intact HEWL protein. It was also shown that fibril formation is accelerated by addition of small aliquots of solution containing pre-formed fibrils (seeding). HEWL fibril formation at pH 1.6 and 65 ^{o}C has been investigated in detail by Mishra and co-workers who suggested fragmentation of 49-101 peptides from full length protein is essential for efficient amyloid fibril formation (**Mishra et. al., 2007**). Mature amyloid fibrils of HEWL are formed after nicked HEWL through a fibril shaving process resulting in fibrils composed of 49-101 or 53-101 fragments. It was also shown that substituting intact HEWL in place of nicked HEWL can slow down fibril formation owing to presence of non-amyloidogenic regions, which act like molecular accelerates. The aggregation pathway of HEWL under acidic conditions has been proposed as follows: amyloid monomers likely to associate into small oligomers of similar size, without a nucleation barrier. The protofibril nucleation begins after population of oligomers reaches a critical threshold concentration. Mishra and his coworkers has define the critical concentration >50 μM for HEWL aggregation at acidic pH 1.6 and 65 ^{o}C also and

for this confirmation they were done concentration dependent 50, 100, 200, 500 μM fibril formation kinetics (**Mishra et al., 2007)**. By Hill and coworker's fibril elongation and it maturity discusses similarly like protofibrils grow as polymers of oligomers, with oligomers adding to the ends of protofibrils. After reaching a contour length of few hundred nanometers, protofibrils apparently self-assemble into much longer and stiffer mature fibrils (**Hill et. al., 2009**). Interestingly, in presence of 5% ethanol solution at pH 2 and 57 °C has been shown to form amyloid fibrils in 25 out of 38 proteins studied (**Aso et. al., 2007**). Three more proteins could be added to this list if 5% trifluoroethanol is employed instead of ethanol, making it 28/38 which implies that acidic pH and elevated temperature is closest to a universal condition to induce amyloid formation. Huang and cowrker suggested that in presence of lower SDS concentration ranging (0.06-0.1 mM) HEWL shows propensity of amyloid aggregates in acidic pH 2.0 (**Huang et al., 2010**).

1.3.1.3 Using ethanol

In the same year, Krebs and co-workers reported formation of HEWL fibrils at acidic pH, however Goda and co-workers showed formation of amyloid protofilament and fibrils with HEWL in presence of 90% ethanol. They proposed that HEWL in ethanol solution shows an increase in helical and sheet content, followed by partial loss of helices and tertiary structure and later β-sheets interact each other to form amyloid protofilaments (**Goda et. al., 2000***)*. Further, in more detail of amyloid fibril formation in presence of ethanol was identified from Fujiwara's group. They have extensively characterized the various structural states of HEWL (2-9 mg/ml) in presence of 0-90% ethanol using small angle X-ray and neutron scattering along with far UV CD (**Yonezawa et. al, 2002**). They proposed an elegant phase diagram to account for fibril formation in presence of different concentrations of ethanol and HEWL. In their mechanism for amyloid fibril formation they proposed that formation of dimers accompanied by large increase in β-sheet structure, and these dimers act as nuclei for protofilaments via a nucleation-dependent polymerisation, further steps followed like protofilaments laterally associates to form amyloid fibrils. In a later study, the same group has suggested a role for electrostatic interactions in fibril formation from protofilaments in 90% ethanol solutions based on dependence with NaCl concentrations (**Fujiwara et. al., 2003**). However, the role of salt has been reported later (**Holley et. al., 2008**), when it was shown that HEWL forms fibrils in 80% ethanol at 22 ºC with agitation in complete absence

of ions. Here a distinct lag phase of seven days followed by a slow growth phase of another seven days is observed.

1.3.1.4 Using guanidine hydrochloride

In a fascinating work, Vernaglia and co-workers have reported that HEWL can be induced to form amyloid fibrils within hours, with moderate concentrations (2-5 M) of GdnCl. At lower concentrations (0-1 M), the protein is not partially unfolded to trigger fibrils formation, while at higher GdnCl concentrations (5-6 M), the protein is fully denatured and fibrils may be disrupted while formation by GdnCl (**Vernaglia et. al, 2004**). It is surprising to observe that the lag phase, and rate of fibril formation depend on GdnCl concentration confirmed using ThT assay. It was strongly believed that partially folded state triggers the formation of fibrils.

1.3.1.5 Using other conditions

Cao and his coworkers studied amyloid aggregation using fully reduced hen egg white lysozyme (HEWL), which is a good model of random coil structure. Their findings suggest that in presence of 90% (v/v) ethanol, the fully reduced HEWL adopts β-sheet secondary structure at pH 4.5 and 5.0, and an α-to-β-transition is observed at pH 4.0. The pH dependence of the initial structure of the fully reduced HEWL in the presence of 90% (v/v) ethanol suggests that Asp and His residues may play an important role for inducing amyloid like structure. (**Cao et al., 2003**). Niraula and co-workers used a zero cysteine (0SS) mutant (Cys-6 replaced by Ser, other seven Cys replaced by Ala) of HEWL and observed formation of amyloid fibrils on incubation in pH 2.0-2.7, 4.0 and 7.5 at 25 ^{o}C from weeks to months (**Niraula et. al., 2004**). They conclude that an unfolded state of HEWL can also form amyloid fibrils failing partially folded state. However the UV treatment based disulfide bond destabilization disrupt the native structure which participates in formation of amorphous aggregates (**Xie et al., 2011)** In 2007, Sasahara and co-workers demonstrated that HEWL can form amyloid fibrils treating with a combination of mechanical agitation (310 rpm), heating using differential scanning calorimetry, high salt (1 M NaCl) at pH 2-6 for 24 hours (**Sasahara et. al., 2007**). Recently it has been found that HEWL can form amyloid fibrils in acidic protic ionic liquids (hydrated ammonium bisulphate) when heated to 60 ^{o}C (**Byrne et al., 2009**). It is important to know from their work that HEWL amyloid fibrils formed using ethanol or acidic pH can be completely dissolved in anhydrous protic ionic liquids like ethyl

ammonium nitrate (EAN). Further, enzymatic assays demonstrated that fibrils formed using ethanol could be redissolved in EAN recovering around ~72% activity. Based on the recovery of significant activity they have suggested that fibrilization could recommend an approach for long term strorage of proteins. It has also found that lysozyme is capable to form globular aggregates as well fibrillar aggregates at physiological pH with interaction of gold nanoparticle (**Zhang et al., 2009**).

1.3.2 Inhibition of lysozyme aggregation

Inhibition of protein aggregation and their deposition in different tissues is essential for therapeutic intervention against different protein misfolding diseases (PMDs), (**Sacchettini & Kelly, 2002; Ross & Poirier, 2004**). Since protein aggregation is a multi-steps process followed by multiple intermediate species, it is difficult to identify a single step or species where potential drugs targets could be used to stop protein aggregation and pathogenicity associated with it. Currently, main approaches against protein misfolding disorders discussed above, although there is no effective cure against PMDs including systemic amyloidosis, there are several approaches explored to reduce the extent of aggregated protein in vitro or in vivo (**Rochet, 2007; Herczenik & Gebbink, 2008**). As it has been known that amyloid fibril formation is generally driven by hydrophobic interactions which are further stabilized by hydrogen bonds forming inter and intramolecular β-sheets of the fibril core. Small molecule compounds are preferred drug candidates as they are small enough to enter inside the fibril structure to destabilize both the hydrogen bonds forming β-sheet of fibril core and hydrophobic interactions among amino acid side chains (**Vieira et al., 2006; Rochet 2007**). Small aromatic compounds, 4-aminophenol (4AP) and 2-amino-4-chlorophenol (2A4CP) inhibit aggregation and disrupt the preformed fibrils from human and hen lysozyme at micromolar concentrations (**Vieira et al., 2006**) although, exact inhibitory mechanism of these molecules are not known. Uses of specific antibodies are promising strategy for inhibiting or reversing the in vitro and in vivo fibril formation by amyloidogenic proteins or peptides (**Schenk, 2002; White et al., 2003**). Using antibody mediated inhibitory approach for protein aggregation; it was shown that a camelid antibody fragment which was raised against wild-type human lysozyme inhibits in vitro aggregation of its amyloidogenic variant, I56T and D67H lysozyme (**Dumoulin et al., 2003; 2005**). Employing chaperone mediated inhibition, Dobson and co-workers demonstrated that clusterin, a ~61 kDa glycoprotein

significantly inhibits aggregation of human lysozyme even at very low concentration (**Kumita et al., 2007**). They proposed that human chaperone, clusterin, binds with oligomeric form of protein but not with native or fibrillar form of protein. With the fact that clusterin is present throughout the human body, it will be really interesting to know the interaction of clusterin with lysozyme which may be used as a therapeutic agent against systemic amyloidosis. With the recent finding it is believed that oligomeric form of protein or pre-fibrillar aggregates are pathogenic in nature, it is crucial to target these species to fight against protein misfolding diseases (**Haass & Selkoe, 2007**). Using oligomer-specific antibody they were observed that oligomers of human lysozyme and other structurally distinct proteins can be detected and their cytotoxicity can be neutralized. On the basis of this observation authors proposed that soluble oligomers form different proteins may have a common structure and they may have common mechanism of pathogenesis (**Kayed et al., 2003**). Protein aggregation is a generic property of polypeptide chains, such that almost all peptides or proteins undergo to self-associate in vitro under appropriate conditions (**Chiti & Dobson, 2006**). Since amyloid fibrils and pre-fibrillar aggregates from non-disease related proteins exhibit similar morphological features and cytotoxicity as observed for disease associated proteins (**Vieira et al., 2007, Bucciantini et al., 2002**) understanding the aggregation mechanism of non-disease associated proteins like HEWL shall help in finding inhibition approaches against systemic amyloidosis and other PMDs. Retarded growth of HEWL aggregates and disaggregation of pre-formed fibrils by different indole derivative was observed at acidic pH (**Morshedi et al., 2007**). It is suggested that binding of indole derivatives with native protein hampers the formation of fibrils while interaction of indole ring with hydrophobic residues helps in disaggregating the pre-formed fibrils. Inhibitory effect of p-benzoquinone and endogenous neurohormone melatonin is also observed against HEWL amyloid formation at acidic pH (**Wang et al., 2006**). Although both compounds suppress lysozyme fibrillization in a concentration dependent manner, p- benzoquinone was found to be more potent inhibitor than melatonin. Comparing the effectiveness of rifampicin and its structural analogue p-benzoquinone against HEWL aggregation, rifampicin is found to be better inhibitor than and p-benzoquinone. Both compounds inhibit formation of β-sheet structure and also reduce the exposure of hydrophobic patches which drives HEWL aggregation (**Lieu et al., 2007**). Eight types of tea Catechins which is polyphenol induce the conversion of preformed hen lysozyme amyloid fibrils to amorphous aggregates (**He et al.,**

2009). The ThT fluorescence assay indicated that the β-sheet content of lysozyme fibrils reduced upon catechin binding. As a result, the hemolytic effect of the fibrils on RBC was attenuated. Both antioxidative potency and hydrophobicity of tea catechins were positively related to the fibril-disruptive activity. Ascorbic acid, R-tocopherol, and phenol did not demonstrate any effect on lysozyme fibril. This fiding may be utilized for the design of novel antiamyloidogenic drugs with a polyphenolic structure. Interestingly, Catechins with a gallic ester bond represented high efficiency in converting lysozyme fibrils to amorphous aggregates. The heterocyclic structure acridine based compounds were identified as potent inhibitors of prion protein (**Korth et al., 2001; May et al., 2003**). Different planar acridine derivatives molecules effectively inhibit lysozyme aggregation (IC50 = 6.5-10 μM) by intercalating between the exposed hydrophobic residues which blocks the interaction between two adjacent β-sheets (**Gazova et al., 2008**). L-Arginine, a basic amino acid which is well known additives being used in the purpose of refolding of recombinant proteins from inclusion bodies (**Arora & Khanna, 1996; Umetsu et al., 2005**). Although the exact mechanism of arginine during refolding is still unknown, it is proposed ball park estimate that it increases surface tension of water and favourably interacts with most amino acids side chains and peptide bonds (**Arakawa et al., 2007**). Moreover, the poor binding of arginine with protein surface is a critical factor in suppressing aggregation (**Arakawa et al., 2007; Arakawa & Tsumoto, 2003**). It was shown that in presence of 0.75 M to 1.0 M, L-arginine, nearly 95% active protein was recovered from denatured lysozyme (**Hevehan & Clark, 1997**). It has also reported that L-arginine also suppress lysozyme aggregation and increase oxidative refolding of protein with concentration upto 1.0 M (**Reddy et al., 2005**). In another hypothesis of inhibiting lysozyme aggregation by arginine, it was proposed that arginine inhibits aggregation by slowing protein–protein association reactions. Preferentially it was excluded from protein–protein encounter complexes, but not from dissociated protein molecules (**Baynes et al., 2005**). Homchaudhuri and coworker have shown that arginine is also potent to inhibiting lysozyme aggregation induced at pH 12.2. This work was demonstrated using time-resolved fluorescence anisotropy of covalently tagged dansyl probe. They have shown that in presence of 0.9 M arginine, the dansyl segmental motion of HEWL-dansyl conjugates was similar to that in absence of arginine at early times, however after nearly two hours this rotational component was significantly faster (3.3-1.9 ns) in comparison to that in absence of arginine (5.3-3.5 ns). The global rotational motion was also

significantly faster (13 ns) in presence of arginine compared to that in its absence (43 ns) at later times. This clearly indicated that arginine inhibits formation of higher oligomers at later times, retaining protein as loosely packed unfolded small oligomer (**Homchaudhuri et. al, 2006**). Recently it was found that arginine controls the heat induced aggregation at isoelectirc point of HEWL (**Tomita et al., 2011**). Apart from small molecules surfactants have also been used as artificial chaperones to assist the refolding of denatured protein and improve the yields of recombinant protein (**Rozema & Gellman, 1996**). Ampiphillic surfactants can inhibit Aβ (1–40) amyloid fibril formation at physiological pH (**Wang et al., 2005**). It was also investigated that where ionic surfactants like sodium dodecyl sulfate (SDS) and cetyltrimethylammonium bromide (CTAB) protect rhodanese, (a mitochondrial enzyme) against thermal aggregation (**Bhattacharyya & Das, 1999**). Recently, it was shown that SDS at concentrations above 0.25 mM suppresses HEWL fibril formation at pH 2, while at lower SDS concentrations (0-0.1 mM), the SDS-HEWL ensemble is fibrillogenic and rich in β-sheet conformation (**Hung et. al., 2010**). It has been considered that intramolecular disulphide bonds in HEWL are essential to retain its structural fold and catalytic activity. However improper disulphide bond formation leads to protein aggregation and fibrillization (**Furukawa et al., 2006**) which can be reduced or suppressed in presence of reducing agent like dithiothreitol (DTT) or cysteine (**Yamamoto et al., 2008**). To inhibit lysozyme aggregation, reduction of HEWL fibrillization with 2 mM DTT was observed by Wang and co-workers. They also observed that inhibitory effect of DTT was possible only if it was added within ~8 days of incubation (**Wang et al., 2010**). From another group, Wang and co-workers also demonstrated that thiol-free compound tris(2-carboxyethyl) phosphine (TCEP) halt HEWL fibrillization through disulfide bond disruption and preventing the α helix-to-β sheet transition of protein at acidic pH (**Wang et al., 2009b**). Stabilizing the native state of protein is another approach against misfolding and aggregation, since it may increase the activation energy barrier, thus slowing the aggregation kinetics and moving away from amyloidgenic state (**Hammarstrom et al., 2003**).

Inhibition of HEWL dimerization at alkaline pH was first observed by Sophianopoulos where different glucose derivatives (NAG and its disaccharide and trisaccharide derivatives) displayed different degrees of inhibition against lysozyme aggregation (**Sophianopoulos, 1969**). The order of their effectiveness against HEWL dimerization was also observed such as, trisaccharide>disaccharide>monosaccharide although, effect of these compounds on fibril

formation was not studied. Besides above mentioned strategies, there are several other approaches where self-assembly of HEWL was inhibited in different experimental conditions.

With Contradiction of several reports, where crowding agents favours aggregation, Liang and co-workers have shown that HEWL amyloid formation can not only be inhibited even significant amount of activity can be recovered at acidic pH by crowding the medium with BSA (100 g/l) either alone or mixed with Ficoll 70 (**Zhou et al., 2008**). Different chemical modifications of lysine residues in lysozyme have influence on amyloid formation in different manner. For example acetylation of the lysine residues promote amyloid formation, while citraconylation (introduction of citraconyl groups to free lysine groups, in order to change their charge at neutral pH from positive to negative and make the adjacent peptide bond resistant to hydrolysis by trypsin) was found to inhibit HEWL aggregation at acidic pH (**Morshedi et al., 2010**).

New reports suggest that nanoparticle have also promising inhibitory effect against the protein misfolding and protein aggregation as for example magnetic nanoparticles of Fe3O4 (with mean hydrodynamic diameter of 26 nm), it was shown that amyloid formation of HEWL can not only be inhibited but it can be reversed or disaggregated in concentration dependent manner (**Bellova et al., 2010**). It was observed that IC50 (ability to inhibit formation of amyloids) of Fe3O4 was 0.654 mg ml^{-1} while DC50 (ability to destroy pre-formed aggregates) was 0.163 mg ml^{-1}.

1.3.3 Motivation and objectives of this work

This thesis deals with the investigations of hen lysozyme aggregation and its inhibition employing various additives and applying strategies in pH 12.2 at room temperature. Motivation to work on this system was, this is a poorly understood aggregation process, particularly fibril formation and its suppression, characterization of ensemble size of intermediate product and its control. Except few, all such investigation has been reported in acidic pH at higher temperature (60-80 °C), requiring longer incubation time to convert into final products like fibrils, thereby making aggregates to form forcefully owing to large positive charge. In spite of, these conditions have own advantages. However, the system like pH 12.2 used for aggregation condition, where HEWL spontaneously aggregate at room temperature owing to near pI 11.3, close to pI it bears low net charge and act as driving force to initiate aggregation. Approaching this system, it can be used as model system for studying the inhibition of hen lysozyme, because hen lysozyme has been used in food industries to preserve fresh fruits and vegetables, tofu bean curd, seafood's, meats and sausages, potato salad, cooked burdock with soy sauce, and varieties of semi-hard cheeses such as Edam, Gouda and some Italian cheeses, hen lysozyme added also to infant feeding formula making properties more resemble like human milk (**Cunningham et al., 1991**). Apart from this, it can use as model system for studying inhibition of human lysozyme aggregation which is responsible for systemic amyloid deposits. New application of this aggregation system can be for making protein nano particles, which can acts like carrier for drug delivery system.

Based on these motivations objective of this work is as follows:

1. Characterization of size and morphology of hen lysozyme aggregates in alkaline pH 12.2.
2. To develop effective strategies for blocking of hen lysozyme aggregation at alkaline pH 12.2.
3. To probe the effect of monomer concentration on hen lysozyme aggregation kinetics and its size in alkaline pH 12.2.

Experimental materials, techniques and conditions

2.1 Materials used

There different kinds of chemicals and materials used to carry out the work, as follows:

Hen egg white lysozyme (HEWL, L6876/L7651) and NATA (N-Acetyl-L-tryptophanamide) were procured from Sigma-Aldrich Chemicals Pvt. Ltd., India. Thioflavin T, ANS (8-anilino-1-naphthalene sulfonic acid ammonium salt), DTNP (2,2'-dithiobis(5-nitropyridine)), DTT (Dithiothreitol), L-Cysteine, Iodoacetamide (I1149), *N,N′,N″*-Triacetylchitotriose, N-Acetyl-D-glucosamine (NAG), Sephadex G-50, Blue dextran, and gel filtration molecular weight marker kit cat, No. MWGF 200-1KT fractionation range 12000-200000 kDa from Sigma–Aldrich Chemicals Pvt.Ltd., India. Dansyl chloride (2-dimethyl aminonaphthalene-6-sulfonyl chloride, D-23) and Dabcyl SE (4-((4-(dimethylamino) phenyl) azo) benzoic acid, succinimidyl ester, D-2245) were purchased from Invitrogen, Molecular Probes™, USA. PD-10 desalting column purchased from GE Health care Pvt. Ltd. India, SDS, and CTAB was purchased from Amresco (Solon, Ohio, USA) and all other chemicals used analytical grade. Sodium dihydrogen phosphate dihydrate, potassium iodide, sodium bicarbonate and sodium thiosulphate ($Na_2S_2O_3$) were purchased from Merck Limited, Mumbai. The solvents like DMSO, DMF were purchased from Merck Limited, Mumbai. For UV-Visible absorbance and fluorescence measurement, quartz cuvettes with 1 cm path length purchased from HELLMA. AFM Cantilevers PPP-NCL-50 (Point probe Plus/ Non- contact/ Long cantilever, part 65-262P) was purchased from Molecular Imaging™, USA. Muscovite mica, V-1 quality was purchased from Electron Microscopy Sciences, USA.

2.2 Methods

2.2.1 Stock solutions

To investigate the hen lysozyme aggregation, concentration of stock solution of HEWL was measured using UV specrophotometric method. It is well known that lysozyme contains aromatic amino acids that absorb UV light at 280 nm. The concentration of HEWL stock solution (10 mg/ml) made in deionised water was verified using extinction coefficient 38,400 $M^{-1}cm^{-1}$ at 280 nm.

To investigate the effects of additive on aggregation, various additives were used such as surfactant (SDS, CTAB) and DTT. These additives 14 mM SDS, 3 mM CTAB and 20 mM DTT were prepared in sodium dihydrogen phosphate buffer, pH 12.2 from their respective stock solution. Samples containing DTT were kept sealed to prevent air oxidation.

For characterization of HEWL aggregates after prior incubation with chitotriose and NAG, the 50mM chitotriose and 250 mM NAG stock solution was prepared in deionised water (MilliQ).

For the free -SH estimation, stock solution of 60 mM L-Cysteine was prepared in deionised water (MilliQ) and 32 mM DTNP was prepared in DMSO, It was vortexed vigorously for complete dissolution, and Stock solution of DTNP was made freshly for every analysis.

2.2.2 Sample preparation for aggregation and control

A different kind of buffer was used to carry out the work as follows: 50 mM Sodium dihydrogen phosphate pH 7.0 for control and pH 12.2 for aggregation study, was prepared in deionised water (MilliQ). For dye labeling 100 mM sodium bicarbonate pH 9 and pH 8.3 was prepared in deionised water (MilliQ).

(A) Sample for aggregation: Diluting from stock solution (10 mg/ml), 120 µM HEWL sample was prepared in 50 mM phosphate buffer pH 12.2 and it was kept for aggregation at room temperature (25-28 °C). Precipitation was not seen while incubation at 25-28 °C for [HEWL < 200µM]. Control sample 120 µM HEWL was prepared in 50 mM phosphate buffer pH 7.0, kept at room temperature (25-28 °C). The sample for 0.3 µM and 0.03 µM (300 &30 nM) was prepared by serial dilution from stock solution.

(B) Sample in presence of surfactants (SDS, CTAB) and DTT: Separately 14 mM SDS and 20 mM DTT from their respective stock solution (stock solution in 50 mM phosphate buffer pH 12.2) were added in 120 µM HEWL, desired volume was maintained from pH 12.2 buffer, whereas for 3 mM CTAB from stock solution (stock solution in 50 mM phosphate buffer pH 12.2) added in 80 µM HEWL sample instead of 120 µM HEWL concentration. At 120µM concentration precipitation was observed in CTAB containing sample. Samples containing

DTT were kept under sealed to prevent air oxidation. All experiments were performed using various biophysical techniques at 25-28 ºC.

(C) Sample in presence of chitotriose: 50 mM chitotriose stock solution was prepared in deionised water (MilliQ), immediately before starting the over night incubation in 10 mM pH 7.3 phosphate buffer. Next 5 mM chitotriose was added in 300 µM HEWL with rest of the volume maintained with 10 mM phosphate buffer pH 7.3. This sample was kept at room temperature overnight. Later it was diluted to 100 µM HEWL containing >1.5 mM chitotriose (from over night incubated sample) in pH 12.2 buffer, and kept for incubation to observe the effect on aggregation.

(D) Sample in presence of NAG: Stock solution of 250 mM NAG was prepared in deionised water (MilliQ), immediately before starting the over night incubation in 10 mM pH 7.3 phosphate buffer. Next 25 mM NAG was added in 300 µM HEWL with rest of the volume maintained with 10 mM phosphate buffer pH 7.3. After making the sample it was kept at room temperature overnight. Later it was diluted to 100 µM HEWL containing >7.5 mM NAG (from over night incubated sample) in pH 12.2 buffer, and kept for incubation to observe the effect on aggregation.

2.2.3 *Labeling HEWL with dansyl and dabcyl probes*

HEWL was covalently labeled with dansyl chloride following the protocol recommended by Molecular Probes with minor modification as reported previously (**Homchaudhuri et al., 2006**). HEWL was labeled with dansyl chloride follows:

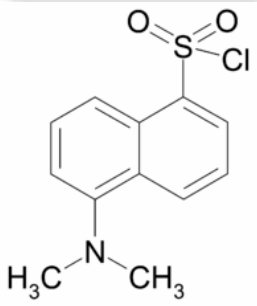

(2-dimethyl aminonaphthalene-6-sulfonyl chloride)

Step 1: HEWL (12 mg) was dissolved in 1 ml of freshly prapred 100 mM sodium bicarbonate pH 9.0 buffer in a glass vial. Dansyl chloride (2-6 mg) was carefully dissolved in 100 µL of DMF in eppendroff tube. Dye stock solution wrapped with aluminium foil and direct light was avoided.

Step 2**:** Dissolved HEWL was stirred using rice magetic beads and 100 µL dansyl chloride added slowly. For the complete reaction sample was stirred continuously for 3 hrs at 4 °C in cold room.

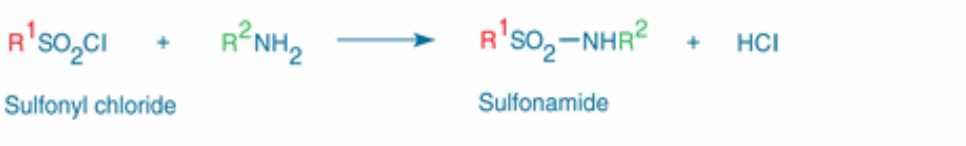

.

Reaction scheme 1: Adopted from Molecular Probes catalog for sulfonyl choride dye with HEWL.

Step 3: After completing the reaction, conjugated HEWL-dansyl was separated using PD10 column. (A) Before eluting the labeled sample, column was equilibrated with 25 ml of 50 mM phosphate pH 7.0 buffer. (B) Then labeled sample was diluted adding 1.5 ml of sodium bicarbonate pH 9.0 buffer, and final volume was 2.6 ml of labeled sample. (C) The 2.6 ml sample was added to column and the flow through was discarded. (D) After the discarding the flow through, 3.5 ml phosphate pH 7.0 buffer was added. (E) Finally four fraction of 1 ml each was collected and it was stored at 4 °C.

Step 4: The HEWL, dansyl concentrations were estimated by measuring the absorbance at 280 nm (ε = 38,400 M^{-1} cm^{-1}), 380 nm (16,000 $M^{-1}cm^{-1}$) The protein to dye labeling ratio in the conjugate were consistently between 2-3.

For labeling HEWL with dabcyl, the protocol suggested by Molecular Probes was followed

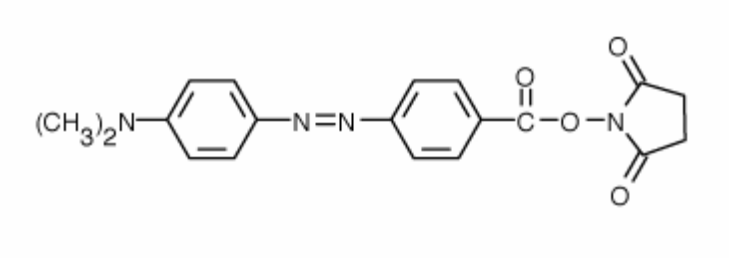

(4-((4-(dimethylamino) phenyl) azo) benzoic acid, succinimidyl ester)

Step 1: HEWL (16 mg) was dissolved in 1 ml of freshly prepared 100 mM sodium bicarbonate pH 8.3 buffer in a glass vial. Dabcyl succimidyl ester (2 mg) was carefully dissolved in 100 µL of DMF in eppendroff tube. Dye stock solution wrapped with aluminium foil and direct light was avoided.

Step 2: Dissolved HEWL was stirred using rice magetic beads and 100 µL dabcyl succinimidyl ester added slowly. For the complete reaction sample continuously was stirred for 2.5 hrs at room temperature.

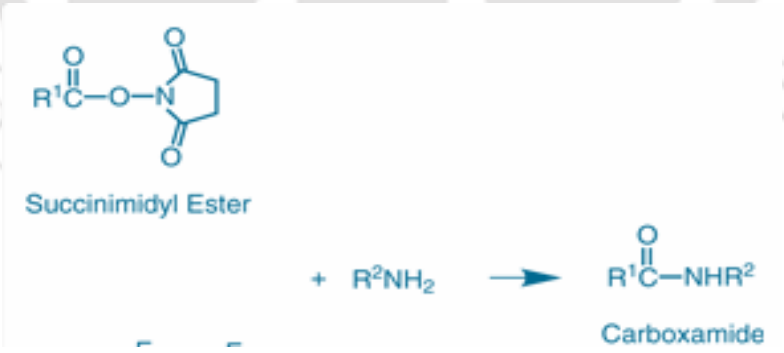

Reaction scheme2: Adopted from molecular probe catalog for succinimidyl ester dye with HEWL.

Step 3: After completing the reaction, conjugated HEWL-dabcyl was separated using PD10 column (Sephadex™ G-25 Medium for group separation of high (M_r > 5000) from low molecular weight substances (M_r < 1000) by desalting and buffer exchange). (A) Before eluting the labeled sample, column was equilibrated with 25 mL of 50 mM phosphate pH 7.0

buffer. (B) Then labeled sample was diluted adding 1.5 ml of sodium bicarbonate pH 8.3 buffer, and final volume was found 2.6 ml of labeled sample. (C) The 2.6 ml sample was added to column and the flow through was discarded. (D) After the discarding the flow through 3.5 ml phosphate pH 7.0 buffer was added. (E) Finally four fraction of each `1 ml were collected and it was stored at 4 °C.

Step 4: The HEWL, dabcyl concentrations were estimated by measuring the absorbance at 280 nm (ε = 38,400 M^{-1} cm^{-1}), and 453 nm (32,000 $M^{-1}cm^{-1}$), respectively. The protein to dye labeling ratio in the conjugate were found consistently 2-3.

2.3 Fluorescence measurements

Fluorescence spectroscopy is widely used to track the molecular events due to its sensitivity, selectivity and wide range of time scale. For this reason, here various types of fluorescence techniques were used to track the HEWL aggregation event and its products.

2.3.1 Fluorescence resonance energy transfer

FRET technique was developed by Stryer and Hauglaivnd. FRET is an ideal probe to study protein–protein interaction (**Stryer and Haugland, 1967**). Therefore fluorescence resonance energy transfer (FRET) was employed to monitor aggregation. Based on the previous study, this technique is very sensitive to track early events of molecule- molecule interactions like association and aggregation. Since early event in protein aggregation is a type of self association, where monomer likely to forms dimers, trimers, and so on. So this process can be tracked easily using the fluorescence resonance energy transfer. FRET, involves the transfer of the excited –state energy from the initially excited donor [D] to an acceptor [A]. The donor molecule emits at shorter wavelengths, which overlaps with the absorption spectrum of the acceptor and energy transfer occurs via non-radiative dipole–dipole interactions. This energy transfer efficiency is highly sensitive to the Forster radius (R_0) ranging between 10–100 Å. The orientation of dipoles between donor and acceptor, rate of energy transfer depends upon the amount of spectral overlap of the emission spectrum of the donor with the absorption spectrum of the acceptor, distance between the donor and acceptor molecule. Forster radius (R_0) is distance at which energy transfer is 50% efficient (i.e, 50 % of excited donor are deactivated by FRET). The magnitude of R_0 is dependent on the spectral

properties of the donor and acceptor dyes. R_0 can be written in terms of mathematical expression

$$R_0 = [8.8x10^{23}. \kappa^2.n^{-4}.QY_D. J(\lambda)]^{1/6} \text{ Å} \qquad 2.3.1.1$$

Where κ^2= dipole orientation factor (range 0 to 4, $\kappa^2 = 2/3$ for randomly oriented donors and acceptors, n= refractive index, J (λ) = spectral overlap integral.

$$J(\lambda) = \int \varepsilon_A(\lambda).F_D(\lambda).\lambda^4 d\lambda cm^3 M^{-1} \qquad 2.3.1.2$$

Where ε_A = extinction coefficient of acceptor, F_D = fluorescence emission intensity of donor as a fraction of the total integrated intensity.

The rate of energy transfer $k_T(r)$ is written as

$$k_T(r) = \left(\frac{1}{\tau_D}\right)\left(\frac{R_0}{r}\right)^6 \qquad 2.3.1.3$$

Where r is the distance between the donor (D) and the acceptor (A) and τ_D is the life time of the donor in absence of energy transfer.

The efficiency of energy transfer for a single donor-acceptor pair at a fixed distance is

$$E = \frac{(R_0)^6}{(R_0^6 + r^6)} \qquad 2.3.1.4$$

The transfer efficiency is generally measured using the relative fluorescence intensity of the donor, in the absence of F_D and presence of F_{DA} of acceptor.

The transfer efficiency can also be calculated from the lifetimes and these respective conditions.

$$E = 1 - \left(\frac{\tau_{DA}}{\tau_D}\right) = 1 - \left(\frac{F_{DA}}{F_D}\right) \qquad 2.3.1.5$$

Experimental measurement of FRET:

For HEWL monomer concentrations 3-120 μM, FRET samples were prepared by mixing 0.5 μM dansyl (donor) and 0.5 μM dabcyl (acceptor) conjugated HEWL with unlabeled HEWL. For 0.3 μM samples, a ten-fold dilution of above concentrations dye conjugated HEWL was

employed with unlabeled HEWL. In samples containing donor alone, the unlabeled HEWL concentration was adjusted to make up for absence of acceptor conjugated HEWL. Keeping a constant ratio of labeled to unlabeled dye was not feasible as that would require 40 µM dye for 120 µM HEWL. FRET experiments were performed using steady state spectrofluorimeter (Fluoromax-3, Jobin-Yvon Horiba Inc., USA). Sample was excited at 380 nm (slit width 1 nm) and emission collected between 400 and 700 nm (slit 5 nm). For 0.3 µM samples, slit width was kept 10 nm. To minimize photobleaching excitation light shutter was kept open only when recording fluorescence. FRET efficiency was calculated from average integrated total emission counts under emission curve of donor alone & donor-acceptor mixture after subtraction of blank. The FRET efficiency results reported are averaged from three sets of experiments. R_0 of dansyl-dabcyl pair is 3 - 4 nm (**Miki and Remedios, 1990; Adair and Engelman, 1994**).

2.3.2 Steady state fluorescence anisotropy

Fluorescence anisotropy is an excellent technique to monitor the rotational motion of fluorophores in the excited state following their excitation using plane polarized light (Lakowicz et al., 1999). Steady-state fluorescence anisotropy (r_{ss}) reflects time integrated average value of the rotational motion of molecules in the excited state that is weighed by quantum yield. This parameter is however dependent both on the fluorescence lifetime and rotational correlation time of the fluorescent probe. The extent of polarization of emission is used to calculate fluorescence anisotropy (r).

At their excited state life time (~10^{-9}s) Brownian rotational motion in fluorophores changes the extent of polarization and these changes can be detected in term of anisotropy as follows

$$r_{ss} = \frac{\int_0^\infty I(t)r(t)dt}{\int_0^\infty I(t)dt} \quad , \quad r_{ss} = \frac{I_{\parallel} - GI_{\perp}}{I_{\parallel} - 2GI_{\perp}} \qquad 2.3.2.1$$

Here r_{ss} is steady-state anisotropy, $I_{||}$ and $I_{\perp}$ indicates the intensity of fluorescence emission when (A) both the excitation and emission polarizers are vertically oriented and (B) when emission polarizer is perpendicular to the excitation polarizer respectively. The factor $G = \frac{I_{HH}}{I_{HV}}$ is the ratio of sensitivity of the detection system for vertically and horizontally polarized light. Anisotropy is an intensity ratiometric measurement and it is independent of the fluorophore concentration in the absence of artifacts, like scattering.

Steady-state fluorescence anisotropy (r_{ss}) measurements (G-factor corrected and dark counts subtracted) were measured using Fluoromax-3 fluorimeter as described previously (**Homchaudhuri et al., 2006**). For HEWL monomer concentrations 3-120 μM, the concentration of dansyl conjugated HEWL was 0.6 μM, while remaining protein was unlabeled. Similarly 0.3 μM HEWL contained 0.1-0.2 μM of the HEWL-dye conjugate. Dansyl-labeled HEWL was excited at 380 nm (slit width = 1 nm) and emission at 438 nm was collected with a slit width between 5-10 nm. Each measurement was done in duplicate, while data reported are averages of at least two such measurements.

2.3.3 Time resolved fluorescence intensity decay and anisotropy decay

Following the pulsed excitation, time dependent intensity decay of sample is measured using time correlated single photon counting (TCSPC) method. For the sample with single lifetime, intensity decay can be written as

$$I(t) = I_0 \exp(-t/\tau) \qquad 2.3.3.1$$

Here $I(t)$ is intensity at any time t, I_0 is the initial intensity and τ is the fluorescence lifetime. As mentioned earlier, fluorescence lifetime is the average amount of the time spent by fluorophore in their excited state before emission. This can be calculated by averaging t over the intensity decay of the sample.

$$< t >= \frac{\int_0^\infty tI(t)dt}{\int_0^\infty I(t)dt} = \frac{\int_0^\infty t\exp(-t/\tau)dt}{\int_0^\infty \exp(-t/\tau)dt} \qquad 2.3.3.2$$

After solving the equation 2.2.3.2 for a single exponential decay, the average time a fluorophore remains in the excited state is equal to the fluorescence lifetime τ.

$$\langle t \rangle = \tau \qquad 2.3.3.3$$

Now assume the case where decay consists of emission from more than one fluorophore or from the same fluorophore but in different environments, then decay is multi-exponential and individual lifetime is needed to be resolved. In these cases

$$I(t) = \sum_i \alpha_i \exp(-t/\tau_i) \quad \text{i} = 3 \qquad 2.3.3.4$$

Here α_i and τ_i indicates the ith fractional amplitude and ith lifetime respectively of the decay component. Sum of all fractional amplitudes is equivalent to unity, $\sum_i \alpha_i = 1$

From the above parameters mean fluorescence lifetime τ_m can be calculated as:

$$\tau_m = \sum_{i=1}^{n} \alpha_i \tau_i \quad \text{i} = 1,2,3 \qquad 2.3.3.5$$

.

Since steady-state observation is an average of the time-resolved phenomenon over the intensity decay of the sample, it is thus imperative to understand the relationship between these two events. For a fluorophore that exhibits a single decay time τ, intensity decay can be represented as

$$I(t) = I_0 e^{-t/\tau} \qquad 2.3.3.6$$

Now steady-state intensity (I_{ss}) can be related with the decay time as follow,

$$I_{ss} = \int_0^\infty I_0 e^{-t/\tau} dt = I_0 \tau \qquad 2.3.3.7$$

Being more sophisticated, time-resolved method is preferred over steady-state. It is independent of the concentration of the fluorophore.

Time- resolved fluorescence anisotropy

This technique has been used to study the rotational dynamics of the fluorescent probe or molecule to which it is covalently attached. Localized fast rotational dynamics of probe around covalently attached position called segmental motion. The other rotational motion in

solution arises contributes from tumbling of entire macromolecule known as global motion, which is also slow (see Fig. 2.2.3.1

The fluorescence anisotropy decay of a rotating spherical body following pulsed excitation is given by

$$r(t) = r_o e^{-t/\theta} = r_o e^{-6Dt} \qquad 2.3.3.7$$

As mentioned above, r_o is initial anisotropy at t = 0, θ is rotational correlation time of the sphere and *D* is the rotational diffusion coefficient. The rotational correlation time, θ, can be obtained by Stokes-Einstein equation as follows

$$\theta = \frac{\eta V}{RT} \qquad 2.3.3.8$$

Where η is bulk viscosity, *V* is hydrodynamic volume of rotating sphere, *R* stands for gas constant and *T* refers for temperature in Kelvin.

For a system with multiple fluorophores or single fluorophore in with multiple rotational components, the anisotropy decay at time t is multi-exponential and will be written as

$$r(t) = r_0 \sum_j \beta_j \exp(-t/\theta_j) \qquad j = 1 \text{ or } 2 \qquad 2.3.3.9$$

Where r_0 is the initial anisotropy in the absence of rotational diffusion, the θ_j are the individual correlation times and β_j are the fractional amplitudes of each correlation times in the anisotropy decay. Biomacromolecules shows multi-exponential decay due to multiple rotational components (see Fig. 2.2.3.1)

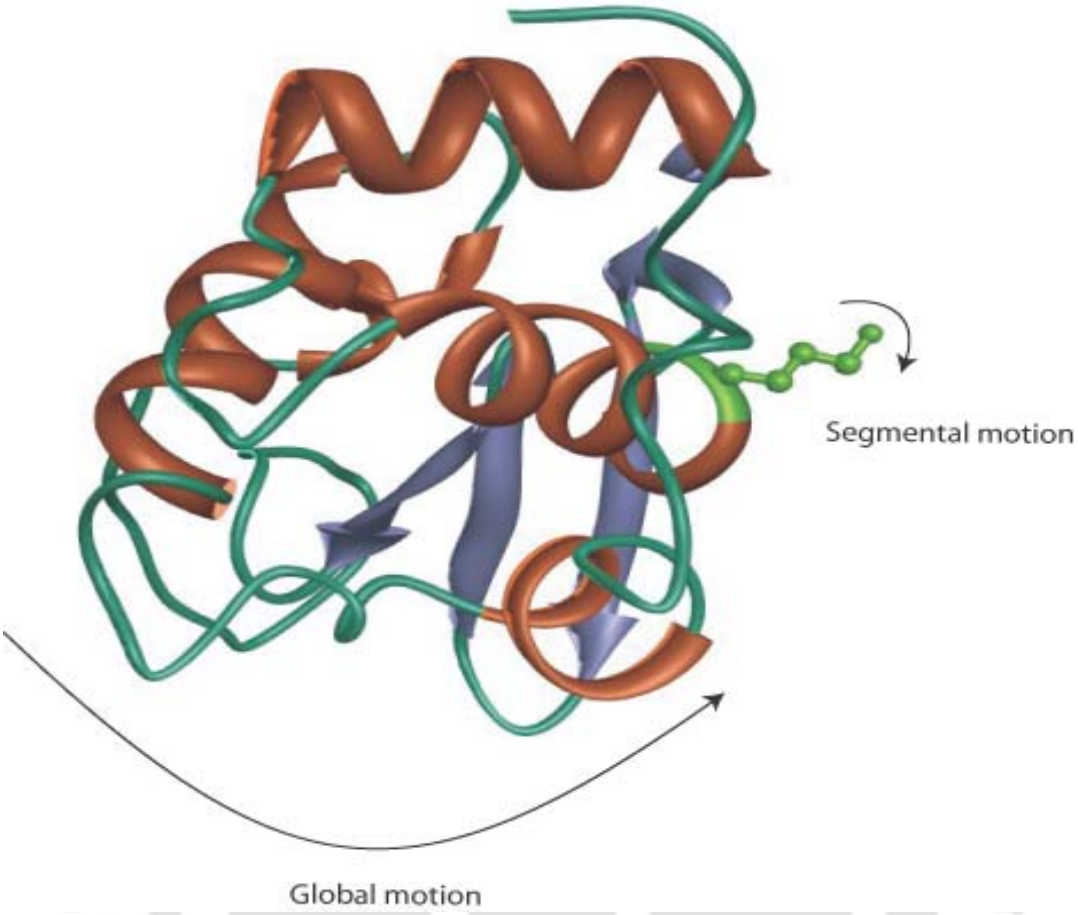

Figure 2.3.3.1: Depicting global and segmental motions in protein.

2.3.3.1 Instrumentation for time-resolved fluorescence measurement

Time-domain fluorescence lifetime or anisotropy decay measurement performed using a sensitive technique called *time-correlated single photon counting* (TCSPC). TCSPC measures the time interval between the exciting pulse and the emitted photon very accurately with a resolution of picoseconds time range. Repeating this "single photon experiment" several times gives the histogram of statistical distribution of arrival time of photons. This statistical distribution is then reconstructed to yield intensity decay of fluorophore(s).

The advantage of the TCSPC technique is required less than one emitted photon per exciting pulse is sufficient. Being a digital technique, TCSPC contains essential components like light source, constant fraction discriminator (CFD), time-to-amplitude convertor (TAC), amplifier,

photomultiplier tube (PMT), and multichannel analyzer. Depending on the emission yield, either forward or reverse mode of TCSPC can be employed. Forward mode counting implies the excitation pulse as a start TAC whereas, in reverse mode emission pulse is used to start TAC and excitation pulse is used to stop TAC.

The experiment starts with repetitive excitation of sample with pulsed light. The fluorescence intensity decay is collected at 54.7 degrees angle from the excitation polarizer. This angle is also called as magic angle. Following the excitation, amplified emission signal is passed through constant fraction discriminator (CFD), avoiding problems associated with pulse height variations and accurately measures the arrival time of the pulse. Now, each pulse is guided towards time-to-amplitude converters (TAC) which generate a voltage ramp that is proportional to the time between the excitation pulse and first arriving emitted photon. After arrival of the first photon from sample, multichannal analyzer (MCA) converts the voltage from TAC to the time channel using an analog to digital converter (ADC). Summing over many pulses the MCA builds up a probability histogram of counts verses time channel. One should continue the experiment until about 10,000-15,000 counts in the peak channel are collected.

As stated earlier that in TCSPC less than one photon is detected per laser pulse, the detection rate is typically 1 photon per 20 excitation pulses. The dead time of electronics prevents detection of another photon resulting from same excitation pulse. Detection of larger number of photons leads to pile up and apparent decay becomes non-exponential.

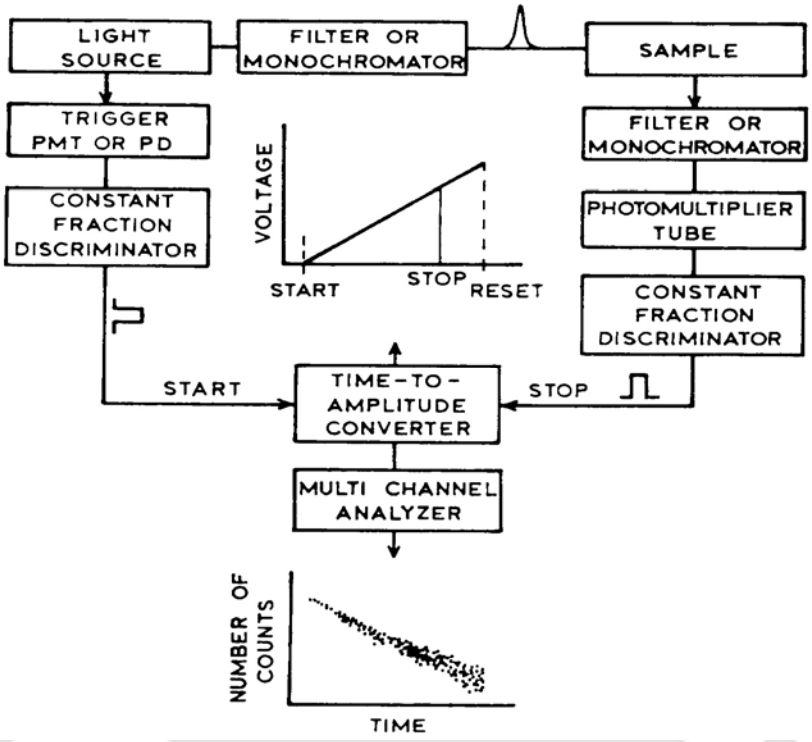

Figure 2.3.3.1 Setup for time-correlated single photon counting. The figure has been adapted from Principle in Fluorescence Spectroscopy by J. R. Lakowicz, second edition, 1999.

Time-resolved fluorescence intensity and anisotropy (G-factor corrected) measurements were carried out in LIFE SPEC II spectrometer (Edinburgh Instruments, Livingston, UK) operating in TCSPC mode, collecting emission decay in 4096 channels using a microchannel plate PMT.

(A) Measurement of tryptophan life time:

Mean fluorescence lifetime of tryptophan was measured by exciting samples with 295 nm nanosecond pulses (IRF fwhm was ~0.6 ns, Nano LED) and collecting subsequent emission at 350 nm with a temporal resolution of 4.883 ps/channel. For tryptophan lifetime measurements, HEWL was diluted to 1.2 μM for monomer concentrations 3-120 μM. however sample containing 0.3 μM was measured directly without further dilution.

(B) Measurement of dansyl-HEWL conjugates life time:

HEWL-dansyl conjugates were excited with 375 nm (EPL-375, picosecond pulsed diode laser, IRF fwhm ~150 ps) and emitted fluorescence from dansyl probe was collected at 440 nm with a temporal resolution of 24.414 ps/channel. For HEWL monomer concentrations 3-120 μM, the concentration of dansyl conjugated HEWL was 1.0 μM, while rest of the protein

was unlabeled. Similarly 0.3 μM contained 0.1 μM of the HEWL-dye conjugate. Each data reported is the average of at least two measurements.

Intensity decays were analysed by iterative reconvolution using the Marquardt-Levenberg algorithm to extract life time(τ_i) and (α_i) as given in equation below.

$$I(t) = \sum_i \alpha_i e^{-t/\tau_i} \quad \text{Where } i = 1\text{-}3 \text{ and } \sum_i \alpha_i = 1.0 \qquad 2.3.3.10$$

Mean fluorescence life time, $\tau_m = \sum_i \alpha_i \tau_i$ 2.3.3.11

(C) Measurement of dansyl-HEWL conjugates anisotropy decay:

Before taking the time-resolved anisotropy measurements of HEWL aggregated sample, G-factor was determined using the ANS in ethanol, where 0.13 ns rotational correlation time (ϕ_1) was found. The raw (G-factor corrected) anisotropy decays were tail fitted using a sum of two exponential (see Eq. 2.3.3.12) two extract the slower rotational correlation time (ϕ_2) corresponding to global motion of the HEWL aggregate.

$$r(t) = A + \beta_1 e^{-t/\phi_1} + \beta_2 e^{-t/\phi_2} \qquad 2.3.3.12$$

Where, A is constant dépendent on G-factor, β_i denotes the amplitude for ϕ_i, ϕ_1 and ϕ_2 refers the fast and slow rotational correlation times, respectively. As the 0.15 ns IRF pulse-width is negligibly small in comparison to the time scale of protein rotational motion (> 4 ns), So the extracted values of ϕ_2 by this tail-fit approach are not affected by consequences of IRF convolution.

2.3.4 Tryptophan fluorescence quenching

The decrease in fluorescence intensity of fluorophore is known as fluorescence quenching. It can occur by many processes like, excited state reaction, molecular rearrangement, energy transfer, ground state complex formation and collisional quenching. There are wide ranges of molecules which decrease fluorescence intensity, acting as a quencher. Molecular oxygen is a commonly considered as quencher if > 0.5 mM present (dissolved oxygen in solvent 10 ppm

= 0.5 mM), which reduces fluorescence intensity possibly by their paramagnetic nature which promote fluorophore to undergo intersystem crossing to the triplet state, whereas heavy atom like iodide exhibit their quenching behavior by spin-orbit coupling. Due to its change and larger size iodide is used to study surface accessibility of fluorophore in macromolecules. Two types of quenching were considered i.e collisonal quenching or dynamic quenching and static quenching. Dynamic quenching is a ground state complexation phenomena.

Collisional quenching occurs when the excited fluorophore experiences contact with an atom or molecule that can facilitate non-radiative transition to the ground state. Common quenchers include O_2, I^-, Cs^+ and acrylamide.

Collisional quenching of fluorophore is described by the Stern-Volmer equation

$$\frac{F_0}{F} = 1 + k_q \tau_0 [Q] = 1 + K_{SV}[Q] \qquad 2.3.4.1$$

In above equation F_0 and F are the fluorescence intensities observed in the absence and presence of quencher respectively, k_q is bimolecular quenching constant, τ_0 is unquenched lifetime of fluorophore, and [Q] is the quencher concentration.

K_{SV} is the Stern-Volmer quenching constant and represented as

$$K_{SV} = k_q \tau_0 \qquad 2.3.4.2$$

In the simplest case, a plot of F_0/F versus [Q] should yield a straight line with a slope equal to K_{SV}. The bimolecular quenching constant k_q reflects the accessibility of the fluorophore to the quencher. For diffusion controlled quenching reaction, k_q is close to $1x10^{10}$ $M^{-1}s^{-1}$. This value is considered as maximum possible value in aqueous solution. Smaller value indicates the shielding of the fluorophore or a low quenching efficiency.

The tryptophan quenching experiment reveals the exposure of tryptophan on the surface of protein. The fluorescence of tryptophan was quenched by adding KI (0 to 0.8 M) as described earlier (**Kumar et al., 2007**). To prevent the formation of iodate (I^{-3}), 0.1 mM sodium thiosulphate was added in stock solution of KI. A fixed concentration (1.2 μM) of aggregated lysozyme was diluted in cuvette for 120 μM or 3 μM monomer concentrations, while for 0.3 μM HEWL, KI was directly added. NATA (5 μM in pH 12.2 buffer) was used as a control. Steady state fluorescence of tryptophan in HEWL was measured by exciting at 295 nm (1 nm slit) and collecting emission between 310–400 nm (slit 20 nm for 0.3 μM, 10

nm for rest). The slopes reported from Stern-Volmer plots were averaged from two sets of experiments.

2.3.5 ANS binding

The concentration of ANS stock (1 mg/ml) in water was checked using extinction coefficient of 4,950 $M^{-1}cm^{-1}$ at 350 nm. The HEWL concentration dependent ANS binding assay was performed by employing a constant (3 μM) HEWL and (10 μM) ANS concentration in cuvette in pH 7 (3 μM) or 12.2 (3 to 120 μM). For 0.3 μM samples (in pH 12.2), ANS was directly added. Steady state fluorescence intensity was measured using Jobin-Yvon Fluoromax-3 spectrofluorometer after excitation at 380 nm (slit = 1 nm). Emission (slit = 16 nm for 0.3 μM, 8 nm for rest) was collected in the range 400-600 nm. Background intensity from Raman scatter or buffer was negligible (<5%) compared to sample emission intensity under identical conditions. The integrated fluorescence is the average area of two independent emission spectra after subtracting the blank emission reported previously.

2.3.6 Thioflavin T binding

Stock solution (~3 mg) of ThT was dissolved in ~3 ml deionised water (MilliQ). The ThT solution was filtered through 0.45 μM filter. Filtered solution was diluted in ethanol and again assayed by UV, taking OD at 416 nm and concentration was calculated using ε = 26620 M^{-1} cm^{-1}. Aliquot of ThT stock solution was kept in -20°C. While fibril binding assay 1mM ThT was maked in deionised water (MilliQ). Further it was diluted to 0.5 mM in 20 mM Gly-Gly pH 8.5 buffer from 1 mM ThT solution. Protein aggregated sample (70 μM –SH blocked and 70 μM control incubated in pH 12.2) and control sample was diluted to 7 μM protein concentration and ~11 μM ThT was added into protein sample, 1ml sample volume was adjusted with 20 mM Gly-Gly pH 8.5 buffer. Binding to fibril, molar ratio of protein to ThT was ~1:2 as described previously (**Wall et al., 1999**). Sample was vortexed and spectra was taken immediately, exciting at 450 nm with 1 nm slit width and subsequent emission between 470 and 550 nm was observed at 5 nm slit width using the Jobin-Yvon Fluoromax-3 spectrofluorometer at different time intervals. Background fluorescence intensity was subtracted from blank. Integrated fluorescence intensity was plotted against time after averaging of independent measurements.

2.4 Atomic force microscopy

2.4.1 Instrumentation and working principle

To study the morphology of aggregates and fibrils structure atomic force microscopy has been employed. The atomic force microscope (AFM) or scanning force microscope (SFM) was invented in 1986 by Binnig, Quate and Gerber. Like all other scanning probe microscopes, AFM utilize is a probe, which is known as Tip, it is fabricated on the end of a cantilever which consists of silicon nitride. The sharp probe moves over the surface of a sample in a raster scan. While raster scanning images are obtained through measuring of the force on a sharp tip (insulating or not) created by the proximity to the surface of the sample. This force is set aside small and at a constant level via a feedback mechanism (see Fig 2.4.1), when the tip is moved sideways it follows the surface contours such as giving trace like topograph sketch. The cantilever with the attached stylus is mounted between the AFM sample and the tunneling tip, which is fixed to a small piezoelectric element called the modulating piezo, which is used to drive the cantilever beam at its resonant frequency. Cantilever bends under the force and these forces can be measured applying the Hook's law formula.

$$F = -k.X, \text{ where k is spring constant, X is displacement} \qquad 2.4.1$$

Magnitude of these forces (non covalent force like attractive and repulsive forces) between the tip and the respective sample detected through detector (photodiode) and magnitude of detector signal transfer to imaging system i.e. digital signal process see Fig. 2.4.1(**Binnig et al., 1986**).

2.4.2 Operational Mode

Contact Mode: In this mode vertical positioned tip raster over the sample with approaching and retracting force. Moving to sideways it follows the surface contours such as giving trace like topograph sketch.

Tapping mode (Ac mode): In this imaging mode stiff or beam type cantilever is preferably used. Basically cantilever vibrates at or near its resonance frequency by an electrical oscillator to amplitude up to 100 nm, So that it can bounce up and down exerting both repulsive and

attractive region of the tip-sample interaction. It also reduces the lateral (side to side) force on the sample because tip spends less time on the surface of the sample. Advantages of this mode, delicate sample can be image without distortion of sample.

True non contact mode (Ac mode): The oscillating tip (at its resonance frequency) never touches the sample, keeping the distance between tip and sample around 10 nm within long range of Vander Waals attractive forces. It is not used for imaging in liquid medium.

MAC mode (magnetic ac mode): Cantilever coated with magnetic material is required for this imaging mode. It oscillate near it resonance frequency by electromagnetic oscillator. It is suitable for both liquid and air imaging methods.

2.4.3 Sample preparation

Prior to preparation of sample, freshly cleaved mica was cleaned using cello tape as much as possible by peeling method. In next step HEWL samples (10 µl) were applied on to freshly cleaved mica in the presence of 10 mM Mg^{2+}, after a few minutes, these were rinsed with 0.2 µm filtered deionized water to remove unadsorbed sample and were dried under nitrogen. HEWL incubated in the presence of SDS and CTAB was eluted through Amersham PD-10 columns to remove free surfactants before preparing the sample for imaging. Sample in presence of chitotriosoe and NAG were diluted 10 fold in incubating buffer prior to sample preparation. Remaing procedure was same like others sample. Samples were imaged in air under AAC or MAC MODE (non contact) in PICO PLUS^{TM} AFM purchased from Molecular Imaging, USA. Cantilever type PPP-MFMR-20 (resonance frequency, 60-70 kHz; Nanosensors) was used for MAC mode, while type PPP-NCL-50 (resonance frequency, 150 kHz; Molecular Imaging) was used for AAC mode. Images were acquired digitally at a scan speed of 1-2 lines/second with 256 data points per line. AFM images were acquired at least three times for every sample conditions

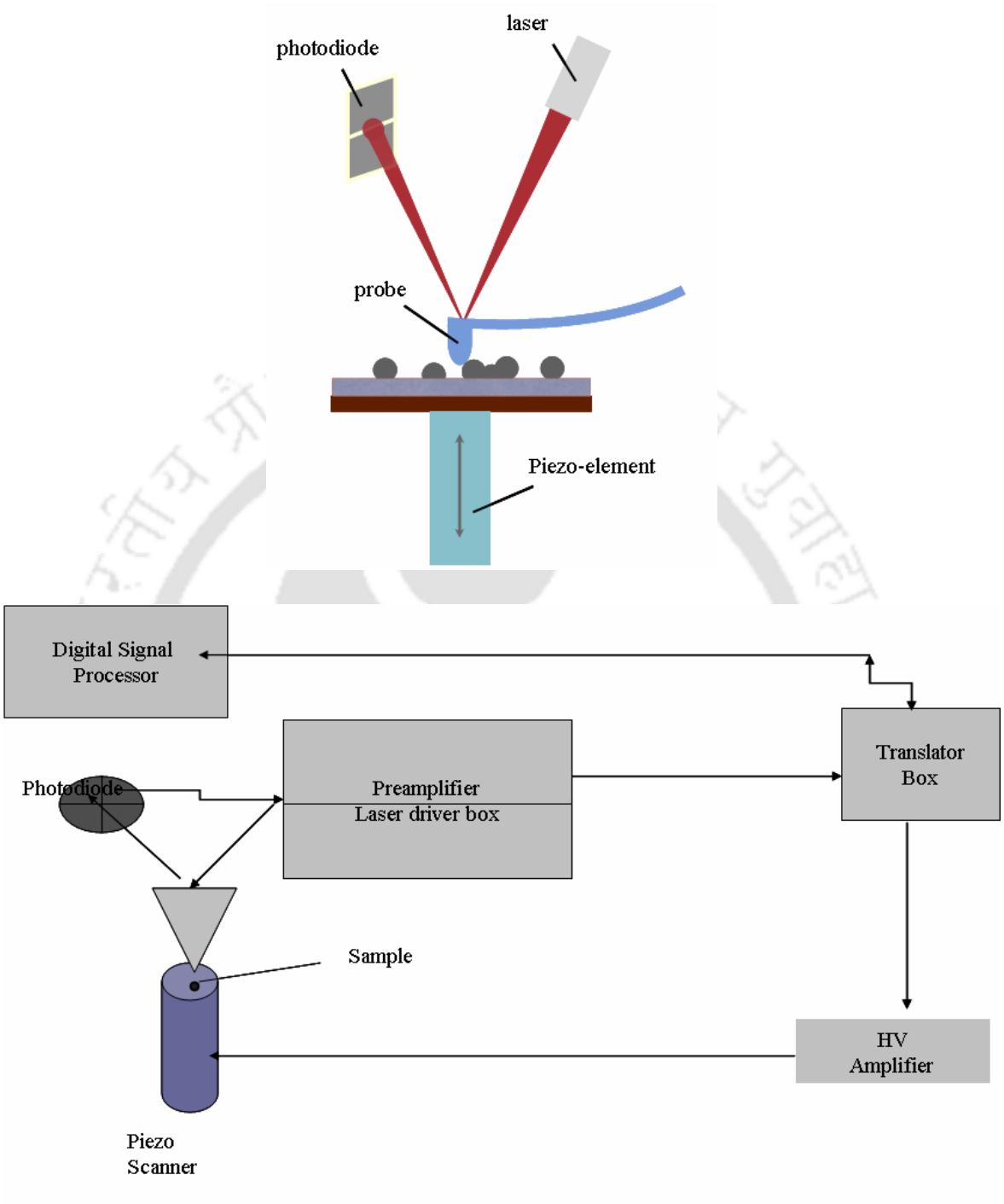

Figure 2.4.1: Top image represents AFM instrument containing individual component and on bottom electronics control system of AFM is shown.

2.5 Size exclusion chromatography

2.5.1 Matrix preparation and column packing

Sephadex G-50 (Fractionation range for globular protein 1.5 kDa- 30 kDa) was used for matrix. Accoding to the product information sheet provided by proprietor, Sephadex G -50 swelling quantity is 1g in 9-11 ml of eluting buffer (50 mM sodium dihydrogen phosphate pH 7). For making the slurry, quantity of sephadex G-50 was decided based on swelling information for the desired column packing volume. The slurry was prepared in 50 mM pH 7 buffer having sodium azide and kept for 24 hours. After making it was ensured that it has swelled well under buffer, it was manually packed in column (1 cm×50 cm;Econo-column®, Bio-Rad) under gravity flow. Finishing this step, newly packed column was equilibrated using 3-4 th column volume manually. After performing the experiment, column was stored in cold room to avoid the microbial growth. It was re equilibrated before using for next experiment.

2.5.2 Eluting sample detection

Size-exclusion chromatography experiments were performed using the Biologic LP Chromatography system (Bio-Rad) equipped with a peristaltic pump and UV optics module permitting detection of eluant using the absorbance at 280 nm. Void volume of column was calculated using blue dextran (2000,000 kDa). Typically ~250 µl of sample was injected for every run and low flow rate was kept like 0.120 ml / min, because setup was assembled with low pressure module. All gel –filtration experiment was carried out at 25 ºC. A matrix with a fractionation range up to~30 kDa was chosen to clearly distinguish the small oligomers of HEWL from the large assemblies that eluted through the void volume. For monitoring the aggregation of 120 µM HEWL in pH 12.2 in absence and presence of surfactants (SDS, CTAB) and DTT, The total volume of matrix in the column was 32 ml. However, matrix column volume was 39 ml for the characterization of aggregates size in absence and presence of prior incubation of chitotriosoe and NAG. The column was washed with the elution buffer (50 mM NaH_2PO_4 at pH 7), employing three times the matrix volume, before loading every fresh sample.

2.6 Free thiol estimation and blocking

Presence of free –SH groups in HEWL was monitored by reacting 2,2′-dithiobis(5-nitropyridine) with the protein as described previously (**Kumar et al., 2008**). Briefly, 50 µM of DTNP (diluted from 3mM stock in DMSO) was mixed with 5 µM of HEWL (diluted from 100 µM HEWL in pH 12.2 buffer) in the reaction buffer (100 mM pH 7, phosphate). However, the concentration dependent accessibility of free –SH was estimated with 2 µM of HEWL diluted (from all three incubated concentration like 20, 50, 120µM) in 300 mM phosphate pH 7 buffer. Higher ionic strength buffer (300 mM) was used to counter the effect of higher pH 12.2 from small concentration sample on absorbance at 387 nm. The mixture was stirred in a vortex mixer for 15 min. The formation of the product 5-nitropyridine-2-thione was confirmed from the characteristic absorption peak near 387 nm where the reactant (DTNP) has negligible absorption. The concentration of free –SH groups was determined by calibrating the absorbance at 387 nm with a standard plot generated using known concentrations of L-cysteine amino acid (0–100 µM) under identical conditions.

The –SH blocking with iodoacetamide procedure was followed as mention in B. Tech project thesis (Mohit 2011). Freshly made stock solution of iodoacetamide was used.The excess iodoacetamide (2 µL of 3 mM) was added to HEWL sample at every 2 hrs, 6hrs, 12 hrs, 24 hrs of incubation time in pH 12.2. Sample containing HEWL with iodoacetamide was kept in dark condition for reaction. The degree of successful blocking was checked after 24 hours using DTNP assay. This protocol was followed as used previously (Kumar et al., 2009). The 60-70% of blocked free –SH was achieved.

Note: Circular Dichroism and Dynamic Light Scattering measurements were carried out with external help.

Monitoring hen egg white lysozyme aggregation in pH 12.2 at room temperature in absence and presence of additives like surfactants (SDS, CTAB) and DTT

3.1 Introduction

Previous study has shown that HEWL aggregates slowly **(Homchaudhuri et al., 2006)** in pH 12.2 at room temperaure. Surfactants are known to act like an artificial chaperone is assisting the refolding of denatured protein and maximize the yields of recombinant protein **(Rozema & Gellman, 1996).** Owing to their ampiphillic nature, surfactants can also inhibit protein aggregation. It has been reported that ampiphillic surfactants can inhibit Aβ (1–40) amyloid fibril formation at physiological pH **(Wang et al., 2005)**. Earlier reports also suggest that ionic surfactants like sodium dodecyl sulfate (SDS) and cetyltrimethylammonium bromide (CTAB) protect rhodanese, (a mitochondrial enzyme) against thermal aggregation **(Bhattacharyya & Das, 1999)**. Other than surfactants some reports stated that in presence of reducing agent like dithiothreitol (DTT) or cysteine, fibrillation of HEWL can be suppressed (**Yamamoto et al., 2008)**. With this background some salient results on the size heterogeneity and morphology of hen lysozyme aggregates in pH 12.2 are presented below.

3.2 Results and discussion

3.2.1 Size of aggregates

Characterization of size and shape of aggregates is essential as well as difficult owing to its heterogeneous population. Previously our lab has shown that steady growth of HEWL aggregates occur at concentrations 4, 40 and 200 μM in alkaline pH 12.2 at room temperature and formation of average size aggregates are concentration dependent (**Homchaudhuri et al., 2006)**. However change in size/shape and heterogeneity inside the aggregate population has not been shown earlier. Similarly effect of surfactants and DTT on the size/shape of HEWL aggregates in pH 12.2 was not investigated. Based on previous finding, size/shape of HEWL at pH 12.2 in absence and in presence of SDS, CTAB and DTT was investigated employing gel filtration experiment.

The elution volume of a protein species from gel-filtration experiment is a good indicator of the overall protein size and shape. Additionally the gel-filtration experiment itself takes a few hours to complete; therefore it was also chosen to monitor irreversible changes in protein size/shape in the timescale of days. Before monitoring the size/ shape of aggregates with and without additives column was calibrated using different molecular weight markers (see Fig. 3.2.1 A) and void volume of the column was calculated using blue dextran (2000 kDa). After that HEWL in pH 7.0 sample incubated at various durations was eluted stepwise. The elution of HEWL incubated at pH 7 was observed as a gaussian profile with an elution peak at ~30 ml. This yield a V_e/ V_o of indicating that eluted sample seems to be monomeric, but not exactly globular, HEWL (14.3 kDa). Figure 3.2.1B shows that that elution profile remains symmetric without change in elution volume even at longer duration like 6 days. Based on these results, it was concluded that HEWL at netural pH 7.0 does not have propensity to aggregate.

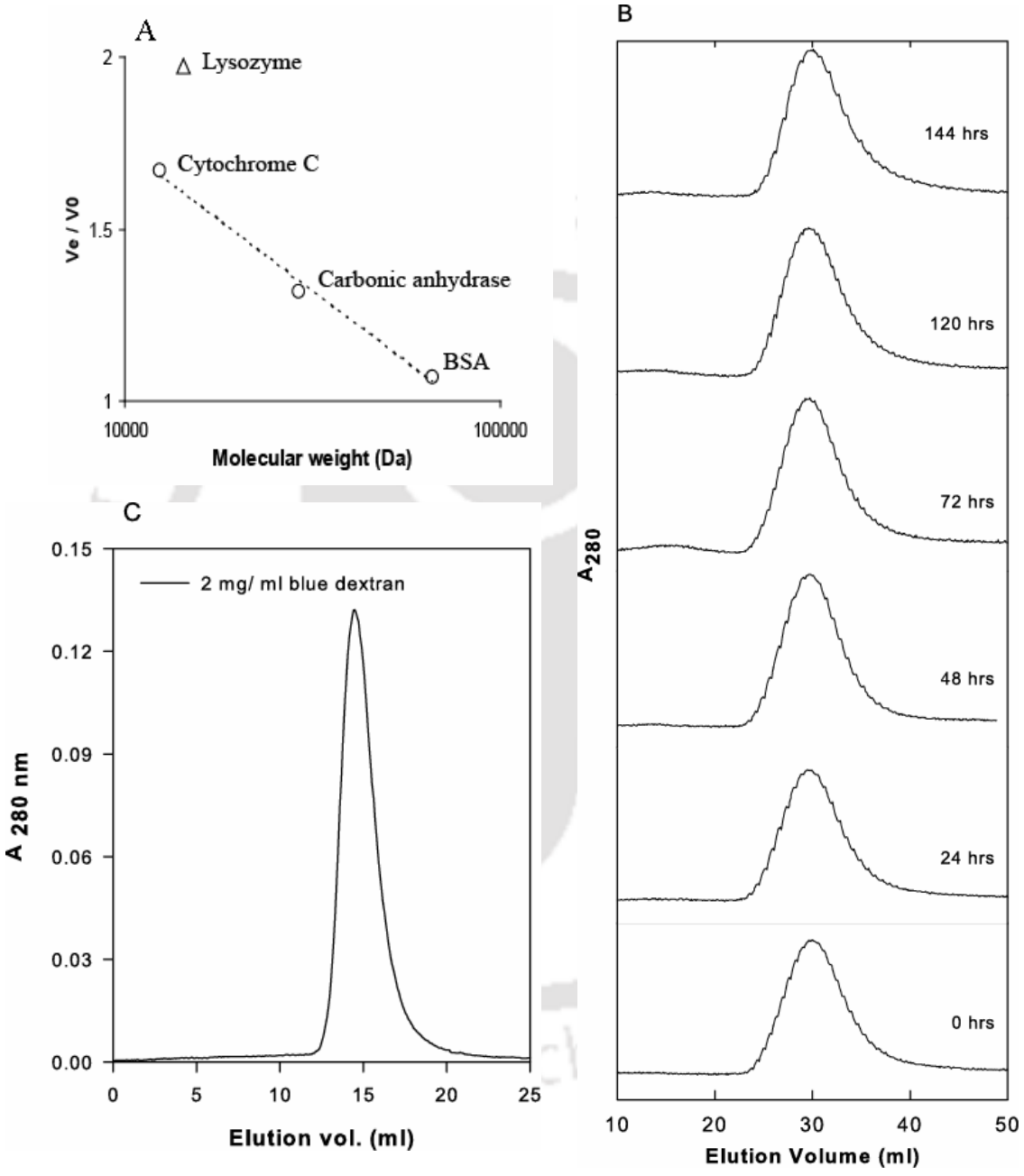

Figure 3.2.1: Gel filtration column calibration plot and elution profile of native HEWL and blue dextran (A) Calibration curve using three standard proteins, namely Lysozyme (14.3 kDa), cytochrome C (12.4 kDa), carbonic anhydrase (29 kDa) and BSA (66 kDa), (B) Elution profiles of 120 μM lysozyme incubated in pH 7 at 298 K for different incubation times. (C) Blue dextran elution (2000000 kDa).

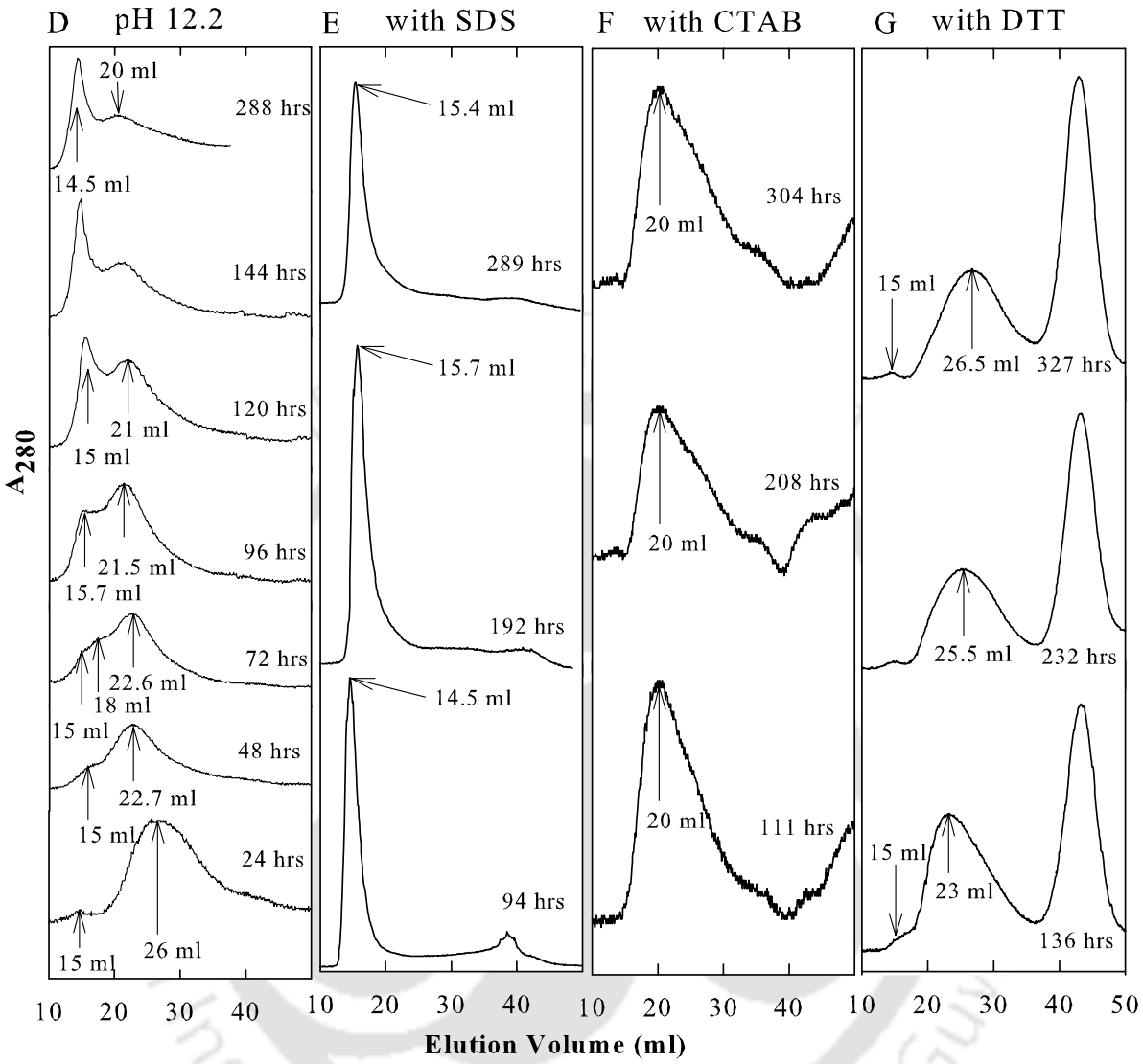

Figure 3.2.1: Gel filtration elution profile of lysozyme, incubated in 12.2 at 298 K for the times indicated, as monitored using absorbance at 280 nm. (D) The elution profiles of 120 μM HEWL. (E) The elution profile of 120 μM HEWL in the presence of 14 mM SDS. (F) The elution profile of 80 μM HEWL in the presence of 3 mM CTAB. (G) The elution profile of 120 μM HEWL in the presence of 20 mM DTT.

Figure 3.2.1 D shows the elution profiles observed for 120 μM HEWL incubated at pH 12.2 for different durations. At 24 h, a broad asymmetrical elution profile was seen with a peak at ~26 ml. A tiny bump is noticed at ~15 ml, whereas at larger elution volumes between 37 and 47 ml a tiny shoulder is also observed. Consequently it is interesting to observe the changes in this elution profile as the duration of exposure at pH 12.2 is gradually increased. At 48 h, the asymmetric distribution started acquiring a bimodal shape, likewise the elution peak had clearly shifted to ~22.7 ml, the shoulder at 37–47 ml is much less pronounced and the bump at ~15 ml is now as distinct shoulder. At 72 h, a third species begin to exist as a small shoulder near ~18 ml, whereas the elution peak at ~22.6 ml remains. At 96 h, elution profile reveals two peaks one at ~15.7 and other at ~21.5 ml were evident. As incubation time progresses to 120 h and later 144 h, the taller peak was appeared at ~15 ml; similarly the peak height at ~21 ml was proportionally reduced. In continuation with elution profile, both of the peaks are marginally shifted to ~14.8 ml and ~21 ml respectively at 144 h. At 288 h, it has observed that the elution profile was fairly similar in shape which was observed at 144 h; however the peaks were now shifted towards ~14.5 ml and ~20 ml. It seems that the species eluted at ~14.5 ml must be a large aggregate, as it matches with the elution volume of blue dextran, which elutes through the void volume (15ml).

Figure 3.2.1 E exhibit the elution profile of 120 μM HEWL incubated at pH 12.2 in the presence of 14 mM SDS. The concentration of SDS was used 10 fold higher to critical micelle concentration (1.36 mM). At 94 h, we observe a tall and narrow peak distribution at ~14.5 ml, matching from the elution volume of blue dextran. This indicates elution of a large-molecular-mass species through the void volume of the matrix. At 192 h, the tall peak profile was persistent although it is now shifted to ~15.7 ml. At 289 h, the elution profile is nearly alike comparing at 192 h, except that a minor shift to ~15.4 ml.

Figure 3.2.1 F shows the elution profile of 80 μM HEWL incubated at pH 12.2 in the presence of 3 mM CTAB. The concentration of CTAB was used 10 fold higher than critical micelle concentration (0.27 mM). At 111 h., it was observed a broad elution profile with a peak at ~20 ml. A small shoulder is able to be seen between 30 and 40 ml, whereas another rising profile is observed from 40 ml onwards. At 208 h, the elution peak is seen slightly broader, otherwise fairly similar to that at 111 h except for the profile after 30 ml. At 304 h, the elution profile is seen also slightly broader, but other feature was similar to 111 h.

Figure 3.2.1 G exhibits the elution pattern of 120 μM HEWL incubated in the presence of 20 mM DTT. DTT concentration was used in 100 fold excess to compensate for losses pH 12.2. At 136 h, we observed a broad elution peak at around 23 ml with a tiny shoulder at ~15 ml. As incubation time reaches to 232 h, this broad peak shifted to ~25.5 ml, while a tiny peak is hardly visible at ~15 ml. At 327 h, this elution peak shifted further to ~26.5 ml, whereas the tiny peak at ~15 ml was fairly intact. At all three time points it was observed a major elution peak consistent at approx. 43 ml that originated possibly from DTT molecules eluting later. At different time periods the peaks were observed between 23, 26.5 ml and at approx. ~15 ml. This arises from HEWL in presence of DTT. The increasing trend of peaks from elution volume (23–26.5 ml) towards 136 to 327 h suggests that HEWL is attaining more compact structure as time progresses. An elution peak in the range of 23–26.5 ml demonstrates that a predominant fraction of the HEWL population is expected to be compact and monomeric in the prolonged presence of DTT. A small fraction of HEWL aggregates or perhaps completely unfolded HEWL may account for the tiny peak at ~15 ml. It is quite evident that presence DTT has a strong influence in inhibiting HEWL aggregation at alkaline pH.

3.2.2 Morphology of aggregates

Subsequent to size heterogeneity analysis, it will be worthwhile to observe the morphology of HEWL aggregates in pH 12.2 in absence and presence of surfactant (SDS, CTAB) and DTT. For this purpose atomic force microscopy was employed. This is an excellent technique to demonstrate the morphological feature of aggregates. Images of the HEWL samples using AFM were acquired at different conditions.

Figure 3.2.2 A reveals topograph image of HEWL at pH 7 which appears monomeric as expected. The z- range (0-30 Å) indicates a flat profile.

Figure 3.2.2 B and C, Top and bottom topograph flattened images shows the heterogeneity in size and shape among aggregates of HEWL after 122 h, 136 h and 288 h of incubation at pH 12.2 in the absence of any additive. Morphology of HEWL indicates a mixture of aggregate population occurs at pH 12.2 and it exist as big aggregates at later time which is consistent with our gel filtration elution profile that eluted via void volume at later time.

Figure 3.2.2 D, Top and bottom topograph images reveal well populated long thread like structures (~20 nm thickness) after continuous incubation for 172 hours in the absence of additives.

However in figure 3.2.2 E bottom, amplitude images with z- range 0-50 nm were found well populated and dense fibrillar structure interwoven to each other and its, rarly seen in other condition. High z-range indicates that fibril is very long and interwoven. They are similar to amyloid fibrils and characteristic to enhanced ThT fluorescence intensity. Interestingly, this is the first report of spontaneous formation of fibrillar structure of HEWL in pH 12.2 at room temperature.

A

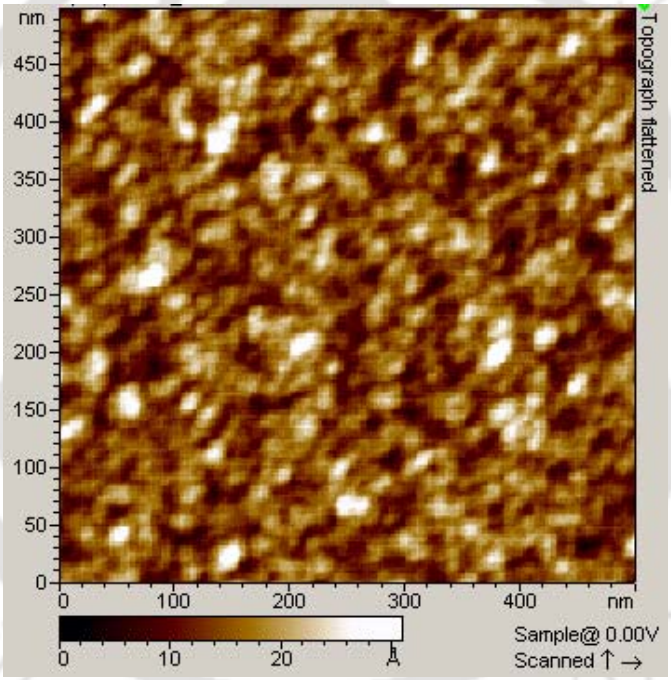

Figure 3.2.2 A: Topograph AFM image of HEWL in pH 7.0 at 298 K, after 96 hours.

B

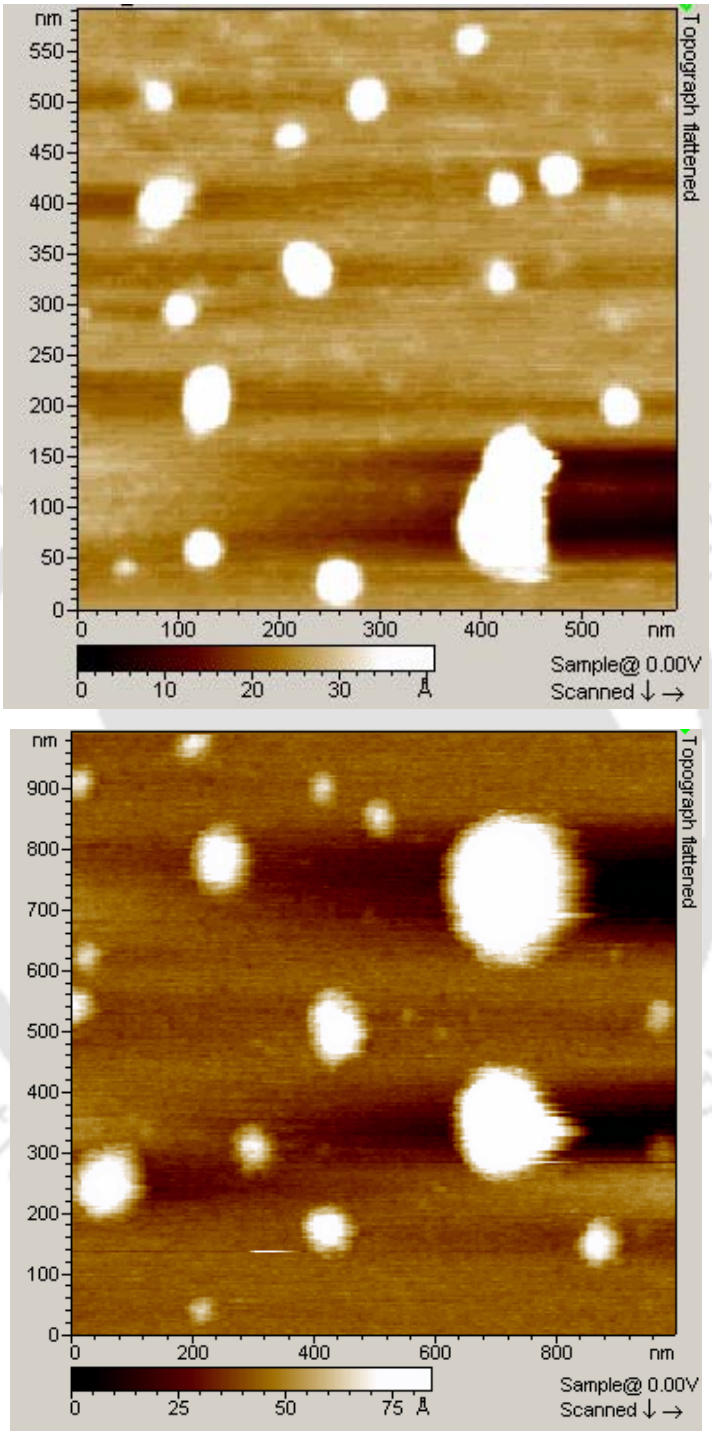

Figure 3.2.2 B: On top topograph AFM image of HEWL in pH 12.2 at 298 K, after 122 hours & bottom AFM image of HEWL in pH 12.2 at 298 K, after 136 hours.

C

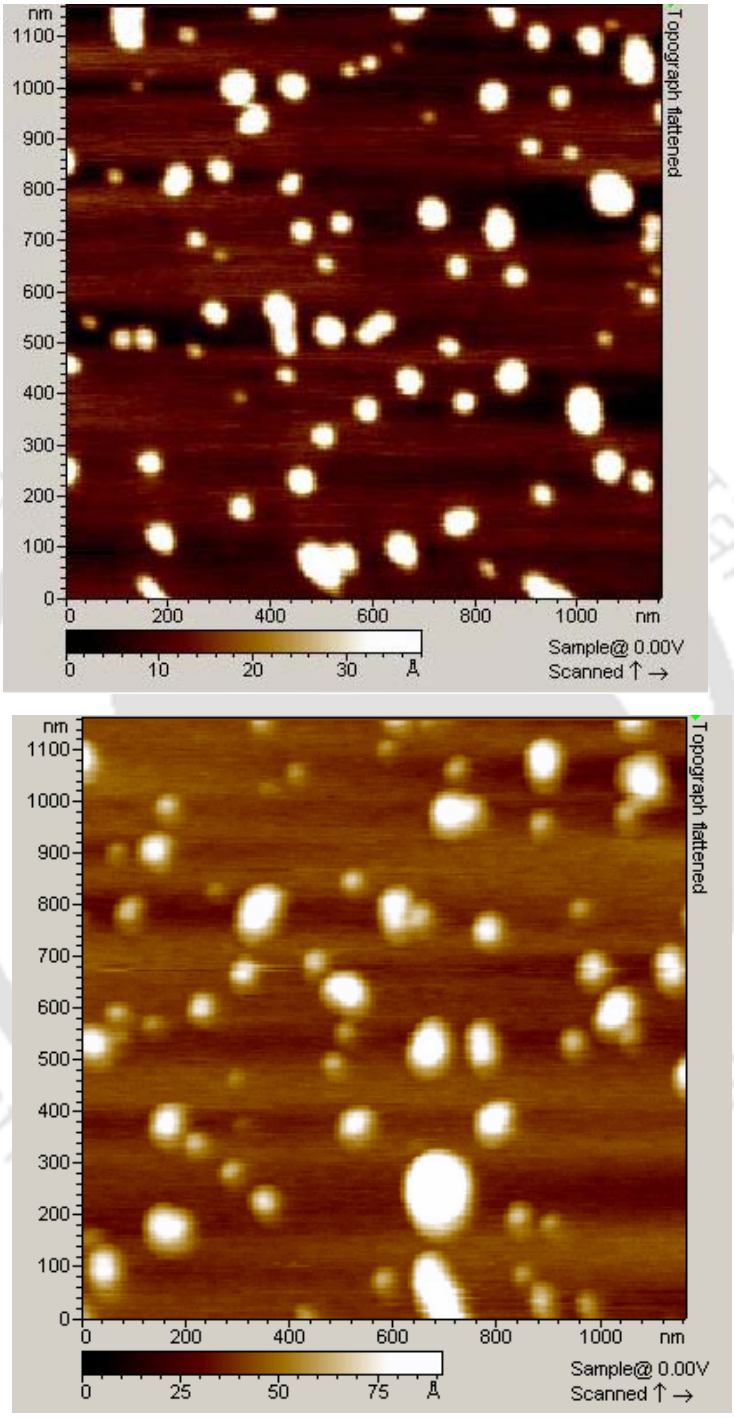

Figure 3.2.2 C: On top & bottom represents topograph AFM image of HEWL in pH 12.2 at 298 K, after 288 hours.

D

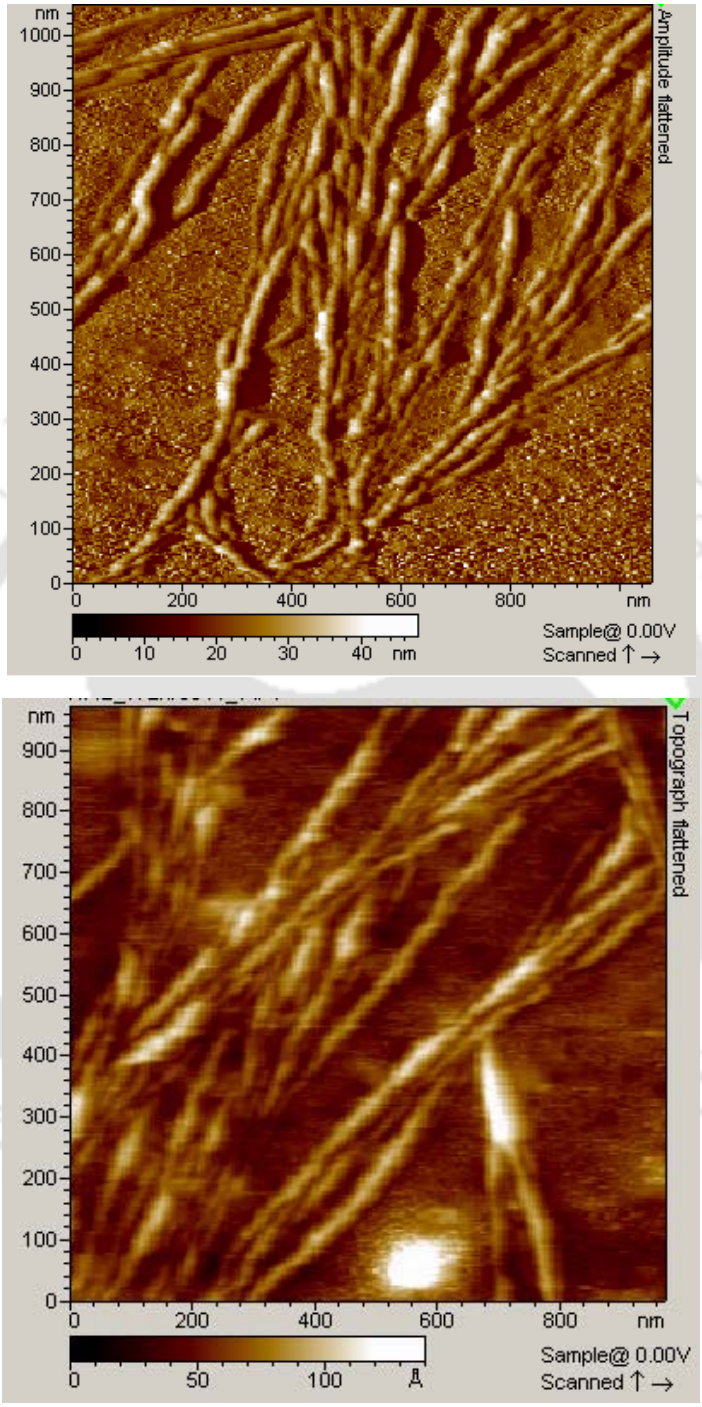

Figure 3.2.2 D: On Top amplitude AFM image represents fibril of HEWL in pH 12.2 at 298 K, after 170 hours. On bottom topograph AFM image of fibril at same condition.

E

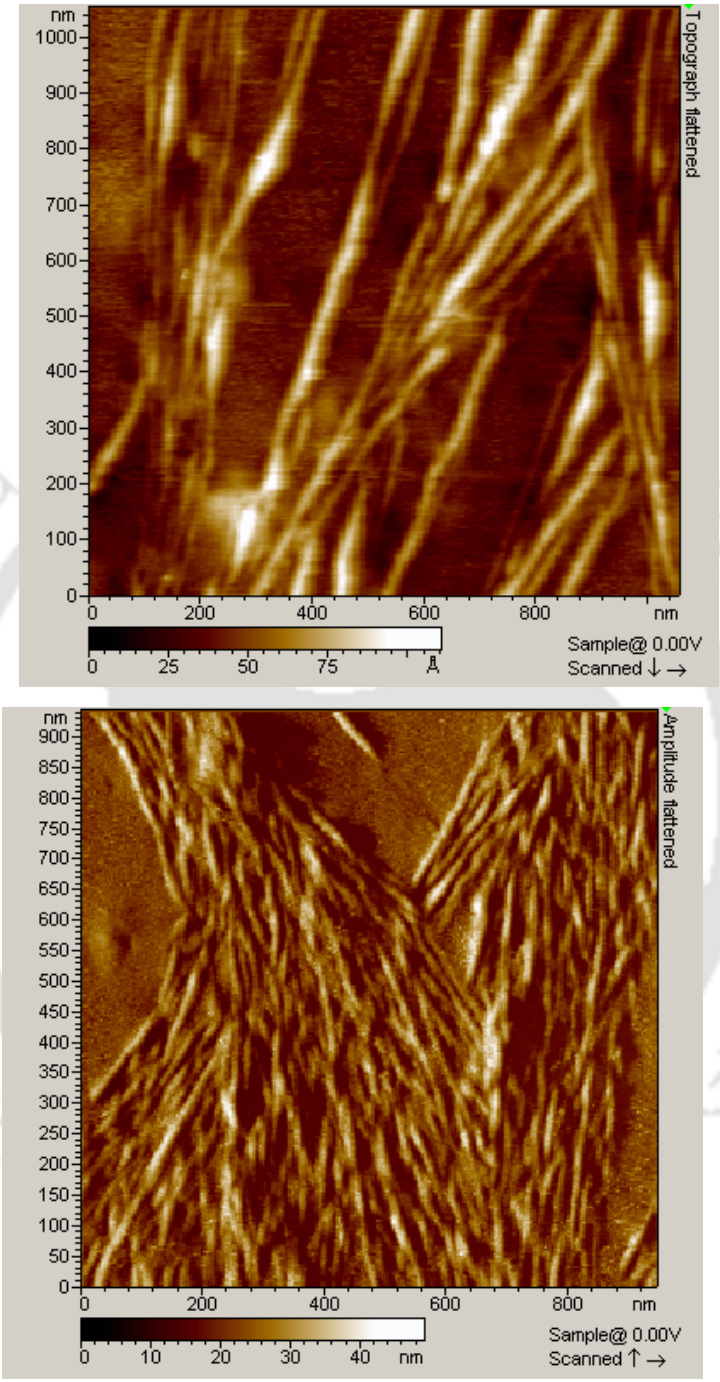

Figure 3.2.2 E: On top topograph & bottom amplitude AFM image of HEWL fibril in pH 12.2 at 298 K, after 170 hours.

In the presence of 14 mM SDS (Fig. 3.2.2 F), Phase images of HEWL-SDS complex was presented like an outer layer of bound micellar SDS to HEWL aggregates. As well as series of small clusters among these big aggregates was also clearly evident. Unlike other samples in figure 3.2.2 F, the z profile was found 0.5V, and in figure 3.2.2 D top & E bottom, z- range was noticed 0-40 nm , whereas z height were noticed in the rage of 40-100 Å for all others images. These observations represent the presence of large species that eluted through the void volume in gel filtration analysis (see Fig. 3.2.1 C).

In contrast, Figure 3.2.2 G revealed comparatively smaller, unbound and single aggregates in the presence of CTAB, which is fairly matches with the higher elution volumes obtained in figure 3.2.1 F.

Figure 3.2.2 H shows that in the presence of DTT, the aggregates are mostly monomeric and compact similar to figure 3.2.2 A, which is native HEWL and consistent with the earlier results also.

F

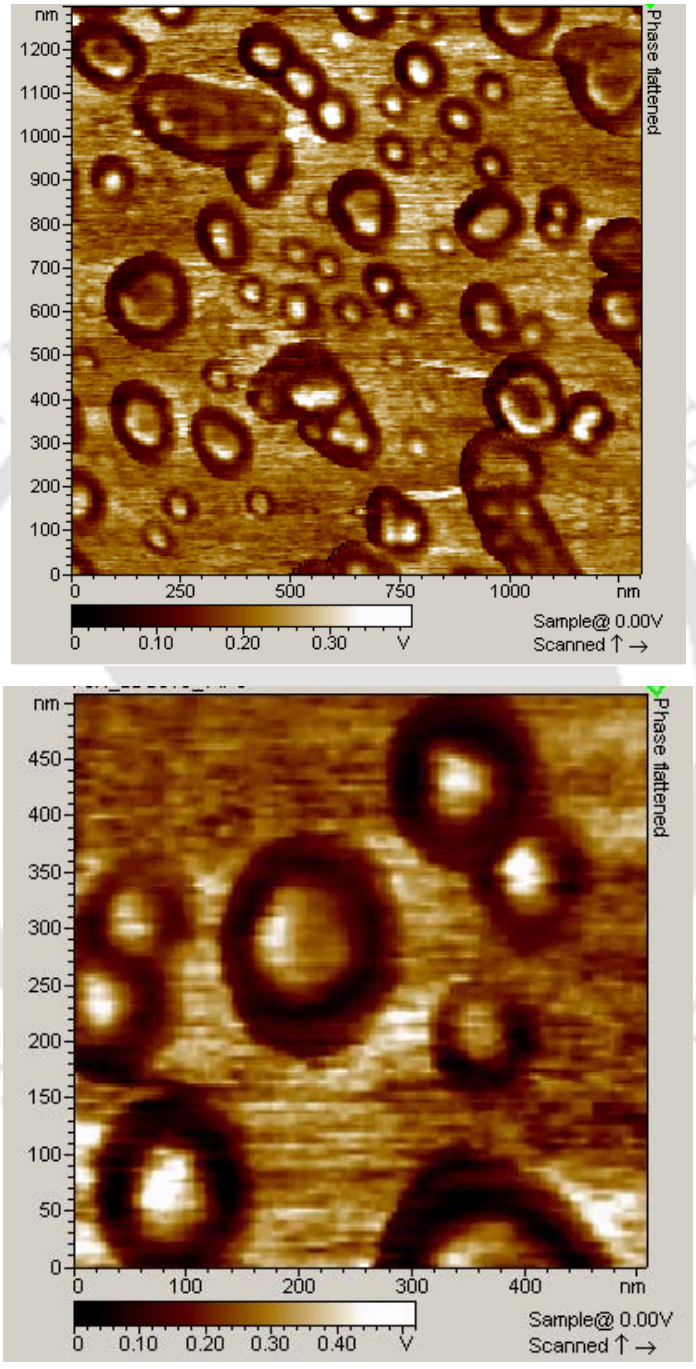

Figure 3.2.2 F: On top & bottom AFM phase image of HEWL in presence of 14 mM SDS in pH 12.2 at 298 K, after 120 hours.

G

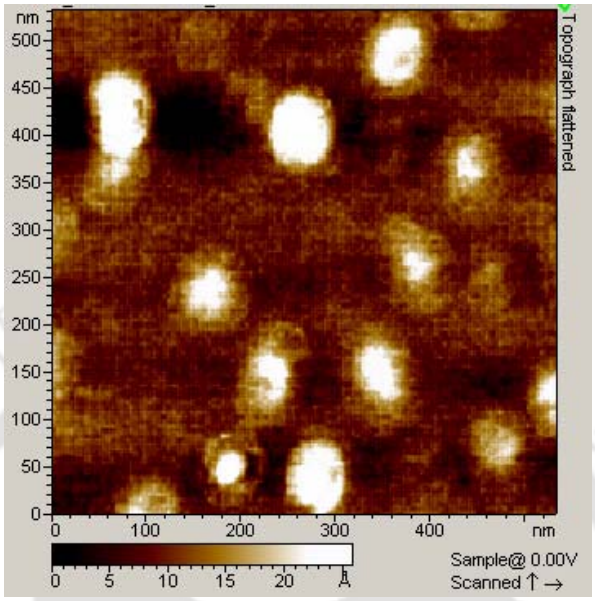

H

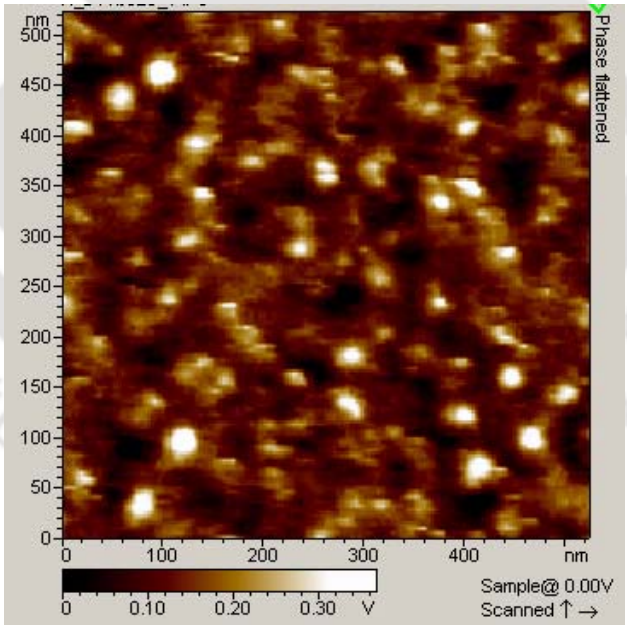

Figure 3.2.2: (G) AFM image of HEWL in presence of 3 mM CTAB in pH 12.2 at 298 K, after 144 h and (H) in presence of 20 mM DTT in pH 12.2 at 298 K, after 120 h.

It is important to discuss the comparative investigation comparing with pH 7 incubated samples, HEWL at pH 12.2 demonstrated time-dependent changes in the elution profiles that clearly reflect the presence of multiple aggregate species with varying size/shape redistribution of population among the different aggregate species with the progression of time. The steady growth and maturation of large aggregates was started prominently from 120 h onwards. This remarkable reorganization among aggregate composition was not revealed from steady-state dansyl fluorescence anisotropy investigation (**Homchaudhuri et al., 2006)** possibly due to time and ensemble averaging. Resolving , the multiple (>2) rotational species occuring from a mixture of multiple- sized aggregates is not feasible using time-resolved fluorescence anisotropy, reason is limitations in data analysis and high signal-to-noise ratio required in data for that purpose. Morphology of multiple aggregate species can discuss from AFM images. It was observed that HEWL forms globular like aggregates and spontaneous growth of fibrillar structure in pH 12.2 which is rarely seen in other condition. At higher concentration (mM) HEWL known to fibril formation at mostly acidic pH with continuous heating and extra treatment (**McAllister et al., 2005, Arnaudov et al., 2005 and Krebs et al., 2005**). Some group has found fibril at pH 9.2 in presence of surfactant (**Moosavi-Movahedi et al., 2007**). HEWL has forms fibril in some different condition also which was reviewed by Swaminathan and coworkers recently (**Swaminathan et al., 2011**). Here it is crucial to address that HEWL forms fibrils spontaneously in pH 12.2, which was not possible at other condition.

In presence of anionic surfactants SDS, it is imperative to discuss the results obtained from figure 3.2.1 E, where shifts observed over subsequent days may perhaps be attributed to structural reorganization inside the HEWL–SDS complex making the SDS-aggregates complex more compact, which matches with AFM figure 3.2.2 F (top & bottom). The minor peak at ~38 ml may be from elution of protein-free SDS molecules that exist. It is worthwhile discussing that, unlike previous studies (**Stenstam et al., 2001**), the surfactant (SDS) and the protein (HEWL), with a pI near ~11.3 (**Wetter et al., 1951**), are both negatively charged. In a similarly charged system, it has been shown previously (**Moren et al., 1999**), using NMR relaxation rates, that protein–surfactant micellar complexes are larger than protein-free micellar aggregates. From figure 3.2.2 F (top & bottom), HEWL-SDS complex was presented like an outer layer of bound micellar SDS to HEWL aggregates. Aggregates appear physically large but their molecular packing loose and disorganized as

evidenced from the fast segmental motion of the dansyl group (**Kumar, 2008**). It has also been argued that the micelle-like interaction between SDS and HEWL at high pH is hydrophobic in nature (**Chatterjee et al., 2002**). The AFM images might be tracking the conglomeration of HEWL monomers in the presence of surfactants. The presence of such surfactant mediated protein networks have been discussed and proposed previously for the lysozyme–SDS complex system (**Stenstam et al., 2001)**.

In presence of CTAB, It is likely that the HEWL–CTAB complex that is heterogeneous in size and shape accounts for the broad elution peak at ~20 ml. Overall, an elution peak at ~20 ml indicates that the protein is reasonably smaller and compact in the presence of CTAB, compare to SDS. A comparatively similar profile at three different times indicates that no major time-dependent changes in aggregate size/shape are taking place in the presence of CTAB. The elution volume observed beyond 35 ml is likely due protein-free CTAB molecules. Using AFM, Morphology of aggregates was also observed globular and smaller in size which is similar to gel filtration results. It is interesting to address that CTAB assist to HEWL aggregate in making compact and smaller size in pH 12.2 compare to SDS (see Fig 3.2.2 G and Fig. 3.2.1 F). Previously, it was shown that the formation of CTAB–denatured lysozyme complex arise at the beginning stage of refolding, effectively inhibited the formation of aggregate, leading to an assist in refolding (**Wang et al., 2005**). In presence of DTT, shifting of elution volume near 23-26.5 ml and appearance of globular and smaller compact morphology from AFM image (see Fig 3.2.2 H) indicates that HEWL exist like more compact and smaller in size similar to native. It is likely that DTT is assisting to disrupt the formation of intermolecular disulfide bond. It is known that disulfide bonds distrupt under alkaline conditions (**Anderson, 1975**), subsequently these may get oxidized again with a different cysteine thiol group leading to disulfide scrambling and intermolecular disulfide bonds which leads to stable growth of aggreates in pH 12.2.

3.3 Conclusions

1. HEWL in pH 12.2 forms multiple species of small and large aggregates.

2. HEWL spontaneously forms fibrils as well as heterogeneous population of globular aggregates in pH 12.2 at room temperature.

3. In presence of surfactant (SDS, CTAB) and DTT, fibril formation was not detected; however differences in size and morphology of globular aggregates were observed

4. DTT has a profound inhibitory effect on aggregation of HEWL at alkaline pH 12.2.

5. Tight bunching among lysozyme fibrils was observed.

Characterization of HEWL aggregates after prior incubation with tri-*N*- acetylchitotriose and N-Acetyl-D- glucosamine (NAG)

4.1 Introduction

The aim of this investigation was to identify if small molecules like enzyme inhibitors can be used to inhibit the aggregation of HEWL at pH 12.2 and facilitate recovery of functional protein. Stabilizing the protein into its native state against misfolding and aggregation by increasing the activation energy barrier for unfolding, can slowdown the aggregation kinetics was studied **(Hammarstrom et al., 2003)**. Previously inhibition of HEWL dimerization at alkaline pH was first observed by Sophianopoulos where glucose derivatives (NAG and its disaccharide and trisaccharide derivatives) displayed different degrees of inhibition against lysozyme aggregation **(Sophianopoulos, 1969)**. The magnitude of their efficacy against HEWL dimerization was observed in order of trisaccharide> disaccharide> monosaccharide; however effect of these compounds on fibril formation was not studied. Does pre-incubation of HEWL with its competitive inhibitor, chitotriose (or its smaller sugar derivatives) at neutral pH 7 have any influence on its aggregation and fibrillogenesis in pH 12.2? In favour of this question important results are represented.

4.2 Results and discussion

4.2.1 Size of aggregates

To get comparative information with respect to size and heterogeneity of HEWL oligomers in presence of additives, size-exclusion chromatography experiments were carried out. The elution volume of the eluting protein species is indicative of its size and shape in solution. Fig. 4.2.1 C shows the elution profiles acquired for control, NAG and chitotriose samples at early (column X) and late (column Y) time of incubation. HEWL at pH 7 showed a single elution peak at ~28 ml (see Fig. 4.2.1 A).

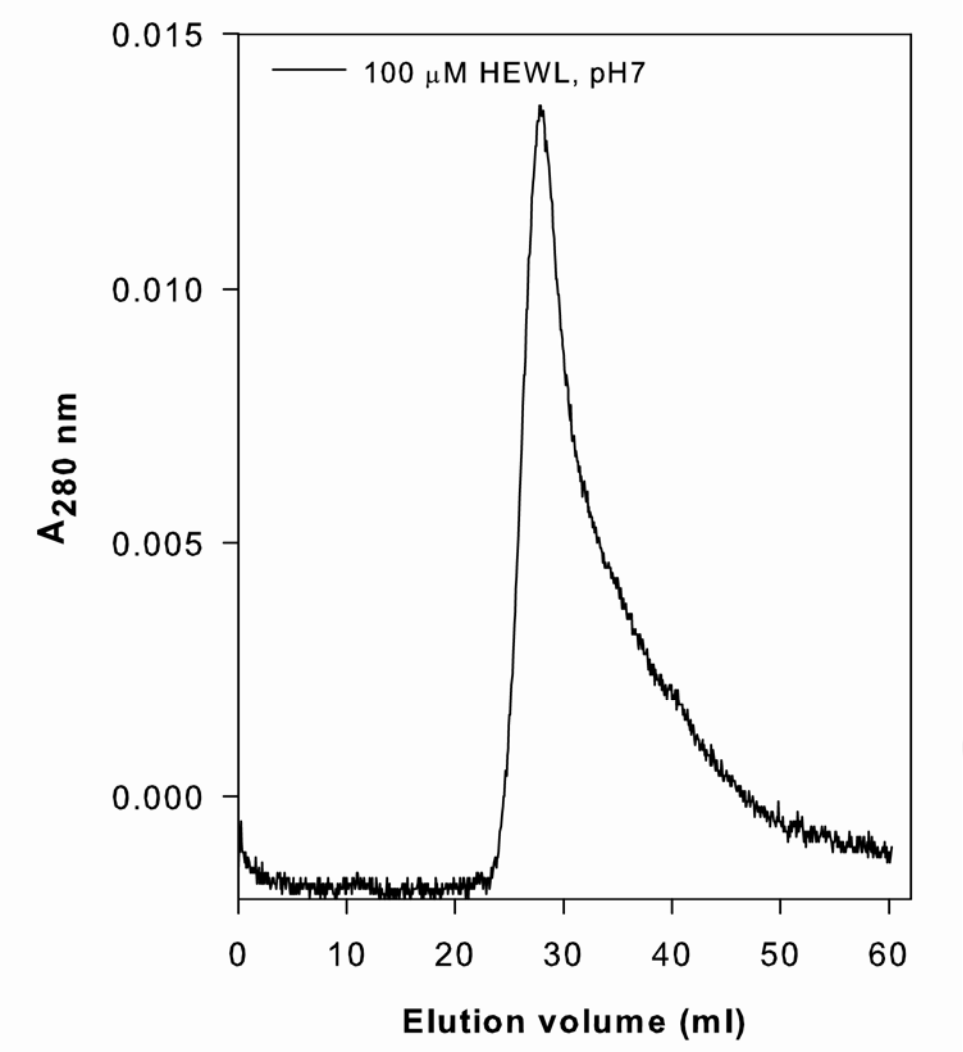

Figure 4.2.1A: Gel filtration elution profiles of lysozyme (100 μM), incubated in pH 7 at 298 K.

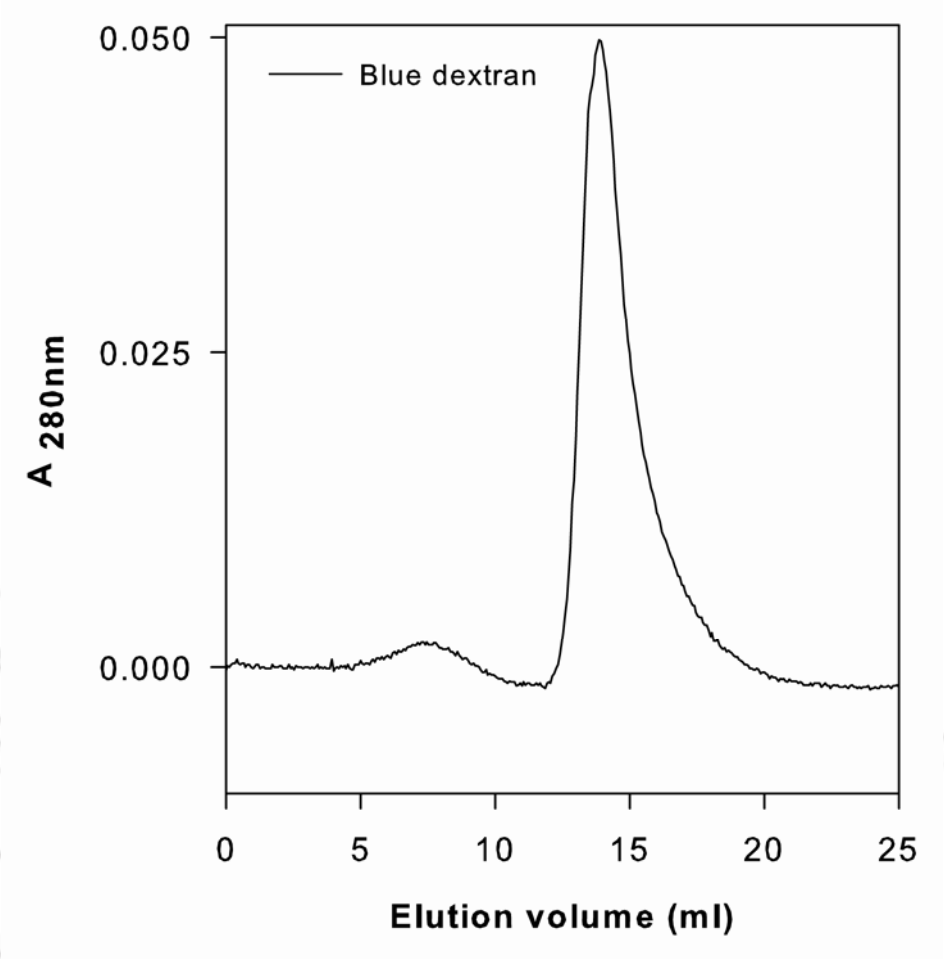

Figure 4.2.1 B: Gel-filtration elution profiles of blue dextran 2 mg/ml.

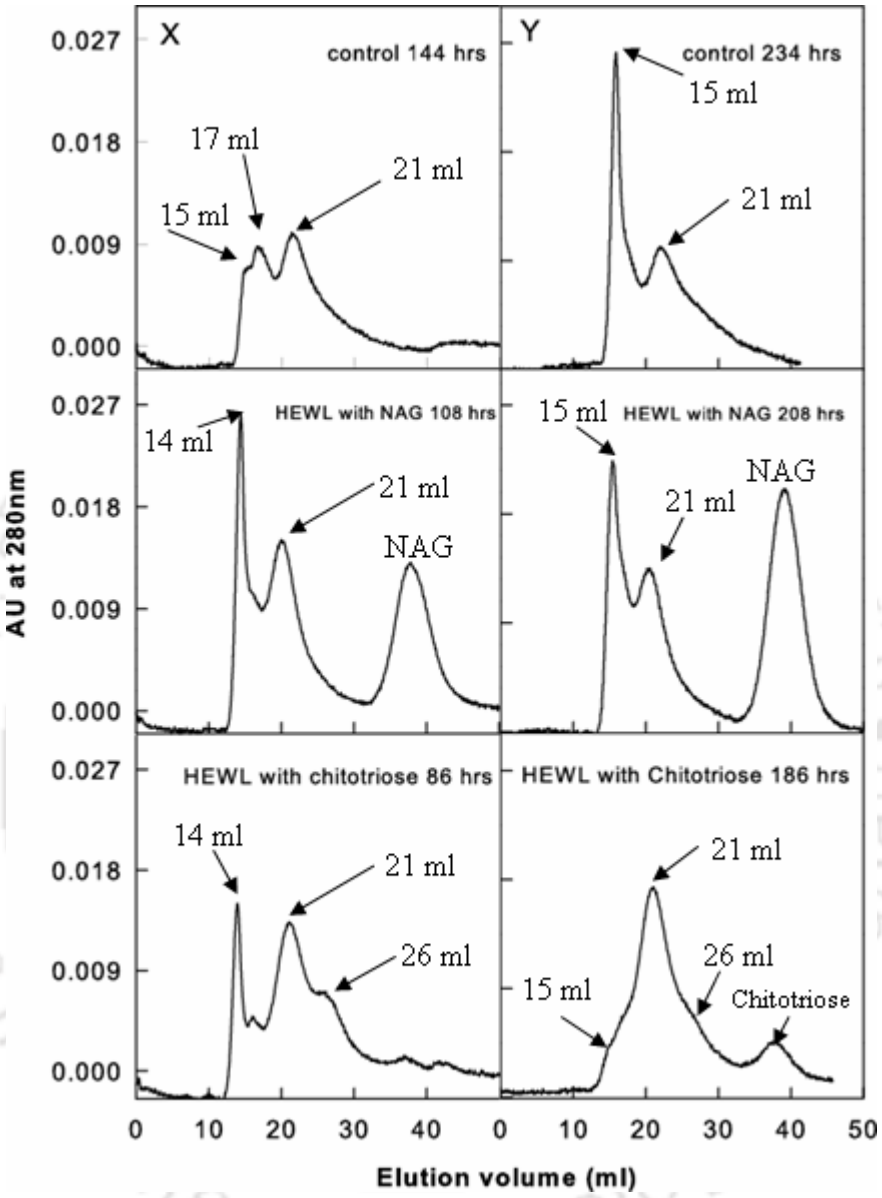

Figure 4.2.1 C: Gel-filtration elution profiles of lysozyme (100 µM), incubated in pH 12.2 at 298 K with or without (control) additives, for the times indicated, as monitored using absorbance at 280 nm. Column X indicates elution profiles at earlier times, while column Y shows the elution profiles after incubation period of ~144 h.

From figure 4.2.1 C, Column 'X' shows elution of a large aggregate tracked as a shoulder (~15 ml) in control, peak at (~14 ml) in NAG and chitotriose samples. Subsequently, peaks at 17 ml (control) and 16 ml (chitotriose) are visible. NAG sample shows a shoulder at 16 ml. Later all three samples display a prominent peak between 21 and 22 ml, which may arise from oligomers of HEWL. At higher elution volumes, Only chitotriose sample shows a clear shoulder at ~26ml in contrast to NAG and control samples. This peak is quite closer to elution volume of native HEWL and is likely to be the sole functional fraction in the mixture of protein. Peaks observed later on at 37–38 ml, in NAG and chitotriose samples may originate from free species of NAG and chitotriose that were in excess. Column 'Y' in Fig. 4.2.1 C reveals a fairly less heterogeneous elution profile after week-long incubation in alkaline pH. Both control and NAG samples show a prominent peak near 15 ml, while chitotriose sample reveals a small shoulder, consistent with SDS-PAGE data that revealed absence of large aggregates (**Kumar et al., 2008**). The prominent peak near 21–22 ml observed in column X and Y is present at almost identical position and similar intensity in all samples, suggesting that the oligomers are stable over several days. Possibly functional species eluting near ~26 ml observed in column X with appearance like shoulder in column Y as perhaps due to its diminished population. Unbound NAG and chitotriose from their respective samples show a rise in intensity at their elution (38–39 ml) in comparison to column X elution profiles. This can happen owing to loss of binding affinity between NAG or chitotriose and HEWL after prolonged incubation periods.

4.2.2 Helical structure

It is worthwhile to observe the helical conformation of HEWL in presence of additives like chitotriose. Previous study has shown that HEWL activity changes in presence of NAG, chitotriose and control samples (**Kumar et al., 2008)**. It means that HEWL may retain native conformations in presence of these additives. To investigate this in detail, the far-UV circular dichroism spectrum of HEWL samples was measured. Fig. 4.2.2 shows that after week-long incubation at pH 12.2, in presence of chitotriose HEWL sample shows a strong positive ellipticity near the 190 nm along and minimum at 208 nm, while in presence of NAG, HEWL sample shows a positive peak at 192 nm along and minimum near 208 nm. The control

sample shows a reduced positive ellipticity near 190 nm in comparison to chitotriose, likewise a minimum at 205 nm that is consistent with earlier data (**Kumar et al., 2008)**. Beyond 210 nm, the CD spectra of NAG and control samples remains fairly similar. The chitotriosoe sample shows a negative ellipticity at 208 nm alongwith a positive band near 190 nm coupled with absence of shoulder at 222 nm in comparison to native HEWL (**Kumar et al., 2008).** This suggests a low, but significant presence of helical content in presence of chitotriose. It apperas control sample possesses significantly reduced helical content in comparison to NAG and chitotriose samples.

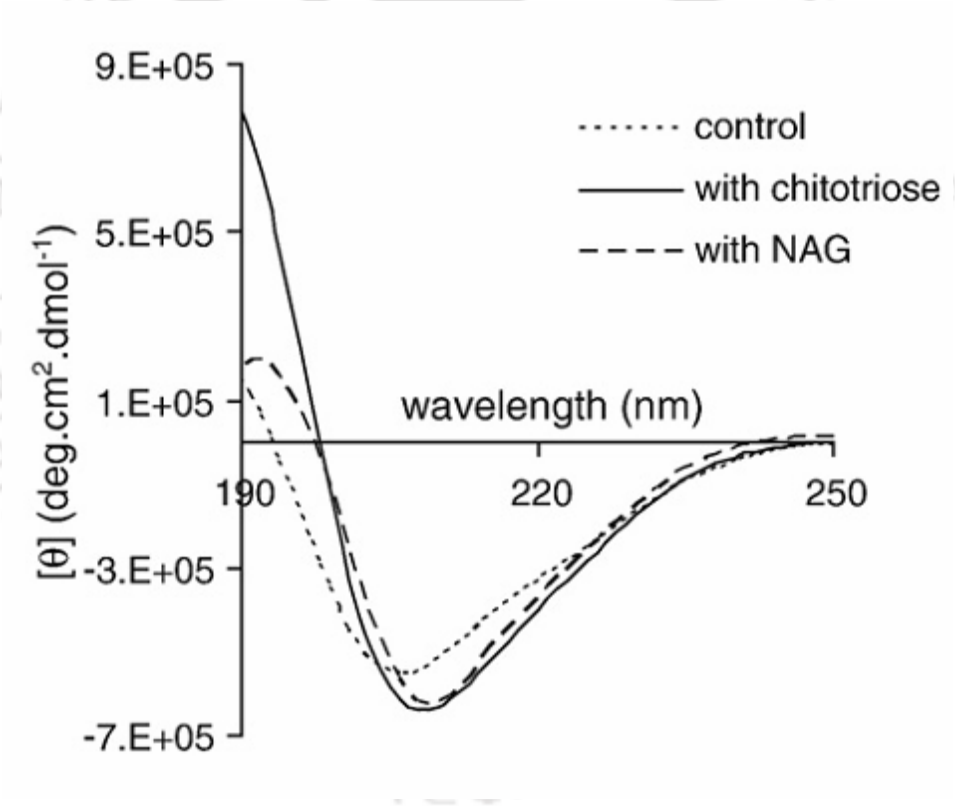

Figure 4.2.2: The far-UV CD spectra of HEWL (molar ellipticity against wavelength), are shown after incubation for 8 days in pH 12.2 at 298 K in presence of different additives as indicated and control. See 'Materials and methods' for more details.

4.2.3 Accessibility of sulfhydryl groups

Earlier work from our group (**Kumar et al., 2008)**, has indicated that intermolecular disulphide bonds between free thiol groups in HEWL play an important role for the stability

and assembly of aggregates at alkaline pH 12.2. Therefore based on this hypothesis, we proceeded to measure the accessibilty of free thiol groups of HEWL in presence of NAG and chitotriose. The concentration of free thiol calculated from the cysteine standard curve see in Fig. 4.2.3 A. Fig. 4.2.3 B shows that while control samples showed a maximum presence of free thiols after three days of incubation, while samples containing NAG or chitotriose revealed significantly lower concentration of free thiols. Moreover, while control samples displayed a steady decrease in concentration [–SH] with time (70–170 h), samples containing NAG and chitotriose showed an early drop of free [–SH] during period of 72–144 h prior to plateauing. The decrease in thiol concentration levels occurs due to formation of intermolecular –S–S-bonds and perhaps inaccessibility of –SH groups to DTNP owing to growth of aggregates. The minor increase in [–SH] for chitotriose samples in comparison to NAG is not significant. Thus it appears that reduced but significant growth of aggregates does occur in presence of NAG or chitotriose also. The thiol accessibility experiments show that concentration of free [–SH] is regionably lower at 72 h (Fig. 4.2.3B) in both NAG and chitotriose samples compare to the control.

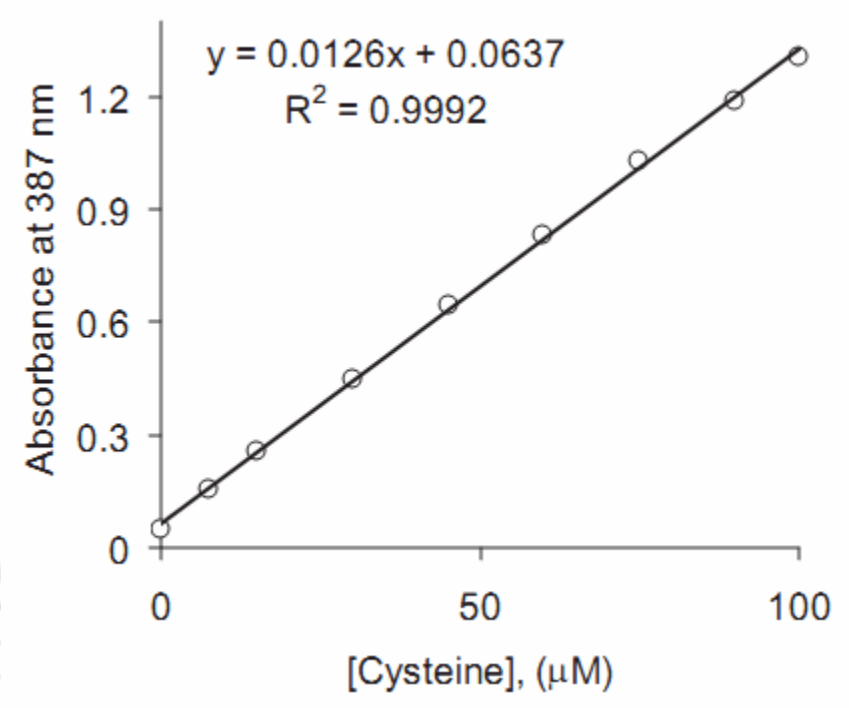

Figure 4.2.3 A: Cysteine standard curve for thiol estimation.

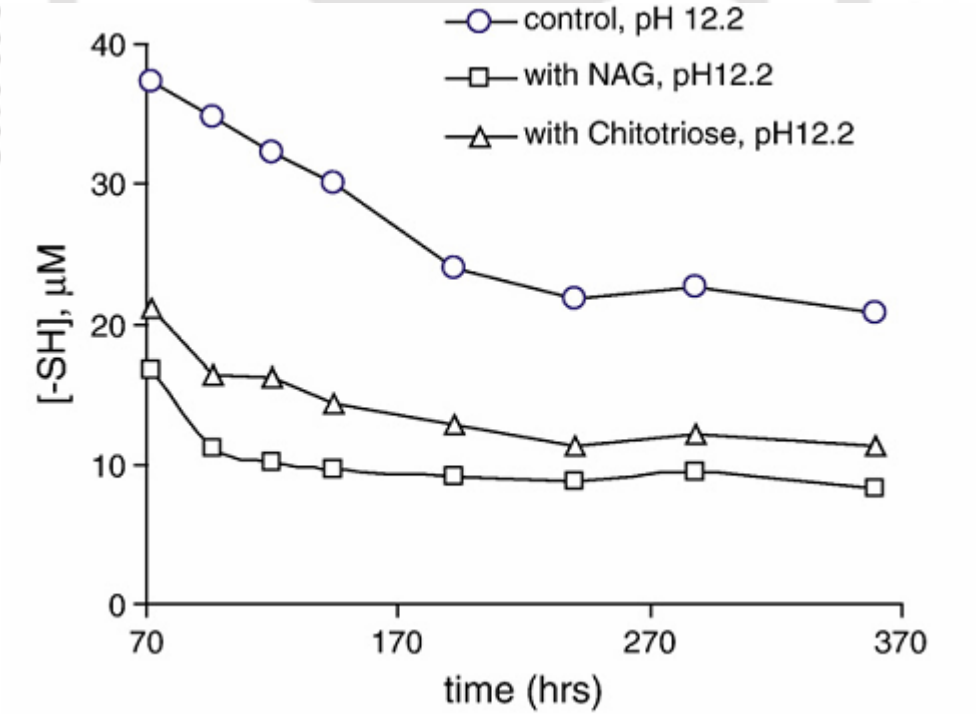

Figure 4.2.3 B: Changes in the concentration of free thiol groups in HEWL (5 µM) at different times subsequent to incubation in pH 12.2 with chitotriosoe and NAG or without additives (control) as indicated.

4.2.4 Morphology

Employing the atomic force microscopy, morphology of HEWL aggregates like fibrillar aggregates and globular aggregates in presence and absence of chitotriose and NAG were investigated. In Fig. 4.2.4 A shows amorphous aggregates of HEWL (~200 nm, long uncorrected axis), while 4.2.4 B reveals ordered aggregates of HEWL resembling amyloid fibrils (~30 nm uncorrected thickness) in the absence of NAG and chitotriose. These observed different morphologies suggest that protein exist as a mixture of amorphous aggregates as well as fibrillar forms in the pH 12.2. Similarly, in presence of NAG at pH 12.2, HEWL was shown a heterogeneous mixture of amorphous aggregates (100–300 nm, uncorrected long axis) in Fig. 4.2.4 C, along with clearly distinguishable fibrils (~ 25 nm thickness) was visible in figure 4.2.4 D. These results are supported from the high fluorescence intensity observed with ThT in HEWL pH 12.2 and in presence of NAG (**Kumar et al., 2008**). In Figure 4.2.4 E and F, show morphology of HEWL with prior overnight incubated in pH 7 of chitotriose under alkaline condition for 41 and 26 days of incubation, respectively. But neither the ordered fibrillar HEWL nor large amorphous aggregates were exhibited in presence of chitotriose, although, small oligomers (~150 nm×50 nm) were found.

A

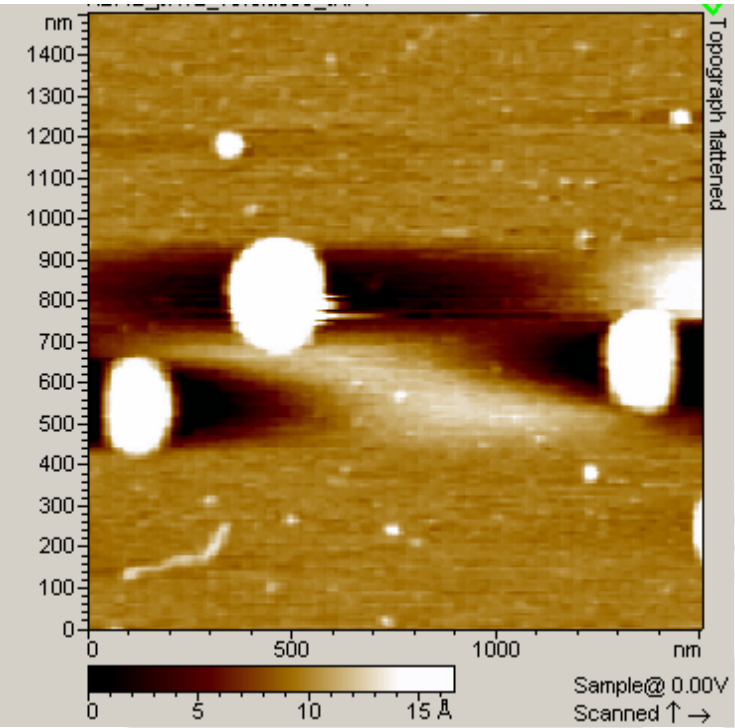

Figure 4.2.4 A: Topograph image of HEWL amorphous aggregates in pH 12.2 at 298 K, after incubation of 37 days.

B

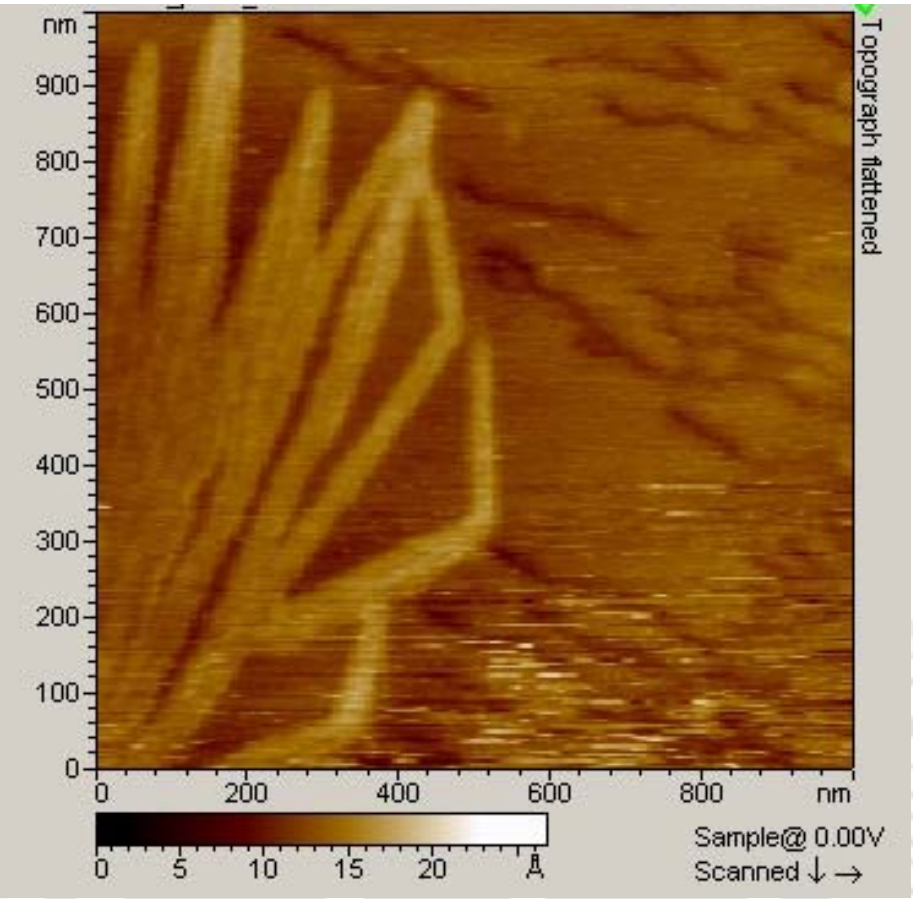

Figure 4.2.4 B: AFM topogarph image of HEWL fibrillar structure in pH 12.2 at 298 K after 37 days of incubation.

C

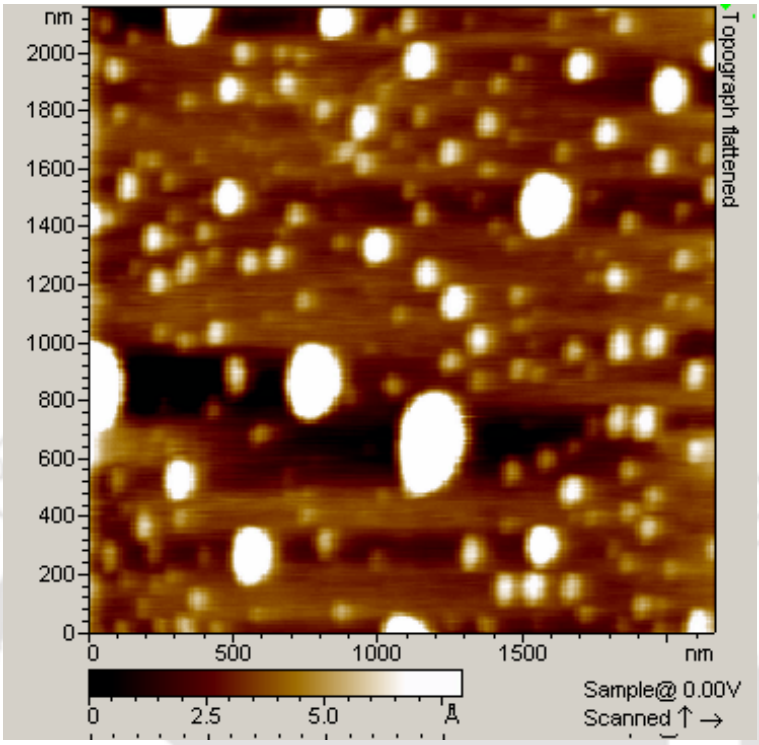

Figure 4.2.4 C: AFM topograph image of HEWL amorphous aggregates in pH 12.2 in presence of NAG, after 25 days incubation period.

D

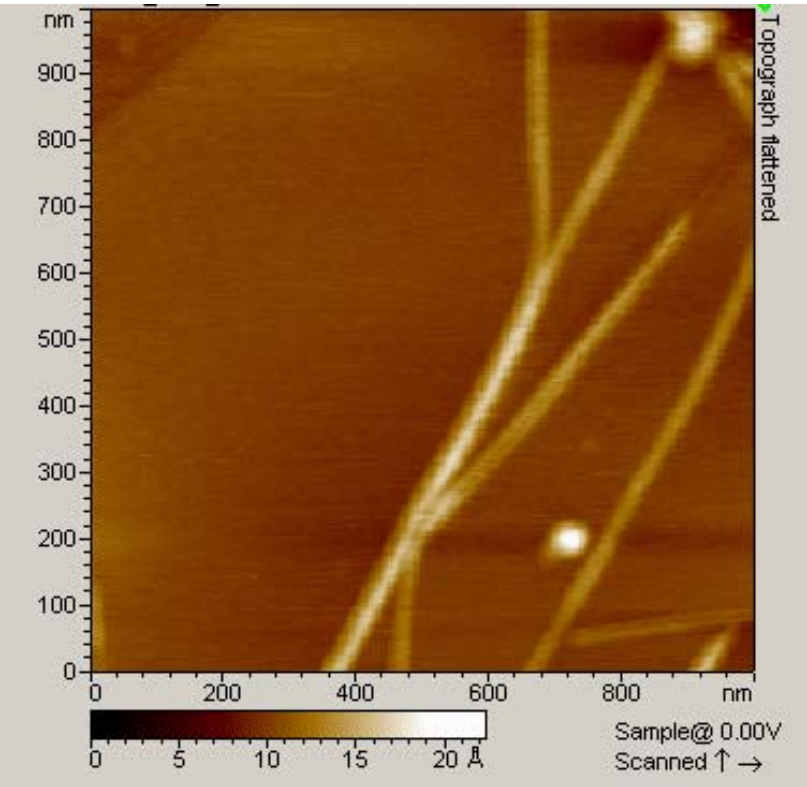

Figure 4.2.4 D: AFM topograph image of HEWL fibrillar structure in pH 12.2 in presence of NAG, after 35 days incubation time.

E

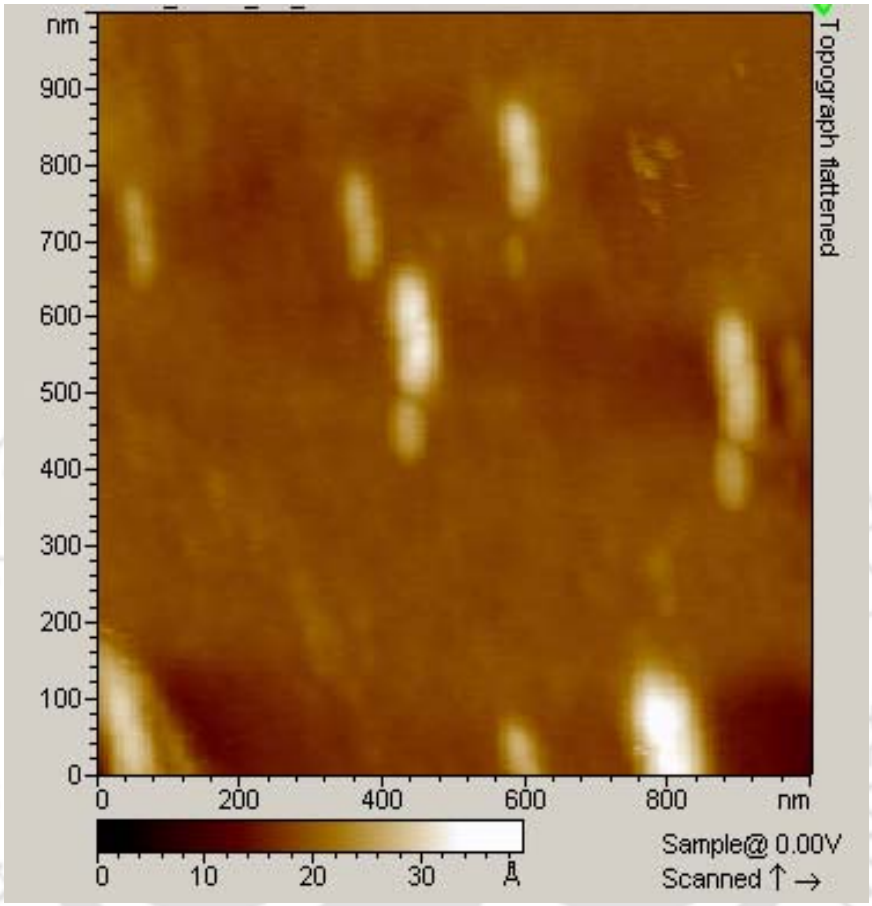

Figure 4.2.4 E: AFM topograph image of HEWL oligomer in pH 12.2 in presence of chitotriose, after 41 days of incubation period.

F

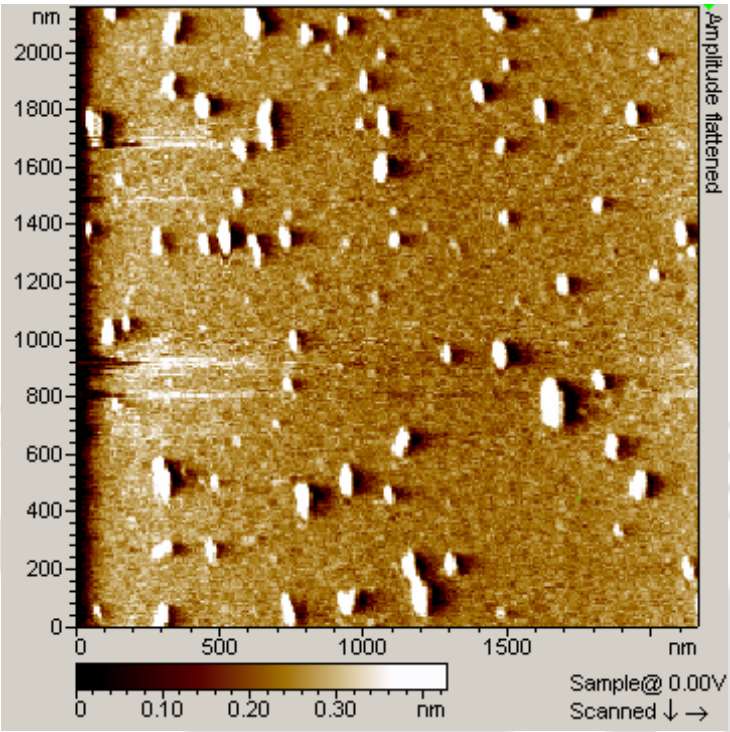

Figure 4.2.4 F AFM amplitude image of oligomer of HEWL pH 12.2 in presence of chitotriose, after 26 days of incubation period.

It will be worthwhile to discuss the results where it was observed change in size of aggregates, exposure of free [–SH], helical content and morphology in presence of chitotriosoe, NAG and control. The gel- filtration elution profile indicates prominently native like HEWL fraction (eluting near 26 ml) at 186 h of incubation, including at 86 h some small fraction seems to be native. With decreasing the size of aggregate, simultaneously helical content was retained, which appears from the CD data (see Fig. 4.2.2). Apart from these, AFM images reveal absence of fibril and the mixture of oligomers, which is consistent from the elution profile of chitotriose (see Fig. 4.2.1 C). All these results display that HEWL oligomerisation is not completely suppressed in prior presence of chitotriosoe, while control sample display fibrillar as well as big globular aggregates, incubated in pH 12.2. Perhaps, in presence of chitotriose HEWL slows down the aggregation kinetics of HEWL at significantly, enabling recovery of a significant fraction of functional protein even

after one week of incubation at alkaline pH. This has also observed from activity of bound chitotriose and NAG to HEWL (**Kumar et al., 2009**). It was observed control sample possesses significantly reduced helical content in comparison to NAG and chitotriose samples. In presence of NAG, gel filtration data display heterogeneous size of aggregates, which could be both larger and smaller aggregates, even at later time of incubation (208 h). It also retains a lower extent of helical content in comparison to chitotriose sample. However different morphology of these aggregates (in presence of NAG) was observed like globular and well organized branched fibrillar structure (see 4.2.4 C & D), which was not seen in presence of other sugar molecule earlier. This is consistent with our gel-filtration result where big aggregates eluted near void volume (~15 ml), while no shoulder was observed near 26 ml.

The free [–SH] results of HEWL with NAG and chitotriose suggest that the presence low level of free [-SH] are either sufficient or does not have role in fibril formation rather larger aggregates formation. This could be due to stabilization of protein sufficiently against unfolding to minimize exposure of disulfide bonds to the alkali.

These findings clearly have evidence that trisugar like chitotriosoe are able to arrest further HEWL aggregation and fibrillization at pH 12.2, whereas the single sugar, NAG does not show any inhibitory effect. With reference to earlier findings, like Sophianopoulos work (**Sophianopoulos et al., 1969**), these finding on suppression of aggregation with NAG and chitotriose are consistent with earlier work and unlike his study, the present investigation was involved with a relatively more dilute protein (~100 μM) and a much harsh pH (12.2). Interestingly, it can address that most of the investigation have been presented on inhibition of HEWL aggregation at acidic pH (~2) using small molecules like, 4-aminophenol and 2-amino-4-chlorophenol (**Vieira et al., 2006**), rifampicin (**Lieu et al., 2007**), indole and its derivatives (**Morshedi et al., 2007**) and p-benzoquinone (**Wang et al., 2006**). Zhou and coworkers showed that crowding HEWL solutions at pH 2 with BSA with or without Ficoll 70 inhibited amyloid fibril formation (**Zhou et al., 2008**). However our investigations demonstrate that inhibitor of lysozyme enzyme like chitotriose significantly suppress the fibrillization in pH 12.2. Putting altogether, our results emphasize to discuss that chitotriosoe could be the screen as inhibitor molecule against the human lysozyme systemic amylodosis. Interestingly, chititriose has shown the binding property to human lysozyme (**Kuramitsu et al., 1975**).

4.3 Conclusions

1. The trisaccharide, tri-*N*-acetylchitotriose inhibits growth of big aggregates which could be used as specific suppressor molecule to arrest the HEWL aggregation at alkaline pH 12.2.

2. The tri-*N*-acetylchitotriose inhibits for further fibrillation but N-acetyl-D-glucosamine favours the fibrillation process of HEWL in pH 12.2 at later incubation time.

3. In comparison to tri-*N*-acetylchitotriose NAG was a less potent suppressor of HEWL aggregation.

4. Free [–SH] level of HEWL with NAG and chitotriose suggest that the presence of reduced level free [-SH] was either sufficient or does not have role in fibril formation. However HEWL amyloidogenic inhibition mechanism not fully studied in presence of chitotriosoe. This can investigate in future at very low concentration of protein where it likely to form oligomer as well as fibrillar structure.

Decrease in size of hen egg white lysozyme aggregates with decrease in monomer concentration from micro to nanomolar in alkaline pH

5.1 Introduction

The terminal products in the protein aggregation pathway, the ordered aggregates like mature amyloid fibrils, have been isolated and structurally characterized (**Nelson et al., 2005**). However, the intermediates in this pathway, like nucleated species and the 'soluble aggregates' or oligomers formed post-nucleation, have proved difficult to isolate and characterize. Ironically, it is these oligomers which are implicated to be toxic in vivo and responsible for cell death (**Bucciantini et al., 2002, Lambert et al., 1998, Walsh et al., 2006**). Knowledge of the factors favoring the growth kinetics of oligomers and amyloid fibrils are critical to develop strategies to control and arrest their formation. The normal physiological concentrations of proteins like Aβ are in the nM range (**Lue et al., 1999, Nitsch, et al., 1995**), yet majority of studies in vitro require concentrations that are far higher (~μM) to induce Aβ aggregation. In order to mimic physiological conditions, it would be worthwhile to investigate protein aggregation at sub-micromolar concentrations. Consequently, proteins and solution conditions that induce aggregation at nM concentrations are ideal models to study. Low monomer concentrations are also likely to facilitate isolation of oligomers which are important players in cytotoxicity. Hen egg white lysozyme (HEWL), which has been shown to form amyloid fibrils in vitro under a plethora of conditions like acidic pH, alkaline pH, disulphide reduction, guanidine hydrochloride, ethanol, mechanical agitation and so on, is currently among the best known model proteins to investigate protein aggregation (**Swaminathan et al., 2011**). Here in this work HEWL used as a model system to investigate the different oligomeric intermediates in HEWL aggregation pathway at pH 12.2 and this can be kinetically trapped and their structural features monitored at near equilibrium by varying the initial monomer concentration between 120 μM and 0.3 μM. Such oligomers are shown to remain proficient to form amyloid fibrils. Our results reveal that average size of these oligomeric intermediates diminishes gradually when monomer concentration is reduced from 120 μM to 0.3 μM.

5.2 Results and discussion

5.2.1 Onset of aggregation measured by fluorescence resonance energy transfer (FRET)

The association of monomers is the initial step of aggregation. Tracking the initial steps in aggregation events require sensitive techniques and for this aim FRET was employed. Previously this event has been studied using FRET between dansyl (donor) and dabcyl (acceptor) probes labeled at N-terminus lysine (**Adair et al., 1994**). Using FRET, an aggregation event was monitored in pH 12.2 at sub-micromolar concentrations. The gradual decrease in emission intensity and change in λ_{max} was shown in Fig 5.2.1C-F and no change was observed in pH 7, Fig. 5.2.1A-B. Based on the integrated area of emission intensity, intermolecular FRET efficiency was calculated (see Eq. in material and methods) from Figure 5.2.1G reveals the rise in intermolecular FRET efficiency with time when dansyl and dabcyl labeled HEWL were mixed with excess of unlabeled HEWL at pH 12.2. The early rise in FRET (0-6 hrs) is followed by saturation after 10 hrs for all monomer concentrations from 0.3 to 120 μM, suggesting that growth of aggregates reaches at equilibrium after 10 hours of exposure in pH 12.2. Here both the magnitude and rate of change in FRET efficiency are observed to increase with decrease in monomer concentration from 120 to 3 μM. The apparent faster kinetics and higher magnitude of FRET efficiency at lower (3 and 0.3 μM) compared to higher (50 and 120 μM) concentrations may be accounted to the effect of dilution. There are 4 unlabeled proteins for every donor/acceptor labeled HEWL at 3 and 0.3 μM, while this number is 238 at 120 μM. The presence of multiple acceptors in the neighborhood of a single donor, which can significantly enhance FRET, is unlikely especially at higher concentrations. For monomer concentrations 3 and 0.3 μM which possess the same ratio of donor or acceptor labeled HEWL to unlabeled HEWL, the marginal increase in FRET efficiency in 0.3 μM is perhaps due to relatively smaller size (more proximity) of oligomers compared to 3 μM. The faster rate of increase in FRET efficiency at 0.3 μM hints appreciable aggregation kinetics at low concentrations. FRET efficiency for 50 μM HEWL was significantly less at pH 7 compared to 12.2, highlighting the role of alkaline pH in promoting association of monomer. The error bars at pH 7 are higher because a small fraction of HEWL can form dimers at neutral pH as reported previously (**Sophianopoulos et al., 1961**).

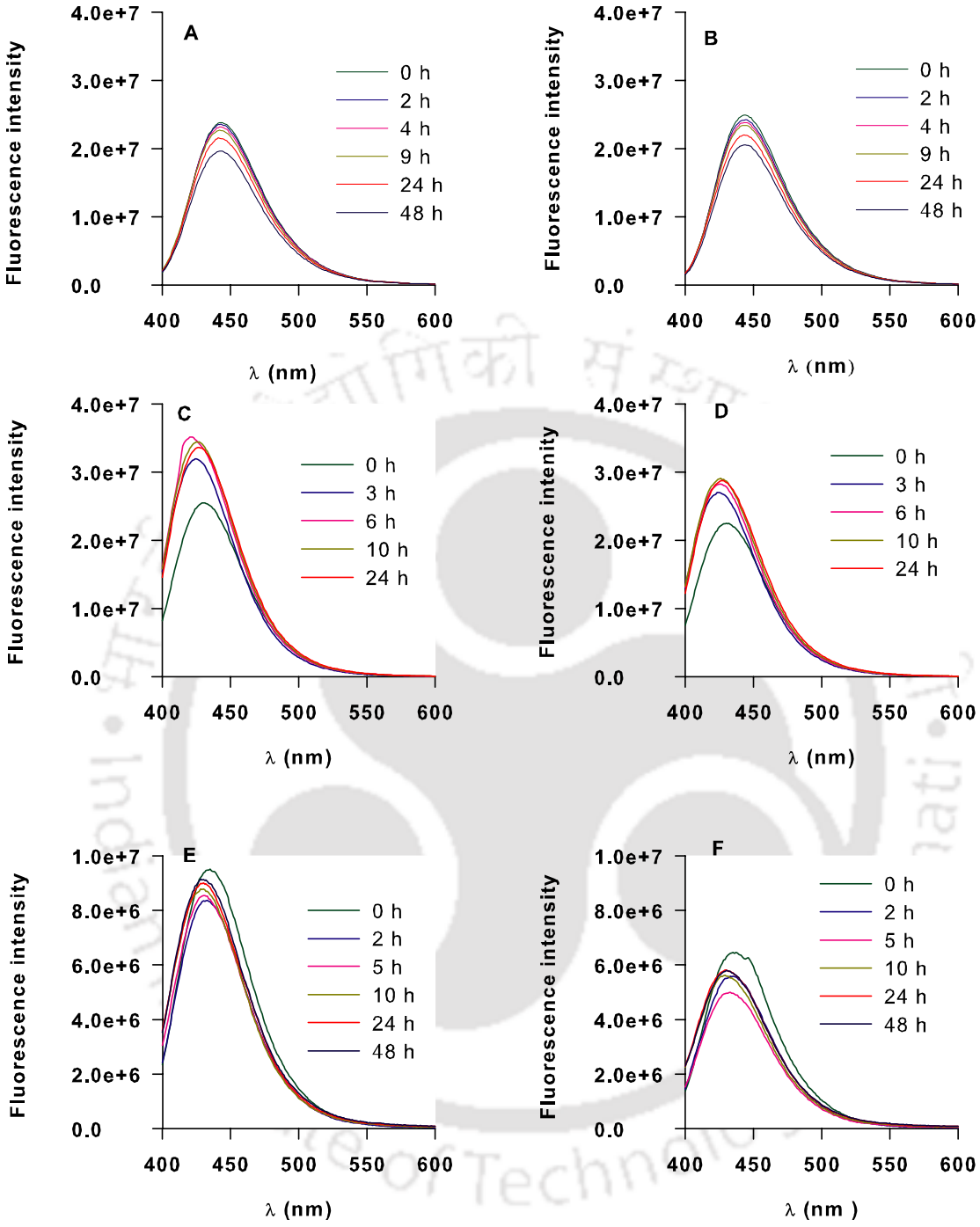

Figure 5.2.1: (A) Spectra of 50 µM HEWL with 0.5 µM dansyl-HEWL at different incubation times in pH 7.0. **(B)** Spectra of 50 µM HEWL with 0.5 µM dansyl-HEWL and 0.5 µM dabcyl-HEWL at different incubation times in pH 7.0. **(C)** Spectra of 120 µM HEWL with 0.5 µM dansyl-HEWL. **(D)** Spectra of 120 µM HEWL with 0.5 µM dansyl-HEWL and 0.5 µM dabcyl-HEWL **(E)** Spectra of 0.3 µM HEWL with 0.05 µM dansyl-HEWL **(F)** Spectra of 0.3 µM HEWL with 0.05 µM dansyl-HEWL and 0.05 µM dabcyl-HEWL. **Fig. C-F** samples were incubated in pH 12.2 at various times.

FRET data fitted using equation give below.

$$r_{ss}(t) = r_{ss}^{\infty} - (r_{ss}^{\infty} - r_{ss}^{0})e^{-kt} \quad 5.2.1$$

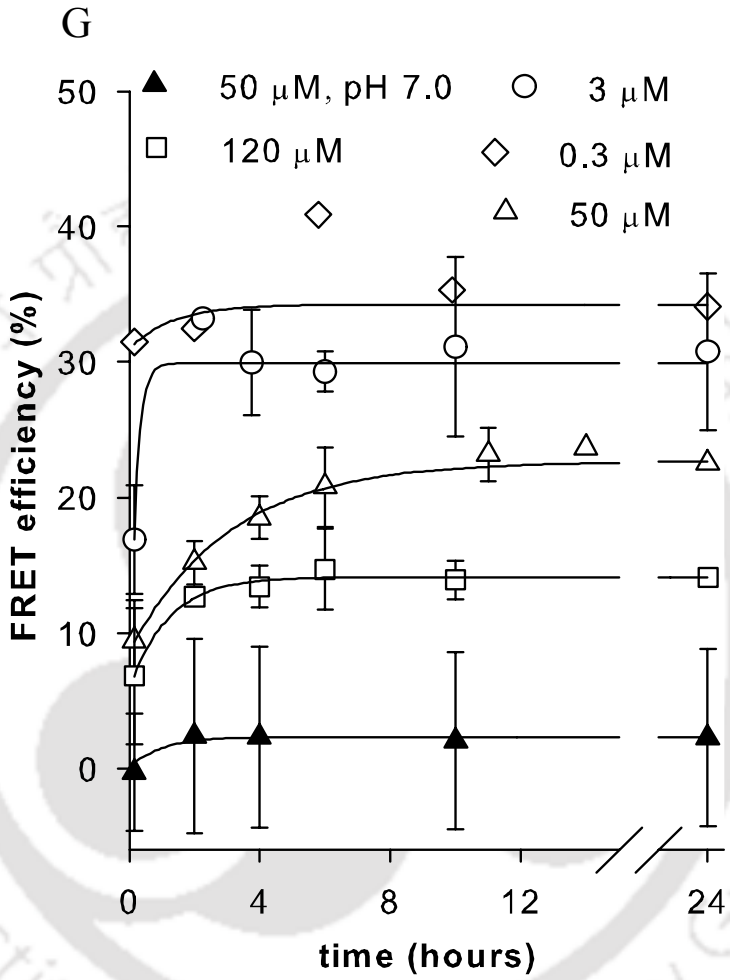

Figure 5.2.1 G: FRET efficiency of HEWL labeled with dansyl-dabcyl pair at different time of incubation in pH 7.0 and pH 12.2.

5.2.2 Changes in local environment inside aggregates

After probing the magnitude and rate of formation of aggregates, it was interesting to investigate the microenvironment in the aggregate interior. The non-polar nature of such interiors, arising from shielding of bulk water, is indicative of the aggregate architecture.

5.2.2.1 Using dansyl conjugated HEWL

Naphthalene derivative, dansyl chloride is well known probe, energetically favors to bind inside a non-polar pocket of the protein. Dansyl probe emission intensity and peak wavelength are dependent on surrounding polarity (**Brand, et al., 1972**); therefore this probe was used for tracking the change in local environment inside aggregates. A fast and profound dip (blue shift) in emission λ_{max}, was noticed for 120 µM HEWL, which is indication of a developing hydrophobic environment around the dansyl probe, (see Fig. 5.2.2.1 A), while lower concentrations show a more gradual and shallower dip trend in emission λ_{max} with time that is noticed clearly concentration dependent. The dip feature reflects growth based changing in molecular packing around dansyl probe inside the aggregate. Similarly, maximal increase in normalized total emission intensity was observed at pH 12.2 for 50 & 120 µM concentrations, while 2 µM & 0.3 µM shown marginal increase and slight dip line, correspondingly. Here too, the magnitudes of changes in quantum yield (0.9-1.4 fold) were clearly proportional to HEWL monomer concentration.

5.2.2.2 Using ANS

A covalently conjugated dansyl probe does not enjoy full freedom to available microenvironments in the entire aggregate sample. Hence ANS was selected for monitoring exposed hydrophobic regions to entire aggregates, which is a well known fluorescent probe which preferentially non-covalently binds to the exposed hydrophobic regions of protein displaying enhanced fluorescence intensity and blue-shifted emission compared to water (**Stryer, 1965 & 1968**). Figure 5.2.2.2 E shows a gradual decline (blue shift) in emission λ_{max} of ANS (see Fig. 5.2.2.2 A-D for spectra) with time, for concentrations 3-120 µM HEWL at pH 12.2, eventually decreasing gradually with lowest value for 120 µM followed by 50, 10 and 3 µM in that order. HEWL at 300 nM is nearly insensitive to ANS perhaps due to lower protein concentration. HEWL at pH 7 is fairly insensitive to ANS due to non-

availability of exposed hydrophobic sites in the native protein. In figure 5.2.2.2 F, the increase in good extent of total normalized intensity with time is displayed by 120 μM, followed by 50, 3 & 10 and 300 nM in progressive order. The concentration dependent trends in both the blue emission spectral shift and increase in quantum yield of ANS with time are consistent with a quantitative increase in number exposed hydrophobic pockets inside growing HEWL aggregates (which attract ANS) as one moves from 0.3 to 120 μM HEWL.

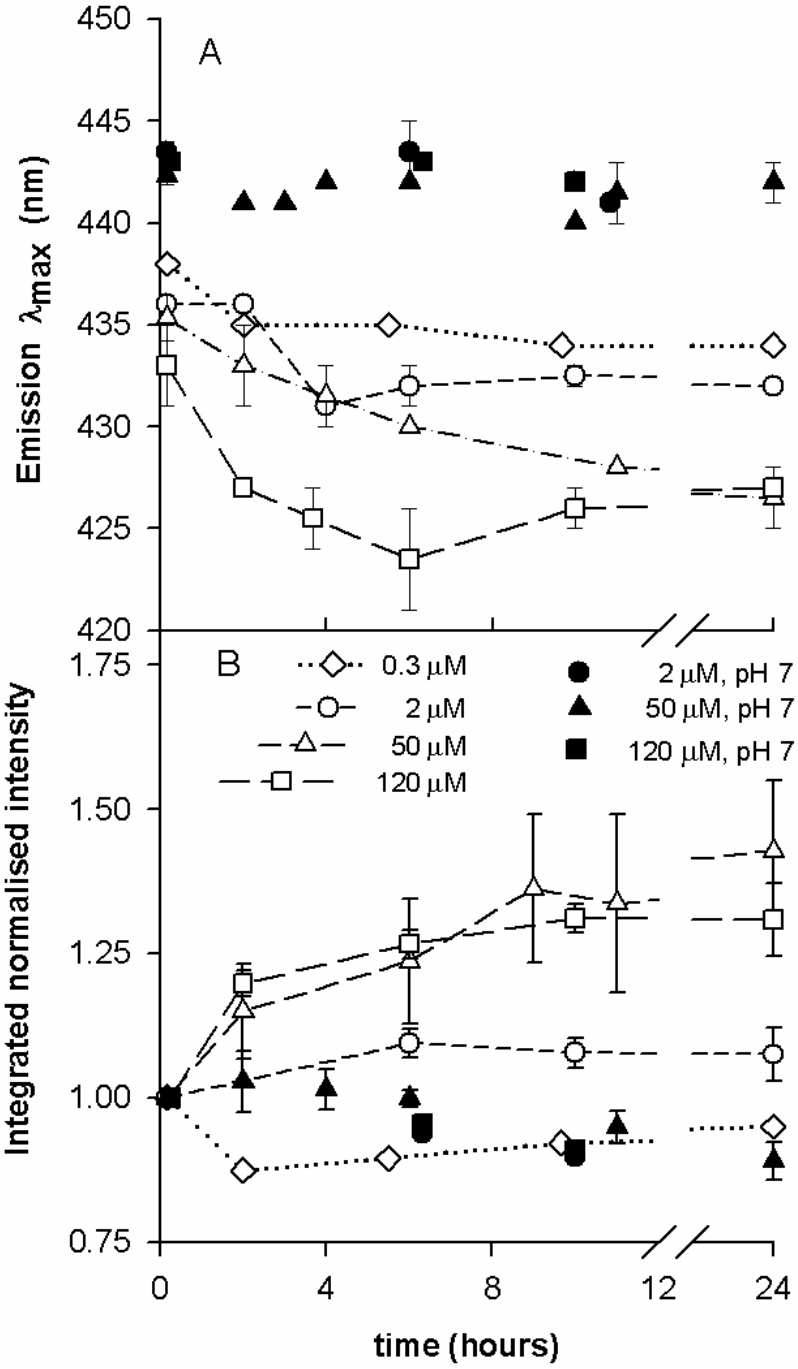

Figure 5.2.2.1: Dansyl-HEWL fluorescence emission. (A) Changes in emission λ_{max}. (B) Integrated normalized emission intensity of dansyl-HEWL conjugates (0.05 μM for 0.3 μM HEWL, 0.5 μM for others) are shown at different time intervals subsequent to incubation of HEWL at concentrations 0.3, 2, 50 & 120 μM in pH 12.2 and 2, 50 & 120 μM in pH 7.

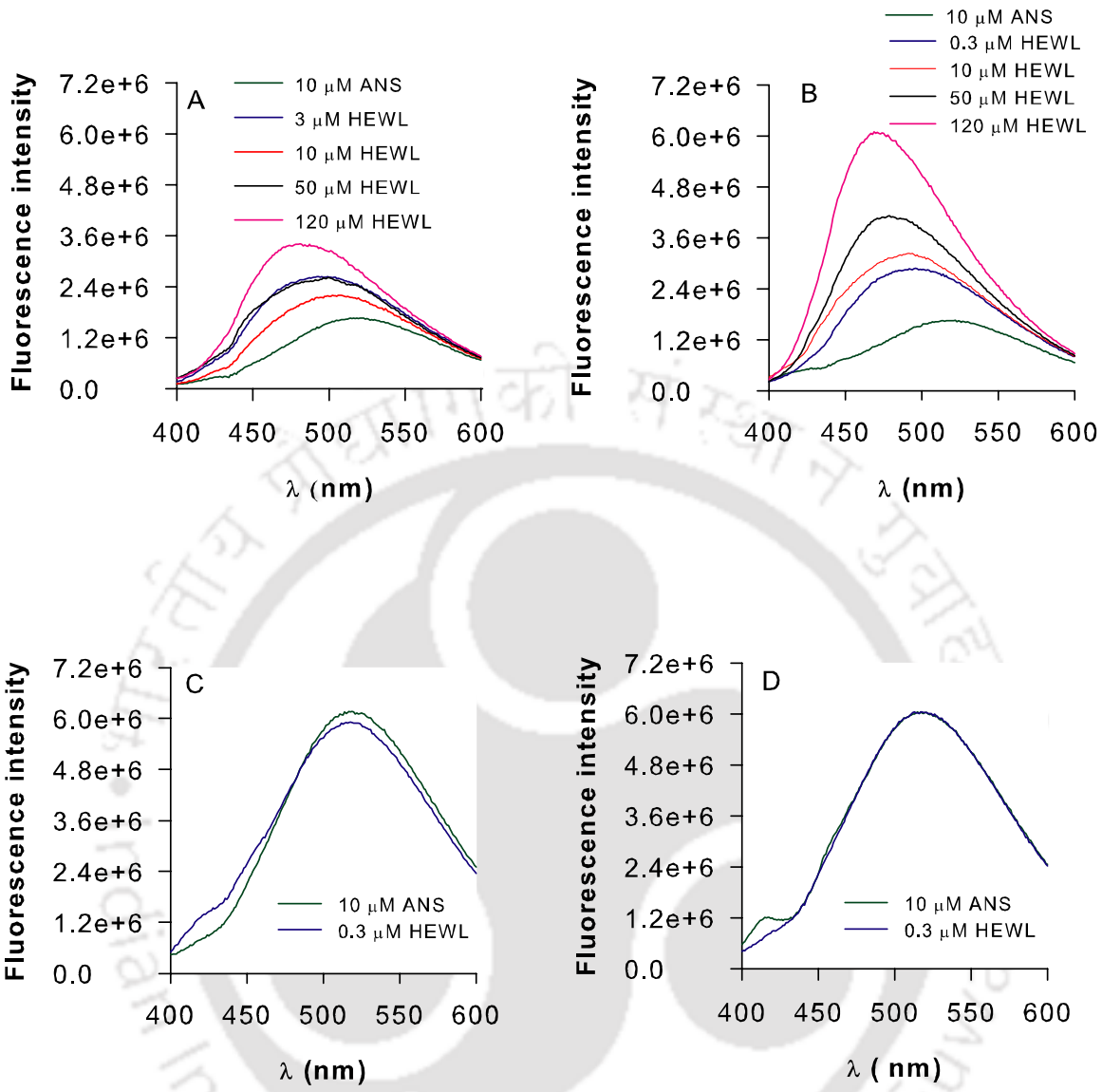

Figure 5.2.2.2: (A) Spectra of 10 µM ANS in absence and presence of HEWL (3 µM in assay cuvette) taken from HEWL samples incubated for 6 hours in pH 12.2 at concentrations 3, 10, 50 & 120 µM. **(B)** Spectra of 10 µM ANS in absence and presence of HEWL (3 µM in assay cuvette) taken from HEWL samples incubated for 24 hours in pH 12.2 at concentrations 3, 10, 50 & 120 µM. **(C)** Spectra of 10 µM ANS in absence and presence of 0.3 µM HEWL incubated for 6 hours in pH 12.2. The sample was excited at 380 nm (1 nm slit width) and emission collected with a slit width of 16 nm. **(D)** Spectra of 10 µM ANS in absence and presence of 0.3 µM HEWL incubated for 24 hours in pH 12.2. The excitation and emission slit width was 1 nm & 8 nm except 0.3 µM emission slit width was 16 nm.

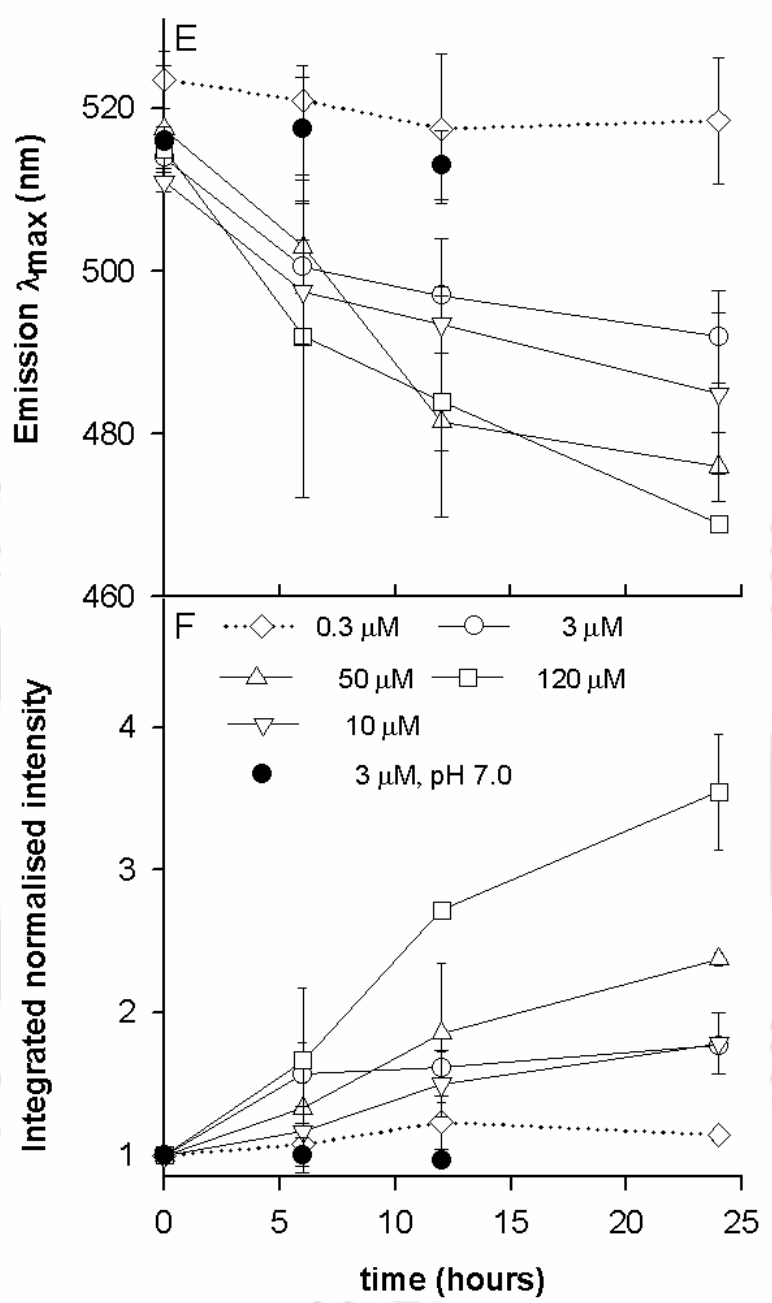

Figure 5.2.2.2: (E) Changes in ANS emission λ_{max}. (F) Integrated normalized emission intensity of ANS (10 μM) in presence of HEWL are shown for different time intervals incubation of HEWL at concentrations 0.3, 3, 10, 50, & 120 μM in pH 12.2 and 3 μM in pH 7.

5.2.2.3 Using tryptophan fluorescence quenching

Tryptophan (trp) is normally buried in the hydrophobic interior of protein; hence accessibility of trp is a good indicator of exposed non-polar regions of a protein in solvent. The average accessibility of six trp residues during growth of HEWL aggregates in pH 12.2 was probed by quenching of trp fluorescence using KI (**Eftink, et al., 1991**). Figure5.2.2.3B reveals the change in bimolecular quenching constant k_q at different times during the growth of HEWL aggregates (see figure 5.2.2.3A for Stern-Volmer plots and Table 5.2.2.1). Unlike ANS and dansyl probe data, variation in k_q with time is less, perhaps due to averaging among trp(s) in varied locations. It is evident that HEWL likely formed oligomers at 300 nM concentration possess exposed hydrophobic residues (trps), confirming significantly higher k_q at all incubation times, compared with oligomers formed with 3 & 120 µM HEWL. The k_q observed for NATA is fairly close to value observed (**Kumar et al., 2007**) in 6 M guanidine HCl (2.4×10^9 $M^{-1}s^{-1}$). Taken together the trp quenching results clearly suggest that average exposure of trp in HEWL aggregates decreases as HEWL monomer concentration is increased. These results also corroborate the aggregates size dependent exposure of trp, which is seen more at lower concentration like 300 nM HEWL, expectedly due to presence of small aggregates, which posses accessible trp. Interestingly the mean fluorescence lifetime of trp at 0.3 µM HEWL shows an increase from 1.9 ns to 2.7 ns over 24 hours (Table 5.2.2.1) unlike 3 and 120 µM samples, indicating a change in environment around trp(s) for 300nM.

A

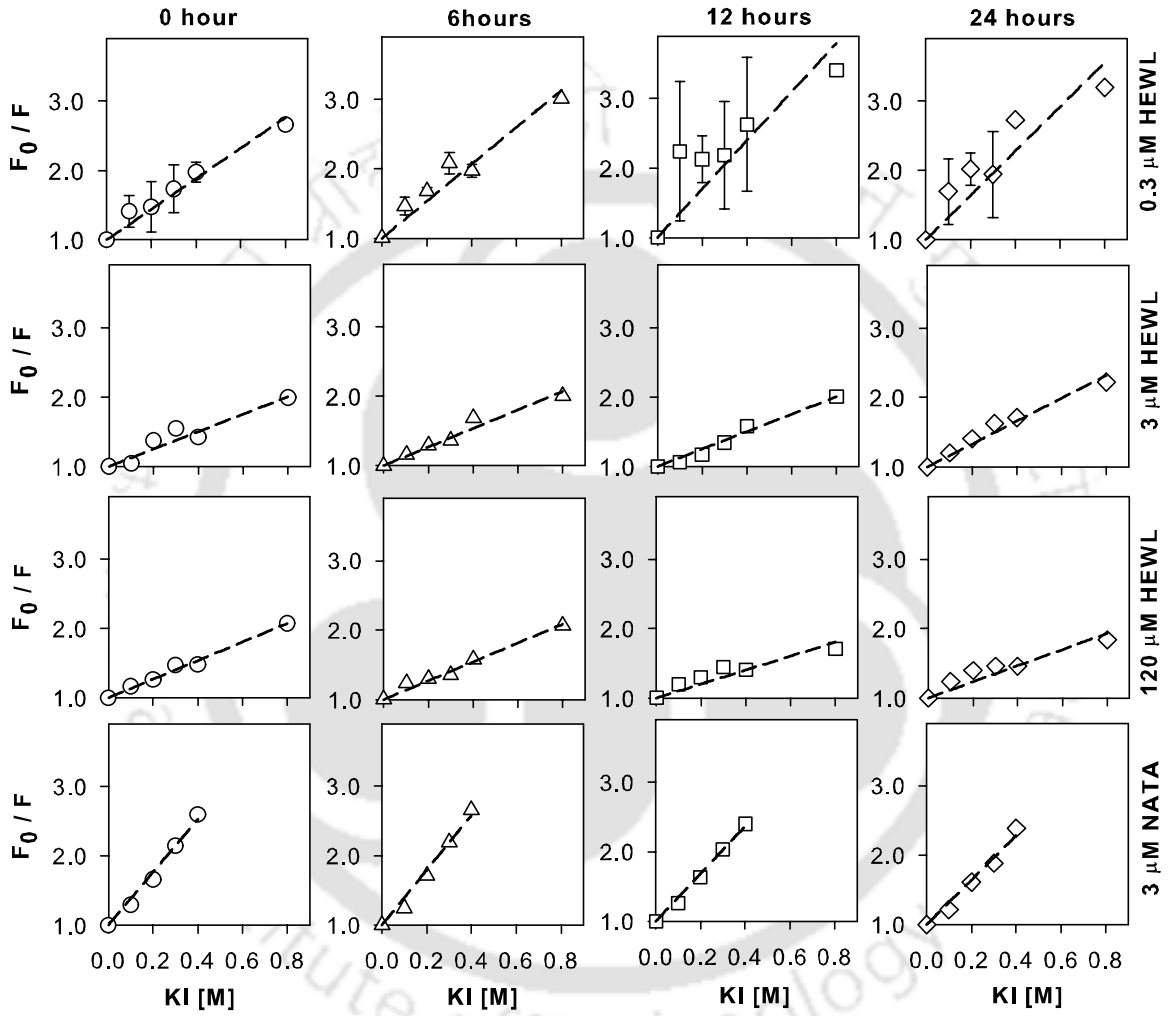

Figure 5.2.2.3 A: Stern-Volmer plots for quenching of tryptophan at pH 12.2 by iodide: Stern-Volmer plots for quenching of tryptophan in 0.3 µM HEWL are shown in top row for different incubation times in pH 12.2 starting from 0 h (leftmost) followed by 6, 12 and 24 hrs (rightmost). Similar plots are shown for 3 µM HEWL (second row from top), 120 µM HEWL (third row) and 3 µM NATA (bottom row). The dashed lines reveal the linear regression fit used to calculate the K_{SV} (see Table 5.2.2.1)

Table 5.2.2.1: Calculation of bimolecular quenching constant k_q from K_{sv} and fluorescence lifetime.

Condition	Incubation time (hrs)	τ_m (ns)	Slope (K_{sv} M^{-1})	k_q ($M^{-1}s^{-1}$ x 10^9)
300 nM HEWL pH 12.2	0	1.90	2.20	1.16
	6	2.15	2.66	1.24
	12	2.26	3.49	1.55
	24	2.69	3.19	1.19
3 µM HEWL pH 12.2	0	2.06	1.28	0.62
	6	1.94	1.34	0.69
	12	1.98	1.25	0.63
	24	2.06	1.65	0.80
120 µM HEWL pH 12.2	0	1.95	1.34	0.69
	6	1.93	1.35	0.70
	12	1.97	1.00	0.51
	24	2.20	1.16	0.53
5 µM NATA pH 12.2	0	1.70	3.81	2.24
	6	1.64	3.96	2.42
	12	1.77	3.43	1.94
	24	1.82	3.21	1.76

B

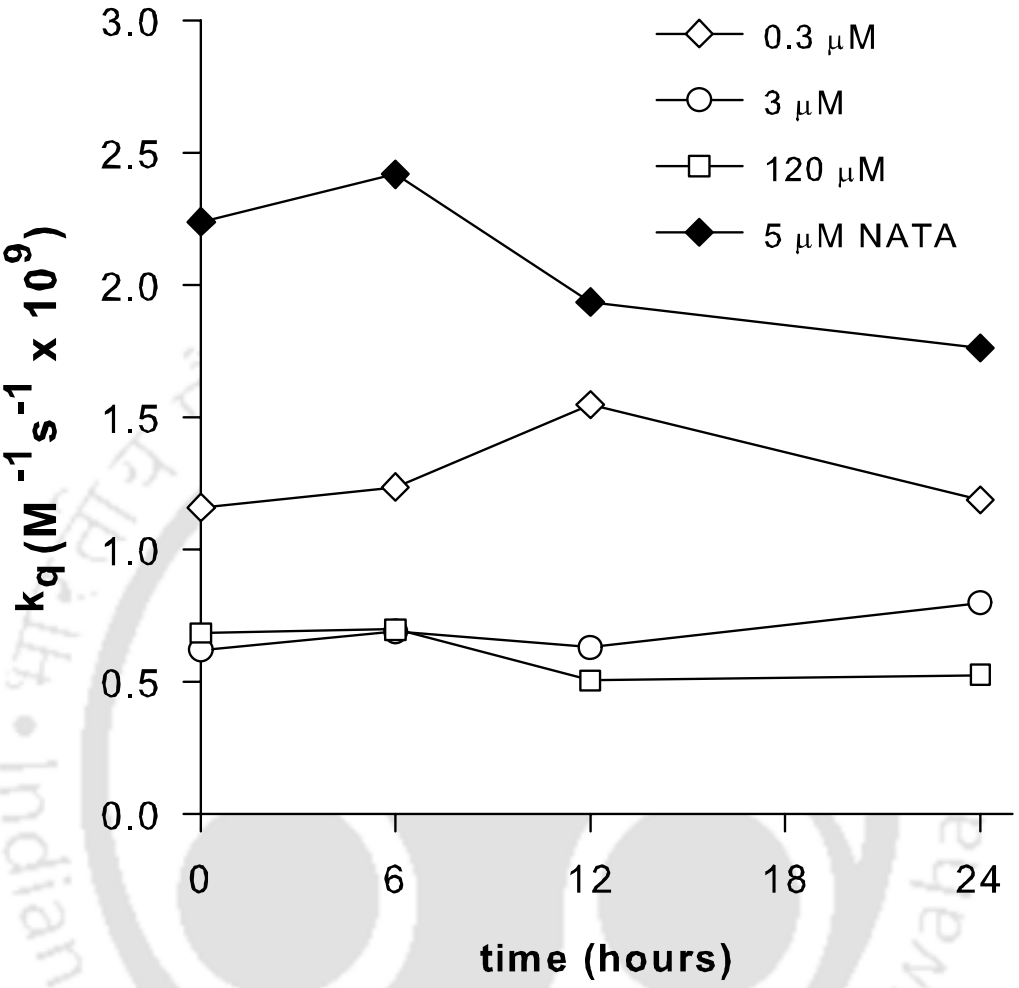

Figure 5.2.2.3 B: Bimolecular quenching constant of tryptophan in HEWL (0.3 μM, 3 μM and 120 μM) and N-acetyl-L-tryptophanamide (NATA, 5 μM) are shown at different time intervals after incubation in pH 12.2.

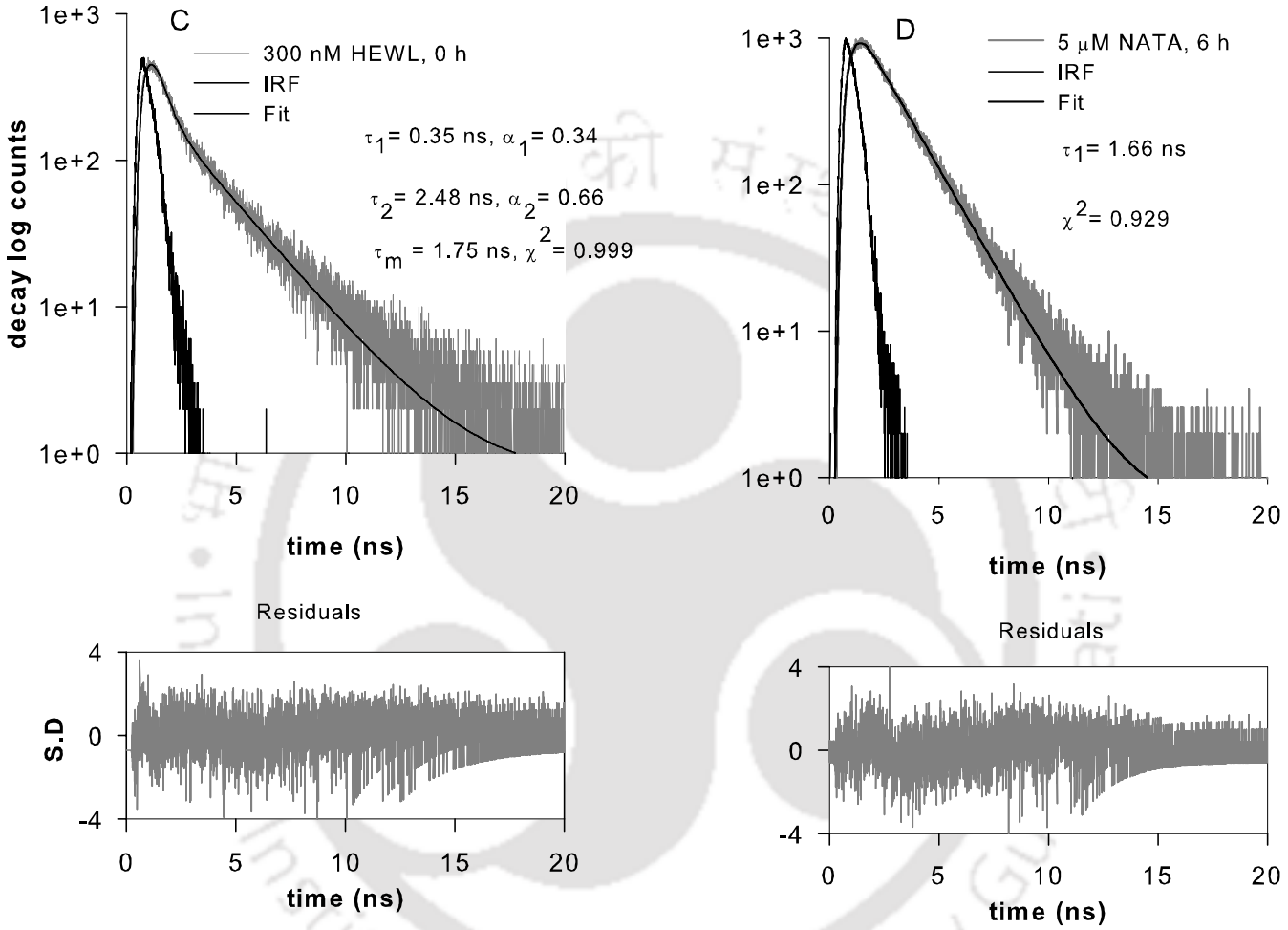

Figure 5.2.2.3: (C) Fluorescence intensity decay of tryptophan in 300 nM HEWL in pH 12.2 at 0 h. (D) Fluorescence intensity decay of NATA in pH 12.2 at 6 h.

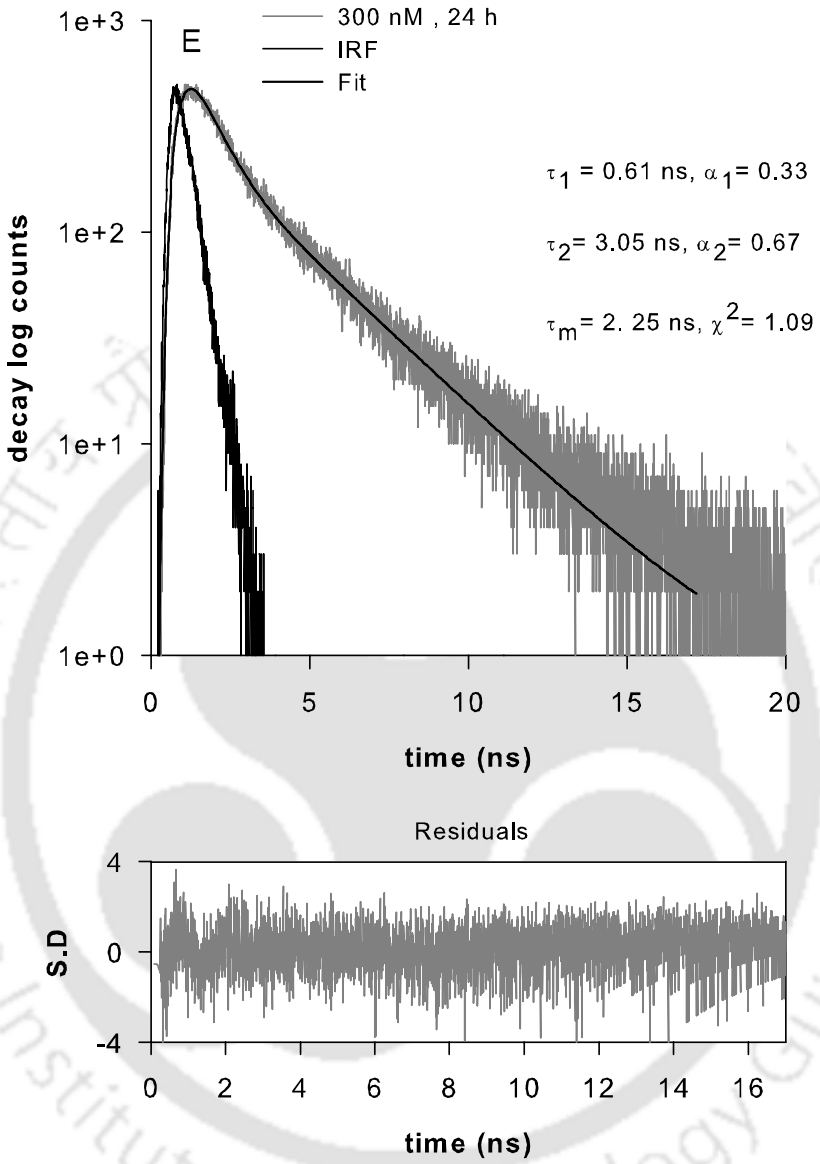

Figure 5.2.2.3 E: Fluorescence intensity decay of tryptophan in 300 nM HEWL in pH 12.2 at 24 h.

5.2.3 Size of aggregates is concentration dependent

Does the growth kinetics and molecular mass of HEWL aggregate depend on monomer concentration? To know these answers, the rotational dynamics of the whole aggregate was investigated at different times post incubation in alkaline pH as a function of monomer concentration. The fluorescence anisotropy of covalently conjugated dansyl probe was employed to measure the Brownian rotational motion of whole aggregate. The long fluorescence lifetime (~13 ns) of the dansyl probe is ideal to monitor the slow global rotation of the large aggregate over a time window of 0-100 ns.

Previous studies from our lab have demonstrated that changes in fluorescence steady state anisotropy (r_{ss}) of the dansyl probe is an excellent indicator for growth changes in HEWL aggregate, since fluorescence lifetime of the conjugated dansyl probe remains fairly invariant with progress of aggregation (**Homchaudhuri et al., 2006, Kumar et al., 2008**). The variation of r_{ss} in dansyl–HEWL conjugates with time of incubation in alkaline pH for multiple monomer concentrations are shown in Fig. 5.2.3 A. It was observed that at pH 12.2, r_{ss} increases gradually during 0-24 hours, for all monomer concentrations from 3 μM to 120 μM, followed by saturation at later times. The magnitude of increase in r_{ss} is strongly concentration dependent, revealing the highest increase for 120 μM followed by 50, 20 & 3 μM in that order. In comparison at 0.3 μM however, the r_{ss} is at its lowest with comparatively little increase during 0-24 hours. The control at pH 7 with 50 μM HEWL, reveals practically no significant change in r_{ss} consistent with earlier observations (**Homchaudhuri et al., 2006**). The fluorescence lifetime of the same dansyl-HEWL aggregates were nearly constant under prolonged incubation times and across monomer concentrations (see Fig. 5.2.3 M and Fig. 5.2.3 N & O) under similar conditions. This implies that increase in r_{ss} occurs owing to slowing of rotational motion in HEWL-dansyl conjugates. The fitted parameters of increase in anisotropy in pH 12.2 for different HEWL concentrations are shown in Table 5.2.3.1. It is evident that rate constant, *k*, for increase in anisotropy (Eq. 5.2.3.1) is almost invariant (0.22-0.27 hr^{-1}) across monomer concentrations, suggesting that each addition of a monomer during oligomer elongation probably has an identical rate. Overall results clearly suggest that at pH 12.2: a) the rotational dynamics of dansyl probe is slowed down with time due to growth of aggregates and b) the growth-dependent slowing in

rotational dynamics of HEWL-dansyl conjugate is clearly proportional to HEWL monomer concentration.

A

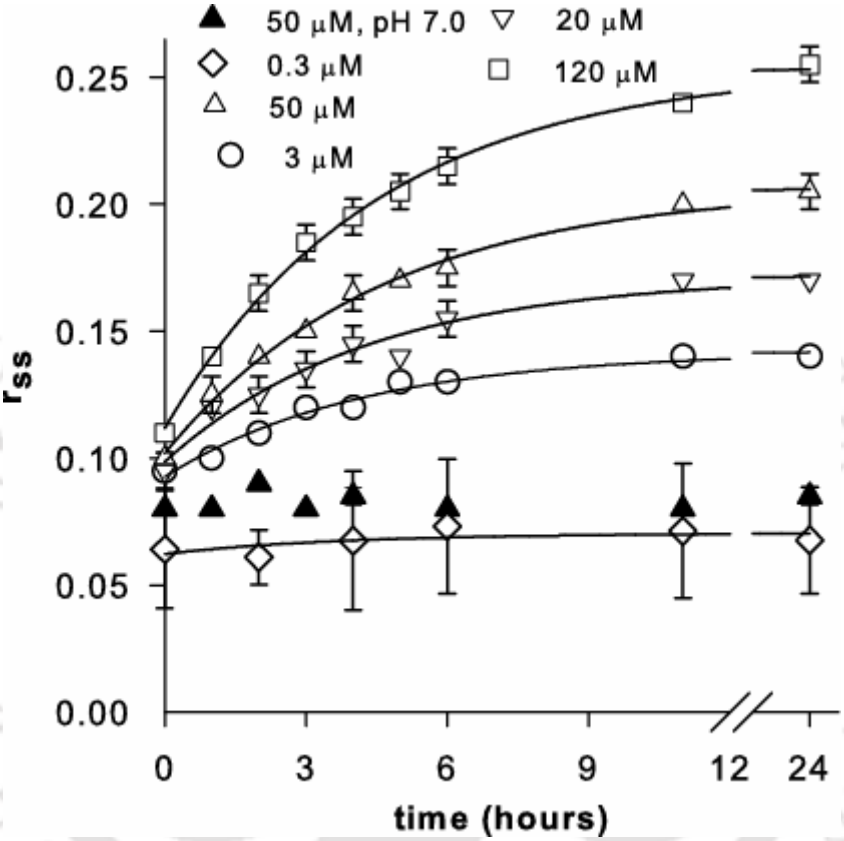

Figure 5.2.3 A: Steady-state anisotropy of dansyl-HEWL: Change in steady state-fluorescence anisotropy of dansyl-HEWL conjugates at different time intervals in presence of 0.3, 3, 20, 50 & 120 μM of HEWL incubated in pH 12.2 and 50 μM in pH 7 is shown along with fitted curve (for pH 12.2 only). See table 5.2.3.1 for parameters extracted from fitting the growth curves. Using equation given below.

$$r_{ss}(t) = r_{ss}^{\infty} - (r_{ss}^{\infty} - r_{ss}^{0})e^{-kt} \qquad 5.2.3.1$$

Where, r_{ss}^{∞} refers to r_{ss} at infinite time, r_{ss}^{0} refers at time $t=0$ and k denotes the rate constant for increasing in anisotropy.

To further confirm these results, time-resolved fluorescence anisotropy measurements were performed. Figure 5.2.3 B-K show the raw anisotropy decay curves for HEWL-dansyl conjugates, after 12 and 24 hours of incubation in alkaline pH 12.2, at multiple concentrations. The decays were tail fitted to a sum of two exponentials (Eq. 5.2.3.2), extracting two rotational correlation times. The slower correlation time (ϕ_2) was interpreted to reveal the average global tumbling rate of the aggregate ensemble in the solution, which is directly proportional to its spherical hydrodynamic volume as per the Stoke-Einstein equation. Figure 5.2.3 L displays a comparative slower correlation time (ϕ_2) and fitted slower correlation time (ϕ_2) was shown in table 5.2.3.2& 5.2.3.3 after 12 and 24 hours. It was shown that at pH 7, ϕ_2 is 4.4 ns, which is a good agreement with previous results (**Nishimoto et al., 1998**), corroborating the predominantly monomeric nature of HEWL at this pH. Interestingly, At pH 12.2, we observe a progressive increase in ϕ_2 as increase monomer concentration from 0.3 μM (~7 ns) to 120 μM (~26 ns). No significant differences in ϕ_2 are noticeable between 12 and 24 hours. It must be emphasize that ϕ_2 values reported here for higher monomer concentrations are more reliable compared to our earlier reports for 40 (**Homchaudhuri et al., 2006**) and 120 μM (**Homchaudhuri et al., 2006**) for two reasons: a) The anisotropy decay here is sampled over a larger time window (0-100 ns), following a complete decay for analysis, b) The decay here is acquired in 4096 time/channels with a better time resolution compared to earlier. Together with results obtained in Fig. 5.2.3 B-K, these data clearly conclude that size of HEWL aggregates increase as the monomer concentration is elevated.

Table 5.2.3.1: Parameters extracted (using equation no. 5.2.3.1) from fits for growth in steady-state anisotropy shown in figure 5.2.3 A

[HEWL]	pH	r_{ss}^{∞}	r_{ss}^{0}	k (hour $^{-1}$)	r^2
0.3 μM	12.2	0.070	0.062	0.274	0.46
3 μM	12.2	0.142	0.093	0.240	0.98
20 μM	12.2	0.172	0.098	0.231	0.97
50 μM	12.2	0.206	0.102	0.218	1.0
120 μM	12.2	0.254	0.117	0.224	1.0

Table 5.2.3.2: Tail fit analysis (using equation no. 5.2.3.2) of anisotropy decays shown in Figure 5.2.3 B-F & Figure 5.2.3 G-K

Figure 5.2.3	HEWL [μM], pH	Incubation time (hours)	A	ϕ_1 (ns)	ϕ_2 (ns)	β_1	β_2	χ^2
B	3, pH 7.0	12	0	0.16	**4.5**	0.08	0.92	1.03
C	0.3 , pH 12.2	12	0	0.12	**7.4**	0.07	0.93	0.97
D	3 , pH 12.2	12	0.006	0.54	**11**	0.03	0.97	1.02
E	20, pH 12.2	12	0.002	0.16	**13**	0.02	0.98	1.04
F	120 , pH 12.2	12	0	0.72	**28**	0.01	0.99	1
G	3 , pH 7.0	24	0	0.14	**4.3**	0.08	0.92	1.1
H	0.3 , pH 12.2	24	0	0.12	**5.3**	0.09	0.91	1.01
I	3 , pH 12.2	24	0.004	0.24	**9.8**	0.03	0.97	1.02
J	20 , pH 12.2	24	0.002	0.54	**15**	0.02	0.98	1.03
K	120 , pH 12.2	24	0	0.76	**26**	0.01	0.99	0.99

Eq. used for fit, $$r(t) = A + \beta_1 e^{-t/\phi_1} + \beta_2 e^{-t/\phi_2} \qquad 5.2.3.2$$

Where, A is constant dependent on G- factor, β denotes the amplitude for ϕ_i, ϕ_1 and ϕ_2 refer to the fast and slow rotational correlation times, respectively. As the 0.15 ns IRF pulse-width is negligibly small in comparison to the time scale of protein rotational motion (> 4 ns), the extracted values of ϕ_2 by this tail-fit approach are not affected by consequences of IRF convolution.

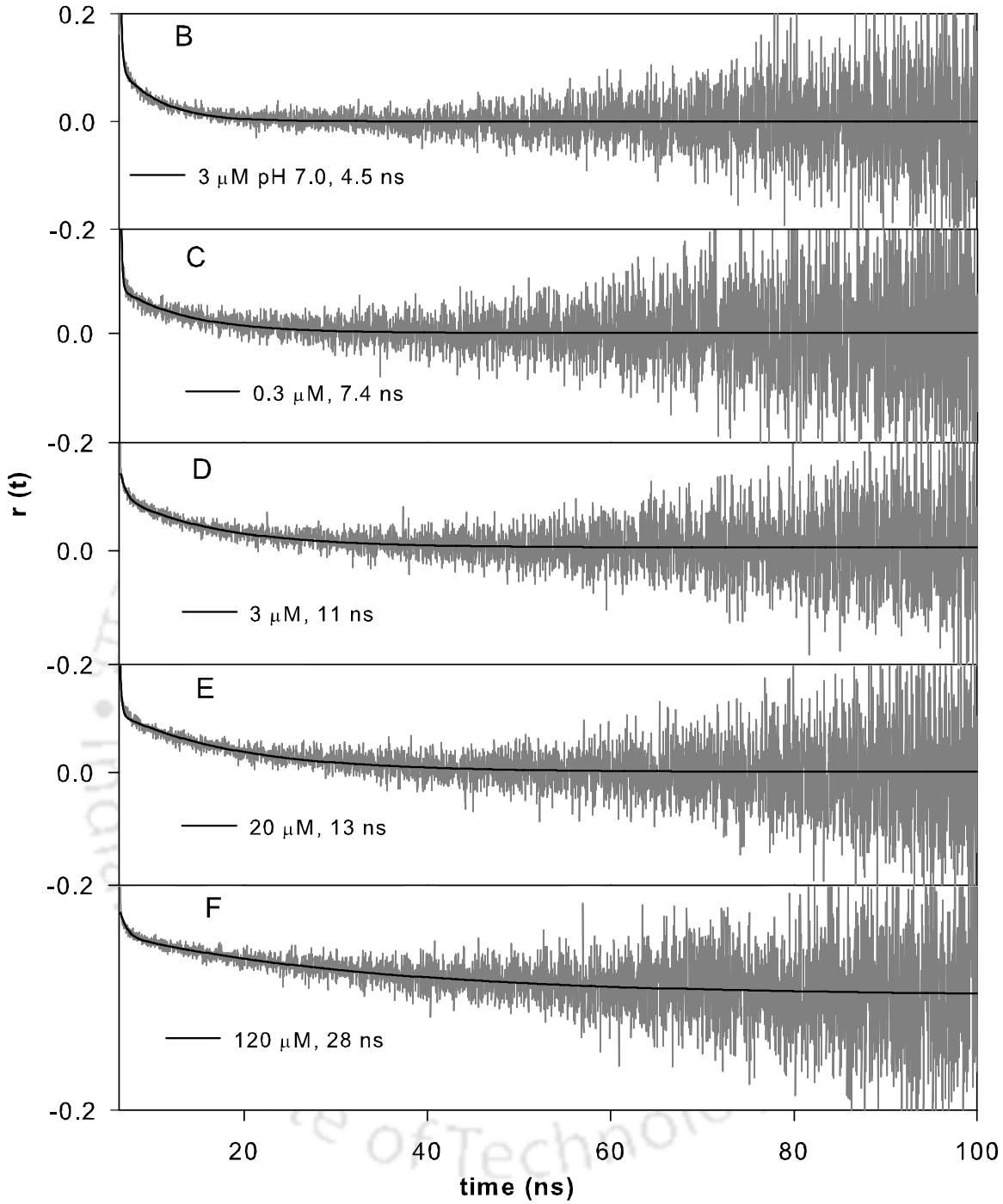

Figure 5.2.3 B-F: Fluorescence anisotropy decay for various concentration of HEWL-dansyl labeled at 12 h, Fig. B for pH 7 and all others are pH 12.2 incubated samples.

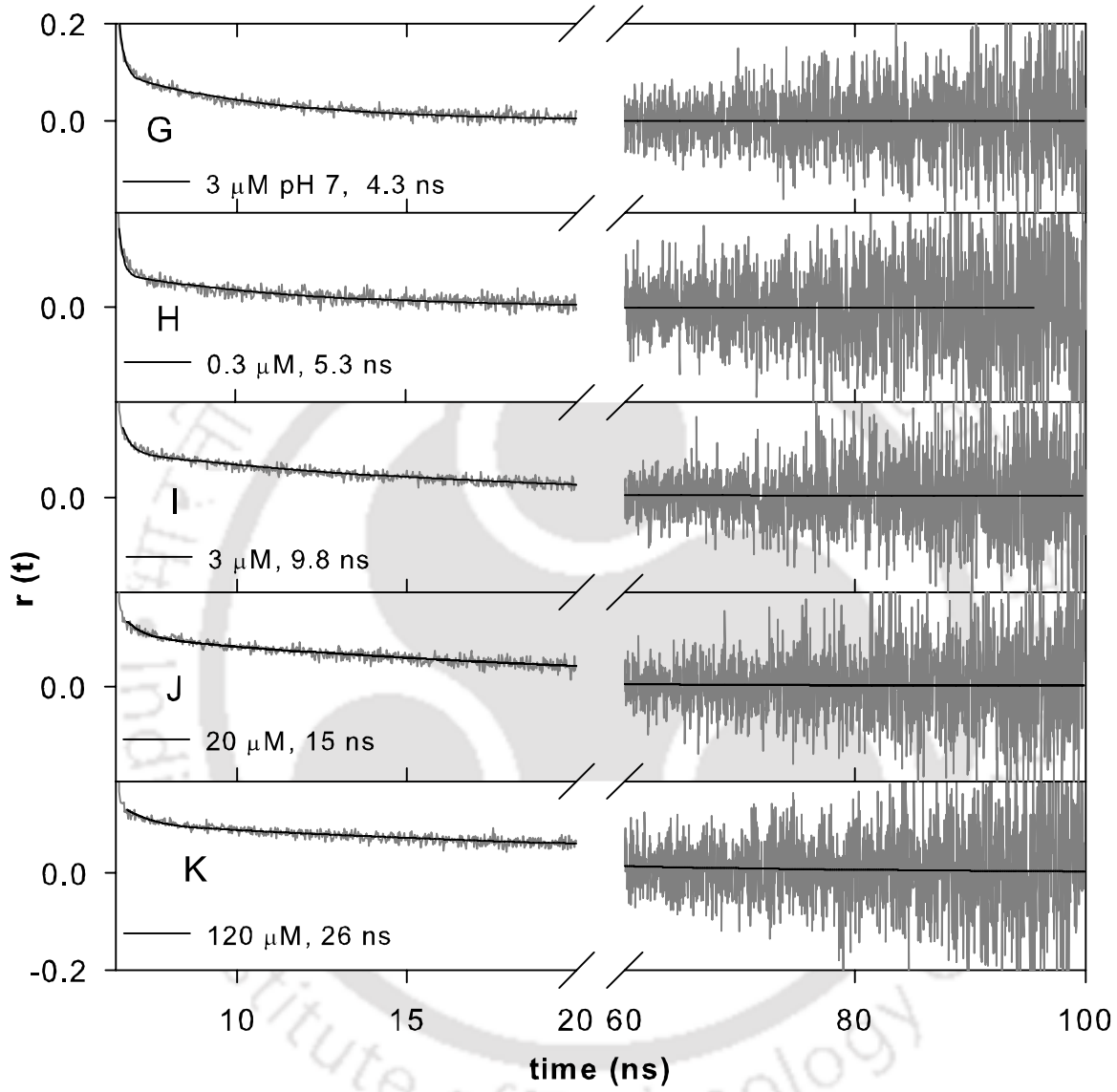

Figure 5.2.3 G-K: Fluorescence anisotropy decay for various concentration of HEWL-dansyl labeled at 24 h, Fig. G for pH 7 and others all are pH 12.2 incubated samples.

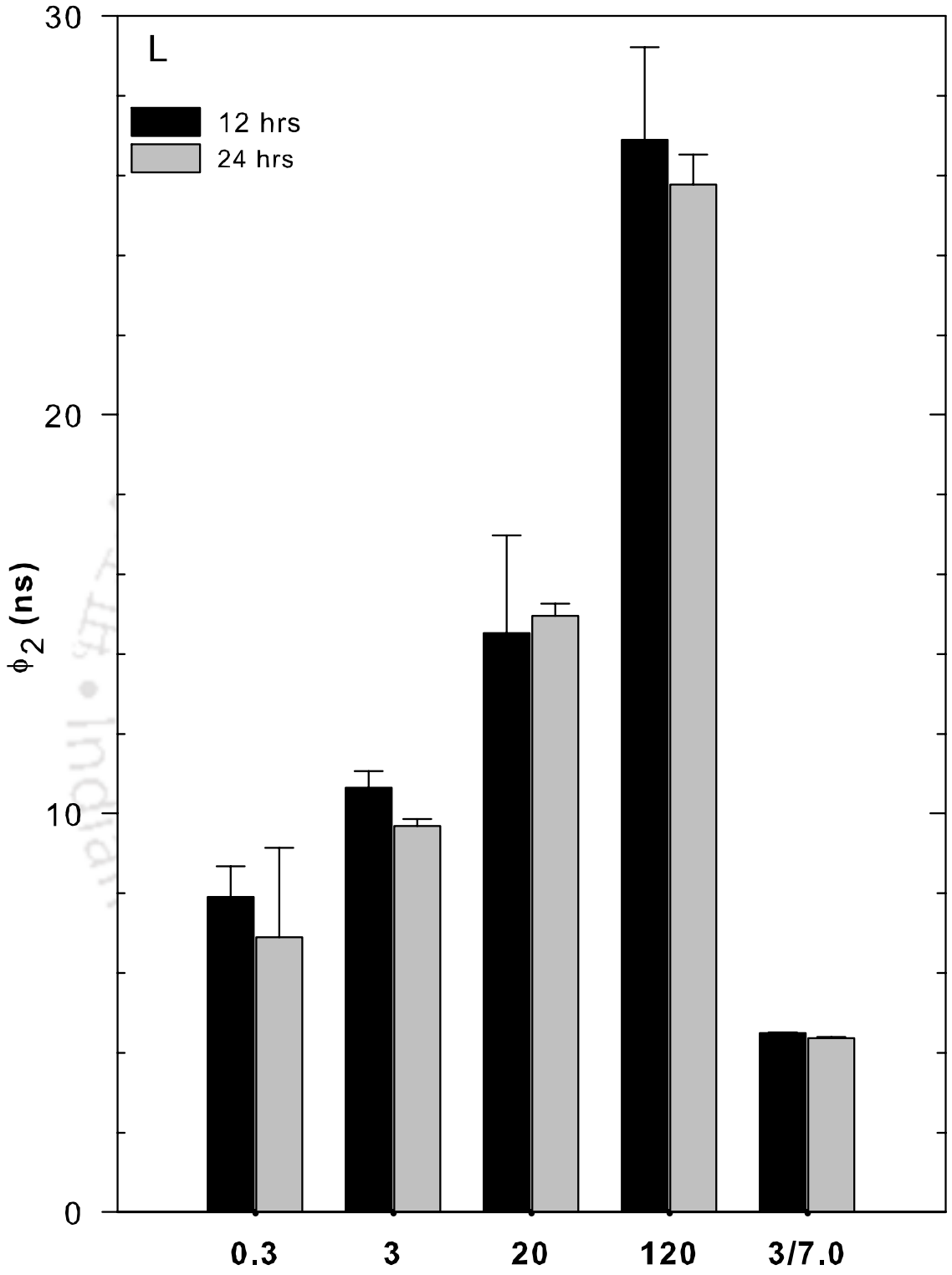

Figure 5.2.3 L: Represents variation in long rotational correlation time (ϕ_2) of dansyl-HEWL labeled with different concentration at 12 and 24 h in pH 12.2 and pH 7.

Table 5.2.3.3: Observed average of global rotational correlation time (ϕ_2)

[HEWL], pH	Time of incubation (hours)	ϕ_2 (ns)
3 μM, pH 7.0	12	4.5 ± 0.0
0.3 μM, pH 12.2	12	7.9 ± 0.8
3 μM, pH 12.2	12	10.6 ± 0.4
20 μM, pH 12.2	12	14.5 ± 2.4
120 μM, pH 12.2	12	26.9 ± 2.3
3 μM, pH 7.0	24	4.4 ± 0.0
0.3 μM, pH 12.2	24	6.9 ± 2.2
3 μM, pH 12.2	24	9.7 ± 0.2
20 μM, pH 12.2	24	14.7± 0.3
120 μM, pH 12.2	24	25.8 ± 0.8

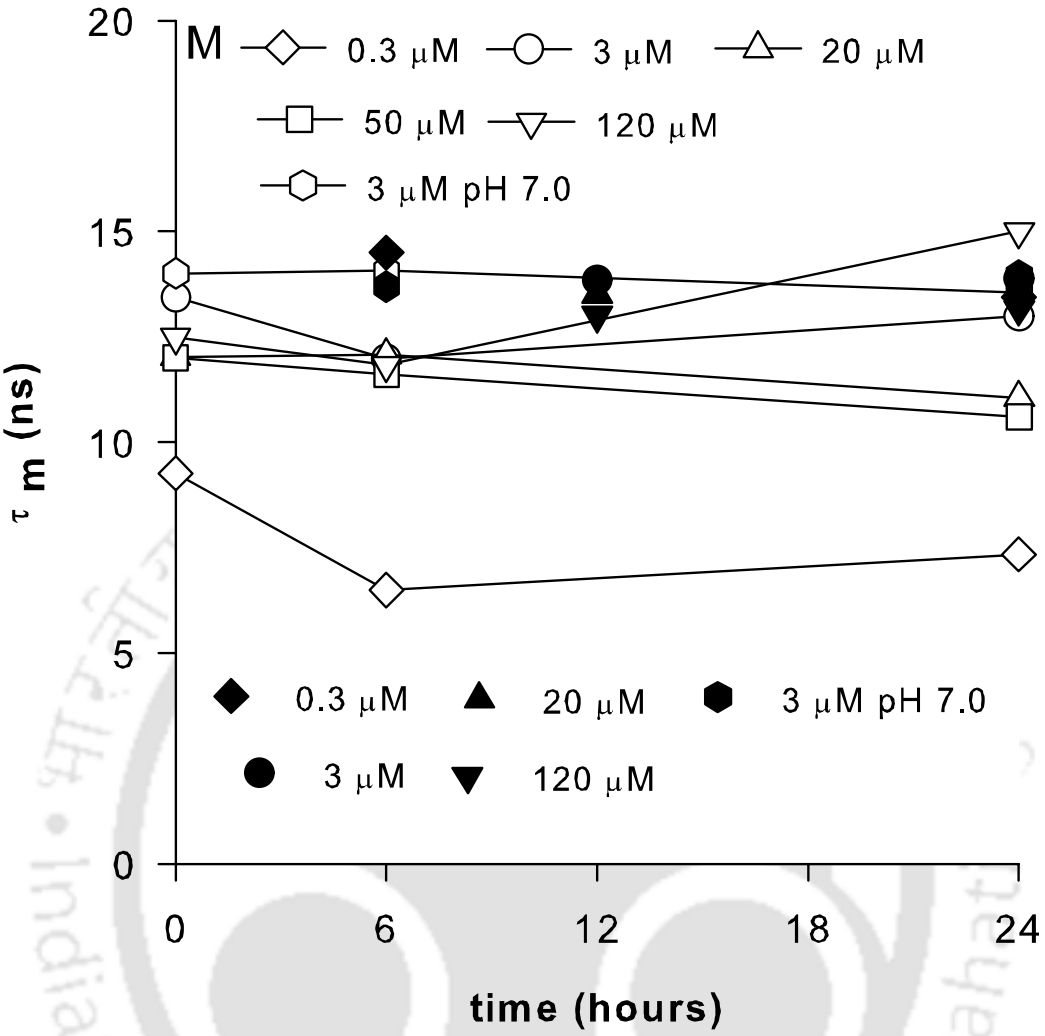

Figure 5.2.3 M: Mean fluorescence lifetime (τ_m) of dansyl-HEWL conjugates: The variation in mean fluorescence lifetime of dansyl probe in dansyl-HEWL conjugates is shown against time of incubation in pH 12.2 for different HEWL concentrations. The filled symbols show the mean lifetime (τ_m), measured from emission collected at 438 nm using a monochromator, while unfilled symbols show mean lifetime measured from whole emission collected using an excitation cutoff filter.

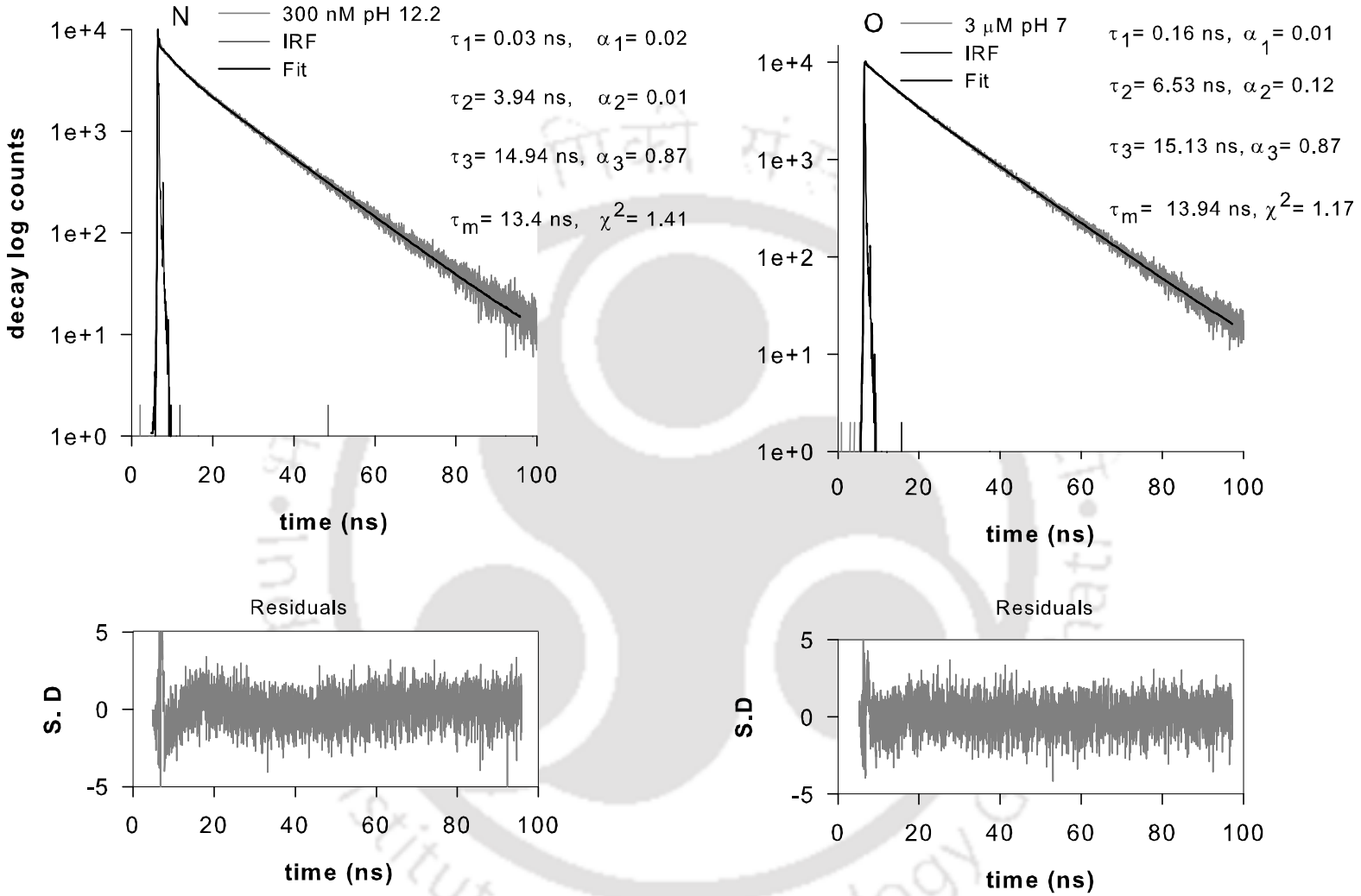

Figure 5.2.3 N & O: Fluorescence intensity decay of labeled dansyl-HEWL incubated in pH 12.2 for 24 h.

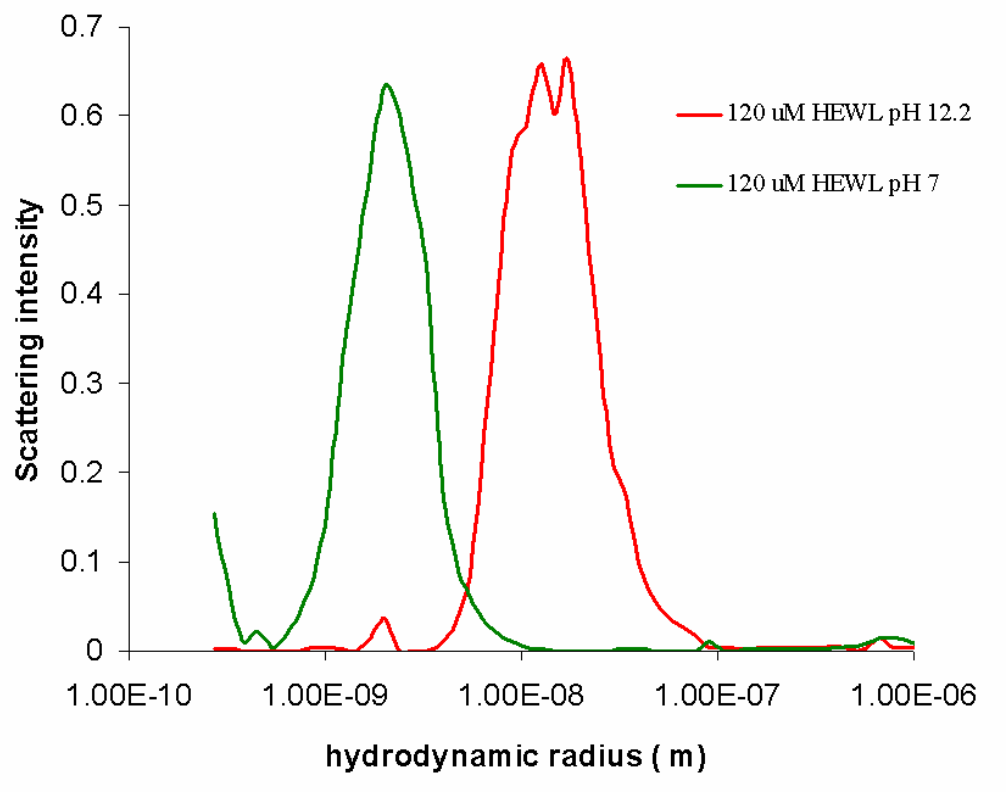

Figure 5.2.3 P: Dynamic light scattering represents HEWL size distribution in pH 12.2 and pH 7 after 26 h incubation.

5.2.4 Accessibility of sulfhydryl group among aggregates

Hen lysozyme contains four disulfide bonds which is prone to cleave after transferring in pH 12.2 and can remain as eight free –SH group. In support of this, earlier work by us has revealed that aggregates in HEWL are stabilized by formation of intermolecular disulfide bonds in later time **(Kumar et al., 2008, Kumar et al., 2009)**. However rate of extent of bond cleaving was unknown, whether it is dependent on monomer concentration or time of incubation in pH 12.2? For this purpose confirmation, presence of free thiol was measured in HEWL aggregate as function of incubation time for monomer concentration like 120, 50, 20 μM (Experiment was not possible below concentration of 20 μM). Figure 5.2.4 A shows that within hours of exposure in alkaline pH, almost all –SH groups in HEWL are accessible to DTNP (see spectra in Fig. 5.2.4 B), which are independent of monomer concentration. These thiols continue to remains accessible to DTNP for duration of 96 hours. DTNP being uncharged, does have the ability to penetrate deeper inside the protein in comparison to its benzoic acid derivative DTNB. The [–SH] concentration however reveals a downward trends suggesting loss of a few –SH bonds perhaps to form intermolecular –S-S- bond. The above results suggest that most if not all thiols in HEWL are free and accessible in the aggregates independently against monomer concentration in the range of 20- 120 μM.

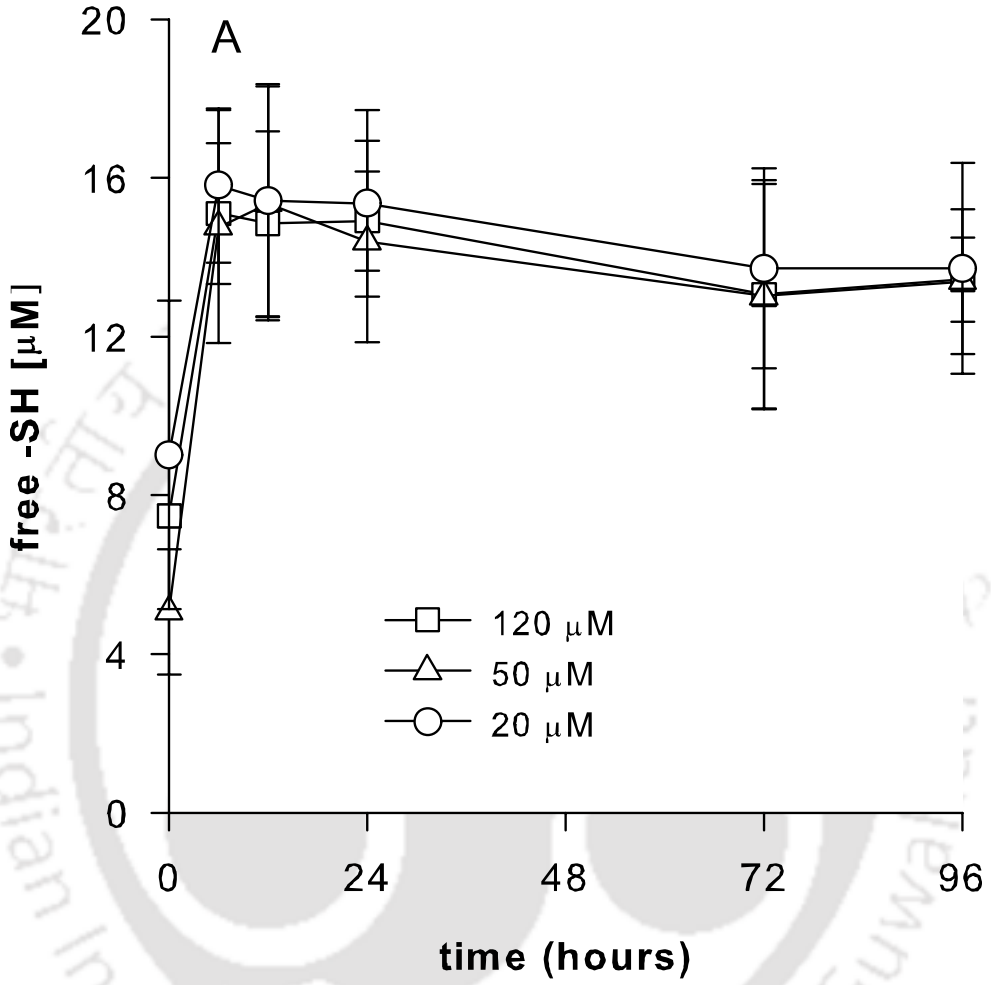

Figure 5.2.4 A: Free –SH present in HEWL incubated in pH 12.2 at various times for different concentrations.

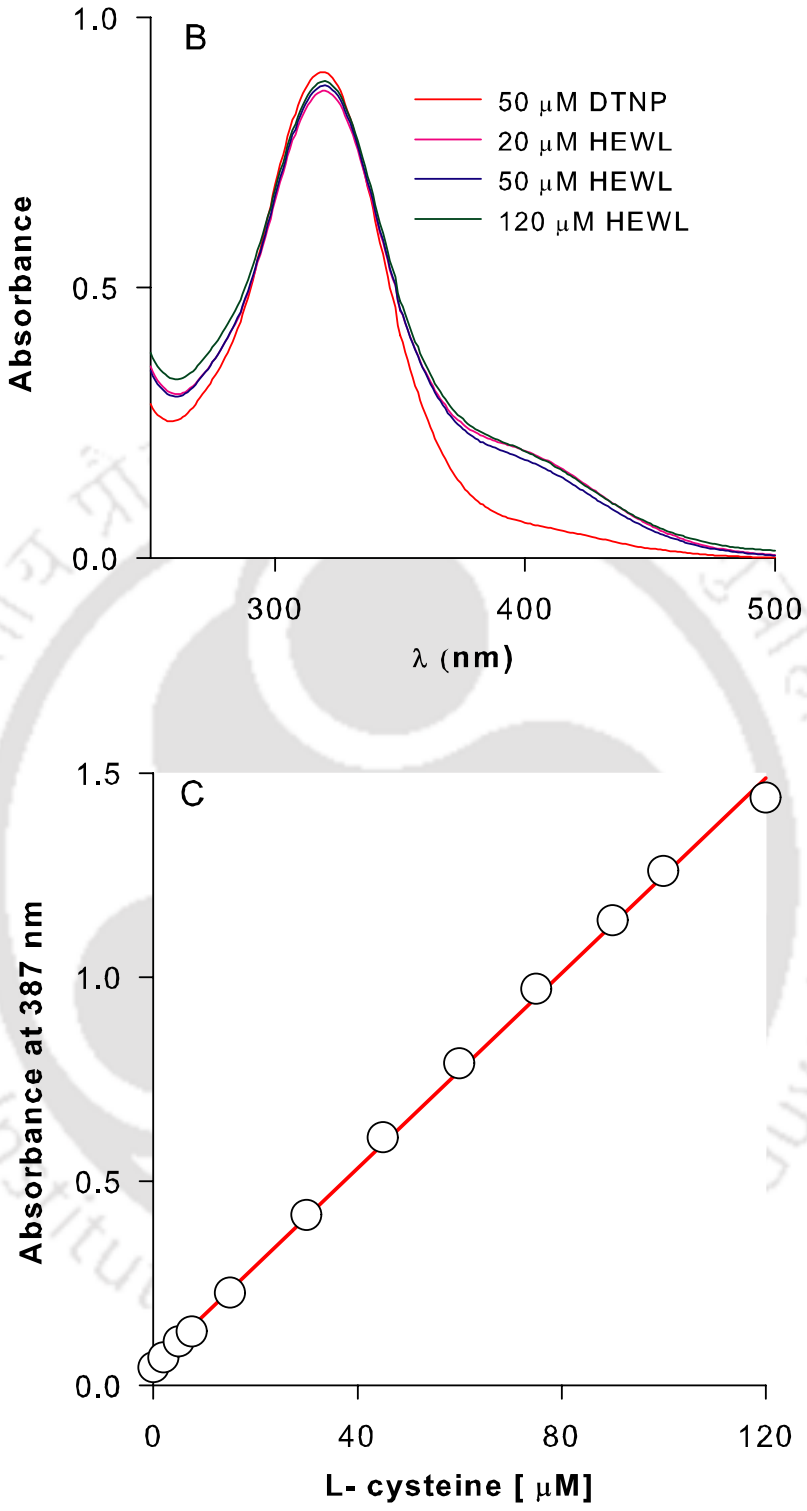

Figure 5.2.4 B: Spectra of DTNP in presence of **free** –SH present in HEWL incubated in pH 12.2 at various time. **Fig. 5.2.4 C:** Cysteine std. curve against various concentrations for calculating –SH, for DTNP assay.

5.2.5 Morphology of aggregates is concentration independent

The external appearance of aggregates can reveal a lot about the nature of the aggregate, including their origin. For this purpose, aggregates formed with different concentration of monomers namely, 0.03 0.3, 3, 50 and 120 µM were observed using AFM after 12 hours of incubation at 301 K in alkaline pH 12.2. In Fig. 5.2.5 A &B morphology of 3 µM pH 7 incubated samples was shown. Its z-height and particle size dimension indicates the 3 µM in pH 7 exist mostly in monomer (**Kumar et al., 2008**). Figure 5.2.5 C reveals the rope like binding morphology of fibril in presence of 3 µM while another image in Fig. 5.2.5 D was presents globular aggregates. Other images depicts branched like fibrillar morphology (see Fig. 5.2.5 E & F) at 3 µM, which has seen also from HEWL in acidic condition (**Arnaudov et al., 2005, McAllister et al. 2005**). Figure 5.2.5 G - M represents the morphology of aggregates in presence of 0.3 µM HEWL in pH 12.2, and Figure 5.2.5 N-Q reveals morphology of aggregates in presence of 30 nM HEWL in pH 12.2. Here both types of aggregates like globular (see Fig 5.2.5 G & Fig. 5.2.5 O), and mostly long (1 to >3 µM) fibrillar aggregates was found. It is interesting to track the fibrillar aggregates of HEWL at nano molar concentrations like 300 nM and 30 nM. Figure 5.2.5 H and I depicts the germination of fibrillar aggregates observed at 0.3 µM monomer concentration. Image 5.2.5 H highlight multiple instances where thin pointed structures (perhaps early fibrils) appear originating in multiple directions from globular aggregates. Some aggregate from another sample is shown in image 5.2.5 I, from where multiple fibrillar structures originate in a radial geometry. Image 5.2.5 J & K dictate fibrils from Fig. 5.2.5 I at higher resolution after a fresh scan. Here it is interesting to observe the twisted protofilaments in the fibril. Apart from different fibrillar feature, long fibrils were noticed at nM concentration range also. From figure 5.2.5 N & P, at 30 nM HEWL concentration long fibril also was shown (1 to >3 µM). Figure from 5.2.5 R indicates crowded, wavy and branched like fibrillar structures, which is observed from 120 µM samples after 12 h of incubation. However from 50 µM HEWL sample unfortunately only globular aggregates was able to tracked (see Fig. 5.2.5 S). In contrast to pH 7, at pH 12.2, images show clumps of protein that resemble globular aggregates with a heterogeneous size distribution as well as long, thread like structures, resembling amyloid fibrils with noticeable branching. These observations using AFM have shown a larger likelihood and predominance of amyloid fibrils at lower monomer

concentrations (≤ 3 μM) than higher at early times (~12 hours). Higher monomer concentrations (50-160 μM) revealed tightly bunched well populated amyloid fibrils at long duration (25-31 days) of incubation in alkaline pH 12.2, probably owing to higher concentrations and their origin in a radial geometry as mentioned above (see Fig. 5.2.5 T-V).

A

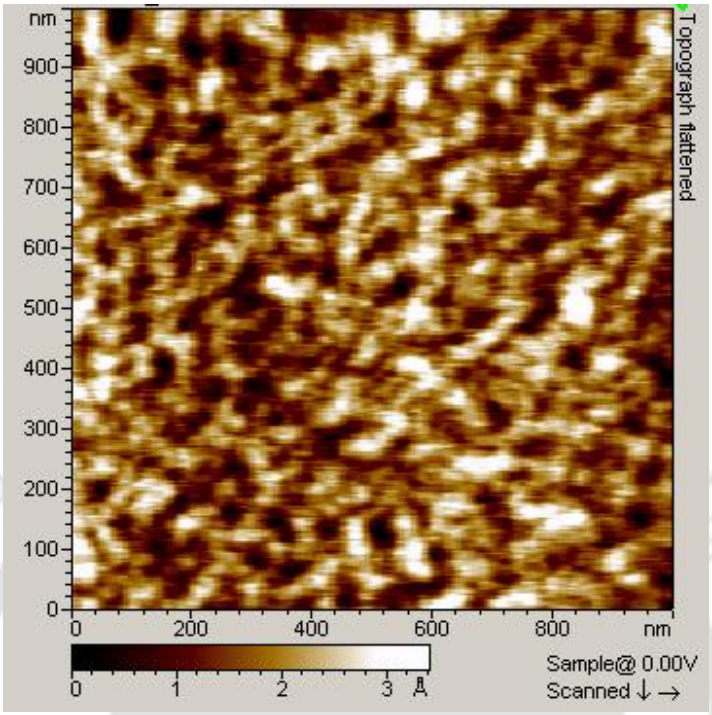

B

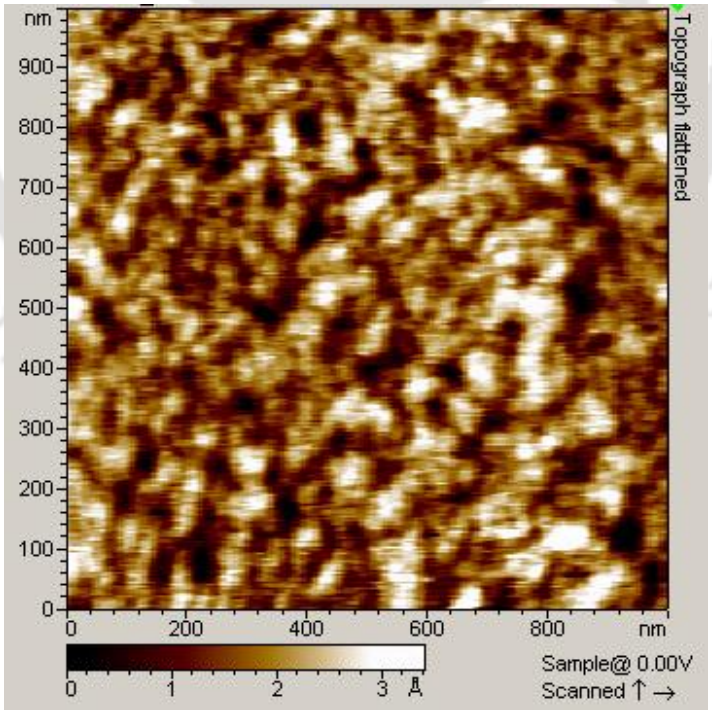

Figure 5.2.5 A & B: Topograph AFM image of 3 μM HEWL in pH 7.0 at 301 K after12 h of incubation.

C

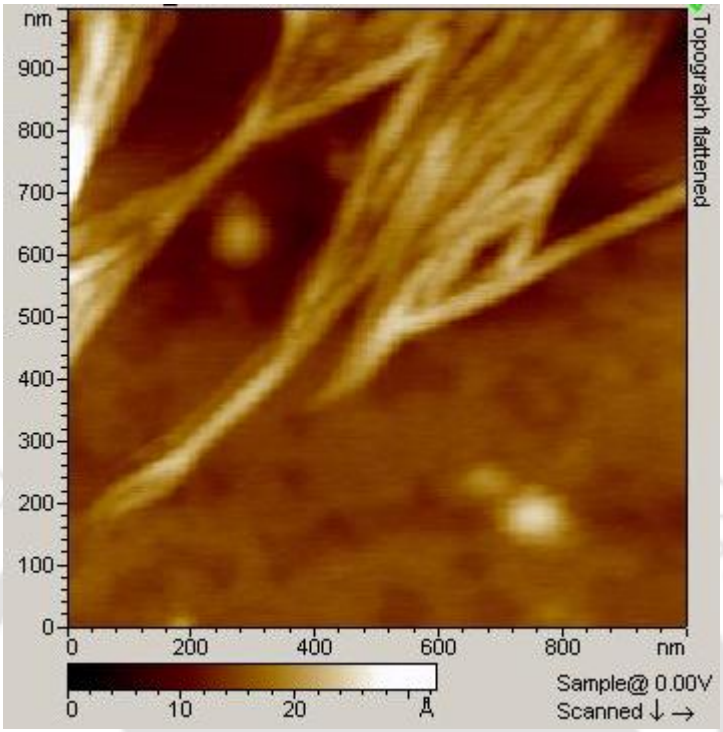

D

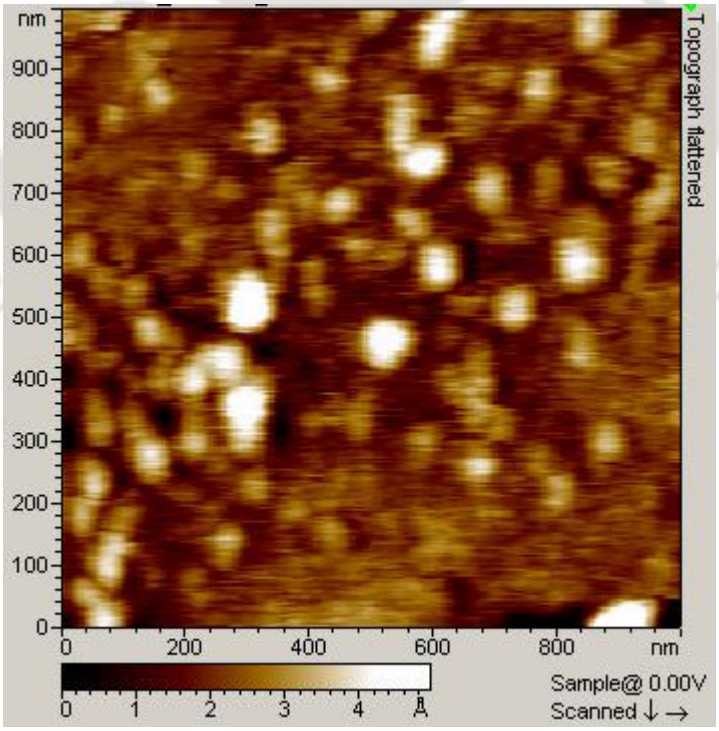

Figure 5.2.5 C & D: Topograph AFM image of 3 μM HEWL in pH 12.2 at 301 K after 12 h of incubation.

E

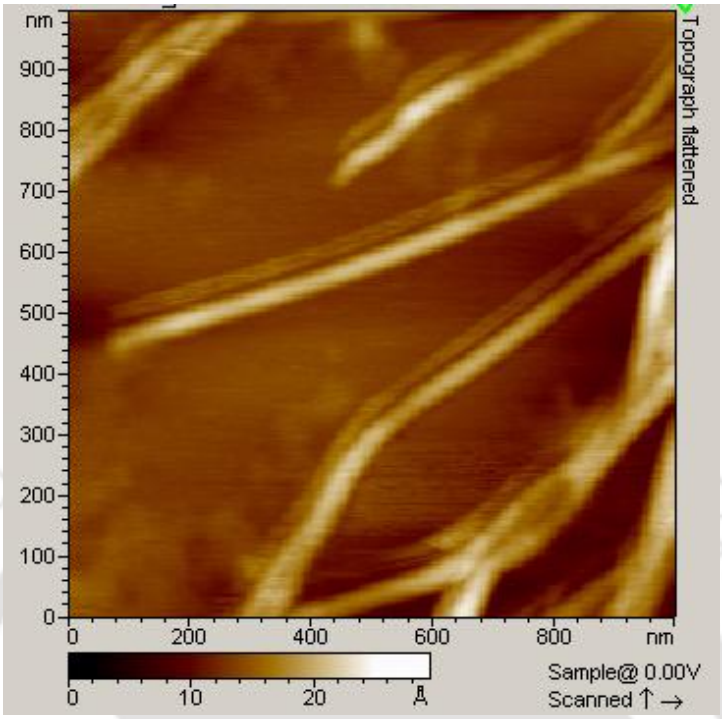

F

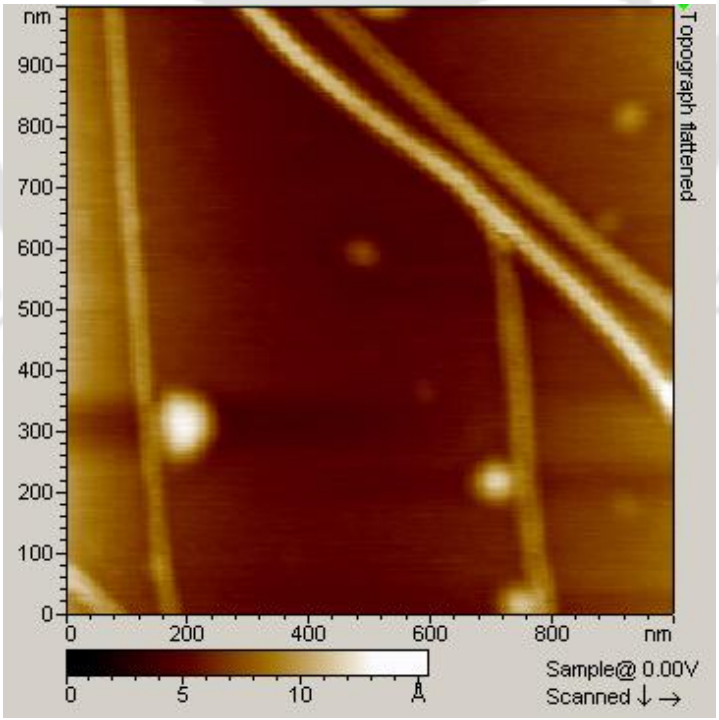

Figure 5.2.5 E & F: Topograph AFM image of 3 μM HEWL in pH 12.2 at 301 K after 12 h of incubation.

G

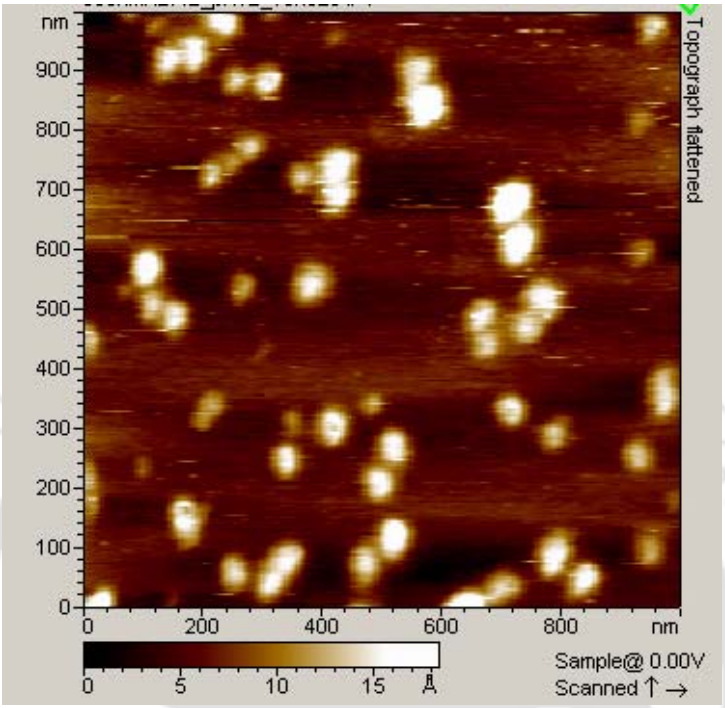

H

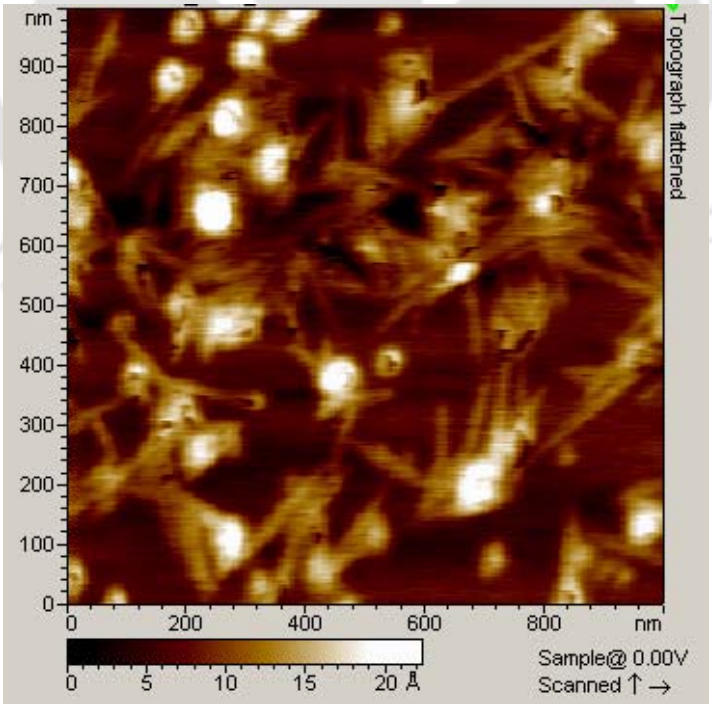

Figure 5.2.5 G & H: Topograph AFM image of 300 nM HEWL in pH 12.2 at 301 K after 12 h of incubation.

I

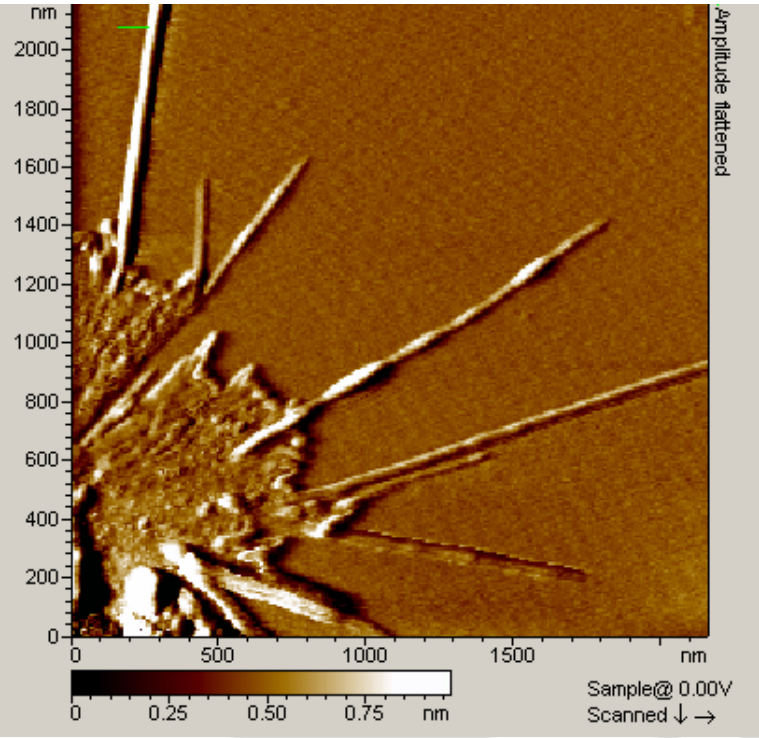

Figure 5.2.5 I: Amplitude AFM image of 300 nM HEWL in pH 12.2 at 301 K after 12 h of incubation.

J

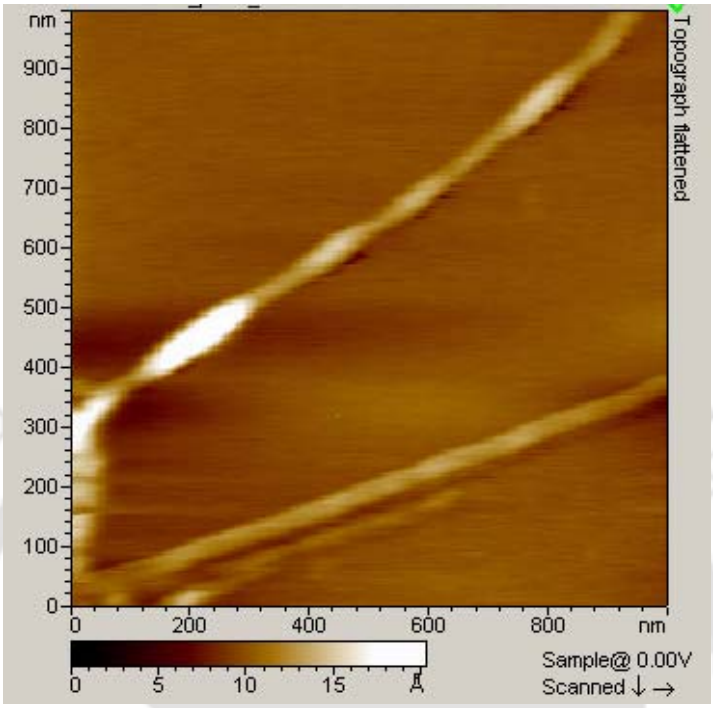

K

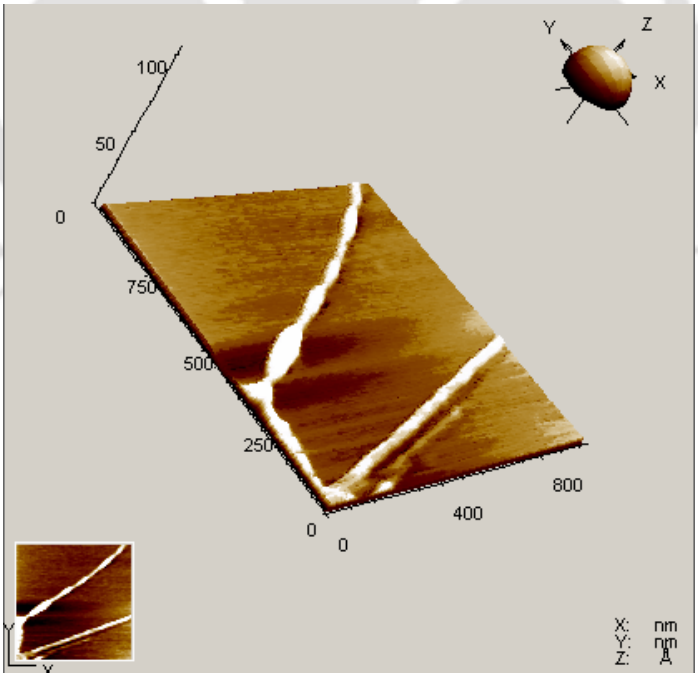

Figure 5.2.5: 300 nM HEWL in pH 12.2 at 301 K after 12 h of incubation.

(J) Represents topograph AFM image **(K)** Represents 3 D of topograph AFM image

L

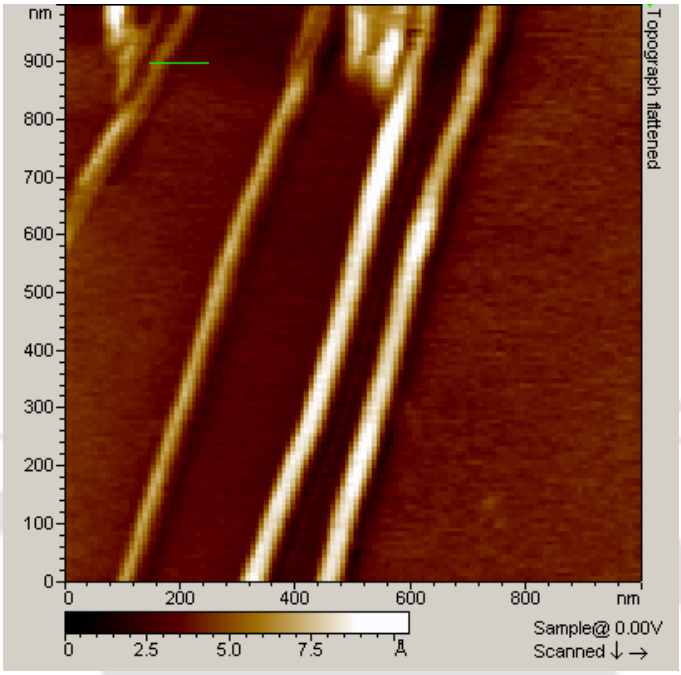

M

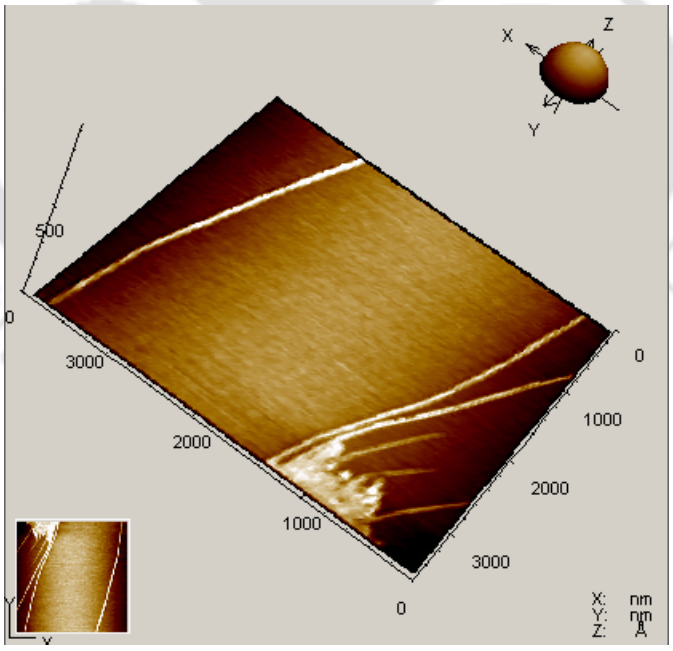

Figure 5.2.5: 300 nM HEWL in pH 12.2 at 301 K after 12 h of incubation.

(L) Represents topograph AFM image **(M)** Represents 3 D of topograph AFM image

N

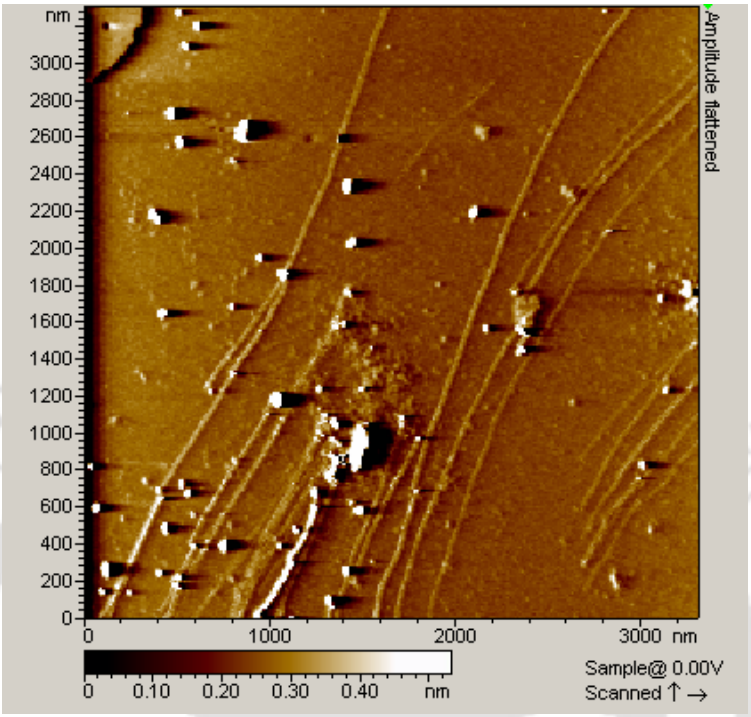

O

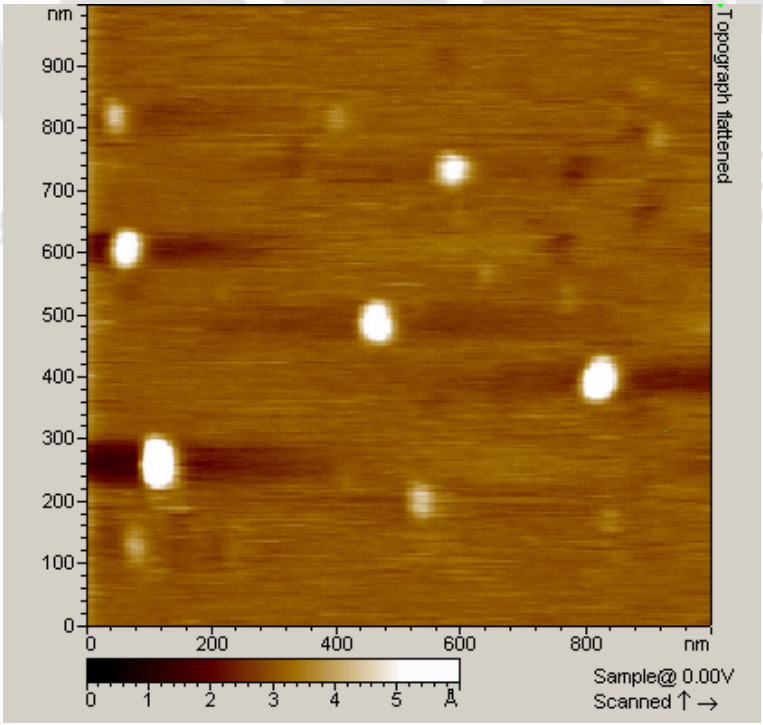

Figure 5.2.5: AFM image of 30 nM HEWL incubated in pH 12.2 for 12 h **(N)** Amplitude image. **(O)** Topograph image.

P

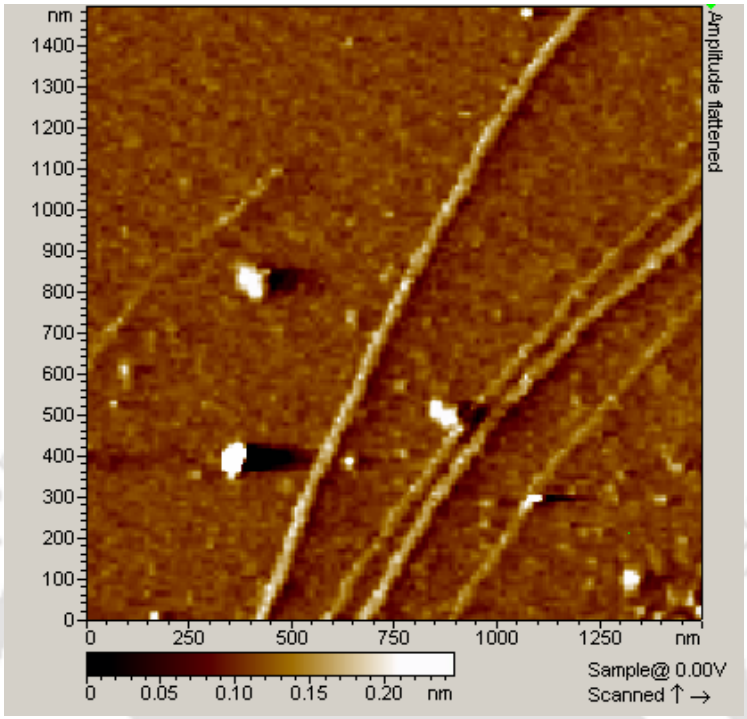

Q

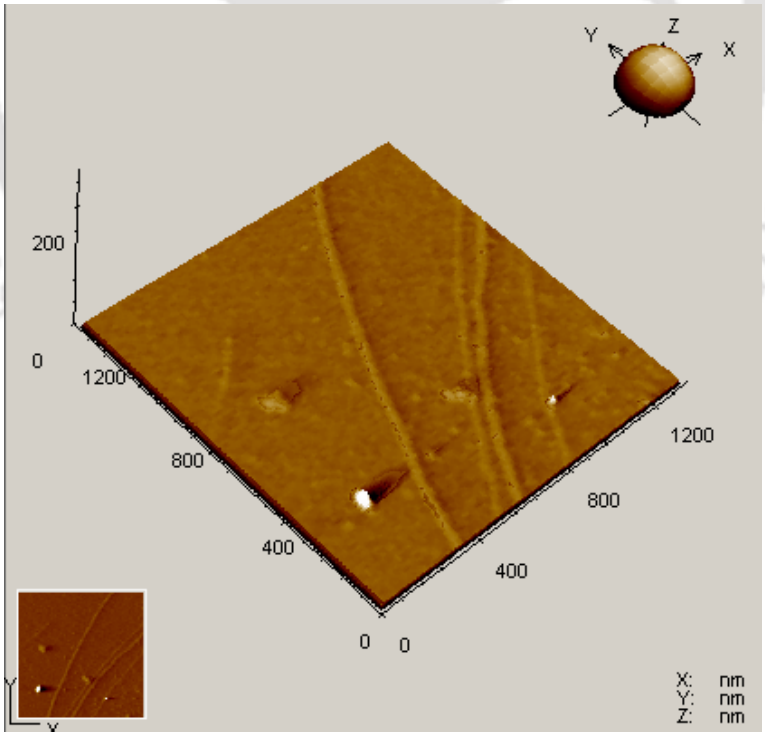

Figure 5.2.5: AFM image of 30 nM HEWL incubated in pH 12.2 for 12 h **(P)** Amplitude image. **(Q)** 3D amplitude image.

R

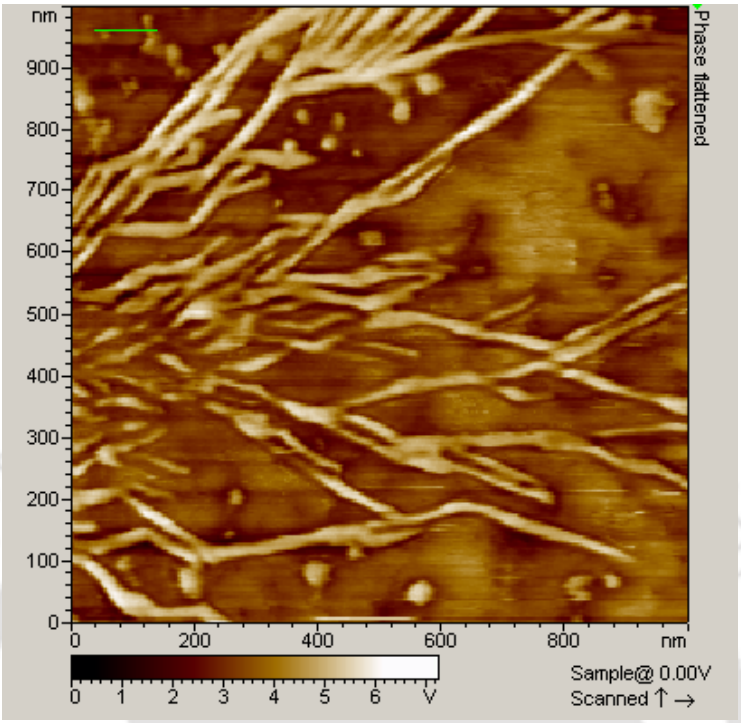

S

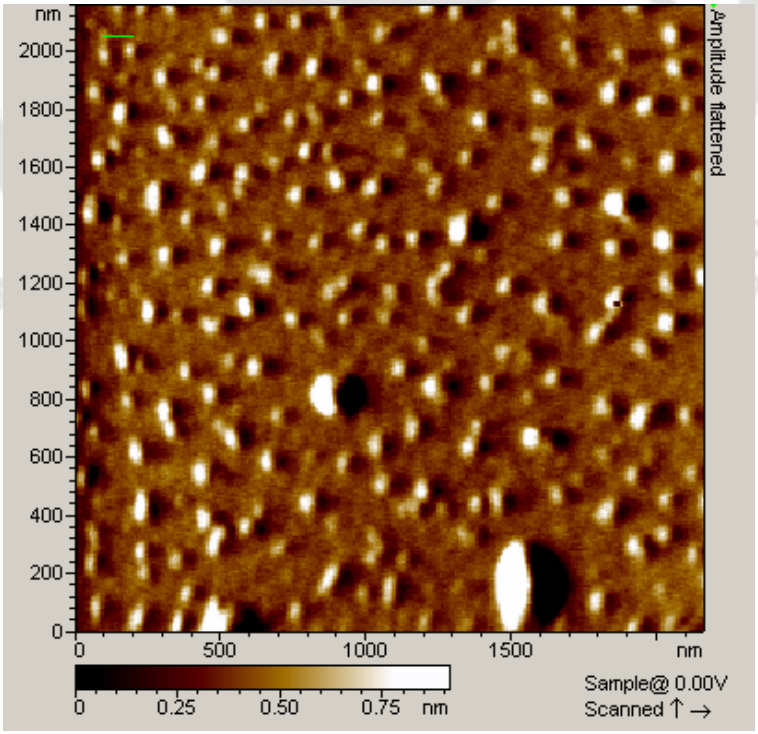

Figure 5.2.5: (R) Topograph AFM image of 120 µM HEWL **(S)** Amplitude image of 50 µM HEWL. Both sample incubated in pH 12.2 for 12 h at 301 K.

T

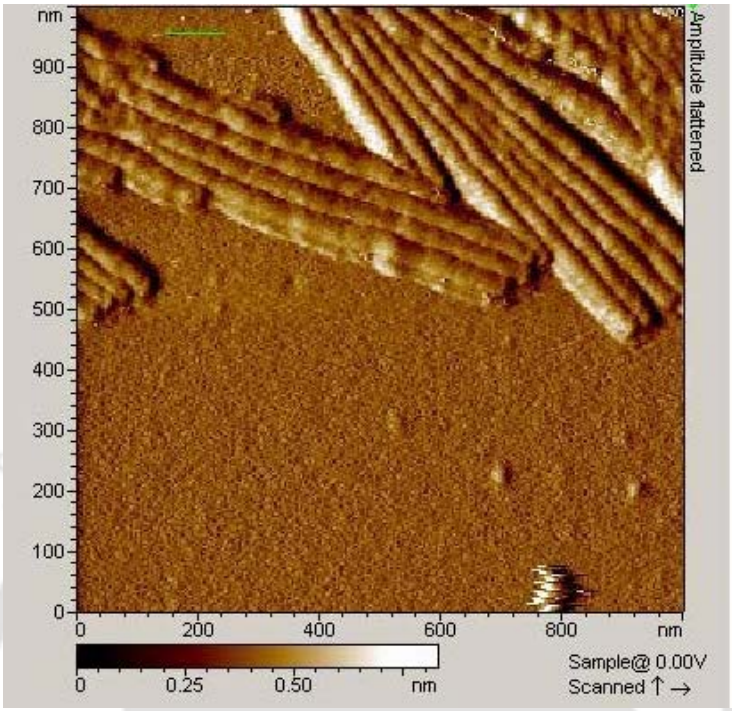

U

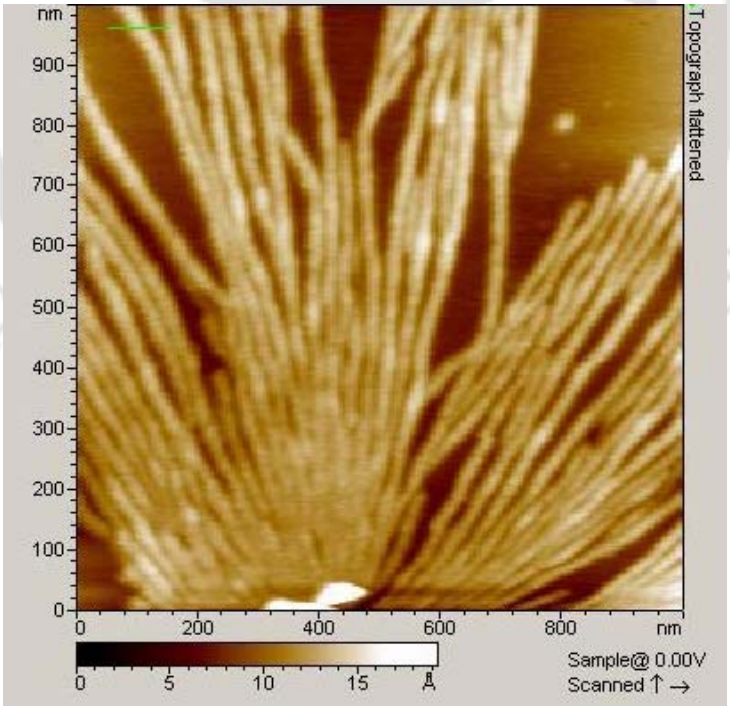

Figure 5.2.5: AFM image of HEWL in pH 12.2 at room temperature. **(T)** Amplitude image of 50 uM after 25 days **(U)** Topograph image of 75 uM after 30 days.

V

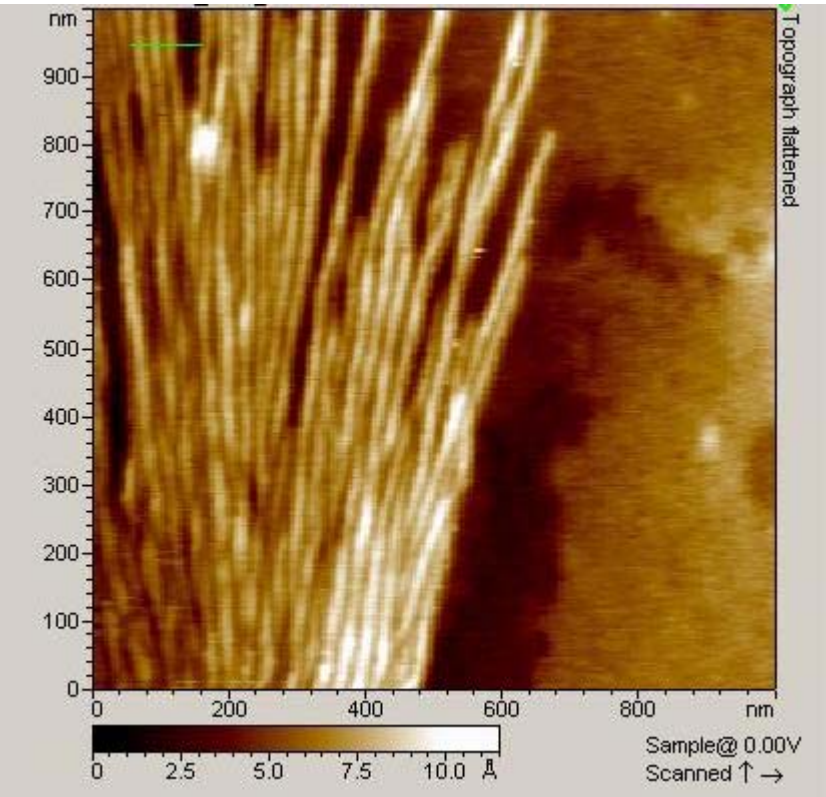

Figure 5.2.5 V: Topograph AFM image of 160 μM HEWL in pH 12.2 at room temperature after 31 days of incubation.

It is worthwhile to discuss that while FRET efficiency nearly saturates after 8 hours (Fig. 5.2.1 G), anisotropy data reveal little change after 11 hours (Fig. 5.2.3 L), ANS emission exhibits profound changes between 0-24 hours for ≥ 3 μM HEWL. This result reflects dynamic rearrangements within the growing aggregate interior, leading to concentration dependent dense molecular packing, therefore favoring an increasingly hydrophobic core. Existence of such molecular packing inside HEWL aggregates after 6 hours has been reported previously from the slow segmental mobility of dansyl probe with 40 (**Homchaudhuri et al., 2006**) and 120 μM (**Kumar et al., 2008**) HEWL. In support of above validation, trp quenching data (Fig. 5.2.2.3 B) indicates two fold higher accessibility for trp(s) in 0.3 μM HEWL compared to aggregates from 120 μM. This argument is further strengthened by the systematic rise of global rotational correlation time (ϕ_2) in dansyl-HEWL conjugates due to

rise in molecular volume arising from growth of oligomers (Fig. 5.2.3 B-K). The oligomers formed with 0.3 μM HEWL are probably growth stalled, small unstructured dimers/trimers with exposed tryptophans and fast rotational tumbling. Assays of free thiols in HEWL (see Fig. 5.2.4 A, B and C) reveal that formation of aggregates during 96 hours of incubation at pH 12.2 are not stabilized by disulphide bonds unlike at later times (**Kumar et al., 2008**). In addition previous experiments with 150 mM KCl have demonstrated that electrostatic forces have no role in holding the aggregates together (**Homchaudhuri 2005**)., As ANS data suggest, It seems that the aggregates are held together predominantly by hydrophobic interactions. Indeed, aggregates stabilized by short-range attractive hydrophobic forces, have been shown to grow bigger in size (**Sahoo et al., 2009**) as observed here. Are HEWL aggregate(s) distributed among multiple/broad range of aggregate sizes *OR* does it form aggregates of a single/narrow range of sizes? Dynamic light scattering (DLS) experiments performed with 120 μM HEWL (lower concentrations like ~20 μM gave poor S/N ratio) incubated for 26 hours in pH 12.2 (see Fig. 5.2.3 P) reveal a broad heterogeneous size distribution (peaks at R_h ~2.0 (monomer), 12.5 & 17.4 nm and shoulders at R_h ~9.0 & 28.7 nm) of the aggregates, clearly support against selective increase in population of a specific oligomer. A previous model of HEWL self-association at pH 6 and 298 K has proposed a two equilibrium association with monomers, dimers and trimers (**Hampe et al., 1982**). The discrepancy in sizes revealed by DLS and time-resolved anisotropy suggests that shapes of the oligomers could be irregular as seen by AFM images. The oligomers formed with different monomer concentrations represent stable equilibrium intermediates in aggregation pathway of HEWL at pH 12.2 that can be isolated and investigated further. The AFM images (Fig.5.2.5 G-M) clearly show that ordered aggregates resembling amyloid fibrils can originate from small oligomers at 0.3 μM. From the low r_{ss} and fast ϕ_2 for 0.3 μM samples, it appears unlikely that these fibrils are present in any detectable amounts in solution. Significant presence of fibrils would have resulted in longer correlation times as reported earlier (**Jha et al., 2009**). Interestingly formation of fibrils directly from globular aggregates suggesting absence of intermediate step like a protofibril. These widely recognized, curly worm-like intermediate structures were never observed by us during AFM imaging of HEWL samples at pH 12.2. Interestingly, the lengths of the fibrils, originating radially in figure 5.2.5 I different, suggesting different rates of their elongation. We observed that at short incubation times (~12 hours), fibrils were more likely to be seen at lower monomer concentrations (≤ 3 μM)

compared to higher (≥ 50 μM) using AFM. Indeed it has been predicted that at high monomer concentrations, rate of molecular contact between a growing fibril and a monomer, varies inversely with protein concentration. Further monomer addition to fibril can be consider through dock-and-lock mechanism, such that the rate-determining step in the monomer addition is the lock phase in which both the preformed oligomer and the monomer undergo combined conformational changes that form a stable antiparallel higher-order oligomer (**Straub et al., 2011**). In view of their small size and unhindered dynamics, oligomers at low concentrations probably adapt their conformation more rapidly to enable locking onto the fibril. Perhaps, lower concentrations allow sufficient relaxation time for oligomers to attain right orientation to lock into ordered aggregates**,** like in protein crystallization (**Zhang et al., 2003**).Generally, protein polymerization has been modeled as either nucleation-dependent polymerization (NDP) or isodesmic (linear) polymerization (**Kumar et al., 2010, Frieden et al., 2007**). The NDP model demands: 1) a lag phase whose duration depends on protein concentration, 2) a critical concentration below which polymerization does not occur, 3) disappearance of lag phase on addition of pre-formed nuclei (seeds), and 4) dependence of rate of polymer elongation on protein concentration. Figure 5.2.3 A clearly shows that features 1 and 4 of NDP model are NOT validated here. Further, investigations using AFM (see Fig. 5.2.5 N-Q) have revealed HEWL aggregation even at concentrations as low as 30 nM. At this concentration (30 nM) globular and fibrillar aggregates was observed. hinting at absence of a critical concentration. Attempts to enhance growth of fibrils by seeding have not been successful either (data not shown). An isodesmic model has been proposed earlier for HEWL (2.8-10 mM) association at pH 4.6 in presence of 0.5 M NaCl with a much lower equilibrium constant of 118 M^{-1} (**Price et al., 1999**). Our observations clearly demonstrate that pH 12.2 is an ideal condition to investigate HEWL aggregation at very low concentration.

5.2.6: Model for HEWL aggregation at pH 12.2

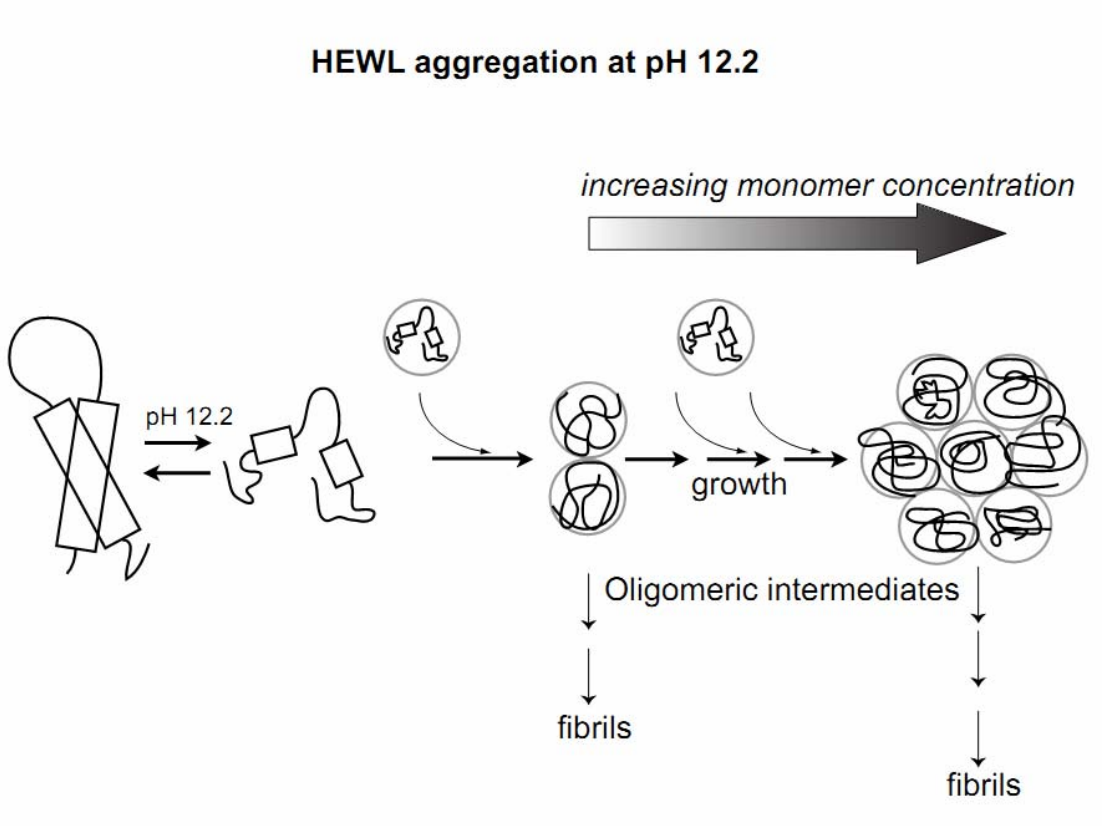

Figure 5.2.6: Represents the possible mechanistic pathway for aggregation in pH 12.2

$$M \xleftrightarrow{pH\ 12.2} B$$

$$B + B \rightleftharpoons B_2 \rightarrow \rightarrow \rightarrow \rightarrow fibrils$$

$$B_2 + B \rightleftharpoons B_3 \rightarrow \rightarrow \rightarrow \rightarrow fibrils$$

$$B_3 + B \rightleftharpoons B_4 \rightarrow \rightarrow \rightarrow \rightarrow fibrils$$

$$B_n + B \rightleftharpoons B_{n+1} \rightarrow \rightarrow \rightarrow \rightarrow fibrils$$

Scheme 1

Figure 5.2.6 and Scheme 1 depicts a possible mechanistic model for HEWL aggregation at pH 12.2 based on the above observations. Exposure to pH 12.2 causes rapid partial unfolding of the native protein M, resulting in monomer B with exposed hydrophobic regions. This triggers the process of aggregation forward forming small oligomers (B_2). Further

spontaneous addition of partially unfolded monomers enables the oligomers to grow bigger (B_3, ..., B_n) in a concentration dependent way. Low concentrations of M kinetically trap the oligomeric intermediates (B_2 and higher) by arresting their growth, however under appropriate conditions or after long times, these oligomers retain the ability to form fibrils. Previous reports based on aggregation and amyloid formation of HEWL at acidic pH stipulate incubation of high monomer concentrations (>1 mM) for several weeks at 37-57 °C (**Krebs et al., 2000, McAllister et al., 2005**). Apparently, the electrostatic repulsions between large positively charged HEWL molecules act as a barrier against amyloid formation. In contrast, the net charge of HEWL at pH 12.2 is likely to be small owing to its pI at 11.3, thus enabling facile formation of oligomers and amyloid fibrils even at sub-micromolar concentrations. Earlier on work with HEWL under acidic condition (pH 1.6 and 65 °C) has shown no amyloid fibril formation with 50 μM lysozyme upto 170 hours, suggesting a critical concentration >50 μM at this condition (**Mishra et al., 2007**). It was also shown that fragmentation of the HEWL polypeptide by acid hydrolysis forming the 49-101 peptides was essential for efficient fibril formation. In contrast, our earlier work (**Kumar et al., 2008**) has shown that significant fragmentation of HEWL at pH 12.2 occurs only after 16 days; hence it is unlikely that fragmentation has any role in fibril formation at alkaline pH after 12 hours. In another work under acidic conditions (1.2 mM HEWL, pH 2.0 with 175 mM NaCl), HEWL monomers have been shown to form uniformly sized oligomers (R_h ~3.8 nm) which after reaching a threshold concentration triggered protofibril nucleation. Later protofibrils grew when oligomers added on to ends of protofibrils (**Hill et al., 2009**). It is thus obvious that changing to alkaline pH has a dramatic influence on the mechanism of HEWL aggregation.

5.2.6 Conclusion

Taken together, our results clearly suggest that the following:

1. Progressive decrease in HEWL monomer concentration causes progressive reduction in size of HEWL oligomers at pH 12.2.
2. Growth of HEWL oligomers with higher monomer concentrations reveal deep hydrophobic interiors in contrast to those formed with lower concentrations of HEWL.
3. Fibril formation of HEWL at pH 12.2 proceeds through an isodesmic mechanism.
4. All oligomers, irrespective of the monomer concentration are competent to form amyloid fibrils.
5. Length and thickness of fibril does not dependent of initial monomer concentration.

Structure and dynamics of s-carboxyamidomethyl cysteine derivative aggregates of hen egg white lysozyme in alkaline pH 12.2 at room temperature

6.1 Introduction

Our previous work has shown that free thiol groups play a role in stable growth of aggregates which follows covalent interaction based aggregation **(Kumar, 2008)**. Other than lysozyme, like β- lactoglobulin undergoes intermolecular covalent aggregation **(Carrotta et al., 2001)**. Hence objective of this work was to suppress HEWL aggregation at pH 12.2 through chemical modification of –SH groups instead of using any external inhibitor, which halts the formation of non native intermolecular disulfide bonds that arise from reduction of –S-S- bonds. For this purpose free -SH was derivatised using iodoacetamide which block the formation of disulfide bond (-S-S-) in pH 12.2. We could successfully block the 50-70% of free –SH group (see Material and Methods), as confirmed by DTNP assay which gives color product reacting with free –SH. Subsequently aggregation phenomena were investigated and significant result presented here.

6.2 Results and discussion

6.2.1 Alteration of exposed hydrophobic regions

Monitoring the alteration of hydrophobic regions is one of the important approaches to ascertain if the growth of aggregates either suppressed or accelerated. Hence it is worthwhile to investigate the exposure of hydrophobic regions of S-carboxyamidomethyl cysteine derivativatized HEWL, which can confirm whether aggregation was hindered or accelerated while incubating in pH 12.2. For this purpose ANS dye was chosen, which binds non covalently to exposed hydrophobic regions and shows enhanced fluorescence intensity with blue shift of emission λ_{max} (**Stryer 1965, Parker et al., 1970**). Using 10 μM ANS dye, the extent of exposed hydrophobic regions in free thiol blocked HEWL and control HEWL in pH 12.2 after 48 hours and 144 hours (see Fig. 6.2.1) was checked. After 48 hours incubation, considerably enhanced ANS fluorescence intensity was observed on binding with thiol

blocked HEWL and red shift of emission $\lambda_{max\ was}$ noticed at 498 nm in contrast to control. However at similar time of incubation, the control HEWL sample showed slightly reduced ANS fluorescence intensity compared to –SH blocked HEWL, where emission λ_{max} was blue shifted to 471 nm. As incubation time progressed to 144 hours, the –SH blocked HEWL and control HEWL bound ANS fluorescence intensity substantially decreased, while emission λ_{max} of HEWL control was similar to 48 hours incubation time. However a marginal blue shift of emission λ_{max} was noticed from –SH blocked sample. The 10 μM ANS alone has not shown enhanced fluorescence intensity and shift from 526 nm emission λ_{max} in pH 12.2. buffer. These results demonstrate that s-carboxyamidomethyl cysteine derivative of HEWL harbours more ANS binding sites that are less non –polar compared to unblocked HEWL. The ANS peak shift from 526 nm to 498 nm indicates that ANS molecules are buried inside moderately hydrophobic sites (non polar environment) of –SH blocked HEWL (**Turner and Brand., 1968**). However control (HEWL pH 12.2) sample possess deeply buried, more non-polar environment for ANS. These results suggest that both HEWL either thiol free or thiol metylated HEWL exist at partially unfolded state in pH 12.2 at 48 h, however the thiol modified HEWL attains slightly flexible structure owing to absence of S-S bonds. Due to its flexible structure ANS is not protected by hydrophobic regions enormously, as confirmed by only slight ANS blue shift.

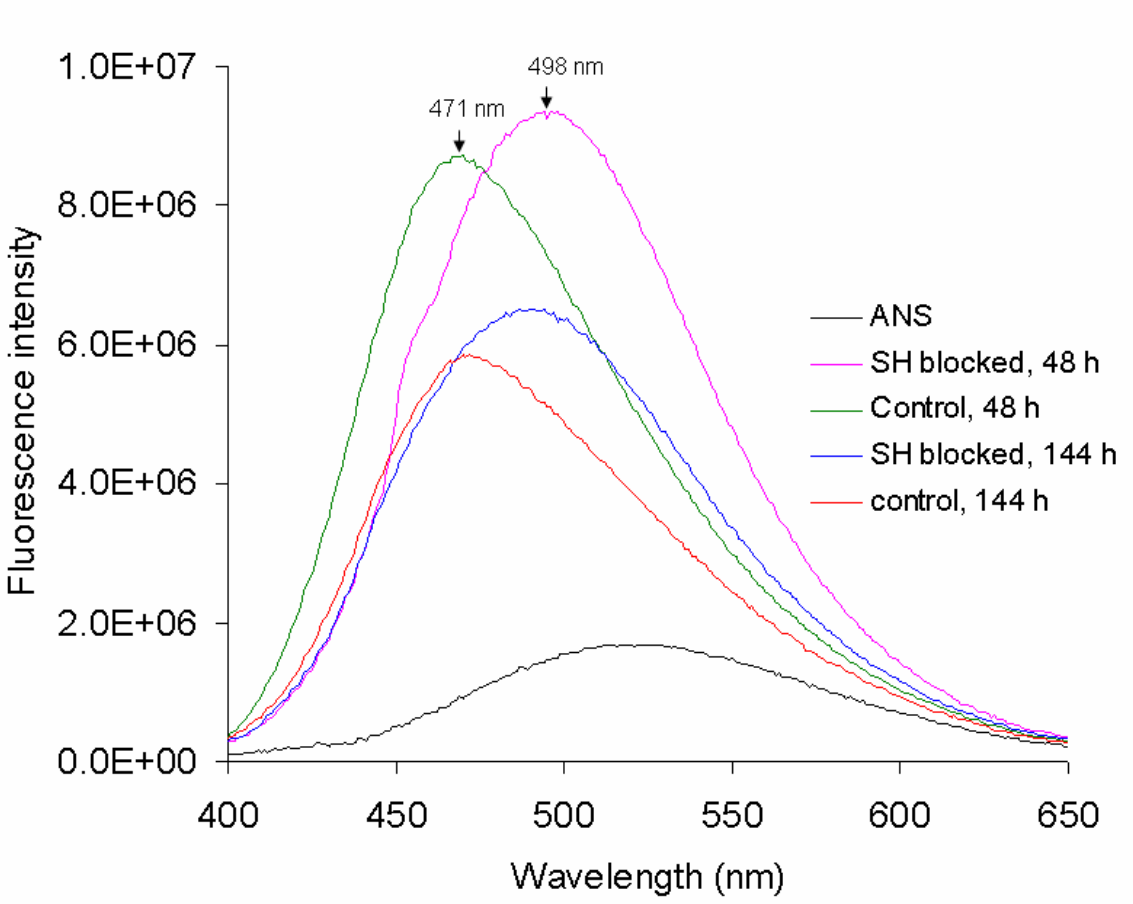

Figure 6.2.1: ANS spectra with thiol blocked HEWL and control, incubated in pH 12.2 at 301 K for different time.

6.2.2 Presence of oligomers/fibrils

Does the S-carboxyamidomethyl cysteine derivative of HEWL affect aggregation steps in pH 12.2, and if so which are the aggregation steps affected by this modification? To ascertain this question, Thioflavin T assay of HEWL S-carboxyamidomethyl cysteine derivative was performed after 48 hours. For detail assay method (see Material and Methods chapter). At 48 hours, normalized ThT fluorescence intensity from derivatised HEWL was found almost half compare to control HEWL pH 12.2 sample (see Fig. 6.2.2), which are known to give enhance ThT intensity after binding with mature fibril with increase in incubation time **(Kumar et al., 2008)**. It is likely that reduced Th T signal occurs due to presence of oligomers alone in sample which are known to bind with ThT (**Carrotta et al., 2001, Ahmed et al., 2010**),

however it has also reported that positive charge of Th-T can interact with negative charge of protein molecules which have no fibrils (**Khurana et al., 2005**).

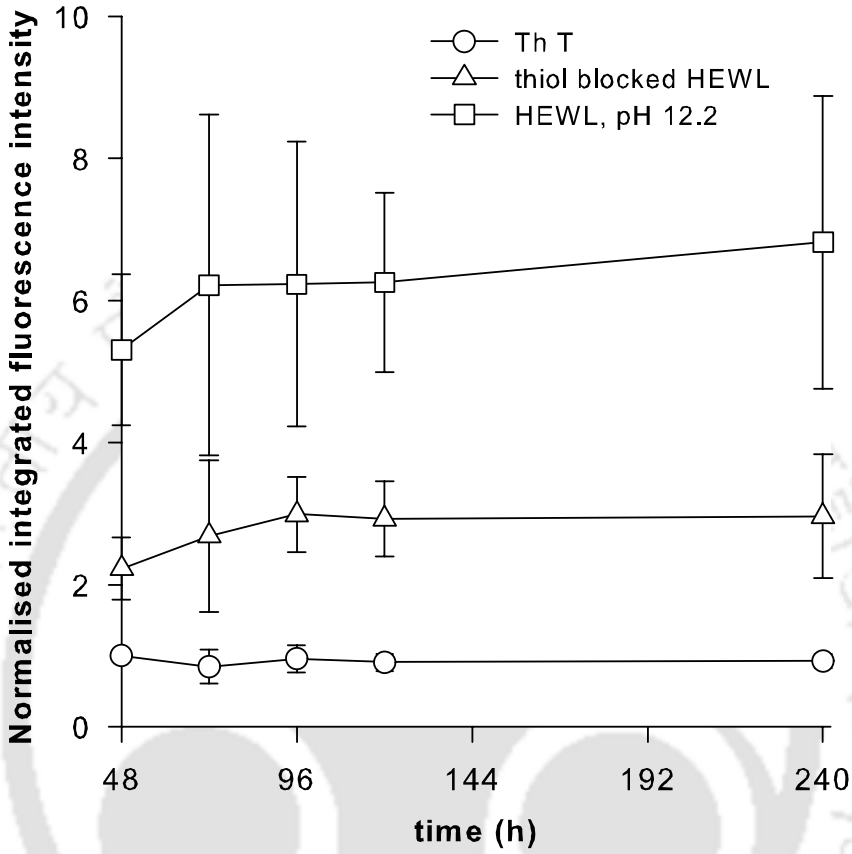

Figure 6.2.2: Thioflavin T assay of thiol blocked HEWL and HEWL (control), incubated in pH 12.2 at 301 K for different duration.

Further, as incubation time progresses from 48 hr to 240 hrs, ThT intensity was remained steady. It has been also noticed that error bar of ThT signal is high and fluctuating between 48 to 240 hours (see Fig. 6.2.2), which suggests a heterogeneous population of oligomers and fibril among different control (unblocked) samples.

6.2.3 Size and dynamics of aggregates

If –SH blocked HEWL likely to forms globular aggregates in pH 12.2., and then further investigation of size and rotational dynamics of entire aggregates is required. In this respect steady state fluorescence anisotropy of dansyl labeled –SH blocked HEWL and dansyl label HEWL (see Material and Methods) was monitored at different incubation time, to measure

the Brownian rotational motion that is proportional to the size of molecules. Since, It has been shown that dansyl is an ideal probe due to its long life time (`~ 13 ns) for measuring the changes in fluorescence steady state anisotropy which indicates the size dependent growth of aggregates **(Homchaudhuri et al., 2006)** From figure 6.2.3 A, we observed that initially r_{ss} value of dansyl probe relatively increasing in both condition thiol blocked HEWL- dansyl conjugates and HEWL conjugates. However the r_{ss} value of dansyl –SH blocked HEWL started saturating in between 12-24 hours and it remains steady (r_{ss} ~ 0.10) even at longer time like 72 hours. Interestingly, the r_{ss} values of dansyl probe conjugates with control sample (HEWL pH 12.2) keep rising and it started to saturate also beyond 24 hours and become steady with higher r_{ss} value (r_{ss} 0.14) at 72 hours. Hence it is worthwhile to explain the how change in r_{ss} affect the rotational dynamics of dansyl conjugates of HEWL. Figure 6.2.3 F and G show the fluorescence intensity decay of thiol blocked and control HEWL-dansyl aggregates. Table 6.2.4 show the variation of mean lifetime (τ_m) with time. It is clear that fluorescence life time of dansyl probe remains unaffected during the rise in r_{ss} shown in figure 6.2.3 A. Hence change in r_{ss} must arise due to change in rotational dynamics of HEWL aggregates. It has also noticed that rate constant, *k* for increasing anisotropy (from Eq. 6.2.3.1) is changing, as seen in table 6.2.1. It means that possibly addition of monomer while oligomerzation occurs at slower rate in thiol blocked HEWL compare to control.

A

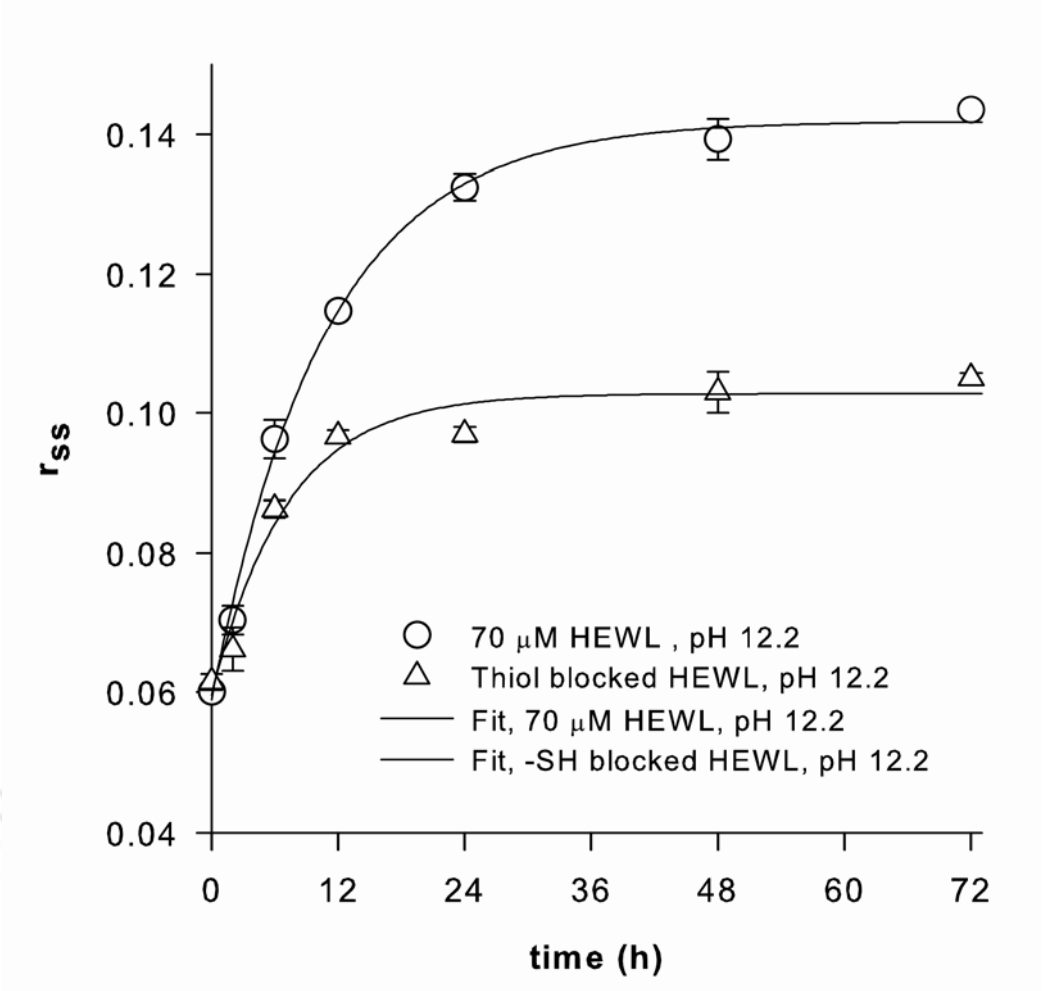

Figure 6.2.3 A: steady state fluorescence anisotropy of dansyl-HEWL thiol blocked and dansyl-HEWL (control) in pH12.2.

Table 6.2.1: Steady state anisotropy fitted parameter recovered for Fig. 6.2.3 A using equation

$$r_{ss}(t) = r_{ss}^{\infty} - (r_{ss}^{\infty} - r_{ss}^{0})e^{-kt} \qquad 6.2.3.1$$

Where, r_{ss}^{∞} represents r_{ss} at infinite time, r_{ss}^{0} represents r_{ss} at $t = 0$. k represents the rate constant for increasing in anisotropy.

Condition HEWL in pH 12.2	r_{ss}^{∞}	r_{ss}^{0}	k (hour $^{-1}$)	R^2
Thiol blocked	0.10	0.06	0.14	0.97
Unblocked thiol	0.14	0.06	0.09	1.0

For obtaining more information, time resolved fluorescence anisotropy decay kinetic measurements were performed to measure the rotational correlation time of aggregates. For this experiment similar dansyl- HEWL conjugates and thiol blocked HEWL conjugates were used and sample incubated in pH 12.2 at 301 K. Measurements were acquired at 32 and 48 hours after incubation (see detail Materials and Methods).

Raw fluorescence anisotropy decay data was fitted using equation

$$r(t) = A + \beta_1 e^{-t/\phi_1} + \beta_2 e^{-t/\phi_2} \qquad 6.2.3.2$$

Where, A is constant dependent on G- factor, β denotes the amplitude for ϕ_i, ϕ_1 and ϕ_2 refer to the fast and slow rotational correlation times, respectively. As the 0.15 ns IRF pulse-width is negligibly small in comparison to the time scale of protein rotational motion (> 4 ns), the extracted values of ϕ_2 by this tail-fit approach are not affected by consequences of IRF convolution.

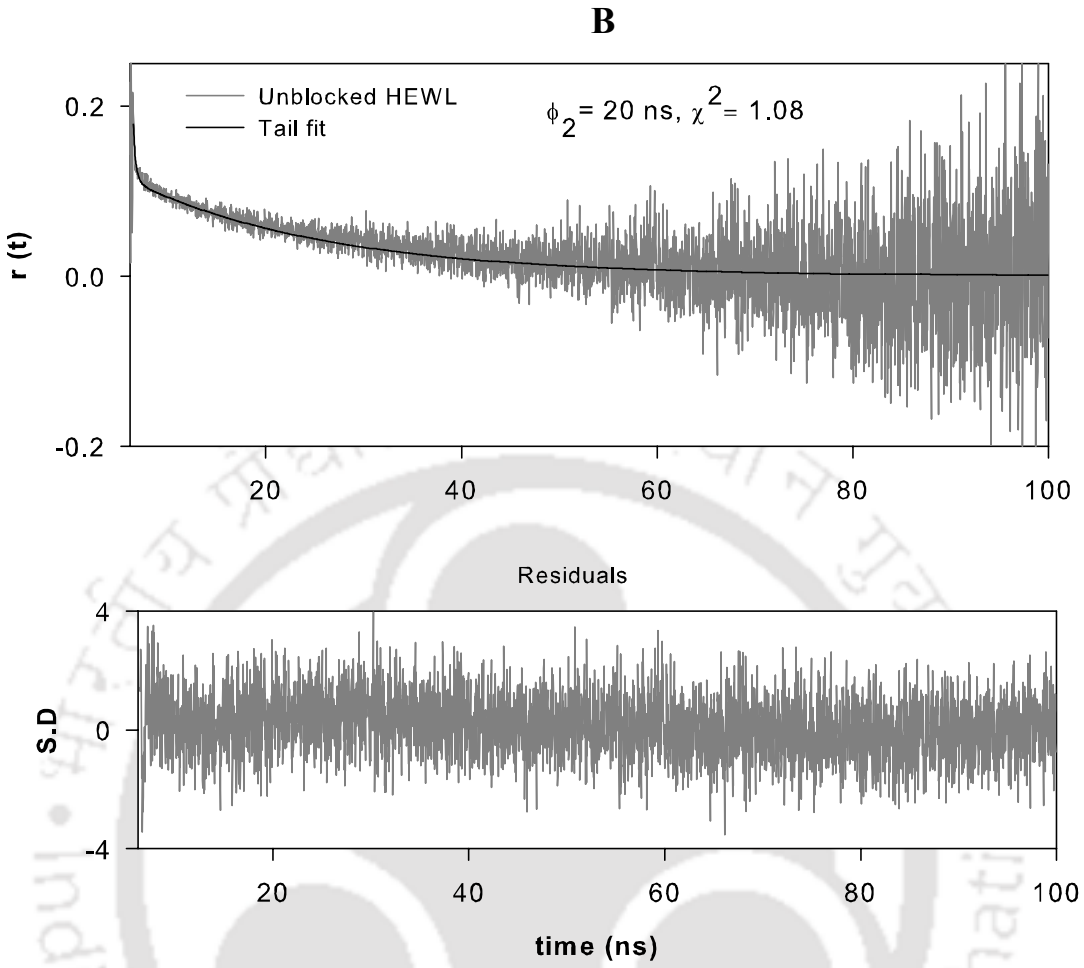

Figure 6.2.3 B: Fluorescence anisotropy decay kinetics of unblocked dansyl- HEWL in pH 12.2 at 32 h.

Raw fluorescence anisotropy decay data was fitted using equation 6.2.3.2

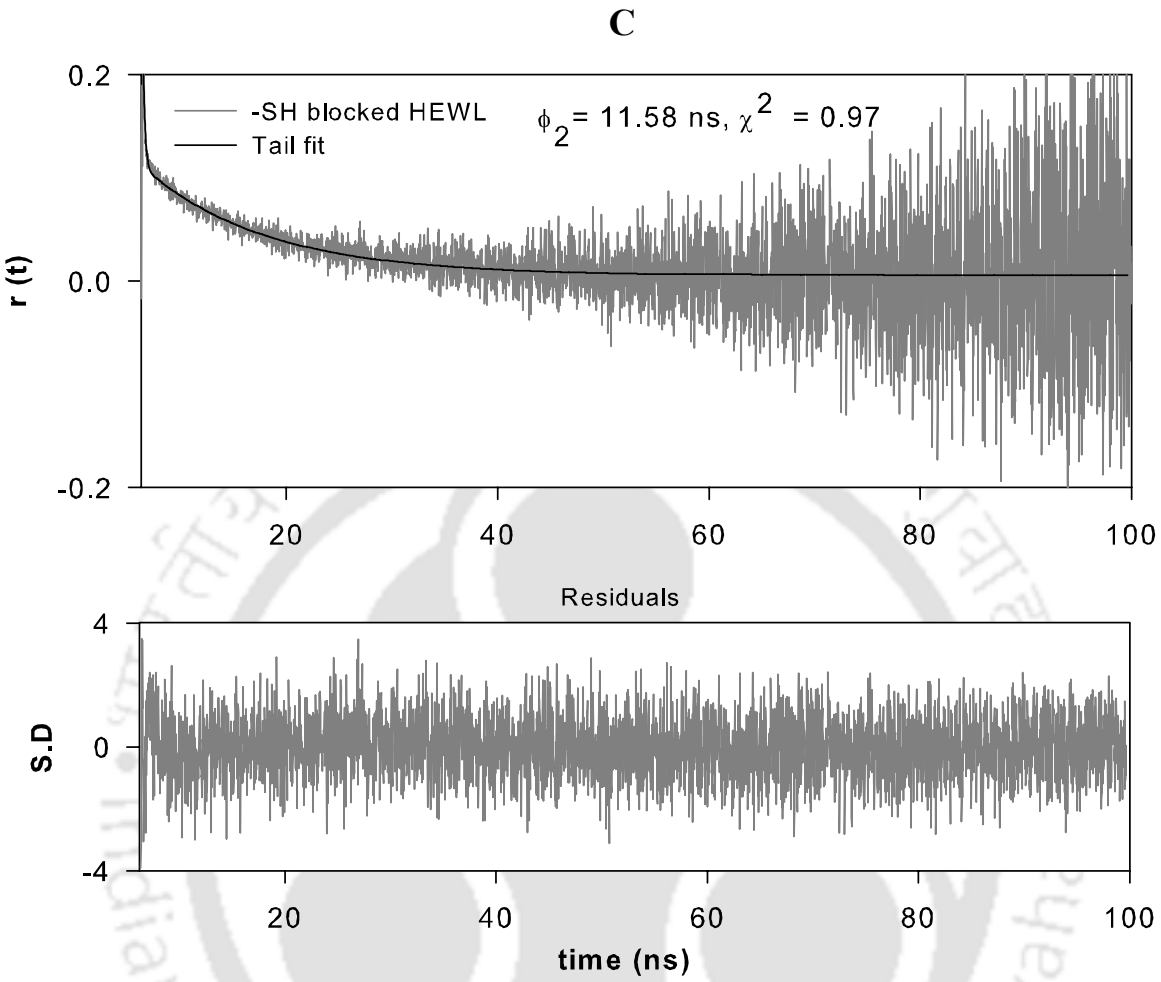

Figure 6.2.3 C: Fluorescence anisotropy decay kinetics of blocked dansyl- HEWL in pH 12.2 at 32 h.

Raw fluorescence anisotropy decay data was fitted using equation 6.2.3.2

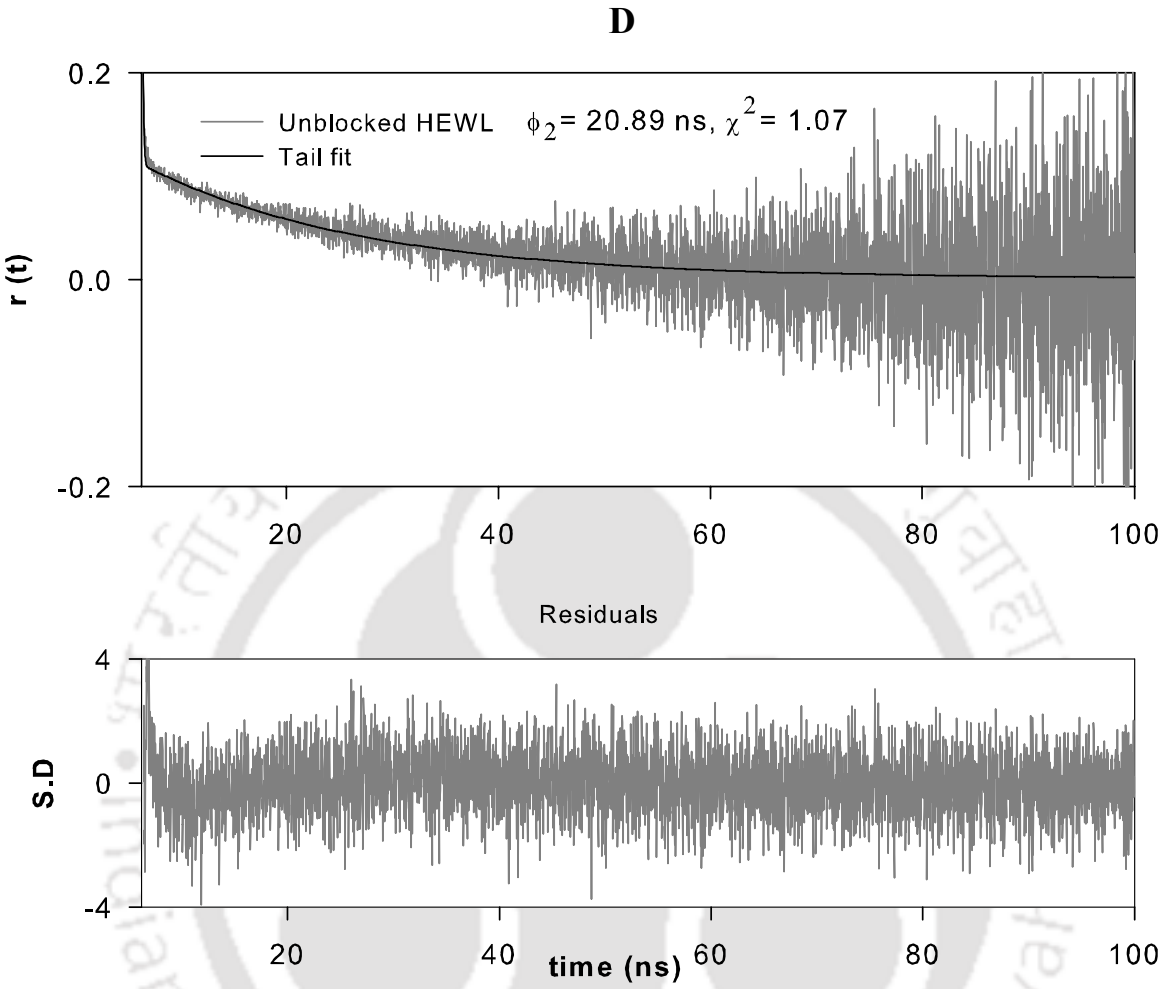

Figure 6.2.3 D: Fluorescence anisotropy decay kinetics of unblocked dansyl- HEWL in pH 12.2 at 48 h.

Raw fluorescence anisotropy decay data was fitted using equation 6.2.3.2

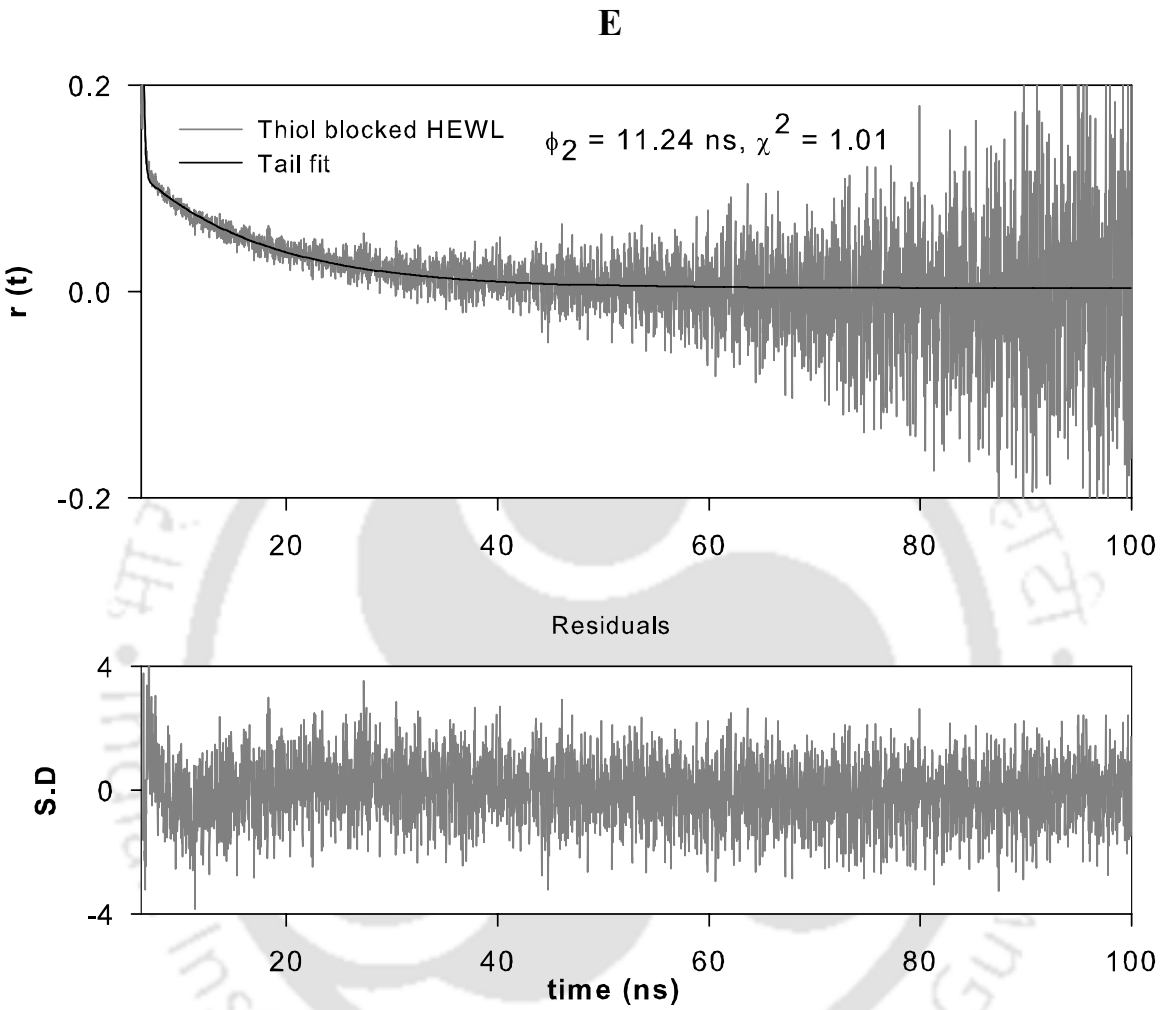

Figure 6.2.3 E: Fluorescence anisotropy decay kinetics of blocked dansyl- HEWL in pH 12.2 at 48 h.

Table 6.2.2: Decay parameter recovered from tail fit analysis for

Fig. 6.2.3 B, C, D & E

Condition HEWL in pH 12.2	Time (hours)	ϕ_1 (ns)	α_1	ϕ_2 (ns)	α_2	χ^2	A
Thiol blocked	32	0.19	0.02	11.58	0.98	0.969	0.005
Unblocked thiol	32	0.3	0.01	20	0.99	1.08	0
Thiol blocked	48	0.1	0.04	11.24	0.96	1.1	-0.001
Unblocked thiol	48	0.07	0.01	20.89	0.99	1.07	0.001

Table 6.2.3: Average long rotational correlation time (ϕ_2) recovered from tail fit analysis

Condition HEWL in pH 12.2	Time (hours)	Average ϕ_2 (ns)	S.D
Thiol blocked	32	11.7	±1.2
Thiol blocked	48	11.6	±0.5
Unblocked thiol	32	21.4	±1.2
Unblocked thiol	48	22.7	±2.5

Figure 6.2.3 B-E represents the raw anisotropy decay curves for thiol unblocked & blocked HEWL-dansyl conjugates, after 32 and 48 hours of incubation at alkaline pH 12.2. Using the raw data the decays were tail fitted to a sum of two exponentials (see Eq. 6.2.3.2), acquiring two rotational correlation times (ϕ). The slower correlation time (ϕ_2) corresponds to the average global tumbling rate of the aggregate ensemble in the solution which is directly proportional to its hydrodynamic volume as per the Stoke-Einstein equation. The average slower correlation time (ϕ_2) with S.D is indicated in table 6.2.3 and individual ϕ_2 has shown in table 6.2.2. The average slower correlation time (ϕ_2) was found lower such as 11.7 ns &11.6 ns for the thiol blocked sample after 32 and 48 hours incubation time compared to unblocked sample at similar time such as 21.4 & 22.7 ns. These data suggest that once free thiol of HEWL is blocked to abolish the formation intermolecular disulfide bonds, the growth

of aggregates in pH 12.2 diminishes as compare to unblocked HEWL. Hence we may conclude that formation of intermolecular disulfide bonds is critical for formation and perhaps stabilization of larger aggregates.

F

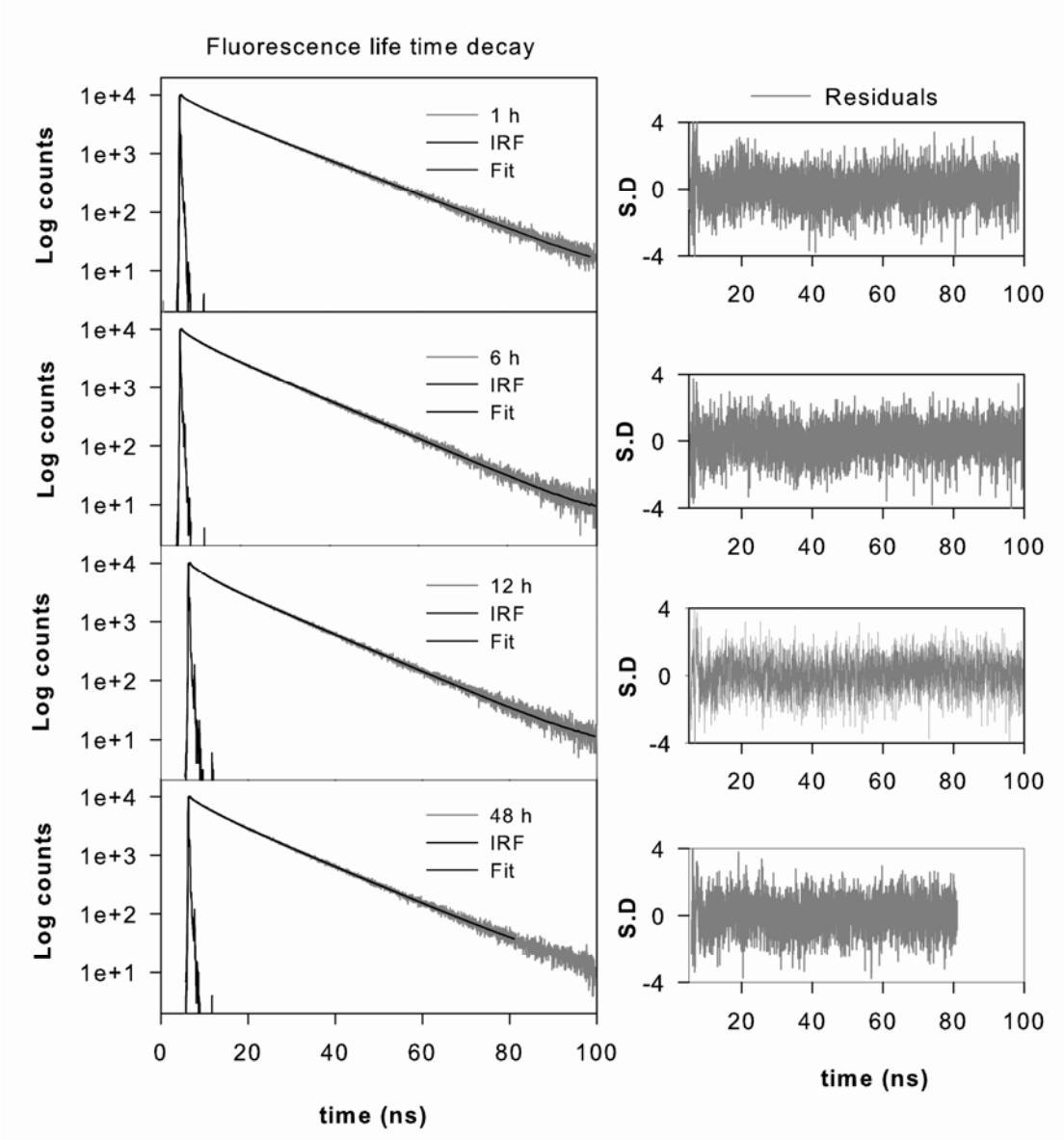

Figure 6.2.3 F: Fluorescence intensity decay of thiol blocked dansyl-HEWL in pH 12.2.

G

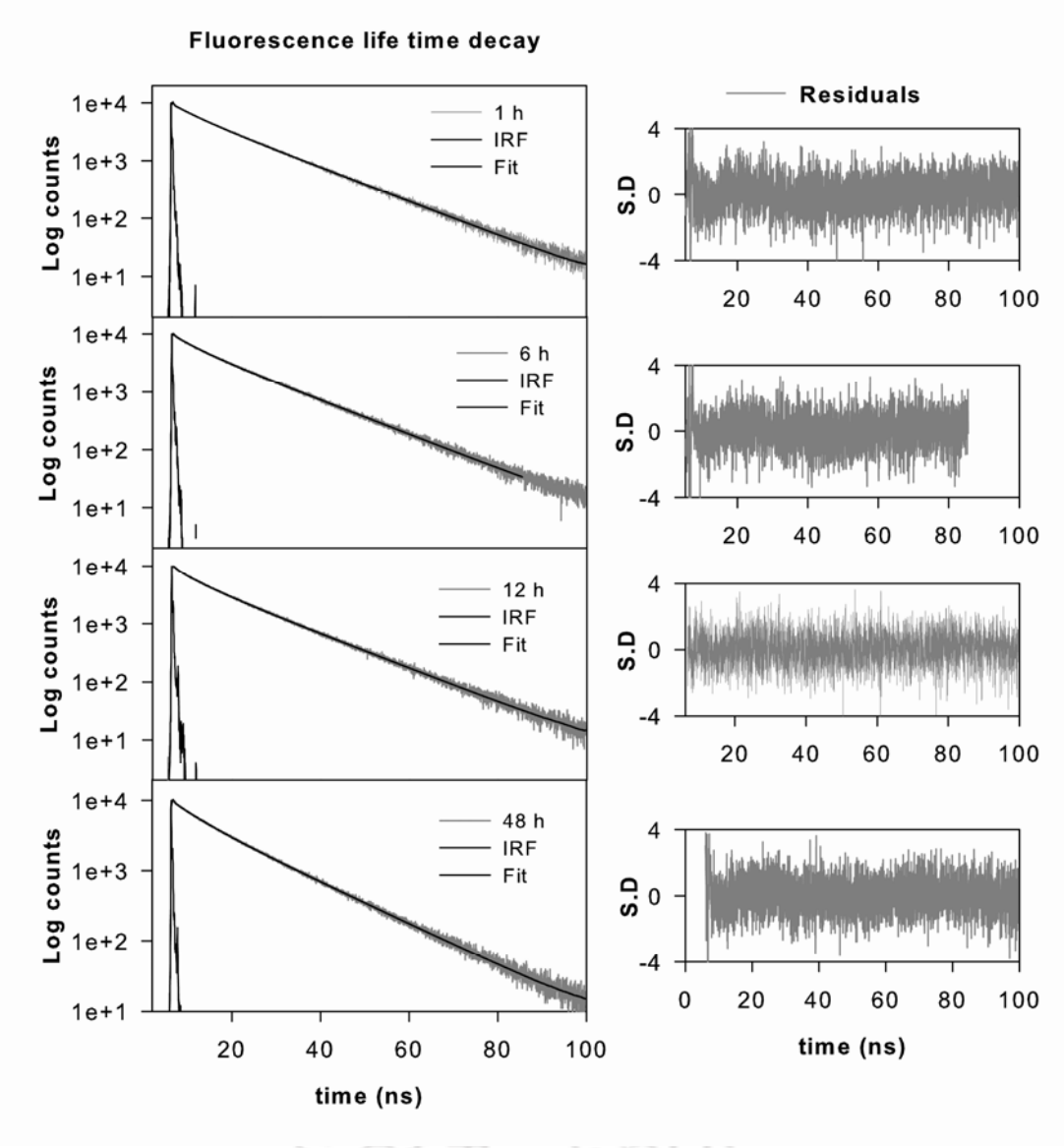

Figure 6.2.3 G: Fluorescence intensity decay of thiol unblocked dansyl-HEWL in pH 12.2.

Table 6.2.4: Fluorescence intensity analysis

Condition	Time (hours)	τ_1 (ns)	α_1	τ_2 (ns)	α_2	τ_3 (ns)	α_3	τ_m (ns)	χ^2
Thiol blocked HEWL, pH 12.2	1	0.17	0.02	4.89	0.08	14.74	0.9	**13.7**	1.1
	6	0.26	0.01	3.92	0.09	13.37	0.894	**12.3**	1.06
	12	0.2	0.02	3.79	0.1	13.78	0.88	**12.5**	1.1
	48	0.28	0.014	4.99	0.12	14	0.87	**12.8**	1.1
HEWL, pH 12.2	1	0.15	0.02	5.06	0.08	14.72	0.99	**15.0**	1.15
	6	0.22	0.01	4.85	0.11	14.58	0.88	**13.4**	1.16
	12	0.78	0.02	5.77	0.14	14.66	0.84	**13.1**	1.04
	48	0.27	0.01	5.42	0.13	14.46	0.86	**13.1**	1.09

6.2.4 Morphology of aggregates

After monitoring hydrophobocity, presence of fibril assay, change in size of aggregates, it is really essential to compare the morphology of 70 μM thiol blocked HEWL and 70 μM unblocked HEWL morphology. For this purpose atomic force microscopy technique was employed. (For detail experimental parameters see in materials and methods). The AFM images were acquired after incubation of thiol blocked and free thiol HEWL in pH 12.2 for various duration. Topograph image was captured at 72 h, shown in Fig. 6.2.4 A, indicating presence of small globular aggregates in large population which appears in *z*-scale ranging from 0-5 Å. It means that aggregates are flat owing to less molecular packing inside aggregates **(Kumar et al., 2008)**. However topograph image with 0-10 Å z-scale shown in Fig. 6.2.4 B at 11 days, indicating as incubation time progresses, small population of large globular aggregates are likely to be seen in thiol blocked HEWL. Interestingly fibrillar structure was not detected while scanning more than hundred spot multiple times. This finding is supporting Th T assay where Th T fluorescence has also seen reduced compare to control. The morphology of free thiol containing HEWL was found like mixture of large and small globular aggregates (see Fig. 6.2.4 C & D) Our earlier report has shown that 75 μM HEWL forms very well matured fibril in pH 12.2 after 30 days **(Swaminathan et al., 2011).**

A

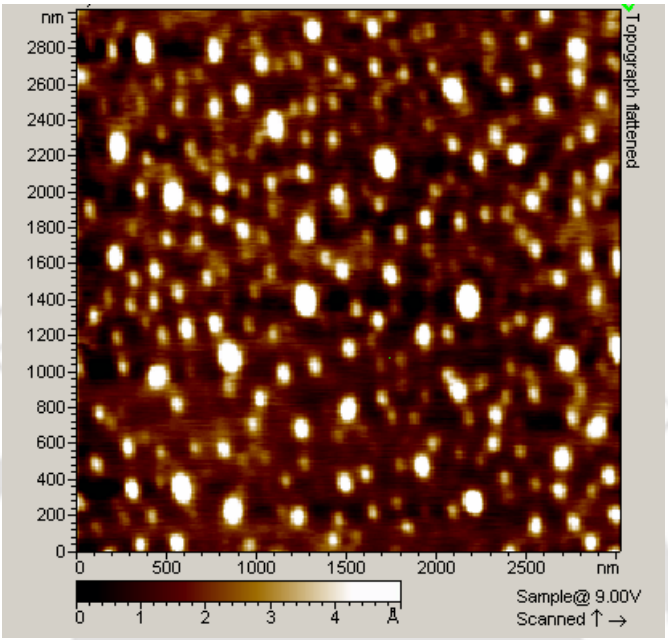

B

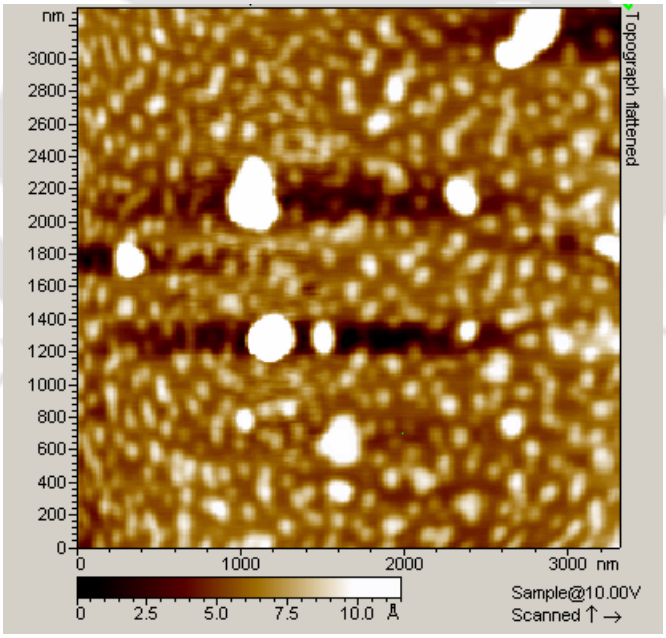

Figure 6.2.4: (A) Topograph AFM image of thiol blocked HEWL in pH 12.2, after 72 h and (B) Topograph AFM image of thiol blocked HEWL in pH 12.2, after 11 days.

C

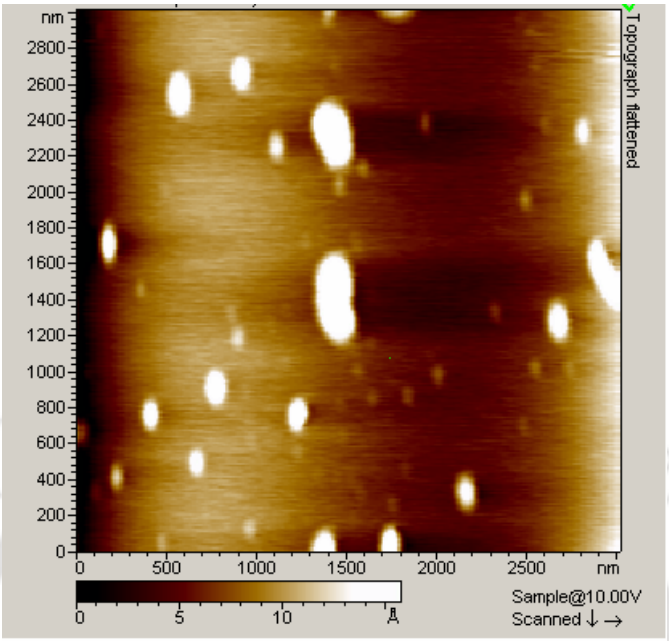

D

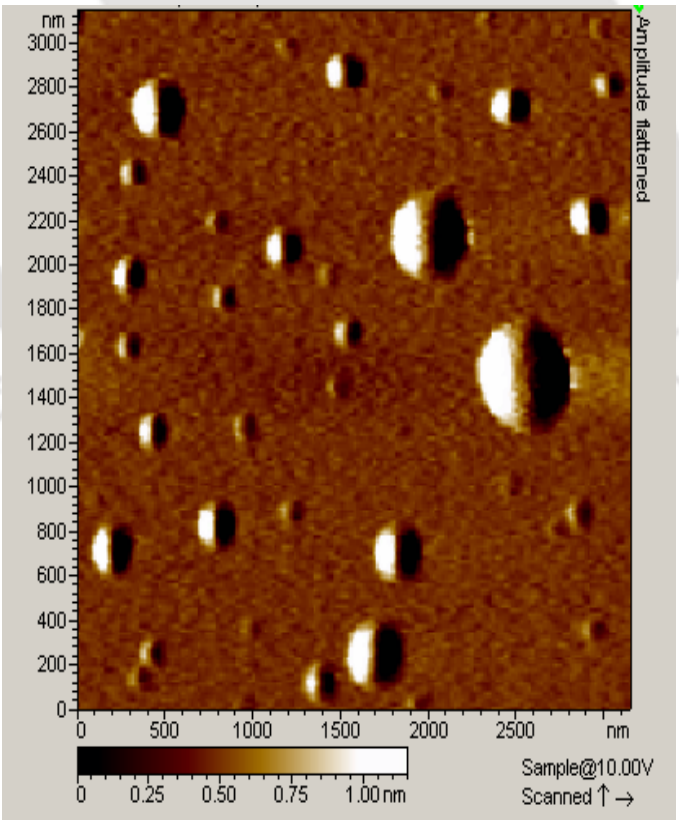

Figure 6.2.4: (C) Topograph AFM image of HEWL in pH 12.2, after 8 days and (D) Amplitude AFM image at similar condition mention in 'C'.

Finally it is imperative to discuss that after modifying the free thiol HEWL are able to form only small globular aggregates but not fibrillar aggregates. What could be reason behind this either role of hydrophobic exposure or abolishing the formation intermolecular disulphide bond? Xie and coworkers discussed that dissociation of disulfide bonds in HEWL disrupt the compact native structure of and triggers to expose of buried hydrophobic residues. These exposed hydrophobic residues interacts each other and self assemble quickly as result amorphous aggregates are formed **(Xie et al., 2011)**. Our findings are also matching from this report such as owing to its flexible conformation, hydrophobic interaction minimizes the molecular interaction which leads to slow down the aggregation process conversely strong hydrophobic interaction actively participates in accelerates aggregation which is evident from HEWL pH 12.2 incubated sample (**Xie et al., 2011, Chiti et al., 2006, Kumar et al., 2008**). It can also justify that intermolecular disulfide bonds play important role to maintain the degree of hydrophobic exposure which favours interaction between the molecules. Results found in Figure 6.2.3 A-E, clearly suggest that size of HEWL aggregates is smaller after blocking the free thiol. It matches the results obtained from AFM image (see 6.2.4 A) where z-height was found less comare to control. It means that aggregates are flat and small owing to less molecular packing inside aggregates **(Kumar et al., 2008)**. It has also reported that free thiol group play a role in growth of HEWL amorphous aggregates **(Xie et al., 2011).**

Recently it has reported that the thiol alkylated human lysozyme is likely to form fibril in pH 2 at different temperature after 24 hours (**Mossouto et al., 2011)**. Contribution of disulfide bonds to stability, folding and amyloid fibril formation in PI3-SH3 domain protein was investigated (**Graña-Montes et al., 20011**). Interestingly, ThT and AFM results are consistent and suggest that fibril formation was suppressed after alkylating free thiol of HEWL in pH 12.2 at room temperature. It seems that intermolecular disulphide bond play a role in fibril formation.

6.2.5 Conclusions

1. Exposed hydrophobic residues are responsible for formation of globular aggregates as seen in –SH blocked and unblocked HEWL samples.
2. Free -SH plays a vital role in growth and stabilization of both amorphous as well as fibrillar aggregates.
3. Modification of free –SH is a useful strategy to inhibit HEWL aggregation at alkaline pH.

References

Adair, B. D. and Engelman, D. M. **(1994)** Glycophorin a helical transmembrane domain dimerize in phospholipid bilayers: A Resonance Energy Transfer Study. *Biochemistry* **33,** 5539–5544.

Ahmed, M., Davis, J., Aucoin, D., Sato, T., Ahuja, S., Aimoto, S., Elliott, J. I, Van Nostrand, W. E and Smith, S. O. **(2010)** Structural conversion of neurotoxic amyloid-beta 1–42 oligomers to fibrils. *Nat. Struct. Mol. Biol.* **17**, 1545–9993.

Alzheimer, A. **(1907)** Uber eine eigenartige Eskrankung der Nirnrinde. *Allg. Z. Psychiatr. Psych. Gerichtl*. **64,** 146- 148.

Anderson, W. L. and Wetlaufer, D. B. **(1975)** A new method for disulfide analysis of peptides. *Anal. Biochem.* **67,** 493–502.

Andreu, J. M, Timasheff, S. N. (**1986**) The measurement of cooperative protein self-assembly by turbidity and other techniques. *Methods Enzymol*. **130**, 47–59.[

Antzutkin, O. N, Balbach, J. J., Leapman, R. D., Rizzo, N. W, Reed, J., Tycko, R. **(2000)** Multiple quantum solid-state NMR indicates a parallel, not antiparallel, organization of β-sheets in Alzheimer's β-amyloid fibrils *Proc. Natl.Acad. Sci*. USA **97,** 13045–50.

Arakawa, T., and Tsumoto, K. (2003). The effects of arginine on refolding of aggregated proteins: not facilitate refolding, but suppress aggregation. *Biochem. Biophys. Res. Commun*. **304**, 148–152.

Arakawa, T., Ejima, D., Tsumoto, K., Obeyama, N., Tanaka, Y., Kita, Y., and Timasheff, S. N. **(2007)** Suppression of protein interactions by arginine: A proposed mechanism of the arginine effects. *Biophys. Chem.* **127**, 1–8.

Arnaudov, L. N. and De Vries, R. **(2005)** Thermally induced fibrillar aggregation of hen egg white lysozyme. *Biophys., J.* **88,** 515-526.

Arora, D., and Khanna, N. **(1996)** Method for increasing the yield of properly folded recombinant human gamma interferon from inclusion bodies. *J. Biotechnol.* **52**, 127–133.

Aso, Y., Shiraki., K. and Takagi, M. **(2007)** Systematic analysis of aggregates from 38 kinds of non disease-related proteins: Identifying the intrinsic propensity of polypeptides to form amyloid fibrils. *Biosci. Biotechnol. Biochem.* **71**, 1313-1321.

Astbury, W. T, Dickinson, S., Bailey, K. **(1935)** The x-ray interpretation of the denaturation and the structure of the seed globulihns. *Biochem J.* **29,** 2351–2360.

Balbach J. J, Petkova, A.T, Oyler, N.A, Antzutkin, O.N, Gordon, D. J, Meredith, S. C., and Tyco, R. **(2002)** Supramolecular structure in full-length Alzheimer's beta-amyloid fibrils: evidence for a parallel beta-sheet organization from solid-state nuclear magnetic resonance. *Biophys. J.* **83**, 1205–1216.

Bauer, H. H., Aebi, U., Haner, M., Hermann, R., Muller, M., Arvinte, T. and Merkle,H. P.**(1995)** Architecture and polymorphism of fibrillar supramolecular assemblies produced by in vitro aggregation of human calcitonin. *J. Struct. Biol.*, **115,** 1–15.

Baxa, U., Cheng, N., Winkler, D. C., Chiu, T. K., Davies, D. R, Sharma, D., Inouye H., Kirschner, D. A, Wickner, R. B and Steven, A. C **(2005)** Filaments of the Ure2p prion protein have a cross-beta core structure. *J. Struct. Biol* **150**, 170–179.

Baynes, B. M., Wang, D. I. C., and Trout, B. L. **(2005)** Role of arginine in stabilisation of proteins against aggregation. *Biochemistry* **44,** 4919–4925.

Bellova, A., Bystrenova, E., Koneracka, M., Kopcansky, P., Valle, F., Tomasovicova, N., Timko, M., Bagelova, J., Biscarini, F. and Gazova, Z. **(2010)** Effect of Fe(3)O(4) magnetic nanoparticles on lysozyme amyloid aggregation. *Nanotechnology.* **21**, 065103

Bhattacharyya, J. and Das, K. P. **(1999)** Effect of surfactants on the prevention of protein aggregation during unfolding and refolding processes comparison with molecular chaperone α-Crystallin. *J. Disp. Sci. Tech.* **20,** 1163-1178.

Binnig, G., Quate, C.F., Gerber, Ch. **(1986)** Atomic force microscope. Phys. Rev.Lett. **56,** 930–933.

Bitan, G., Kirkitadze, M. D., Lomakin, A., Vollers, S. S., Benedek, G. B. and Teplow, D. B. **(2003)** Amyloid beta -protein (Abeta) assembly: Abeta 40 and Abeta 42 oligomerize through distinct pathways. *Proc. Natl .Acad. Sci. U S A.* **100**, 330-335.

Blake, C. C. F., Johnson, L. N., Mair, G. A., North, A. C. T., Phillips, D. C. and Sarma, V. R. **(1967b)** Crystallographic studies of the activity of hen egg white lysozyme. Proc. Roy. Soc. **167B,** 378-388.

Blake, C. C. F., Koenig, D. F., Mair, G. A., North, A. C. T., Phillips, D. C. and Sarma, V. R. **(1965)** Structure of Hen egg-white lysozyme:A three-dimensional fourier synthesis at 2 Å resolution. *Nature* **206,** 757-761.

Blake, C. C. F., Mair, G. A., North, A. C. T., Phillips, D. C. and Sarma, V. R. **(1967a)** On the conformation of the hen egg-white lysozyme molecule. Proc. Roy. Soc. **167B,** 365.

Blow, D. M, Chayen, N. E, Lloyd, L. F, Saridakis, E. **(1994)** Control of nucleation of protein crystals. *Protein Sci.***3**, 1638–1643.

Bohrmann, B., Adrian, M., Dubochet, J., Kuner, P., Müller, F., Huber, W., Nordstedt, C. and Döbeli, H. **(2000)** Self-assembly of beta-amyloid 42 is retarded by small molecular ligands at the stage of structural intermediates. *J. Struct. Biol.* **130**, 232-246.

Brand, L. and Gohlke, J. R. **(1972)**. Fluorescence probes for structure. *Annu. Rev. Biochem.* **41**, 843-868.

Bucciantini, M., Giannoni, E., Chiti, F., Baroni, F., Formigli, L., Zurdo, J., Taddei, N., Ramponi, G., Dobson, C. M., and Stefani, M. **(2002)** Inherent toxicity of aggregates implies a common mechanism for misfolded disease. *Nature* **416**, 507-511.

Byrne, N. and Angell, C. A. **(2009)** Formation and dissolution of hen egg white lysozyme amyloid fibrils in protic ionic liquids. *Chem. Commun.* 1046–1048.

Campioni, S., Mannini, B., Zampagni, M., Pensalfini, A., Parrini, C., Evangelisti, E., Relini, A., Stefani, M., Dobson, C. M., Cecchi, C. and Chiti, F. **(2010)** A causative link between the structure of aberrant protein oligomers and their toxicity. *Nat .Chem. Biol.* **6**, 140-147.

Canet, D., Last, A. M, Tito, P., Sunde, M., Spencer, A., Arche, D. B, Redfield, C., Robinson, C.V, Dobson, C. M. **(2002)** Local cooperativity in the unfolding of an amyloidogenic variant of human lysozyme. *Nature Struct. Biol.* **9,** 308–314.

Canfield, R. E. **(1963)** The amino acid sequence of egg white lysozyme. *J. Biol. Chem.* **238,** 2698-2707.

Cao, A., Hu, D. and Lai, L. **(2004)** Formation of amyloid fibrils from fully reduced hen egg white lysozyme. *Protein Sci.* **13**, 319-324

Chapman, M. R, Robinson, L. S, Pinkner, J. S, Roth, R., Heuser J., Hammar, M., Normark, S. and Hultgren, S. J. **(2002)** *Escherichia coli* curli operons direct amyloid fiber formation. *Science* **295,** 851-855.

Chatterjee, A., Moulik, S. P., Majhi, P. R. and Sanyal, S. K. (**2002**) Studies on surfactant–biopolymer interaction. I. Microcalorimetric investigation on the interaction of cetyltrimethylammonium bromide (CTAB) and sodium dodecylsulfate (SDS) with gelatin (Gn), lysozyme (Lz) and deoxyribonucleic acid (DNA). *Biophys. Chem*. **98**, 313–327.

Carrotta, R., Bauer, R., Waninge, R. and Rischel, C. **(2001)** Conformational characterization of oligomeric intermediates and aggregates in beta-lactoglobulin heat aggregation. *Protein Sci*. **10**, 1312-1318.

Chiti F., Taddei N., Baroni F., Capanni C., Stefani M., Ramponi G., Dobson C. M. **(2002)** Kinetic partitioning of protein folding and aggregation. *Nat. Struct. Biol*. **9,** 137–143.

Chiti, F. and Dobson, C. M. **(2006)** Protein misfolding functional amyloid and human disease. *Annu. Rev. Biochem*. **75,** 333-366.

Chiti, F. and Dobson, C.M. **(2009)** Amyloid formation by globular proteins under native conditions. *Nature Chem. Biol.* **5,** 15-22.

Chiti, F., Taddei, N., Bucciantini, M., White, P., Ramponi, G., and Dobson, C. M. **(2000)** Mutational analysis of the propensity for amyloid formation by a globular protein. *EMBO J.* **19,** 1441–1449.

Citron, M. (2002) Alzheimer's disease: Treatment in discovery and development. *Nat. Neurosci.* (Suppl.) 5, 1055-1057.

Clamp, M., Fry, B., Kamal, M., Xie, X., Cuff, J., Lin, M. F., Kellis, M., Lindblad-Toh, K. and Lander, E. S. **(2007)** Distinguishing protein-coding and noncoding genes in the human genome. *Proc. Natl. Acad. Sci. U S A* **49**, 19428-19433.

Cohen, A. S. **(1986)** General introduction and a brief history of the amyloid fibril, in Marrink, J., and Van Rijswijk, M. H. (Eds.), Amyloidosis, 3–19, Nijhoff, Dordrecht.

Collins, R. S., Douglass, A., Ronald D. Vale, R. D. and Weissman, S. L. **(2004)** Mechanism of prion propagation: Amyloid growth occurs by monomer addition. *PLoS. Biol.* **2**: e321.

Costa, P. R., D. A. Kocisko, B. Q. Sun, P. T. Lansbury, and R. G. Griffin. (**1997**) Determination of peptide amide configuration in a model amyloid fibril by solid-state NMR. J. Am. Chem. Soc. **119**, 10487–10493.

Creighton, T. E. **(1990)** Review on protein folding. *Biochem. J.* **270,** 1-16.

Cunningham, F.E., Proctor, V.A and Goetsch, S. J (**1991**) Egg-white lysozyme as a food preservative: an overview. *World's Poultry Sci. J.* **47**, 141-163.

Demidov V. V. **(2004)** Nanobiosensors and molecular diagnostics: A promising partnership. *Expert. Rev. Mol. Diagn.* **4,** 267–268.

Ding, H., Wong, P. T., Edgar L. Lee, E. L., Gafni, A. and Steel, D. G., **(2009)** Determination of the oligomer size of amyloidogenic protein β-amyloid (1–40) by single-molecule spectroscopy. *Biophys. J*. **97,** 912-921.

Dobson, C. M. **(1999)** Protein misfolding, evolution and disease. *Trends Biochem. Sci*. **24,** 329–332.

Dobson, C. M. **(2004)** Principles of protein folding, misfolding and aggregation. Semin. *Cell Dev. Biol.* **15**, 3 -16.

Dobson, C. M., Evans, P. A. and Radford, S. E. **(1994)** Understanding how protein fold: The lysozyme story so far. *Trend. Biochem. Sci*. **19,** 31-37.

Dumoulin, M., Canet, D., Last, A. M., Pardon, E., Archer, D. B., Muyldermans, S., Wyns, L., Matagne, A., Robinson, C. V., Redfield, C., and Dobson, C. M. **(2005)** Reduced global cooperativity is a common feature underlying the amyloidogenicity of pathogenic lysozyme mutations. *J. Mol. Biol.* **346**, 773–788.

Dumoulin, M., Last, A. M., Desmyter, A., Decanniere, K., Canet, D., Larsson, G., Spencer, A., Archer, D. B., Sasse, J., Muyldermans, S., Wyns, L., Redfield, C., Matagne, A., Robinson, C. V., and Dobson, C. M. **(2003)** A camelid antibody fragment inhibits the formation of amyloid fibrils by human lysozyme. *Nature* **424**, 783-788.

Eftink, M. R. **(1991)** Fluorescence quenching: Theory and applications. *In Topics in Fluorescence Spectroscopy*, **2** Principles. J. R. Lakowicz, editor. Plenum Press.

Eisert, R., Felau, L. and Brwon, L., R. **(2006)** Methods for enhancing the accuracy and reproducibility of congo red and thioflavin T assays. *Anal. Biochem.* **353,** 144-146.

Evans, K. C., Berger, E. P., Cho, C. G, Weisgraber, K. H, Lansbury, P.T. (1995) Apolipoprotein E is a kinetic but not a thermodynamic inhibitor of amyloid formation: Implications for the pathogenesis and treatment of Alzheimer's disease. *Proc Natl Acad Sci USA*.**92,** 763–767.

Fandrich, M. and Dobson, C. M. **(2002)** The behaviour of polyamino acids reveals an inverse side chain effect in amyloid structure formation. *EMBO J*. **21**, 5682–5690.

Fernandez, C. O., Hoyer, W., Zweckstetter, M., Jares-Erijman, E. A., Subramaniam, V., Griesinger, C., and Jovin, T. M. (2004) NMR of alpha-synuclein-polyamine complexes elucidates the mechanism and kinetics of induced aggregation. *EMBO J.* **23,** 2039–2046.

Ferrao-Gonzales, A.D., Souto, S.O., Silva, J.L., and Foguel, D. **(2000)** The pre aggregated state of an amyloidogenic protein: Hydrostatic pressure converts native transthyretin into the amyloidogenic state. *Proc. Natl. Acad. Sci.* **97**, 6445–6450.

Fink, A. L. **(1998)** Protein aggregation: Folding aggregates, inclusion bodies and amyloid. *Fold Des* **3**, R9–R23.

Fleming, A. **(1922)** On a remarkable bacteriolytic element found in tissues and secretions. *Proc. Roy. Soc.* **93B** , 306-317.

Forman, M. S., Trojanowski, J. Q., and Lee, V. M. **(2004)** Neurodegenerative diseases: a decade of discoveries paves the way for therapeutic breakthroughs. *Nat. Med.* **10,** 1055- 1063.

Fowler, D. M, Koulov, A. V., Balch, W. E., Kelly, J. W. **(2007)** Functional amyloid from bacteria to humans. *Trends Biochem Sci.* **32,** 217-224.

Fradinger, E.A., Maji, S.K., Lazo, N.D. and Teplow, D.B. **(2005)** Studying amyloid beta-protein assembly in: Amyloid Precursor Protein (Xu, W.X.a.H.,Ed.), 83–110, CRC Press, Boca Ration, London, New York, Washington, DC.

Frieden, C. **(2007)** Protein aggregation processes: in search of the mechanism. *Protein Sci.* **16,** 2334–2344.

Friedreich, N. K., A. Zur Amyloidfrage. **(1859)** *Virchows Arch. Pathol. Anat.* **15,** 50- 65.

Fujiwara, S., Matsumoto, F., and Yonezawa Y. **(2003)** Effects of salt concentration on association of the amyloid protofilaments of hen egg white lysozyme studied by time-resolved neutron scattering. *J. Mol. Biol.* **331**, 21-28.

Furukawa, Y., Fu, R., Deng, H. X., Siddique, T., and O'Halloran, T. V. **(2006)**. Disulfide crosslinking protein represents a significant fraction of ALS-associated Cu, Zn-superoxide dismutase aggregation in spinal cords of model mice. *Proc. Natl. Acad. Sci. U.S.A.* **103**, 7148–7153.

Gazova, Z., Bellova, A., Daxnerova, Z., Imrich, J., Kristian, P., Tomascikova, J., Bagelova, J., Fedunova, D., and Antalik, M. **(2008)** Acridine derivatives inhibit lysozyme aggregation *Eur. Biophys. J.* **37**, 1261–1270.

Gharibyan, A. L., Zamotin, V., Yanamandra, K., Moskaleva, O.S., Margulis, B.A., Kostanyan, I.A., Morozova-Roche, L.A. **(2007)** Lysozyme amyloid oligomers and fibrils induce cellular death via different apoptotic/necrotic pathways, *J. Mol. Biol.* **365** 1337–1349.

Ghosh, P., Kumar, A., datta, B. and Rangachari, V. **(2010)** Dynamics of protofibril elongation and association involved in Ab42 peptide aggregation in Alzheimer's disease. *BMC Bioinformatics* **11** (Suppl 6): S24.

Giasson, B. I., Forman, M. S., Higuchi, M., Golbe, L. I., Graves, C. L., Kotzbauer, P. T., Trojanowski, J. Q. and Lee, V. M. **(2003)** Initiation and synergistic fibrillization of tau and alpha-synuclein. *Science* **300**, 636-640.

Goda, S., Takano, K., Yamagata, Y., Nagata, R., Akutsu, H., Maki, S., Namba, K., and Yutani, K. **(2000)** Amyloid protofilament formation of hen egg lysozyme in highly concentrated ethanol solution. *Protein Sci.* 9, 369–375.

Gosal, W. S., Morten, I. J., Hewitt, E. W., Smith, D. A., Thomson, N. H. and Radford, S. E. **(2005)** Competing pathways determine fibril morphology in the self-assembly of beta2-microglobulin into amyloid. *J .Mol .Biol.* **351**, 850-864.

Graña-Montes, R., Groot de , N. S., Castillo, V., Sancho, J., Velazquez-Campoy, A., Ventura, S., (2011) Contribution of disulfide bonds to stability, folding and amyloid fibril formation: The PI3-SH3 domain case. *Antioxidants & Redox Signaling*.

Griffiths, J. M., Ashburn, T. T., Auger, M., Costa, P. R., Griffin, R. G. and Lansbury, P. T., Jr. **(1995)** Rotational resonance solid-state NMR elucidates a structural model of pancreatic amyloid. *J. Am. Chem. Soc.* **117,** 3539-3546.

Guijarro, J. I., Sunde, M., Jones, J. A., Campbell, I.D., and Dobson, C.M. **(1998)** Amyloid fibril formation by an SH3 domain. *Proc. Natl. Acad. Sci.* **95**, 4224–4228.

Haass, C., and Selkoe, D. J. **(2007)** Soluble oligomers in neurodegeneration: lessons from the Alzheimer's amyloid beta-peptide. *Nat. Rev. Mol. Cell Biol.* **8**, 101–112.

Hameed, M., Ahmad, B., Fazili, K. M., Andrabi, K. and Khan, R. H. **(2007)** Different molten globule-like folding intermediates of hen egg white lysozyme induced by high pH and tertiary butanol. *J. Biochem. (Tokyo)* **141**, 573–583.

Hameed, M., Ahmad, B., Khan, R. H., Andrabi, K. I. and Fazili, K. M. **(2009)** Tertiary butanol induced amyloidogenesis of hen egg white lysozyme (HEWL) is facilitated by aggregation-prone alkali-induced molten globule like conformational state. *Protein Pept. Lett.* **16**, 56-60

Hammarstrom, P., Jiang, X., Hurshman, A. R., Powers, E. T. and Kelly, J.W. (2002) Sequence-dependent denaturation energetics: a major determinant in amyloid disease diversity. *Proc. Natl. Acad. Sci. USA* **99**, 16427–16432.

Hammarstrom, P., Wiseman, R. L., Powers, E. T. and Kelly, J. W. **(2003)** Prevention of transthyretin amyloid disease by changing protein misfolding energetics. *Science* **299**, 713–716.

Hanssen, O. **(1908)** Ein Beitrag zur Chemie der amyloiden Entartung. *Biochem. Z.* **13,** 185 -198.

Hampe, O. G., Tondo, C. V. and Hasson-Voloch, A. **(1982)** A biophysical model of lysozyme self-association. *Biophys J.* 39:77-82.

Harper, J. D., and Landsbury, P. T. J. (**1997)** Models of amyloid seeding in Alzheimer's disease and scrapie: mechanistic truths and physiological consequences of the time-dependent solubility of amyloid proteins. *Annu. Rev. Biochem*. **66**, 385–407

He, J., Xing, Y. F., Huang, B., Zhang, Y. Z. and Zeng, C. M. **(2009)** Tea catechins induce the conversion of preformed lysozyme amyloid fibrils to amorphous aggregates. *J. Agric. Food. Chem.* **57**, 11391-11396

Herczenik, E., and Gebbink, M. F. B. G. **(2008)** Molecular and cellular aspects of protein misfolding and disease. *FASEB J*. 22, 2115-2133.

Hevehan, D. L., and Clark, D. B. E. **(1997)** Oxidative renaturation of lysozyme at high concentrations. *Biotechnol. Bioeng.* **54**, 221-230.

Hill, S. E., Robinson, J., Matthews, G. and Muschol, M. (2009) Amyloid protofibrils of lysozyme nucleate and grow via oligomer fusion. Biophys J. 96, 3781-3790

Holley, M., Eginton, C., David Schaefer, D., and Brown, L. R. (**2008)** Characterization of amyloidogenesis of hen egg lysozyme in concentrated ethanol solution. *Biochem. Biophys.Res. Commun.*, **373**, 164-168.

Homchaudhuri, L. **(2005)** Ph.D. *Thesis*. Indian Institute of Technology Guwahati. India.

Homchaudhuri, L., Kumar, S. and Swaminathan, R. (2006) Slow aggregation of lysozyme in alkaline pH monitored in real time employing the fluorescence anisotropy of covalently labeled dansyl probe. *FEBS Lett.* **580**, 2097-2101.

Hoshino, M., Katou, H., Hagihara, Y., Hasegawa, K., Naiki, H. and Goto, Y. **(2002)** Mapping the core of the β (2)-microglobulin amyloid fibril by H/D exchange. *Nat. Struct. Biol.* **9,** 332–336

Huang, B., He, J., Ren, J., Yan, X. Y. and Zeng, C. M. **(2009)** Cellular membrane

Hung, Y-Tz., Lin, M-S., Chen, W-Y., and Wang, S. S-S. (2010). Investigating the effects of sodium dodecyl sulfate on the aggregative behavior of hen egg-white lysozyme at acidic pH. *Colloids and Surfaces B: Biointerfaces* **81,** 141–151.

Jain, N., Bhattacharya, M. and Mukhopadhyay, S. **(2011)** Kinetics of surfactant-induced sggregation of lysozyme studied by fluorescence spectroscopy. *J Fluoresc.* **21**, 615-625.

Jarrett, J. T, and Lansbury, P.T Jr. **(1993)** Seeding "one-dimensional crystallization" of amyloid: a pathogenic mechanism in Alzheimer's disease and scrapie? *Cell*, **73,** 1055-1058.

Jha, A., Udgaonkar, J. B. and Krishnamoorthy, G. **(2009)** Characterization of the heterogeneity and specificity of interpolypeptide interactions in amyloid protofibrils by measurement of site-specific fluorescence anisotropy decay kinetics. *J. Mol. Biol.* **393,**735-752.

Jimenez, J. L, Nettleton, E. J, Bouchard, M., Robinson, C. V, Dobson, C. M, Saibil H. R. **(2002)** The protofilament structure of insulin amyloid fibrils. *Proc Natl Acad Sci USA* **99**, 9196-9201.

Jimenez, J. L., Tennent, G. A., Pepys, M. B., and Saibil, H. R. **(2001)** Structural diversity of ex vivo amyloid fibrils studied by cryo-electron microscopy. *J. Mol. Biol.* **311**, 241-247.

John, V., Beck, J. P., Bienkowski, M. J., Sinha, S., Heinrikson, R. L. (2003) Human beta-secretase (BACE) and BACE inhibitors. *J. Med.Chem.* **46,** 4625- 4630.

Johnson, L. N. and Phillips, D. C. (**1965)** Structure of some crystalline lysozyme-inhibitor complexes determined by X-ray analysis at 6 Å resolutions. *Nature* **206,** 761-763.

Jolles, J., Jauregui-Adell, J. and Jolles, P. **(1963)** The chemical structure of Hen's egg –white lysozyme: Detailed study. *Biochim. Biophys. Acta.* **78,** 668-689.

Jolles, P. **(1964)** Recent developments in the study of lysozymes. *Angew. Chem. Int. Ed. Engl*. **3**, 28-36.

Kallberg, Y., Gustafsson, M., Persson, B., Thyberg, J., and Johansson, J. **(2001)** Prediction of amyloid fibril-forming proteins. *J. Biol. Chem.* **276** 12945–12950.

Kayed, R., Head, E., Thompson, J. L., Mclntire, T. M., Milton, S. C., Cotman, C. W., and Glabe, C. G. **(2003)** Common structure of soluble amyloid oligomers implies common mechanism of pathogenesis. *Science* **300**, 486–489.

Kelly, J. W. **(1998)** the alternative conformations of amyloidogenic proteins and their multi-step assembly pathways. *Curr. Opin .Struct .Biol.* **8**, 101–106.

Kheterpal, I., Cook, K. D. and Wetzel, R. **(2006)** Hydrogen/deuterium exchange mass spectrometry analysis of protein aggregates. *Meth. Enzymol.* **413,** 140– 66.

Kodaka, M., (**2004)** Interpretation of concentration-dependence in aggregation kinetics. *Biophys. Chem.* 109, 325–332.

Korth, C., May, B. C. H., Cohen, F. E., and Prusiner, S. B. **(2001)** Acridine and phenothiazine derivatives as pharmacotherapeutics for prion disease. Proc. Natl. Acad. Sci. USA. **98**, 9836–9841.

Krebs, M. R. H., Wilkins, D. K., Chung, E. W., Pitkeathly, M. C., Chamberlain, A. K., Zurdo, J., Robinson, C. V. and Dobson, C. M. **(2000)** Formation and seeding of amyloid fibrils from wild-type hen lysozyme and a peptide fragment from the β-Domain. *J. Mol. Biol*. **300,** 541–549.

Krishnan,R., Lindquist, S. L. **(2005)** Structural insights into a yeast prion illuminate nucleation and strain diversity. *Nature* **435**,765-772.

Khurana, R., Coleman, C., Ionescu-Zanetti, C., Carter, S. A., Krishna, V., Grover, R. K., Roy, R., Singh, S. **(2005)** Mechanism of thioflavin T binding to amyloid fibrils. *J. Struct. Biol.* **151**, 229–238.

Kumagai, I. (2005). Nondenaturing solubilization of β2 microglobulin from inclusion bodies by L-arginine. *Biochem. Biophys. Res. Commun.* **328**, 189–197.

Kumar, S., and Udgaonkar, J. B. **(2010)** Mechanism amyloid formation by proteins. *Current Sci.* **98,** 639-656.

Kumar, S., and Swaminathan, R. **(2007)**. Employing the fluorescence anisotropy and quenching kinetics of tryptophan to hunt for residual structures in denatured proteins. *J. Chem. Sci.* **119**,141-145.

Kumar, S., Ravi, V. K. and Swaminathan, R. **(2008)** How do surfactants and DTT, affect the size, dynamics, activity and growth of soluble lysozyme aggregates? *Biochem. J.* **415**, 275-288.

Kumar, S. **(2008)** Exploring the structure and dynamics of proteins in non-native states using fluorescence spectroscopy. *Ph.D. Thesis,* Indian institute of Technology Guwahati.

Kumar, S., Ravi, V. K. and Swaminathan, R. **(2009)** Suppression of lysozyme aggregation at alkaline pH by tri-N-acetylchitotriose. *Biochim. Biophys. Acta.* **1794**, 913-920.

Kumita, J. R., Poon, S., Caddy, G. L., Hagan, C. L., Dumoulin, M., Yerbury, J. J., Stewart, E. M., Robinson, C. V., Wilson, M. R., and Dobson, C. M. **(2007)** The extracellular chaperone clusterin potently inhibits human lysozyme amyloid formation by interacting with prefibrillar species. *J. Mol. Biol.* **369**, 157–167.

Kuramitsu, S., Ikeda, K., Hamaguchi, K., Miwa, S., Nakashima, K. **(1975)** Binding of N-Acetyl-chitotriose to human lysozyme *J. Biochem.* (Tokyo) **78,** 327–333.

Ladiwala, A. R., Dordick, J. S. and Tessier, P. M. **(2011)** Aromatic small molecules remodel toxic soluble oligomers of amyloid beta through three independent pathways. *J Biol. Chem.* **286**, 3209-3218

Lakowicz, J.R. (1999) Principles of Fluorescence Spectroscopy, Kluwer Academic/Plenum Press, New York.

Lambert, M. P., Barlow,A. K., Chromy, B. A., Edwards, C., Freed, R., Liosatos, M., Morgan, T. E., Rozovsky, I., Trommer, B. and Viola, K. L. **(1998)** Diffusible, nonfibrillar ligands from Aβ1-42 are potent central nervous system neurotoxins. *Proc. Natl. Acad. Sci. USA.* **95**, 6448-6453.

Landau, M., Sawaya, M. R, Faull, K. F, Laganowsky, A., Jiang, L., Sievers, S. A., Liu, J., Barrio, J. R., Eisenberg, D. **(2011)** Towards a Pharmacophore for Amyloid. *PLoS. Biol* 9(6): e1001080. doi:10.1371/journal.pbio.1001080.

Landau, M., Sawaya, M. R., Faull, K. F., Laganowsky, A., Jiang, L., Sievers, S. A., Liu, J., Barrio, J. R. and Eisenberg, D. **(2011)** Towards a pharmacophore for amyloid. *PLoS Biol.* **9**, e1001080.

Lansbury, P. T., Costa, P. R., Griffiths, J. M., Simon, E. J, Auger, M., Halverson, K. J, Kocisko, D. A, Hendsch, Z. S, Ashburn, T. T, Spencer, R. G. S, Tidor, B., Griffin, R. G. **(1995)** Structural model for the beta-amyloid fibril based on interstrand alignment of an antiparallel-sheet comprising a C-terminal peptide. *Nat. Struct. Biol* **2,** 990–998.

LeVine, H. **(1999)** Quantification of b-sheet amyloid fibril structures with thioflavin T. *Meth. Enzymol.* **309,** 274–284.

Lewy, F. Paralysis agitans. **(1912)** In Pathologische Anatomie. Handbuch der Neurologie; Lewandowski, M., Abelsdorff, G., Eds.; Springer Vertag: Berlin, Germany, 920 -933.

Li, J.; Zhu, M.; Rajamani, S.; Uversky, V. N.; Fink, A. L. **(2004)** Rifampicin Inhibits Alpha-Synuclein Fibrillation and Disaggregates Fibrils. *Chem. Biol.* **11,** 1513- 1521.

Lieu, V. H., Wu, J. W., Wang, S. S. S., and Wu, C.H. **(2007)** Inhibition of amyloid fibrillization of hen egg-white lysozymes by rifampicin and p-benzoquinone. *Biotechnol. Prog.* **23**, 698-706.

Lomakin, A., Chung, D. S, Benedek, G. B, Kirschner, D. A, Teplow, D. B. **(1996)**. *Proc. Natl. Acad. Sci. USA* **93**, 1125–1129.

Lue, L. F., Kuo, Y. M., Roher, A. E., Brachova, L., Shen, Y., Sue, L., Beach, T., Kurth, J. H., Rydel, R. E. and Rogers, J. **(1999)** Soluble amyloid beta peptide concentration as a predictor of synaptic change in Alzheimer's disease. *Am. J. Pathol*. **155**, 853-862.

McAllister, C., Karymov, M. A., Kawano, Y., Lushnikov, A. Y., Mikheikin, A., Uversky, V. N. and Lyubchenko, Y. L. **(2005)** Protein interactions and misfolding analyzed by AFM force spectroscopy. *J Mol Biol.* **354,** 1028-1042.

Mankar, S., A. Anoop, A., Sen, S., and Maji, S. K. **(2011)** Nanomaterials: amyloids reflect their brighter side. Nano Reviews **2,** 6032

Marcon, G., Plakoutsi, G., Canale, C., Relini, A., Taddei, N., Dobson, C. M., Ramponi, G. and Chiti, F. **(2005)** Amyloid formation from HypF-N under conditions in which the protein is initially in its native state. *J. Mol .Biol.* **347**, 323-335.

Margittai, M. and Langen, R. **(2008)** Fibrils with parallel in-register structure constitute a major class of amyloid fibrils: molecular insights from electron paramagnetic resonance spectroscopy. *Q. Rev. Biophys.* **41,** 265–297.

Maurois, A. **(1963)**. "The Life of Sir Alexander Fleming" Penguin, London

May, B. C. H., Fafarman, A. T., Hong, S. B., Rogers, M., Deady, L. W., Prusiner, S. B., and Cohen, F. E. **(2003)** Potent inhibition of scrapie prion replication in cultured cells by bis-acridines. *Proc. Natl. Acad. Sci. USA.* **100**, 3416–3421.

Merlini, G., and Bellotti, V. **(2003)** Molecular mechanisms of amyloidosis. *N. Engl. J. Med.* **349**, 583–596.

Minton, A. P. **(2001)** *J. Biol. Chem.* **276**, 10577–10580.

Mishra, R., Sorgjerd, K., Nystrom, S., Yen-Chi Yu, A. and Hammarstrom, P. **(2007)** Lysozyme amyloidogenesis is accelerated by specific nicking and fragmentation but decelerated by intact protein binding and conversion. *J. Mol. Biol.* **366,** 1029–1044.

Moosavi-Movahedi, A. A., Pirzadeh, P., Hashemnia, S., Ahmadiana,S., Hemmateenejad, B., Amania,B., Saboury, A.A., Ahmad, F., Shamsipur, M., Hakimelahi, G.H., Tsai, F., Alijanvand, H.H., and Yousefi, R. **(2007)** Fibril formation of lysozyme upon interaction withsodium dodecyl sulfate at pH 9.2. *Colloids and Surfaces B: Biointerfaces* **60**, 55–61.

Morozova-Roche, L. A., Zurdo, J., Spencer, A., Noppe, W., Receveur, V., Archer, D. B., Joniau, M., and Dobson, C. M. **(2000)** Amyloid fibril formation and seeding by wild-type human lysozyme and its disease-related mutational variants. *J. Struct. Biol.* **130**, 339-351.

Moren, A. K., Nyden, M., Soderman, O. and Khan, A. (**1999**) Microstructure of protein–surfactant complexes in gel and solution-an NMR relaxation study. *Langmuir* **15**, 5480–5488.

Morshedi, D., Ebrahim-Habibi, A., Moosavi-Movahedi, A. A. and Nemat-Gorgani, M. **(2010)** Chemical modification of lysine residues in lysozyme may dramatically influence its amyloid fibrillation. *Biochim. Biophys. Acta.* **1804**, 714-722

Morshedi, D., Rezaei-Ghaleh, N., Ebrahim-Habibi, A., Ahmadian, S. and Nemat-Gorgani, M. **(2007)** Inhibition of amyloid fibrillation of lysozyme by indole derivatives-possible mechanism of action. *FEBS J.* **274**, 6415-6425.

Mossuto, M. F., Bolognesi, B., Guixer, B., Dhulesia, A., Agostini, F., Kumita, J. R., Tartaglia, G. G., Dumoulin, M., Dobson, C. M. and Salvatella, X. (2011) Disulfide bonds reduce the toxicity of the amyloid fibrils formed by an extracellular protein. *Angew. Chem. Int. Ed Engl*. **50**, 7048-7051.

Nag, S., Sarkar, B., Bandyopadhyay, A., Sahoo, B., Sreenivasan, V. K., Kombrabail, M., Muralidharan, C. and Maiti, S. **(2011)** Nature of the amyloid-beta monomer and the monomer-oligomer equilibrium. *J .Biol. Chem.* **286**, 13827-13833.

Necula, M., Kayed, R., Milton, S. and Glabe, C. G. **(2007)** Small molecule inhibitors of aggregation indicate that amyloid beta oligomerization and fibrillization pathways are independent and distinct. *J Biol Chem*. **282**, 10311-10324.

Nelson, R., Sawaya, M. R., Balbirnie, M., Madsen, A. O., Riekel, C., Grothe, R. and Eisenberg, D. **(2005)** Structure of the cross-beta spine of amyloid-like fibrils. *Nature* **435**, 773–778.

Niraula, T.N., Konno, T., Li, H., Yamada, H., Akasaka, K., and Tachibana, H. **(2004)** Pressure-dissociable reversible assembly of intrinsically denatured lysozyme is a precursor for amyloid fibrils. *Proc. Natl. Acad. Sci. U.S.A.* **101**, 4089–4093.

Nitsch, R. M., Rebeck, W., Deng, M., Richardson, U. I, Tennis, M, Schenk, D. B., Pelfrey, C., Lieberburg, I., Wurtmann, R. J. and Hytman, B. T. **(1995)** Cerebrospinal fluid levels of amyloid β-protein in Alzheimer's disease: inverse correlation with severity of dementia and effect of apolipoprotein E genotype. *Ann Neurol.* **37,** 512–518.

Nishimoto, E., Yamashita, S., Szabo, A. G. and Imoto, T. **(1998)** Internal motion of lysozyme studied by time-resolved fluorescence depolarization of tryptophan residues. *Biochemistry* **37,** 5599-5607.

Oosawa, F., Asakura, S., Hotta, K., Nobuhisa,I., Ooi, T. **(1959)** G–F transformation of as actin fibrous condensation. *J. Polym. Sci.* **37**, 323–336.

Orte, A., Birkett, N. R., Clarke, R. W., Devlin, G. L., Dobson, C. M. and Klenerman, D. **(2008)** Direct characterization of amyloidogenic oligomers by single-molecule fluorescence. *Proc. Natl. Acad .Sci. U S A.* **105**, 14424-14429

Otzen, D. E., Kristensen, O., Oliveberg, M. **(2000)** Designed protein tetramer zipped together with a hydrophobic Alzheimer homology: A structural clue to amyloid assembly. *Proc. Natl. Acad. Sci*. **97**, 9907–9912.

Parker, C. W. and Osterland, C. K. **(1970)** Hydrophobic Binding Sites on Immunoglobulins. *Biochemistry* **9,** 1074-1082.

Patterson, K. R., Remmers, C., Fu, Y., Brooker, S., Kanaan, N. M., Vana, L., Ward, S., Reyes, J. F., Philibert, K., Glucksman, M. J. and Binder, L. I. **(2011)** Characterization of prefibrillar tau oligomers in vitro and in Alzheimer disease. *J .Biol. Chem.* **286**, 23063-23076

Pedersen, J. S., Dikov, D., Flink, J. L., Hjuler, H. A., Christiansen, G., and Otzen, D. E **(2006)** The changing face of glucagon fibrillation: structural polymorphism and conformational imprinting *J. Mol. Biol.* **355**, 501–523.

Pepys, M. B., Hawkins, P. N., Booth, D. R., Vigushin, D. M., Tennent, G. A., Soutar, A. K., Totty, N., Nguyen, O., Blake, C. C. F., Terry, C. J., Feest, T. G., Zalin, A. M. and Husan, J. J. **(1993)** Human lysozyme gene mutations cause hereditary systemic amyloidosis. *Nature.* **362,** 553-557.

Petkova, A. T., Leapman, R. D., Guo, Z., Yau, W. M., Mattson, M. P. and Tycko, R. **(2005)** Self-propagating, molecular-level polymorphism in Alzheimer's beta-amyloid fibrils. *Science.* **307**, 262-265.

Phillips, D. C. **(1966)** The three-dimensional structure of an enzyme molecule. *Sci. Amer*. **215,** 78-90.

Phillips, D. C. **(1967)** The hen egg white lysozyme molecule. *Proc. Natl. Acad. Sci. USA.* **57,** 484-495.

Price, W. S., Tsuchiya, F., Arata. Y. **(1999)** Lysozyme aggregation and solution properties studied using PGSE NMR diffusion measurements. J. Am. Chem. Soc. 121:11503-11512.

Rafii, M. S. and Aisen, P. S. (2009) Recent developments in Alzheimer's disease therapeutics. BMC Med. **7**, 7

Reddy, R. C. K., Lilie, H., Rudolph, R. and Lange, C. **(2005)** L-Arginine increases the solubility of unfolded species of hen egg white lysozyme. *Protein Sci*. **14**, 929–935.

Reixach, N., Crooks, E., Ostresh, J. M, Houghten, R. A, Blondelle, S. E. (2000) Inhibition of β-amyloid induced neurotoxicity by imidazopyridoindoles derived from a synthetic combination library. *J. Struct. Biol.* **130**, 247–258.

Ritter, C., Maddelein, M.L., Siemer, A.B., Luhrs, T., Ernst, M., Meier, B.H., Saupe, S.J. and Riek, R. **(2005)** Correlation of structural elements and infectivity of the HET-s prion. *Nature* **435,** 844–848.

Rochet, J. C. (**2007**). Novel therapeutic strategies for the treatment of protein-misfolding diseases. *Exp. Rev. Mol. Med.* **9**, 1-34.

Romberg, L., Simon, M. and Erickson, H. P. **(2001)** Polymerization of Ftsz, a bacterial homolog of tubulin. Is assembly cooperative? *J. Biol. Chem*. **276**, 11743–11753.

Ross, C. A. and Poirier, M. A. **(2004)** Protein aggregation and neurodegenerative disease. *Nature Med*. **10**, S10-S17.

Rozema, D. and Gellman, S. H. **(1996)** Artificial chaperone-assisted refolding of denatured-reduced lysozyme: modulation of the competition between renaturation and aggregation. *Biochemistry* **35,** 15760–15771.

Sacchettini, J. C. and Kelly J. W. (2002) Therapeutic strategies for human amyloid diseases.*Nature Rev. Drug Dis*. **1**, 267-275.

Sahoo, B., Nag, S., Sengupta, P. and Maiti, S. **(2009)** On the stability of the soluble amyloid aggregates. *Biophys. J.* **97,** 1454–1460.

Sasahara, K., Yagi, H., Naiki, H. and Goto, Y. **(2007)** Heat-induced conversion of beta(2)-microglobulin and hen egg-white lysozyme into amyloid fibrils. *J Mol Biol.* **372**, 981-991

Sawaya, M. R., Sambashivan, S., Nelson, R., Ivanova, M. I., Sievers, S. A., Apostol, M. I., Thompson, M. J., Balbirnie, M., Wiltzius, J. J., McFarlane, H. T., Madsen, A.O., Riekel, C. and Eisenberg, D. (2007) Atomic structures of amyloid cross-beta spines reveal varied steric zippers. Nature 447, 453–457.

Schenk, D. **(2002)** Amyloid-beta immunotherapy for Alzheimer's disease: the end of the beginning. *Nature Rev. Neurosci.* **3,** 824–828.

Schneider, R., Schumacher, M. C., Mueller, H., Nand, D., Klaukien, V., Heise, H., Riedel, D., Wolf, G., Behrmann, E., Raunser, S., Seidel, R., Engelhard, M. and Baldus, M. **(2011)** Structural Characterization of Polyglutamine Fibrils by Solid-State NMR Spectroscopy. *J .Mol. Biol.* doi:10.1016/j.jmb.2011.06.045

Sekhar, A., and Udgaonkar, J. B. **(2011)** Fluoroalcohol-Induced modulation of the pathway of amyloid protofibril formation by Barstar. *Biochemistry* **50,** 805–819.

Skerget, K., Vilfan, A., Pompe-Novak, M., Turk, V., Jonathan P. Waltho, J. P., Dusan Turk, D. and Zerovnik, E. **(2009)** The mechanism of amyloid-fibril formation by stefin B: Temperature and protein concentration dependence of the rates. *Proteins.* **74,** 425-436.

Sophianopoulos, A. J. **(1969)** Association Sites of Lysozyme in Solution: The active site. *J. Biol. Chem.* **244**, 3188-3193.

Sophianopoulos, A. J. and Van Holde K. E. **(1961)** Evidence for dimerization of lysozyme in alkaline solution. *J. Biol. Chem.* **236,** PC82–PC83.

Sophianopoulos, A. J., and Van Holde, K. E. **(1964)** Physical studies of muramidase (lysozyme) II: pH dependent dimerization. *J. Biol. Chem.* **239**, 2516-2524.

Sorci, M., Silkworth, W., Gehan, T. and Belfort, G. **(2011)** Evaluating nuclei concentration in amyloid fibrillation reactions using back-calculation approach. *PLoS One.* **6**, e20072.

Spencer, R. G. S., Halverson, K. J., Auger, M., McDermott, A. E., Griffin, R. G., Lansbury, P. T. **(1991)** An unusual peptide conformation may precipitate amyloid formation in Alzheimer's disease: application of solid-state NMR to the determination of protein secondary structure. *Biochemistry* **30,**10382–10387.

Stefani M, Dobson C. M. **(2003)**. Protein aggregation and aggregate toxicity: new insights into protein folding, misfolding diseases and biological evolution. *J. Mol. Med.* **81,** 678–99.

Stenstam, A., Khan, A. and Wennerstrom, K. (**2001**) The lysozyme-dodecyl sulfate system. An example of protein-surfactant aggregation. *Langmuir* **17**, 7513–7520.

Straub, J. E. and Thirumalai, D. **(2011)** Toward a molecular theory of early and late events in monomer to amyloid fibril formation. *Annu. Rev. Phys. Chem.* **62**,437-463.

Stryer, L. (**1965)** The interaction of a naphthalene dye with apomyoglobin and apohemoglobin: A fluorescent probe of non-polar binding sites. *J. Mol. Biol.* **13**, 482-495.

Stryer, L. **(1968)** Fluorescence Spectroscopy of Proteins. *Science* **162**, 526-533.

Sunde, M. and Blake, C. **(1997)** The structure of amyloid fibrils by electron microscopy and X-ray diffraction. *Adv. Protein. Chem.* **50,** 123–159.

Sunde, M., Blake, C. C. **(1998)** From the globular to the fibrous state:protein structure and structural conversion in amyloid formation. *Q. Rev. Biophys.* 1998, **31**, 1 -39.

Sunde, M., Serpell, L. C., Bartlam, M., Fraser, P. E., Pepys, M. B. and Blake, C. C. **(1997)** Common core structure of amyloid fibrils by synchrotron X-ray diffraction. *J. Mol. Biol.* **273,** 729–739.

Swaminathan, R., Ravi,V. K. Kumar, S. Kumar, M. V. S. and N. Chandra. **(2011)**. Lysozyme: A model protein for amyloid research. *In Adv. Prot. Chem. Struct. Biol.* **84** R. M. Donev (editor) (in press).

Tanaka, M., Machida, Y. and Nukina, N. **(2005)** A novel therapeutic strategy for polyglutamine diseases by stabilizing aggregation-prone proteins with small molecules. *J Mol Med (Berl).* **83**, 343-352.

Thompson, R. (1940). Lysozyme and its relation to the antibacterial properties of various tissues and secretions. Arch. Pathol. 30, 1096-1134.

Tomita, S., Yoshikawa, H. and Shiraki, K. **(2011)** Arginine controls heat-induced cluster-cluster aggregation of lysozyme at around the isoelectric point. *Biopolymers,* doi: 10.1002/bip.

Toyama BH, Kelly MJS, Gross JD, Weissman JS: **(2007)** The structural basis of yeast prion strain variants. *Nature* **449,** 233-237.

Trexler, A. J., and Nilsson, M. R. **(2007)** The formation of amyloid fibrils from proteins in the lysozyme family. *Curr. Protein Pept. Sci.* **6**, 537-557.

Trusova, V., M., Gorbenko, G. P., Sarkar, P., Luchowski, R., |Akopova, I., Patsenker, L., D., Klochko, O., Tatarets, A., L., Kudriavtseva, Y., O., Terpetschnig, E., A., Gryczynski, I. and Gryczynski, Z.

(2010) Forster resonance energy transfer evidence for lysozyme oligomerization in lipid environment. *J. Phys. Chem B*, **114,** 16773-16782.

Turner, D. C, Brand L. **(1968)** Quantitative estimation of protein binding site polarity. Fluorescence of N-arylaminonaphthalenesulfonates. *Biochemistry* **10,** 3381-3390.

Umetsu, M., Tsumoto, K., Nittaa, S., Adschiri, T., Ejima, D., Arakawa, T., and Uversky, V. N., Talapatra, A., Gillespie, J. R., Fink, A. L. **(1999)** Protein deposits as the molecular basis of amyloidosis: I. Systemic Amyloidoses. *Med. Sci. Monit.* **5,** 1001-1012.

Umetsu, M., Tsumoto, K., Nittaa, S., Adschiri, T., Ejima, D., Arakawa, T., and Kumagai, I. **(2005)**. Nondenaturing solubilization of β2 microglobulin from inclusion bodies by L-arginine. *Biochem. Biophys. Res. Commun.* **328**, 189–197.

Uversky V. N, Fink, A. L. **(2004)**. Conformational constraints for amyloid fibrillation: the importance of being unfolded. *Biochim. Biophys. Acta* **1698,** 131–153.

Uversky, V. N., Kabanov, A. V., Lyubchenko, Y. L. J. **(2006)** Nanotools for megaproblems: Probing protein misfolding Diseases using nanomedicine modus Operandi. *Proteome Res.* **5,** 2505-2522.

Uversky, V. N., Talapatra, A., Gillespie, J. R., Fink, A. L. **(1999)** Protein deposits as the molecular basis of amyloidosis: II. Localized amyloidosis and neurodegenerative disordres. *Med. Sci. Monit.* **5,** 1238 -1254.

Van Gool, W. A., Kuiper, M. A., Walstra, G. J. M., and Bolhuis, P. A. **(1995)** Concentration of amyloid protein in cerebrospinal fluid of patients with Alzheimer's disease. *Ann. Neurol.* **37,** 277 – 279.

Vasilescu, M., Angelescu, D., Almgren, M. and Valstar, A. **(1999)** Interactions of Globular Proteins with Surfactants Studied with Fluorescence Probe Methods *Langmuir* **15**, 2635 2643.

Vernaglia, B. A., Huang, J. and Clark, E. D. (2004) Guanidine hydrochloride can induce amyloid fibril formationfrom hen egg-white lysozyme. *Biomacromolecules* **5**, 1362-1370.

Vieira, M. N. N., Figueroa-Villar, J. D., Meirelles, M. N. L., Ferreira, S. T. and De Felice, F. G.**(2006)** Small molecule inhibitors of lysozyme amyloid aggregation. *Cell Biochem. Biophys* .**44**, 549-553.

Vieira, M. N. N., Forny-Germano L., Saraiva, L. M., Sebollela, A., Martinez, A. M. B., Houzel, J-C., De Felice, F. G., and Ferreira, S. T. **(2007)** Soluble oligomers from a non-disease related protein mimic Aβ induced tau hyperphosphorylation and neurodegeneration. *J. Neurochem.* **103**, 736–748.

Villegas V., Zurdo J., Filimonov V. V., Aviles F. X., Dobson C. M. and Serrano L. **(2000)** Protein engineering as a strategy to avoid formation of amyloid fibrils *Protein. Sci.* **9**, 1700–1708.

Virchow, R. **(1854)** Cellulose-Frage. Virchows Arch. Pathol. Anat. **6,** 416 426.

Wall, J., Murphy, C. L., Solomon, A. **(1999)** In Vitro immunoglobulin light chain fibrillogenesis.

Methods Enzymol. **309,** 204-217.

Walsh, D. M., Klyubin, I., Fadeeva, J. V., Cullen, W. K., Anwyl, R., Wolfe, M. S., Rowan, M. J. and Selkoe, D. J. **(2002)** Naturally secreted oligomers of amyloid beta protein potently inhibit

hippocampal long-term potentiation in vivo. *Nature*. **416**, 535-539.

Wang, J., Lu, D., Lin, Y. and Liu, Z. **(2005)** How CTAB assists the refolding of native and recombinant lysozyme. *Biochem. Engg. J.* **24**, 269-277.

Wang, S. S. S., Chen, Y. T. and Chou, S. W. **(2005)** Inhibition of amyloid fibril formation of β-amyloid peptides via the amphiphilic surfactants. *Biochim. Biophys. Acta.* **1741,** 307–313.

Wang, S. S. S., Chen, P. H. and Hung, Y. Tz. **(2006)** Effects of *p*-benzoquinone and melatonin on amyloid fibrillogenesis of hen egg-white lysozyme. *J. Mol. Catal. B: Enzym*. **43**, 49-57.

Wang, S. S. S., Liu, K. N., and Lu, Y. C. **(2009b)** Amyloid fibrillation of hen egg-white lysozyme is inhibited by TCEP. *Biochem. Biophys. Res. Commun.* **381,** 639–642.

Wang, S. S., Liu, K. N. and Wang, B. W. (2010) Effects of dithiothreitol on the amyloid fibrillogenesis of hen egg-white lysozyme. *Eur Biophys J.* **39**, 1229-1242

Westermark, G.T., Johnson, K.H. and Westermark, P. **(1999)** Staining methods for identification of amyloid in tissue. *Meth. Enzymol.* **309**, 3–25.

Wetter, L. R. and Deutsch, H. F. **(1951)** Immunological studies on egg white proteins IV. Immunochemical and physical studies of lysozyme. *J. Biol. Chem.* **192,** 237–242.

White, A. R., Enever, P., Tayebi, M., Mushens, R., Linehan, J., Brandner, S., Anstee, D., Collinge, John., and Hawke, S. **(2003)** Monoclonal antibodies inhibit prion replication and delay the development of prion disease. *Nature* **422**, 80–83.

Williams, A. D., Portelius, E., Kheterpal, I., Guo, J. T., Cook, K. D., Xu, Y., and Wetzel, R. (2004) Mapping Ab amyloid fibril secondary structure using scanning proline mutagenesis. *J. Mol. Biol.* **335**, 833–842.

Winner, B., Jappelli, R., Maji, S. K., Desplats, P. A, Boyer, L., Aigner ,S., Hetzer, C., Loher, T., Vilar, M., Campioni, S., Tzitzilonis C., Soragni, A., Jessberger S., Mira H., Consiglio, A., Pham, E., Masliah, E., Gage, H. F. and Riek, R. **(2011)** In vivo demonstration that α-synuclein oligomers are toxic. *Proc. Natl. Acad. Sci. USA* **108,** 4194-4199.

Wood, S. J, MacKenzie, L., Maleeff, B., Hurle, M. R, and Wetzel, R. (**1996**) Selective inhibition of Abeta fibril formation. *J. Biol .Chem.* **271,** 4086–4092.

Wurth, C., Guimard, N.K, Hecht, M.H. **(2002)** Mutations that reduce aggregation of the Alzheimer's Abeta42peptide: an unbiased search for the sequence determinants of Abeta amyloidogenesis. *J. Mol. Biol.* **319,** 1279–1290.

Xie, J., Qin, M., Cao, Y. and Wang, W. **(2011)** Mechanistic insight of photo-induced aggregation of chicken egg white lysozyme: The interplay between hydrophobic interactions and formation of intermolecular disulfide bonds. *Proteins.* **79**, 2505-2516

Yamamoto, K., Yagi, H., Ozawa, D., Sasahara, K., Naiki, H. and Goto, Y. **(2008)** Thiol compounds inhibit the formation of amyloid fibrils by β2-microglobulin at neutral pH. *J. Mol. Biol.* **376,** 258–268.

Yonezawa, Y., Tanaka, S., Kubota, T., Wakabayashi, K., Yutani, K., and Fujiwara, S. **(2002)**. An insight into the pathway of the amyloid fibrilformation of hen egg white lysozyme obtained froma small-angle x-ray and neutron scattering study. *J. Mol. Biol.* **323**, 237–251.

Zerovnik, E., Stoka, V., Mitric, A., Guncar, G., Grdadolnik, J., Staniforth, R. A., Turk, D. and Turk, V., **(2011)** Mechanisms of amyloid fibril formation: focus on domain-swapping. *FEBS Journal. doi: 10.1111/j.1742-4658.2011.08149.*

Zhang, D., Neumann, O., Wang, H., Yuwono, V. M., Barhoumi, A., Perham, M., Hartgerink, J. D., Wittung-Stafshede, P. and Halas, N. J. **(2009)** Gold nanoparticles can induce the formation of protein-based aggregates at physiological pH. *Nano Lett.* **9**, 666-671.

Zhang, J., Liu, X. Y. **(2003)** Effect of protein-protein interactions on protein aggregation kinetics. *J. Chem. Phys.* **119**, 10972-10976.

Zhang, R., Hu, X., Khant, H., Ludtke, S. J., Chiu,W., Schmid, M. F., Frieden, C. and Lee, J. M. **(2009)** Interprotofilament interactions between Alzheimer's Abeta1–42 peptides in amyloid fibrils revealed by cryoEM. *Proc. Natl. Acad. Sci.* USA **106**, 4653–4658.

Zhao, D., Moore, J. S. **(2003)** Nucleation–elongation: A mechanism for cooperative supramolecular polymerization. *Org .Biomol. Chem.* **1,** 3471–349.

Zhao, J., Yu, X., Liang, G. and Zheng, J. **(2011)** Structural polymorphism of human islet amyloid polypeptide (hIAPP) oligomers highlights the importance of interfacial residue

Zhou, B. R., Zhou, Z., Hu, Q. L., Chen, J., and Liang, Y. **(2008)**. Mixed macromolecular crowding inhibits amyloid formation of hen egg white lysozyme. *Biochim. Biophys. Acta.* **1784,** 472–480.

List of publication

Journals

1. Kumar, S., **Ravi, V. K.** and Swaminathan, R., **(2008)** How do surfactants and DTT, affect the size, dynamics, activity and growth of soluble lysozyme aggregates? *Biochem. J.* **415**, 275-288.
2. Kumar, S., **Ravi, V. K.** and Swaminathan, R., **(2009)** Suppression of lysozyme aggregation at alkaline pH by tri-N-acetylchitotriose. *Biochim. Biophys. Acta.* **1794**, 913-920.
3. Swaminathan, R., **Ravi, V. K.,** Kumar, S., Kumar, M. V. S. and Chandra, N., (**2011**) Lysozyme: A Model protein for amyloid research. *In. Adv. Prot. Chem. Struct. Biol.* **84,** (in press) Elsevier.
4. **Ravi, V. K.,** Chandra, N. and Swaminathan, R. (**xxxx**) Decrease in size of hen egg white lysozyme aggregates with decrease in monomer concentration from micro to nanomolar in alkaline pH. (*To be submitted*)
5. **Ravi, V. K.,** Goel**,** M. and Swaminathan, R. (xxxx) Structure and dynamics of s-carboxyamidomethyl cysteine derivative aggregates of hen egg white lysozyme in alkaline pH 12. 2 at room temperature (To *be submitted*).

Conferences /Workshop / Posters / Short term courses attended

1. **Ravi, V. K.,** Singh, K. D., Reddy, C. N., Iyer, A. and Swaminathan, R (2011) Decrease in size of hen egg white lysozyme aggregates with decrease in monomer concentration from micro to nanomolar in alkaline pH. Abstracted published in *Biophysical Journal* **100** (3) pp. 538a
2. Singh, K. D., Iyer, A., Reddy, C. N., **Ravi, V. K.** and Swaminathan, R. (2010) Aggregation of hen lysozyme protein at nanomolar concentrations in alkaline pH: A fluorescence correlation spectroscopy investigation. Poster presented at IIT

Guwahati held on 3-4 th December 2010 "National conference on Frontiers in chemical sciences" organized by Department of Chemistry.

3. Singh, K. D., Iyer, A., Reddy, C. N., **Ravi, V. K.** and Swaminathan, R (2010) Aggregation of hen lysozyme protein at nanomolar Concentration in alkaline pH: A Flurorescence Correlation Spectroscopy Investigation. Poster presented at NEHU Shilong held on 8th-13 th November, 2010 "National workshop on fluorescence correlation spectroscopy and biophotonics (FCS-2010)" at department of chemistry in collaboration with TIFR Mumbai.
4. **Ravi, V. K.,** Chandra, N. and Swaminathan, R. (2010) Oligomerisation, Fibrillation and activity of hen lysozyme in alkaline medium: A concentration dependent investigation. Abstract published in *Biophysical Journal* **98** (3) pp 252a.
5. **Ravi, V. K.,** Chandra, N. and Swaminathan, R. (2009) Aggregation of hen lysozyme at alkaline pH monitored at different concentration, Fluorescence 2009, Fluorescence in biology an international conference on fluorescence from March16th-19th organized by Tata Institute of Fundamental Research (TIFR), Mumbai.
6. Kumar, S., **Ravi, V. K.** and Swaminathan, R. (2008) How Does SDS, CTAB and DTT affect the size, rotational dynamics and growth Kinetics of soluble lysozyme aggregates? Abstract published in *Biophysical Journal* **94** (2) pp 933-946.
7. National Workshop on Fluorescence Correlation Spectroscopy from 7th -24thMar (2009). The workshop was a part of the Department of Information & Technology (DIT), Govt. of India sponsored research project entitled "Construction and multi-site commissioning of multiple fluorescence correlation spectrometers (FCS, a single molecule biophotonic tool)"[Project No. 12(4)/2007-PDD, Principal Investigator: Dr.Sudipta Maiti, TIFR, Mumbai, co-Investigator: Dr. Sivaprasad Mitra, NEHU, Shillong].
8. Short term course on" Advanced Experimental Techniques held at IIT Guwahati from 6 th – 10 th Feb 2006 under Quality Improvement programme (AICTE sponsored).

9. Regional Seminar on ”Intellectual Property & Innovation management in Knowledge era” from 5 th – 6th May 2010 at IIT Guwahati sponsored by NRDC, Govt. of India.